SOIL EROSION IN BINĠEMMA-SAN BLAS VALLEY – A MULTISCALE AND MULTITEMPORAL APPROACH

Shirley Muscat

A dissertation submitted in partial fulfilment of the requirements for the degree of

Master of Science at the Institute of Earth Systems

Master of Science in Rural and Environmental Sciences

Institute of Earth Systems

University of Malta

March 2025

L-Università ta' Malta

FACULTY/INSTITUTE/CENTRE/SCHOOL Institute of Earth Systems

DECLARATIONS BY POSTGRADUATE STUDENTS

(a) Authenticity of Dissertation

I hereby declare that I am the legitimate author of this Dissertation and that it is my original work.

No portion of this work has been submitted in support of an application for another degree or qualification of this or any other university or institution of higher education.

I hold the University of Malta harmless against any third party claims with regard to copyright violation, breach of confidentiality, defamation and any other third party right infringement.

(b) Research Code of Practice and Ethics Review Procedures

I declare that I have abided by the University's Research Ethics Review Procedures. Research Ethics & Data Protection form code IES-2022-00033.

As a Master's student, as per Regulation 77 of the General Regulations for University Postgraduate Awards 2021, I accept that should my dissertation be awarded a Grade A, it will be made publicly available on the University of Malta Institutional Repository.

ABSTRACT

Accelerated soil erosion is a global issue which directly and indirectly impacts the surrounding environment in various ways. In the Mediterranean region, soil erosion is typically more severe. Therefore, this study aimed to estimate the total annual soil loss in the San Blas and Binġemma valley, a small watershed in Gozo, Malta using the RUSLE equation, at two different spatial resolutions. The use of two spatial resolutions was to determine if a coarse 30 m DEM could be used if a finer DEM was unavailable. Through comparison between soil loss estimates obtained from ASTER GDEM and LiDAR-derived DEM of 30 m and 1 m spatial resolution respectively, it was determined that while ASTER GDEM tends to overestimate, the positive correlation between the two datasets is very strong and despite their slight difference, ASTER GDEM can be used to obtain soil loss estimates over the valley, especially to determine hotspot areas of high soil erosion values. Another aim was to estimate historical soil losses in the same valley. The estimates cover a period between 1957 and 2021 with approximately 10-year intervals. Future soil loss predictions for 2050 under SSP 2-4.5 and SSP 5-8.5 were also estimated using precipitation data from CMIP6. Findings showed that mean past estimates fluctuated slightly but had a decreasing trend, with means ranging between 2-7 t/ha/yr in all the past years estimated. Future soil loss predictions were found to be lower, especially for SSP 5-8.5 which had a mean soil loss of 0.87 t/ha/yr.

TABLE OF CONTENTS

LIST OF TABLES

LIST OF FIGURES

LIST OF ABBREVIATIONS

AOI – area of interest

ASTER GDEM – Advanced Spaceborne Thermal Emission and Reflection Radiometer Global Digital Elevation Model

CMIP – Coupled Model Intercomparison Project

DEM – Digital Elevation Model

EPIC – Erosion-Productivity Impact Calculator

ERA – Environment and Resources Authority

ESA – European Space Agency

FAO – Food and Agricultural Organization

IPCC – Intergovernmental Panel for Climate Change

KE – kinetic energy

LiDAR – Light detection and ranging

METI – Japan's Ministry of Economy, Trade and Industry

MFI – Modified Fournier Index

MMMF model – Modified Morgan-Morgan-Finney model

MODIS – Moderate Resolution Imaging Spectroradiometer

NASA – National Aeronautics and Space Administration

NDVI – Normalized Difference Vegetation Index

NIR – Near InfraRed

RCP – Representative Concentration Pathway

RUSLE – Revised Universal Soil Loss Equation

SOM – soil organic matter

SSP – Shared Socioeconomic Pathway

USGS – United States Geological Survey

USLE – Universal Soil Loss Equation

ACKNOWLEDGEMENTS

I would like to express my sincere gratitude to my supervisor, Prof. Charles Galdies, for his constant support, guidance, and feedback throughout this research.

I am also deeply grateful to Dr. Anthony Sacco for his advice and for providing access to laboratory facilities.

I would also like to extend a profound thanks to my parents, sister, and partner for their unwavering support and encouragement throughout this challenging but rewarding journey.

Additionally, I would like to acknowledge the following organizations, data sources, and platforms whose data was imperative to this study. The Meteorological Office MIA plc. for their historical meteorological data. The Planning Authority for their historical orthophotos and their 2018 LiDAR DEM. United States Geological Survey (USGS) for providing access to Landsat 8 Surface Reflectance data and Google for providing the Earth Engine platform, which facilitated data access and processing. The Ministry of Economy, Trade, and Industry (METI) of Japan and the U.S. National Aeronautics and Space Administration (NASA) for providing the ASTER Global Digital Elevation Model (GDEM). WorldClim and each of the CMIP6 and CMIP5 modelling groups, the Program for Climate Model Diagnosis and Intercomparison, and the World Climate Research Programme's Working Group on Coupled Modelling for producing, archiving, and making available their model output.

1. INTRODUCTION

1.1. Background

Soil erosion is defined by the Food and Agricultural Organization (FAO) as 'the accelerated removal of topsoil from the land surface through water, wind or tillage' (FAO & ITPS 2015, p. 100). Soil erosion has a wide variety of impacts. It directly affects the soil through decreases in soil fertility, but it also has other effects, such as pollution and water quality degradation of streams, rivers, lakes, and seas (Eash et al. 2016). It is thus a problem for agriculture as well as for natural ecosystems. This is why management is needed. Management can be in the form of agronomical measures or engineering measures. Determining which is the best management option is done by estimating the amount of soil erosion occurring, which can be done through a number of models and equations (Bhat et al. 2019) or through in-situ methods (de Oliveira Salumbo 2020). Models include the empirical USLE (Universal Soil Loss Equation) and RUSLE (Revised Universal Soil Loss Equation), the physically based WEPP (Water Erosion Prediction Project), EPIC (Erosion-Productivity Impact Calculator), and EUROSEM (European Soil Erosion Model), and the conceptual AGNPS (Agricultural Non-Point Source Pollution) and SWAT (Soil and Water Assessment Tool), among others (Raza et al. 2021; de Oliveira Salumbo 2020). In situ methods include splash cups, field plots, H-flumes, and erosion pins. Furthermore, rainfall simulation, tracers, and aerial photography may also be used to help determine the amount of soil loss taking place (Hu & Liu 2021; de Oliveira Salumbo 2020).

Nowadays, natural phenomena need to also be considered in the context of climate change. Soil erosion has been affected by climate change for a long time, with human attention on this phenomenon dating back to the 1940s (Bryan & Albritton 1943). The effects can be subdivided into direct and indirect effects, with direct effects being related to precipitation changes in pattern, amount, and intensity. Meanwhile, indirect effects are caused by the temperature increase, which in turn affects soil moisture and vegetation cover; and anthropogenic reasons, such as alteration of planting and harvesting dates, and a different choice of crops grown due to the altered climate regime (Nearing et al. 2004; Li & Fang 2016). The increased challenge of climate change, which will probably alter soil erosion rates, requires even better management to ensure that accelerated rates of erosion are controlled (Nearing et al. 2004). Management includes calculating an estimate of soil loss under future climate change projections to help determine a soil conservation plan. This estimate can be calculated using soil erosion models in conjunction with climate models (Li & Fang 2016).

1.1.1. Area of Interest

The area of interest (AOI) is the San Blas and Binġemma Valley situated in Nadur, Gozo, Malta. The valley is located on the north-east of Gozo between the San Blas and Ramla headlands (figure 1-1). Despite having two names, San Blas and Binġemma Valley is one valley which is divided into the tarmacked landward part and the seaward part without a path. The valley ends in San Blas Bay.

Figure 1-1: Map of San Blas and Binġemma Valley (Edited from Google Earth, 2021).

1.2. Justification of Study

One aspect of the study is to compare the use of coarse and fine topographical data over the AOI to determine if coarse data is usable and reliable when fine data is unavailable. Coarse data, with spatial resolutions ranging from 30 m to several kms, while often readily available, can misrepresent small areas by considering them part of a bigger area and merge features together, thereby losing accuracy. Undoubtedly, when available, fine data yields very accurate results. However, a number of constraints can hinder the use of fine data. This includes no data available due to lack of surveys taken with high resolution technology; long revisit periods, and high computational costs (Wang et al. 2022). Considering these limitations, sometimes it is necessary to use coarser data. Using coarse data, for DEMs as well as for climate models and other satellite products, over small areas is especially of interest to Malta due to the size of the islands. This study therefore aims to estimate soil erosion using two different spatial resolutions (1 m from Light Detection and Ranging (LiDAR) surveys and 30 m from ASTER Global Digital Elevation Model (ASTER GDEM)) and then compare the results. This will help to determine whether certain satellite products, in this case ASTER GDEM, are of use to the Maltese Islands or not. If reliable, using such data, which is readily available, would be very beneficial as it would save money and time from conducting field visits or from conducting LiDAR surveys when they are not already available.

Another aspect of the study is soil erosion change in the AOI. Between 1957 and 2021 soil erosion in the San Blas and Binġemma valley has increased in severity but decreased spatially (Muscat 2022). However, whether the change is a gradual trend or whether it is constantly changing is unknown. Therefore, this study's aim to map and estimate soil erosion patterns in the AOI for intermediate years between 1957 and 2021 will fill in this knowledge gap and answer the question as to whether the soil loss is constant or fluctuating. This better understanding of the soil erosion patterns is important as it allows for better soil conservation planning and management, which is essential for healthy productive soils. Good management of soils and effective soil erosion measures are necessary for the agricultural industry. While the industry itself can sometimes damage soil, it is of utmost importance as it is the backbone of food security. In fact, San Blas and Binġemma valley is partially under agricultural production and so it is important to understand and manage soil resources in the valley. This is along with the fact that soil erosion creates other problems, not just agricultural ones, such as water pollution (Issaka & Ashraf 2017).

Using future climate projections is another important aspect of this study as it investigates any potential soil erosion changes which result from future climate change. In their assessment report for the Intergovernmental Panel for Climate Change (IPCC), Ali et al. (2022) predict a decrease in total precipitation, but an increase in intensity; an increase in length, intensity, and frequency of heat waves; sea level rise; and an increased surface temperature over the Mediterranean region. Such changes to precipitation and temperature will result in a number of impacts on

soil and agriculture including on soil organic carbon, soil organisms, soil water, and crop production (Brevik 2012; Galdies et al. 2016). These aspects are likely to be present in the Maltese Islands, along with water stress due to increased water demand because of the longer growing season and increased droughts. This will in turn increase soil salinity and alkalinity leading to land abandonment and dilapidation of agricultural infrastructure and finally to increased soil erosion (Galdies et al. 2016; Climate Change Committee for Adaptation 2010). Another impact of climate change felt in the Maltese Islands is the presence of pests which is reported to have increased, likely due to the warmer climate and the introduction of new pests (Galdies et al. 2016). Galdies et al. (2016) also found that most Gozitan farmers reported a productivity decrease in both crop and livestock production. Understanding these impacts and how the soil will be affected is essential in determining the best measures to adopt to best conserve and maintain soil under the future climatic conditions.

1.3. Research Questions

This study requires three research questions. They are as follows:

1. Can coarse topographic data be used accurately for small valleys such as those found in the Maltese Islands, when finer data is unavailable?
2. Has there been a substantial difference in the estimated annual total soil lost as well as its distribution during the period of analysis?
3. Will there be a substantial change between estimated current soil erosion and predicted future soil erosion under climate change projections?

1.4. Aims

To satisfy the above research questions, this study has three aims, which are to:

1. Estimate the soil erosion in the AOI at different spatial resolutions, using both coarse and fine data.
2. Map soil erosion patterns and estimate total annual soil loss in the AOI for intermediate years from 1957 up to 2021, with intervals of approximately 10 years.
3. Estimate the future potential soil erodibility for the AOI on the basis of variables derived from multi-model climate projections.

In order to meet the study's aims, several methods are required. For Aim 1, regarding the use of coarse data for soil loss estimates, two DEMs will be used with a spatial resolution of 1 m and 30 m respectively. The 1 m DEM will be upscaled to match the 30 m DEM. Both DEMs will be used to calculate the topographic factor, which will in turn be used as one of the inputs to the RUSLE equation to estimate soil loss in the AOI. For Aim 2, rainfall and soil erosivity will be determined via appropriate equations, alongside a 1 m DEM and, orthophoto interpretation to determine crop cover in the AOI during the study period. These parameters will then be used as inputs to RUSLE to estimate soil loss in the valley at approximately 10-year intervals since 1957. For Aim 3, data from climate models will be used to determine future rainfall erosivity. Meanwhile, vegetation data will be determined from NDVI. Since projected NDVI for the future is not readily available, a proxy-based approach will be

implemented. A relationship will be determined between past NDVI and two variables which affect vegetation, and the relationship will be applied to future data to estimate future NDVI. Projected soil loss estimates will then be determined using RUSLE. A detailed description of the methodology will be provided in chapter 3 of this work.

2. LITERATURE REVIEW

2.1. Introduction

Soil erosion is a normal and necessary process, where soil particles are detached, transported, and deposited elsewhere (Eurostat 2020). This process is referred to as natural erosion. However, another type of soil erosion, accelerated erosion, which affects soil through a number of agents, causes soil to be eroded at rates much faster than normal erosion (Webb et al. 2014). This in turn leads to soil deterioration and degradation. Such erosive agents can be either anthropogenic or natural and can include water and wind as well as animals, plants, glaciers, snow, and of course human interference (Zachar 1982). While human interference often accelerates soil erosion, certain activities and management practices may also lead to inhibited erosion (Zachar 1982). Soil erosion often begins gradually in agricultural fields without much visible evidence. This ensures that the problem is not given due importance and proper soil erosion control measures are not adopted until the soil has already undergone an amount of topsoil loss (Zachar 1982).

2.2. Historical Perspective

Since the beginnings of agriculture human interference has greatly affected the environment, including regarding soil erosion (Dotterweich 2008). A shift in the land

use from natural vegetation to agriculture left areas susceptible to soil erosion, while the introduction of tillage operations meant soil surfaces were smoothed and compacted, thereby increasing runoff and erosion on slopes (James 2013). In recent years, farmers have removed rubble walls and hedgerows separating fields in order to create larger fields, leading to increased soil erosion (Baudry et al. 2000). In fact, human influence can be considered in each of the five soil forming factors, with some even considering humanity the sixth soil forming factor (Richter 2007; Dudal 2002). In Malta, agriculture dates back to prehistoric times with agricultural tools dating back to the neolithic period. It was also well documented in the Roman period. Reconnaissance by the Knights of St. John before they came to Malta describe the islands as capable of decent crop production despite having only sparse vegetation and a lack of water. From the mid-19th century onwards, agriculture started to decline as more of the population started to work in secondary and tertiary production (Busuttil 1993).

Land ownership in Malta also had an effect in reducing agriculture. Land belonged to either: the state (civil government and war department), the church, private individuals, or freeholders (farmer-owned). The state and the church leased the land often on an emphyteutical lease, which were often of a very long duration. The highest percentage of agricultural land was under private ownership, sometimes emphyteutical and sometimes normal rent. However, private ownership was decreasing due to the increase in building sites after WWII. Amount of freehold land

is difficult to estimate as many farmers are not sure if their land is freehold or under a long emphyteutical lease (Busuttil 1993).

Busuttil (1993) also mentions some of the problems which Maltese agriculture has faced, and in some cases is still facing. These issues hinder agricultural production but often lead to a change in land use from crop production to abandoned land, which can affect soil erosion values. Issues include:

- Demographics, with many Maltese farmers being from an older generation resulting in an aging farming population; many also have low levels of education which results in reluctance to take up modern techniques, ignorance of production costs, and soil degradation issues such as fertilizer misuse.
- Migration, post war in 1946 due to a reduction in jobs. This led to massive emigration, largely to Australia, which helped lead to a decrease in full-time farmers.
- Monetary issues faced by farmers along with the lack of sufficient government incentives also contributes to the decrease in full-time farmers.
- Land fragmentation, reduces the size of fields owned by individual farmers therefore, reducing the farmer's output and income.

2.3. Types of Soil Erosion

Soil erosion occurs either due to chemical or physical processes. Chemical processes include chemical denudation where mineral soil particles are weathered and removed off-site via suspension or solution and organic soil particles can be weathered via decomposition. However, physical processes are dominant in mineral soils (Verheijen et al. 2009). This involves soil removal via external forces, such as water and wind leading to three different classifications of erosion: water, wind, and tillage erosion

2.3.1. Water Erosion

One of the major agents of water erosion is precipitation. This can be in the form of rain, hail, or snow, all of which influence soil erosion (Zachar 1982). This erosivity depends on the kinetic energy of the precipitation (Laws 1941). Rain impacts soil loss from three perspectives: raindrops, surface runoff, and subsurface runoff. Regarding raindrops, vegetation reduces their kinetic energy and thereby reduces raindrop erosion (Zachar 1982). An extreme positive correlation between rainfall erosivity and soil loss was found in a study by Yuan et al. (2021). Rainfall intensity in particular, is especially important and can lead to rainfall being considered the biggest contributor to soil loss. This is because it is a highly influential factor in determining the amount of runoff generated and soil splash erosion occurring (Yuan et al. 2021). Some studies

have even showed that rainfall intensity is a bigger contributor than rainfall amount regarding soil loss amounts (Shi & Wang 2015; Tang et al. 2015; Yao et al. 2015). Comparing the contribution of rainfall intensity, antecedent moisture conditions and slope gradient to soil loss and runoff, Ziadat and Taimeh (2013) found that rainfall intensity is always the biggest contributor in both cultivated and uncultivated soils. Rainfall intensity is so vital to soil erosion that in the USLE model it is considered in the rainfall erosivity factor (Wischmeier & Smith 1978). Hail also impacts soil loss as it has high levels of kinetic energy leading to soil surface destruction and washing away of soil particles. Snow influences soil loss as runoff is increased during thawing. Frost also disaggregates soil and the cold freezes soil into an impermeable layer or doesn't allow percolation due to frozen permafrost. This increases runoff and thereby increases soil erosion (Zachar 1982).

2.3.1.1. Raindrop Erosion

Raindrop impact, or splash erosion, is when raindrops hit the ground and their energy is used to break the soil particles' bonds, thereby breaking the soil aggregates, and releasing small soil particles (Kinnell 2005). On slopes with an inclination of 10%, after disaggregation, 75% of splash material moves downhill (Ellison 1944). Breakdown of soil aggregates is the beginning of both soil erosion as well as of soil sealing (Ellison 1945). Surface sealing is when detached soil particles undergo washing in, which is displacement of soil particles into soil pores, and after compaction by raindrops, form a surface seal (McIntyre 1958). Surface seal formation is common in cultivated silty

soils, and it increases erosion as it decreases water infiltration and increases runoff (Robinson & Woodun 2008). Slacking can also help in surface seal formation. Slacking is when soil aggregates break down into smaller aggregates due to rapid wetting (Yoder 1936). Under antecedent saturated conditions, slacking is dominant while raindrop impact and particle displacement is dominant under unsaturated conditions (Vaezi et al. 2017).

Vaezi et al. (2017) found that raindrop impact contributed to the deterioration of soil physical properties, such as compaction, crusting and aggregate breakdown. The higher the rainfall intensity, the more soil deterioration. Raindrop impact induced soil detachment is correlated with the ratio of flow depth and rain diameter (Gabet & Dunne 2003). In their study, Vaezi et al. (2017) also linked soil erosion to rainfall intensity. Raindrop impact was the highest with rainfall intensities of 20 mm/h and 30 mm/h. Higher intensities allowed the formation of a water layer on the soil surface which protected against raindrop impact. This reduction in raindrop impact meant less soil erosion taking place (Vaezi et al. 2017).

While raindrop impact is of major importance to soil detachment and runoff disturbance, it does not have the biggest effect on transport (Kinnell 2005; Lu et al. 2016). In fact, transportation is mostly carried out via surface runoff and rain splash (Lu et al. 2016). However, raindrop impact still has a small effect on transportation. Kinnell (2005) observed four detachment and transport systems for soil water erosion:

1. Detachment via raindrops and transport via raindrop splash (RD-ST).
2. Detachment via raindrops and transport via raindrop induced flow (RD-RIFT).
3. Detachment via raindrops and transport via flow (RD-FT).
4. Detachment via flow and transport via flow (FD-FT).

2.3.1.2. Flow Erosion

Overland flow, an aspect of surface runoff, is a thin sheet of water flowing over the land surface. It is a shallow and unconcentrated flow which is also termed sheet flow, the first in the three stages of water erosion – sheet, rill, and gully. Sheet erosion leads to the erosion of a moderately uniform layer of soil (Kilinc & Richardson 1973). These thin layers of soil are eroded consecutively, with erosion often not being visible (Owoputi and Stolte 1995).

The amount of runoff in a rainfall event is dependent on rainfall characteristics, such as intensity and duration, as well as soil characteristics, vegetation, and topography (Critchley et al. 1991). Detachment is mainly influenced by soil cohesion, i.e. soil texture and soil organic matter (SOM) and rainfall characteristics, i.e. raindrop diameter, distribution, velocity and kinetic energy. On the other hand, transport is influenced by availability of detached particles, size distribution, diameter and shape of soil grains, rainfall excess and surface slope (Kilinc & Richardson 1973).

Impact erosion is a big factor in detachment. At the beginning of a rainfall event, erosion is mainly caused by raindrop impact. This is because the soil surface seal would not have formed yet, and the infiltration rate will be high. As soil sealing begins, the infiltration rate decreases while the generation of surface runoff increases (Wang et al. 2023a). In fact, most detached particles are transported via overland flow. This is when the infiltration rate is exceeded and since there is no more capacity for water in the soil, water flows on the surface instead. Detachment and transport rates of overland flow are influenced by the surface slope and the depth and velocity of the flow (Kilinc & Richardson 1973). Flow erosion, or runoff, is especially important on slopes as it determines the amount of transportation (Toy et al. 2002).

2.3.1.3. Rill Erosion

Rills are small channels in the soil, which can be up to 30 cm in depth. A characteristic of rills is that they can be filled in via tillage (Foster 1982; Govers et al. 2007). They form as overland flow concentrates into channels due to surface microtopography. Rills often form between crop rows and along tillage marks (Gilley 2005). Rills both detach and transport sediment (Owoputi & Stolte 1995). Material transported originates both from the rill itself as well as from the interrills (Gilley 2005). Differences between rill and interrill erosion include the processes which dominate detachment and transport of sediment. Rills suffer mainly from overland flow and raindrop impact is considered negligible, whereas interrill erosion employs both

processes (Owoputi & Stolte 1995). Another difference is that interrill erosion is size selective, with finer particles being more erodible (Asadi et al. 2011). This is considered to be because of the insufficient transport capacity of overland flow (Parsons et al. 1991). Meanwhile rill erosion is less size selective (Shi et al. 2012). Another difference between the two is that interrill erosion is usually found on upper slopes while rill erosion is affected more by slope length and steepness (Govers & Poesen 1998).

Rill erosion is influenced by various factors. These include rainfall, runoff, soil, topography, vegetation, and tillage (Sun et al. 2013). A relationship between rainfall and rills is evident with soil loss via rills increasing with an increase in rainfall KE (Wang 1998 as cited in Sun et al. 2013). The relationship between runoff and rills is more complex with studies sometimes achieving contradictory results. Despite this, it is often considered that runoff directly and majorly affects rill erosion (Sun et al. 2013). Soil's effect is also complex as soil includes a wide range of properties which may affect rill erosion. Physical soil properties, such as bulk density, water content, and particle composition, affect the infiltration capacity and the soil's shear strength, which in turn affect rill erosion (Li et al. 2010). Soil erodibility is another of the major aspects which rill erosion is dependent on. With regards to topography, slope length, shape, and gradient affect rills. Increasing slope gradient increases rill erosion, however, this is no longer the case once the slope reaches a particular threshold (Liu et al. 2001). Vegetation has multiple methods to affect erosion. These include intercepting rainfall, increasing infiltration, increasing resistance to flow, increasing soil strength, with plant roots binding soil particles to reduce rill erosion (Woo et al.

1997). Tillage is also an important consideration when discussing rill erosion. Certain equipment can trigger rills and tillage itself can alter soil infiltration, runoff, and soil erodibility, thereby affecting rill erosion (Li et al. 2010).

2.3.1.4. Gully Erosion

Gully erosion is when concentration and channelization increase, and gullies are created (Kilinc & Richardson 1973). Gullies are deep channels that cannot be filled in with tillage and thus permanently alter the landscape. They form where runoff concentrates, often near the upper side of intermittent streams. Runoff may expand and deepen the gully, and exposed banks may also collapse into the gully due to undercutting. Gullies are considered active when their walls are not vegetated and inactive when vegetation is present (Gilley 2005). Gully erosion is often accelerated by land use change, extreme climatic events, and a long antecedent history (Valentin et al. 2005). Intensive cultivation can also accelerate gullying as the depletion of SOM decreases the soil's structural stability and increases surface crust formation, runoff, and gullying (Valentin 2004). Meanwhile, ephemeral gullies are small channels which continuously form in the same place on the landscape. They serve as a primary drainage system for the field. However, they are temporary as they can be filled in with normal tillage operations (Gilley 2005). Ephemeral gullies are usually dendritic but are sometimes parallel to rills, making them difficult to distinguish from large rills.

2.3.1.5. Piping Erosion

Piping or tunnel erosion is the formation of subterranean tunnels via sediment removal by percolating waters. The tunnels range in diameter from a few millimetres to several metres and tend to form a drainage network (Goudie 2013). Subsurface erosion is not studied as much as surface erosion processes and it is not considered in many widely used soil water erosion models such as the USLE, RUSLE or WEPP (Bernatek-Jakiel & Poesen 2018). Piping is affected by weather and climate, soil properties, topography, and land use and land management (Bernatek-Jakiel & Poesen 2018). It is found worldwide, mainly in arid and semi-arid areas, but can also be found under many different climates and with different soil types (Goudie 2013; Bernatek-Jakiel & Poesen 2018). In Europe three piping-prone soils are Xerosols (Calcisols), Luvisols, and Histosols, although piping can also occur with other soil types (Faulkner 2006). Piping involves particle detachment via the shear force of water and also mass movement when the walls and roof of the tunnel collapse due to gravity (Bernatek-Jakiel & Poesen 2018).

2.3.2. Wind Erosion

Wind erosion is the detachment, transport, and deposition of soil material by wind. Wind erosion creates onsite and offsite impacts (Zobeck & Van Pelt 2011). Onsite impacts include the removal of fine chemically active aspects of the soil, such as plant

nutrients (Zobeck & Fryrear 1986). This affects the soil fertility and due to the loss of fine material, the infiltration and water-holding capacity are reduced (Zobeck & Van Pelt 2011). Soil particles being transported may also sandblast crops, thereby damaging them (Fryrear & Downes 1975). There are also impacts which don't affect the agriculture system, such as visibility reduction, due to the suspended particles, which is dangerous to traffic. This is one of the effects of fugitive dust, which is dust that has been transported great distances. It has numerous offsite impacts on the environment, health, industry, and transport (Zobeck & Van Pelt 2011).

Detachment, or entrainment, is when the wind, through drag and lift forces, overcomes the gravitational and cohesive forces of the soil. Rolling particles may also detach particles via abrasion (Zobeck & Van Pelt 2011). Transportation by wind can occur in three ways: creep, saltation, or suspension. Creep is when relatively large particles roll on the surface due to either the direct force of the wind or when saltating particles collide with them. Saltating particles are smaller than creeping particles. They bounce on the surface with heights of a few metres. Saltation either starts by the force of the wind or as other saltating particles dislodge new particles. Suspended particles are relatively small and are often entrained due to saltating particles abrading larger particles. The smallest of these can travel thousands of kilometres (Zobeck & Van Pelt 2011).

Wind erosion is influenced by the following factors:

- Climate
- Wind and atmospheric characteristics
- Sediment supply, depending on soil and soil surface properties
- Vegetation characteristics
- Farming practices

Wind is the energy source for wind erosion, but soil characteristics have a lot of control on whether erosion occurs or not. These characteristics include soil texture, where coarse soils erode easier; SOM; mineralogy, where calcareous soils erode more than noncalcareous soils (Zobeck & Van Pelt 2011); soil moisture, where an increase in moisture leads to an increase in the threshold velocity of particle entrainment (Belly 1964); surface roughness, aggregate properties, and surface crust, which limits wind erosion (Zobeck & Van Pelt 2011). In fact, unless loose, erodible material is present on the surface crust, there is usually no wind erosion. Loose erodible material is usually present in higher quantities on sandy soils (Zobeck & Van Pelt 2011).

Vegetation is another important factor in controlling and limiting wind erosion. In humid and sub-humid climates, under the native vegetation of forests, grasslands and managed pastures, wind erosion is limited. However, in arid and semi-arid climates, the native vegetation does not offer full protection from the wind. In semi-

arid climates, under the native vegetation of grasslands, shrublands, savannas, and woodlands, wind erosion is present (Zobeck & Van Pelt 2011). When the land is under crop production, wind erosion increases. This is because of surface smoothing and native vegetation removal. Conventional tillage also increases wind erosion (Zobeck & Van Pelt 2011). Farming practices that increase the risk of wind erosion include numerous operations such as ploughing, planting, weeding, seeding, baling, mowing, etc. (Nordstrom & Hotta 2004). On the other hand, management practices include windbreaks, strip-cropping, cover crops, plant residue, tillage in a way that creates patterns perpendicular to the prevailing wind, and which increases surface roughness (Nordstrom & Hotta 2004).

2.3.3. Tillage Erosion

Tillage erosion is the movement of soil particles from the topsoil layer during tillage operations. It is not immediately evident but takes numerous years of tillage for the erosion to be seen (Van Oost et al. 2006). Tillage erosion is a gravity-driven process; thus slope gradient is highly influential. Tillage erosion usually results in soil loss on the shoulder slopes and soil accumulation on the toe slopes (figure 2-1). This pattern

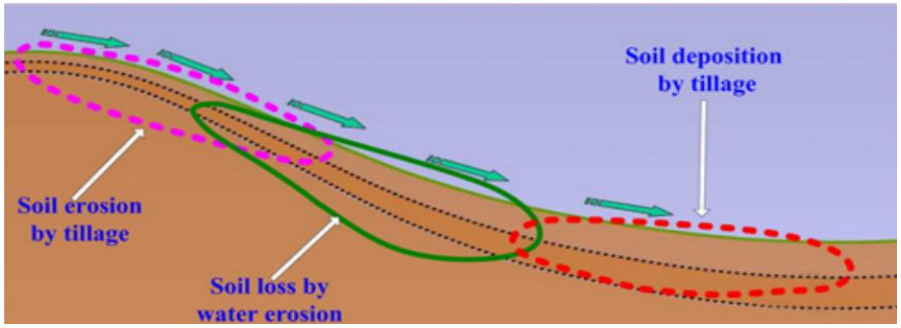

Figure 2-1: Areas on a Slope Affected by Tillage and Water Erosion (Wang et al. 2016).

results in smoothing of the land as upslope areas lose soil to downslope areas. This is in comparison to water erosion patterns, which usually focus erosion in rills, interrills, and gullies which often form on other parts of the slope (Van Oost et al. 2006). Wang et al. (2016) found that tillage erosion further increased water erosion. This was through mechanisms like rill infilling, in which tillage directly delivers soil to rills. Another mechanism is that excessive tillage results in the presence of subsoil at the surface. This increases the soil's susceptibility to water erosion (Wang et al. 2016).

Tillage erosion depends on a number of parameters including:

- Implement type
- Tillage direction, depth, and speed
- Field shape and size
- Soil properties such as bulk density, texture, moisture, etc.
- Slope gradient and curvature

Tillage erosivity increases exponentially with tillage depth. Tillage direction is also important as tillage along a contour is much more beneficial in terms of soil conservation than up and down slope ploughing (Van Oost et al. 2006). Tillage erosion is of two types: topography-based, and field boundary-based. Field boundary-based tillage erosion is especially important in parcelled landscapes made up of small fields as it is the result of field boundaries. Meanwhile topography-based tillage erosion results from a change in slope and it is more common in large fields which often make use of heavy agricultural machinery (Van Oost et al. 2006).

2.4. Factors Affecting Water Erosion

The factors influencing water erosion can be divided into two broad categories: rainfall erosivity and soil erodibility. Rainfall erosivity is the energy (KE) which through the action of falling raindrops and flowing water has the power to detach and transport soil particles. Considerations of rainfall erosivity include raindrop diameter and the frequency of high intensity storms (White 2006). On the other hand, soil erodibility depends on the interactions between a number of soil properties, such as: soil texture, SOM, infiltration capacity, soil structure, and the soil's shear strength. There are also a number of other factors which affect the soil erodibility. These include the length and gradient of a slope. Gradient is influential because a high gradient gives soil and water high potential energy which can become kinetic energy. Length of slope is impactful because the longer the slope, the more surface runoff and the higher the velocity of the flow (White 2006). Management practices also affect soil erodibility as they alter other properties, for example: terraces which reduce slope length and retain water for increased infiltration. Another important factor is crop cover, which protects the soil against rainfall erosivity as well as helps bind the soil with plant roots (White 2006).

Rainfall and soil erosivity are affected by a number of factors. A study in Jordan used twelve slopes with six different slope angles, where each slope angle had a site under barley cultivation and the other site was a rangeland. Different antecedent soil moisture conditions and rainfall intensities were then used at each site to calculate

soil erosion. The authors, Ziadat and Taimeh (2013), found that, of these factors, rainfall intensity was the dominant factor. However, a pre-wetted soil, could undergo erosion even from small rainfall intensities due to its moisture content already being high before the start of the rainfall event. Soil which was already wet suffered more erosion whether it was cultivated or not. This is due to the decreased infiltration rate, which increases runoff and soil loss amounts, as well as the formation of a surface crust, which further adds to the decreased infiltration rate. Under uncultivated conditions, the problem is even worse as the surface crust does not undergo progressive formation as in the cultivated soil. It is instead already there due to lack of tillage; this means there is higher runoff amounts as well as a higher rate of detachment and transport of soil particles. They also found that moisture content was the main driver of soil loss on cultivated land, while on uncultivated land the main driver was slope steepness. Increases in slope steepness still increased soil erosion in cultivated plots but it was less notable (Ziadat & Taimeh 2013).

Rainfall intensity is another one of the factors of rainfall erosivity which greatly affects soil loss. A study by Berger et al. (2010) conducted laboratory experiments to investigate rill initiation under differing rainfall intensities and slope angles. The steeper the slope, the more soil was lost from the system, despite the rill systems being similar in energy expenditure and rill density. The increase in soil loss was thus most likely due to the rill depth, which was larger on steep slopes. This was done under a constant rainfall intensity, when this was changed, it became evident that rainfall intensity had bigger impacts on the factors being investigated, and erosion

and rill dynamics increased (Berger et al. 2010). Another study simulated different storm patterns with differing rainfall intensities. The patterns of rainfall intensity studied were increasing; increasing, followed by decreasing; decreasing; and decreasing, followed by increasing. Soil loss was found to be the highest under the storm regime with increasing rainfall intensity, followed by increasing then decreasing; decreasing then increasing; and the least amount of soil loss was recorded under the storm regime of decreasing rainfall intensity (Mohamadi & Kavian 2015).

Vegetation itself is a very important aspect which affects water erosion (Igwe et al. 2017). This is due to the fact that the presence of vegetation can reduce runoff and soil erosion via processes such as interception and root binding. Interception helps in reducing splash erosion and thus decreases soil particle detachment, while root binding increases infiltration and increases the resistance of the soil to detachment by surface flow (de Baets et al. 2007). In the Loess Plateau of China, revegetation efforts have led to a decrease in erosion in the area. The plant cover and the management practices led to an erosion decrease of 119% while rainfall erosivity contributed -28% in a study period between 1986-2015 (Jin et al. 2021). It is not just the presence of vegetation which affects erosion, but also species diversity of the vegetation present. In a field experiment on a simulated dike, it was found that annual soil loss increased when species diversity decreased. One of the reasons for this was the insurance or compensation effect, which was taking place when *Festuca rubra*, planted next to *Plantago lanceolata*, was decreasing the increased erosion

occurring due to Plantago extinctions in the winter of the study (Berendse et al. 2015).

Cerdà et al. (2021) researched how soil erosion differs according to which species makes up the plant cover. The 4 plants considered were all from a Mediterranean shrubland recovering after a fire event, and were *Ulex parviflorus*, *Pistacia lentiscus*, *Quercus coccifera*, and *Rosmarinus officinalis*. The authors found that the plant sprouters (*Pistacia lentiscus* and *Quercus coccifera*) caused less runoff than the plant seeders (*Ulex parviflorus* and *Rosmarinus officinalis*) by x2.4. This reduction in runoff by the sprouters was mirrored by a higher reduction in soil erosion rates under the sprouters' cover (Cerdà et al. 2021). Mohammad and Adam (2010) also investigated the role of different vegetation types in terms of contribution to soil erosion. Five different vegetation covers were considered: *Pinus halepensis*-planted forests, natural vegetation with the dominant vegetation being *Sarcopoterium spinosum*, natural vegetation with *Sarcopoterium spinosum* removal, cultivated land, and deforestation. The least amount of runoff was exhibited under the *Pinus halepensis* forest and the *Sarcopoterium spinosum*-dominated natural vegetation. Runoff significantly increased under deforestation when compared to the forest, and under *Sarcopoterium spinosum* removal plots and cultivated land when compared to *Sarcopoterium spinosum*-dominated natural vegetation (Mohammad & Adam 2010).

Another aspect of land cover is land abandonment, which can affect both the crop cover and management factor of the RUSLE equation. Rodrigo-Comino et al. (2018)

studied the effects of land abandonment on soil erosion in Spain in vineyards, almond orchards, and olive and orange orchards. Soil erosion after abandonment differed according to what had been the previous crop cover. Soil detachment was reduced in olive and orange orchards after abandonment, no difference was recorded in the vineyards, and increased soil loss in the almond orchards was recorded. These results could be due to the dense vegetation cover which developed in the abandoned orange and olive orchards, while a lack of vegetation resulted in rill and crust formation in abandoned vineyards and almond orchards. It is important to note that in this study, orange and olive orchards were located on terraced slopes unlike almond orchards and vineyards (Rodrigo-Comino et al. 2018).

Surface roughness is also an aspect which can affect soil loss. A study by Zhao et al. (2021) investigated tillage-induced surface microrelief under different rainfall intensities, durations and two slope angles. The tillage patterns investigated were depressions and mounds and troughs and ridges. Compared to a smooth slope, both tillage patterns were capable of limiting soil loss when the rainfall duration was less than 60 minutes, and the rainfall intensity was less than 90 mm/hr. However, when either the rainfall intensity or the duration of the rainfall was greater than these measurements, sediment from the tillage patterns was higher than that recorded from the smooth slope. Furthermore, it was noted that the tillage pattern of troughs and ridges could prevent soil loss more than the depression and mounds pattern, despite the same conditions they were under (Zhao et al. 2021).

There are then also a number of factors which influence the aforementioned factors influencing soil erosion. These include socio-economic factors which affect the management factor and crop cover. Some of these factors include labour availability and rural depopulation, which can allow terraces to fall into a state of disrepair; economic incentives which encourage cheap food production; economic returns, where off-site impacts borne by society do not encourage farmers to conserve soil; etc. (Boardman et al. 2003). Land use policies are some of the most important socio-economic factors which affect soil loss. Such policies are usually in the form of subsidies, guaranteed prices, and protective policies. These policies rarely take the environment into consideration and so decisions encouraging erosion and degradation are constantly taken (Boardman et al. 2003).

2.5. Effects of Climate Change on Soil Erosion

Since weather and climate are a factor contributing to soil erosion, it stands to reason that climate change will impact soil erosion. Climate change is expected to affect soil in a number of ways, with one of the main ways being through precipitation (Li & Fang 2016). This includes altering rainfall erosivity due to changing precipitation totals and intensity (Nearing et al. 2004; Mondal et al. 2016). A study in the U.S., using two coupled atmospheric-ocean global climate models (AOGCMs), found that some areas showed a decline while others showed an increase in rainfall erosivity over 80 years (Nearing 2001). Another study in central India found that the projected rainfall erosivity rose, mirroring the increase in the projected rainfall (Mondal et al.

2016). Another study by Busico et al. (2023) estimated historical and future soil loss predictions in Portugal under different RCP (Representative Concentration Pathway) scenarios. Both RCP4.5 and RCP8.5 had lower soil loss predictions than historical estimates. The slightly higher erosion values under RCP8.5 was attributed to the increase of extreme climatic events (Busico et al. 2023).

Among the many effects of climate change, increased extreme precipitation in many different regions is one of the changes. Extreme precipitation includes both an increase in rainfall amount and rainfall intensity, both of which affect rainfall erosivity. An increase of rainfall intensity stems from climate change-induced higher temperatures which allow the atmosphere to hold more water vapour as well as increase evaporation rates. Higher levels of evaporation mean more water vapour is available in the atmosphere. This results in higher levels of moisture convergence which releases latent heat, which further enhances the storm. The increased water vapour in the atmosphere leads to an increase in precipitation intensity, which may be even greater than the moisture increase (Trenberth 2011). As aforementioned, many studies found that an increase in rainfall intensity leads to increased runoff generation and higher soil losses (Yuan et al. 2021; Wu et al. 2018). Of course, rainfall amount, another factor which can affect rainfall erosivity, is still considered an important factor which affects the amount of soil eroded. In fact, soil erosion is often seen to increase with increasing precipitation (Li & Fang 2016; Nearing et al. 2004). A study by Galdies et al. (2022) in Gozo, Malta was in line with other findings as soil erosion decreased with a decrease in precipitation.

Another effect of precipitation changes due to climate change is the shifting precipitation patterns. Negligible changes in wind coupled with increased evaporation and water available lead to wet regions becoming wetter while dry regions get drier as moisture is transported to the convergence zones from the divergence zones (Trenberth 2011; Tabari 2020). This precipitation shift can also influence soil erosion. Areas getting drier have less protective vegetation cover and so suffer more from both water and wind erosion (Naorem et al. 2023; Ghiloufi et al. 2016). On the other hand, areas getting wetter experience increased surface runoff leading to increased erosion (Eekhout et al. 2018; Jia et al. 2022). Another change regarding precipitation is that snowfall extremes are decreasing to give way to rainfall extremes. Ombadi et al. (2023) found this to be the case in the Northern Hemisphere's snow-dominated regions. Furthermore, increasing temperatures may release organic carbon in the soil providing a positive feedback loop for soil organic carbon and its role in global warming. A study found this trend more pronounced in coarse-textured soils than in fine-textured soils (Hartley et al. 2021).

Another way that climate change is set to influence soil erosion rates is through land use change (Nearing et al. 2004; Eekhout & de Vente 2022). This is an extremely complicated factor and is thus often not considered in studies concerning projected soil loss (Nearing et al. 2004; Eekhout & de Vente 2022). It includes aspects such as the increase in decomposition rate due to higher temperatures and moisture levels; more vegetation because of more rainfall; and more evaporation due to higher temperatures; among others (Nearing et al. 2004). Climate change will also impact

the vegetation itself, for example, species distribution and root density (Peñuelas & Boada 2003). These aspects can affect interception and throughfall as well as runoff (Morgan & Nearing 2010). The projected increase in precipitation is often considered to increase soil erosion. However, this is not always the case. Increased precipitation also increases vegetation cover, which in turn can reduce soil erosion (Langbein & Schumm 1958; Li & Fang 2016). Lavee et al. (1999) found that soil erosion rates increased in a Mediterranean climate under increased aridity conditions. The same concept of vegetation change resulting from aridity leading to more erosion was found in other studies (Ruiz-Sinoga & Diaz 2010). Temperature changes can also cause vegetation changes, where increasing temperatures led to decreased soil loss due to an increase in vegetation (Li & Fang 2016).

The management and adaptation to climate change by farmers is also another thing which affects soil erosion rates. This could include the increased use of conservation tillage and changing of tillage implements, and altering the harvesting and planting times, among other practices (Li & Fang 2016). Guo et al. (2018) compared the runoff and sediment load in an impacted period to those in a baseline period to determine the contribution of human impact and climate change. They found that human activities contributed 126.54% to the total change in annual average runoff experienced, with human influence accounting for a 37.9 m^3/s decrease and climate change accounting for a 7.95 m^3/s increase (Guo et al. 2018). This shows that despite the harmful effects of climate change on soil erosion, human management and agricultural practices can still help to conserve soil and limit erosion.

2.6. Climate Models

Climate models are sets of mathematical equations used to describe and predict the future climate. They use long periods of collected climatic data and are based on both the physical and chemical elements in the climatic system as well as on the land, ocean, and atmosphere systems (Reichle 2023). Climate models can be of three types:

- Earth Balance Models (EBMs)
- Earth Models of Intermediate Complexity (EMICs)
- General Climate Models (GCMs)

EBMs are simple climate models which take into account the incoming and outgoing energy to and from Earth. They can calculate surface temperature, but they are one dimensional models in the direction of Earth's latitude instead of being global models. EMICs are three dimensional and can predict future climate up to 10,000 years. However, they fail to consider the interaction of humans with nature, and they also have a coarse resolution. GCMs are also three dimensional but they have a better spatial resolution (Reichle 2023). GCMs simulate changes in the Earth's energy budget so that they can 3D model variables such as storms, temperature, pressure, wind, humidity, and precipitation with a time evolution (Bader et al. 2008; Abiodun & Adedoyin 2016). They do this by using grids, where a 2D horizontal mesh is merged with the sub-divided vertical layers of the atmosphere, creating the 3D grid. Different algorithms are then used by different models to solve the same primitive dynamical

equations (Bader et al. 2008). GCMs simulate variables globally at a coarse resolution which varies from about 250 - 600 km.

Global climate models can also be downscaled into finer resolution models called regional climate models (RCMs), with spatial resolutions ranging from 25 – 50 km (Chokkavarapu & Mandla 2019). Downscaling is when coarse large area models are transformed to have higher resolutions but cover smaller areas (Benestad et al. 2008). The main downscaling methods are either dynamical or statistical. Dynamical can be further subdivided into limited-area models, which cover a specific region and are also known as RCMs; stretched grid models, which are global but have a spatial resolution which varies horizontally; and uniformly high-resolution atmosphere-only GCMs (Bader et al. 2008). RCMs are a type of dynamical downscaling made using a GCMs boundary conditions or reanalysis from global data sets (Abiodun & Adedoyin 2016).

Climate models provide climate projections, often until the year 2100. Many of these projections make part of the Coupled Model Intercomparison Project's phases 5 and 6 (CMIP 5 and CMIP 6). The projections obtained have been downscaled according to the protocols established by the Coordinated Regional Climate Downscaling Experiment (CORDEX) (Copernicus n.d.). Climate projections are given for a number of scenarios based on emissions and temperature changes. Some scenarios consider a continued usage of fossil fuels while others consider an emission reduction. The use of different scenarios represents the uncertainty in future human actions. The

first three sets of time-dependent scenarios were emission-based, however, the representative concentration pathways (RCPs) are radiative-forcing scenarios, i.e. they are based on the radiative forcing change at the tropopause by 2100 as compared to preindustrial levels. There are four RCPs according to the change in watts per square metre: +2.6, +4.5, +6.0, and +8.5 (Hayhoe et al. 2017).

The latest scenarios also use the shared socioeconomic pathways (SSPs) in conjunction with the RCPs. The SSPs predict possible socioeconomic development in the future. They began as narratives and then models were used to make them useful to climate modelling and match them to the RCPs (Ann Arbor 2021). The following SSPs are available:

- SSP1 – low challenges
- SSP2 – intermediate challenges
- SSP3 – high challenges
- SSP4 – adaptation challenges dominate
- SSP 5 – mitigation challenges dominate

Climate modelling and downscaling have been used worldwide; however, they are not free from problems. Firstly, GCMs are too coarse and so often have inaccurate climate variation for large areas (Chokkavarapu & Mandla 2019). The downscaled RCMs are limited as any error in the parent GCM is redone in the RCM (Benestad et al. 2008). Another problem is that vertical transportation processes and sub-grid

processes, like cloud formation cannot be resolved by model grids like horizontal processes. Instead, they are solved by parameterizations, or approximations. Parameterizations are mathematical representations of processes which can be made via numerical and scale analysis as well as by fluid dynamical filtering (Bader et al. 2008). The problem with parameterizations is that they have more uncertainties (Sweeney 2009). Another limitation of climate modelling is that it relies heavily on computer power. It determines the spatial resolution as well as the parameterizations needed. Since climate models are not completely accurate, they need to be evaluated. Some important techniques used for this include comparing the output of the model to past and present observations, simulating the past climate, and using multi-model model ensemble methods (Eyring et al. 2019; Abiodun & Adedoyin 2016). An example of a multi-model ensemble is CMIP by the World Climate Research Programme (WCRP). It gathers a number of atmospheric-oceanic GCMs (AOGCMs) and Earth System Models (ESMs) for more robustness and less uncertainties in climate modelling.

Climate projections have been used for future soil loss predictions and the resulting soil conservation management plans (Borelli et al. 2020; Hateffard et al. 2021; Marcinkowski et al. 2022; Panagos et al. 2021; Segura et al. 2014). Many studies have showed the models' usefulness in such situations. Panagos et al. (2021) used 19 GCMs from CMIP5 over RCP2.6, RCP4.5, and RCP8.5 to determine future rainfall erosivity predictions over the EU and UK. This was paired with projections from the CAPRI (Common Agricultural Policy Regional Impact Analysis) model for future land

use change predictions so that the RUSLE equation could be calculated. It was found that land use change increases crop cover and so decreases erosion by 3% but rainfall erosivity increases by 15.7-25.5% leading to an increased mean erosion rate of 13-22.5% over the EU and UK depending on the RCP scenario, with RCP8.5 having the most predicted erosion. Targeted use of vegetation in high-risk erosion areas will likely drastically reduce soil erosion (Panagos et al. 2021).

Another study used CMIP5's RCPs (2.6, 4.5, 8.5) to estimate soil loss using RUSLE over central Iran. Soil loss was predicted to increase in 2070 under RCP2.6 and 8.5 but decrease in rangelands and increase slightly under other land uses under RCP4.5 (Hateffard et al. 2021). Marcinkowski et al. (2022) used RUSLE to estimate soil loss for 2021-2050 and 2071-2100 under RCP 4.5 and 8.5 using nine EURO-CORDEX model scenarios over Poland. The average projected soil erosion was seen to progressively increase at 7% and 8% for the near future under RCP 4.5 and 8.5 respectively, and at 13% and 18% under the far future scenario under RCP 4.5 and 8.5 respectively (Marcinkowski et al. 2022). A similar study in the USA studied how rainfall erosivity (R) changes from 1970 to 2090 under nine different climatic conditions using three GCMs for three emission scenarios. Results showed that rainfall erosivity increases with time over all nine climatic conditions, but it varies spatially with catchments in the north having strong trends and those in the west having the weakest trends (Segura et al. 2014). A local study which focused on future soil loss predictions was conducted by Galdies et al. (2022). The study used 8 GCMs from CMIP6 for four SSPs (21-2.6, 2-4.5, 3-70, and 5-8.5) for four time periods (2021-2040, 2041-2060, 2061-

2080, and 2081-2100) to determine future projected soil estimates for the Ramla valley in Gozo, Malta. Contrastingly, their findings indicate a decrease in soil erosion is projected for the Ramla valley under future SSP scenarios due to a decrease in precipitation over the Maltese Islands (Galdies et al. 2022).

2.7. Erosion Risk and Assessment

While soil erosion is a problem found worldwide, some areas are more susceptible than others. The Mediterranean is one such area. This increased susceptibility stems from numerous things, including long periods of dryness followed by heavy episodes of rain; steep slopes; and fragile soils. Meanwhile northwestern Europe suffers less soil erosion as rain is distributed evenly throughout the year and the slopes are relatively gentler (van der Knijff et al. 2000). Using a relatively coarse spatial resolution of 50 m, a 2015 Maltese study found that 19.33% of the total land area was in danger of moderate to severe erosion. Least erosion was recorded on flatter land with good management and erosion control strategies, i.e. the northeast and central areas. Meanwhile, in the northwest and in Gozo, erosion was found to vary greatly with low erosion on plateaus and well-vegetated plateau flanks, and high erosion risk on steep plateaus with poor cultivation techniques and lacking proper erosion control strategies (Sultana 2015). Soil properties and topography both influence the risk of soil erosion in an area; however, vegetation cover is found to be a major controlling factor to actual erosion (Akbari et al. 2022). Assessing the soil

erosion risk and the soil loss taking place are important management techniques as it allows management plans and practices to be implemented.

Soil erosion can be estimated or assessed in a number of ways. Both measurements and models are important for erosion control. Erosion models require calibration and validation from actual measurements, while measurements are hard to extrapolate in space and time (Stroosnijder 2005). Indirect measurements, known as indicators, may also be used (Erskine 2017). Gullies can have actual measurements taken of them via remote sensing technology, this could include either visual inspection or automatic identification (Wang et al. 2021). Remote sensing is also often used to determine inputs to models. Erosion can be measured directly on-site or in the lab through four ways:

- Channel cross-section change: channel cross-sections are measured at intervals, this is repeated shortly after and compared with the first reading. The volume lost is calculated.
- Surface elevation change: erosion pins are placed in the soil and the distance between the pin's top and the surface is measured.
- Weight change: particles detached via rain splash erosion are captured in splash cups. Trays are used to collect particles washed away from plots. Later they are weighed.
- Sediment collection from erosion plots: either the total flow and sediment for a short period of time or a known fraction of the flow and sediment are collected.

Furthermore, dams can also help determine the erosion rate by simply comparing the reservoir's current water depth to its original depth. Another technique is through the use of tracers, albeit rarely used for human accelerated erosion. It involves comparing the radio nuclide Caesium 137's decay activity in a soil profile to that of an undisturbed plot (Stroosnijder 2005).

Soil erosion models are an alternative method to estimate soil erosion in an area. They use mathematics to simplify complex erosional mechanisms and can be subdivided into empirical and physically based models. Empirical or statistical models use long-term field observations and measurements to correlate factors controlling erosion with the soil loss taking place. Some examples include the USLE, RUSLE, and the Modified Universal Soil Loss Equation (MUSLE) (Ketema & Dwarakish 2019). On the other hand, physical models are based on the laws of conservation of mass and energy and on theoretical erosional procedures. Such models require a lot of high-resolution data and include models such as WEPP, AGNPS, SWAT, EUROSEM, and CREAMS (Chemicals Runoff, and Erosion from Agricultural Management Systems). The choice of model depends on what is required of it, available data, time, and money. Empirical models are preferred for specific situations and with areas containing limited data (Ketema & Dwarakish 2019).

2.8. RUSLE Equation

The Revised Universal Soil Loss Equation (RUSLE), developed by Renard et al. (1997), is a commonly used soil erosion assessment method which has been used globally, under a number of different climatic regimes and with many different soil types. It uses five factors to estimate the total annual soil loss in an area in tons per hectare. It can be used at a watershed scale. RUSLE is calculated using the following equation:

$$A = R * K * LS * C * P$$

Where:

A = the total annual soil lost in tons per hectare

R = the rainfall erosivity factor

K = the soil erodibility factor

LS = the slope length and gradient factor

C = the crop cover factor

P = the practice and field management factor

The RUSLE equation's main benefits are its simplicity and limited inputs, making it extensively used, especially in data-scarce areas (Benavidez et al. 2018). RUSLE is also well-used in the Maltese Islands (Sultana 2015; Galdies et al. 2022). Despite its

extensive use, RUSLE also has a number of disadvantages and limitations. These are often applicable to all the models in the USLE family and include:

- Upscaling
- Regional applicability
- Validation
- Representation of different erosion types

The original USLE model was based on small-scale agricultural plots in the USA. This results in uncertainties when upscaling to a catchment or regional scale as well as when applying the model to different climates and land uses (Kinnell 2010; Naipal et al. 2015). Validating data is another potential difficulty as observational soil erosion data is not always available (Benavidez et al. 2018). This means that any model errors might not be detected. A review by Benavidez et al. (2018) of studies which compared RUSLE and USLE to observational data found that (R)USLE results range from under-estimation to over-estimation. Under-estimation was often due to gully erosion and mass wasting, neither of which is included in (R)USLE. Over- and under-estimates could also be due to differences in temporal and spatial resolutions as well as timescales between observed and modelled estimates. Another possibility for the differences between modelled and observed estimates may also be because of the way observed data is obtained. For example, occasional grab samples from streams do not fully represent (R)USLE's annual estimate. Often when the (R)USLE sub-factors are adjusted for regional applicability, the model's errors are reduced (Benavidez et al. 2018). Another highly mentioned limitation is that the (R)USLE only estimates

sheet and rill erosion and ignores all other erosion types, including gully erosion, which can lead to under estimations. It also ignores deposition which can lead to over-estimations (Wischmeier & Smith 1978; Naipal et al. 2015). In general, USLE and RUSLE both tend to underestimate high average annual soil losses and overestimate low average annual soil losses (Kinnell 2010).

While the RUSLE greatly follows the structure of the original USLE, improvements have modified the model to make it more process based. This includes a change to all the sub-factors' equations. One of the main changes was in the C-factor estimation which in RUSLE can be estimated from vegetation form and tillage practices instead of experimental plots as in the USLE (Merritt et al. 2003). Other changes include creating a guide to estimate the K-factor when the USLE's nomograph is not applicable. RUSLE also has a more linear relationship for slope steepness, with USLE giving a 10% error in slope steepness leading to a 20% error in estimated soil loss and RUSLE improving the values by reducing them by approximately half. The LS-factor is also improved as it varies with susceptibility to rill erosion (Renard et al. 1991).

2.8.1. R-Factor

The R-factor is the rainfall and runoff factor in the USLE and RUSLE equations. It is also termed rainfall erosivity as it serves to consider the effect of rainfall and its intensity on soil erosion. While in this case it is specifically for the USLE family of equations, other soil erosion models consider rainfall erosivity in some way as it is a

very important parameter for soil erosion (Rasooli 2022). The R-factor can be calculated in different ways, using varying parameters, however, the original which was derived by Wischmeier (1959) and Wischmeier and Smith (1958) was calculated by assuming that when everything but rainfall is constant, soil loss is directly proportional to the total storm energy (E) times the maximum 30-minute intensity (I_{30}). E reflects the volume of runoff and rainfall while I_{30} reflects the peak rates of detachment since erosion increases with rainfall intensity (Renard et al. 1997). A disadvantage of this factor is that it ignores irrigation and snowmelt (Wischmeier 1959). In RUSLE, the USLE's R-factor was improved by adding improvements for ponded water and frozen soils (Renard et al. 1997).

A major problem with the original R-factor equation by Wischmeier and Smith (1958) is that it requires large amounts of rain gauge data. Renard and Freimund (1994) recommended at least 20 years of rainfall data for RUSLE calculation using its R-factor equation. Furthermore, the data needs to be able to determine the rainfall intensity, and so hourly data is necessary. This disadvantage is one of the reasons why numerous different equations were developed to obtain the R-factor using different parameters, under different climatic regimes. Different studies use different equations including those by:

- Roose (1977),
- Kassam (1992),
- Arnoldus (1980),
- Renard and Freimund (1994),

These equations use a number of parameters including a combination of mean annual rainfall, monthly rainfall, daily rainfall, number of years of observation, a storm's 30-minute maximum intensity, and a number of different constants, among other parameters (Ghosal & Bhattacharya 2020).

Being the factor which includes rainfall, its intensity, and its effect on soil loss, the R-factor will be affected by climate change. In Japan, Shiono et al. (2013) conducted a study to investigate the effects that climate change will bring about on rainfall erosivity in local farmlands. Their results showed that the R-factor is expected to increase under future climate change scenarios. This is both because of changes in precipitation totals and precipitation intensity (Shiono et al. 2013). In China, another study, by Wang et al. (2023b), had similar findings. Under both SSP1-RCP2.6 and SSP5-RCP8.5, and for both the short-term and the long-term, the R-factor is expected to increase. The authors suggest that a main cause is the higher chance of extreme precipitation events (Wang et al. 2023b). On the other hand, a study in Crete achieved quite different results. An increase in rainfall erosivity is projected under RCP2.6 but a decrease in rainfall erosivity is projected for RCP8.5. The results for RCP2.6 can be attributed to the higher erosive power of the rain and the minimal change in precipitation amount. Meanwhile, the RCP8.5 results can be attributed to the decline in precipitation totals (Grillakis et al. 2020).

2.8.2. K-Factor

The K-factor is the soil's susceptibility to erosion and shows how soil characteristics can influence soil erosion (Renard et al. 1997). This includes aspects such as texture, structure, porosity, and organic matter (Ghosal & Bhattacharya 2020). Soil texture is one of the biggest determiners of soil loss. Soils rich in clay are less eroded due to high particle cohesion and resistance to detachment. On the other hand, soils rich in sandy particles have high transport resistance because of a larger particle size. This leaves loam and silt-rich soils as the most prone to erosion (FAO 2019). Soil texture, along with soil structure, permeability, porosity, and antecedent moisture, influence the infiltration rate of a soil. This rate is very important to soil erosion as higher infiltration rates mean less surface runoff and less erosion and vice versa. Whether water infiltrates a soil or becomes runoff depends on not only the infiltration rate but also on the rainfall intensity and drop size, and on the slope gradient (FAO 2019). Other determiners of soil erosion include organic matter content. SOM helps to bind the soil aggregates together, making the soil more resistant to erosion (FAO 2019). Surface roughness is another determiner. This is because a rough surface creates more friction against surface runoff, thereby reducing its erosivity. A rough surface can be created either through rock fragments or large aggregates formed by tillage (FAO 2019).

The K-factor was originally determined for USLE in the field by Wischmeier and Smith (1978) using a plot of 22.1 m slope length and a 9% slope angle, under a continuous

fallow which is ploughed up and down the slope and is considered as how much soil is lost in an EI unit. It can also be calculated in a number of other ways. These include the equation by Wischmeier and Smith (1978) which requires the percentage of the different textural classes, the percentage organic matter, the soil structure code, and the permeability class for the soil. The RUSLE's K-factor is also determined based on soil properties. However, it includes changes regarding seasonal variability, rock fragments, and volcanic soils to improve the model's accuracy (Renard et al. 1997).

Adjustments for rock fragments was necessary in the RUSLE because when rock fragments are on the soil surface, soil detachment is reduced. However, when they are in the soil profile, infiltration is reduced instead. RUSLE considers the influence of rock fragments in the soil profile in the K-factor determination by adding adjustments to the permeability class. The influence rock fragments have on the soil surface is considered in the C-factor (Renard et al. 1997). Seasonal variation is needed due to soil freezing, changes in soil texture and soil water. This seasonal variation is obtained by relating the K-factor to periods without frost and the annual R factor (Renard et al. 1997).

Apart from the nomograph (Wischmeier et al. 1971) and equation (Wischmeier and Smith 1978) for the original USLE model, the K-factor can be calculated through a number of different equations which make use of different soil parameters. Sharpley and Williams (1990) used some of the concepts found in the nomograph to create another model based on particle size distribution and organic matter.

A study by Yang et al. (2024) compares four methods of calculating the K-factor with a measured K-factor from literature. The methods include the USLE-K (Wischmeier & Smith 1978), RUSLE2-K (Renard et al. 1997), EPIC-K (Sharpley & Williams 1990), and Dg-K (Römkens et al. 1997). All methods displayed a similar spatial pattern, with higher K-factor values in northern and central Asia, western Europe, and southern North America. However, out of the four methods, the RUSLE2-K method performed the best when compared with the measured K-factor. This was followed by USLE-K and EPIC-K, with the Dg-K method performing the worst in comparison to the measured-K (Yang et al. 2024).

2.8.3. LS-Factor

The LS-factor considers the topography of the area under study. It can be divided into the L-factor and the S-factor, where the L-factor refers to slope length and the S-factor refers to slope steepness (Renard et al. 1997). Wischmeier and Smith (1978) considered slope length to be the horizontal distance between the runoff's source to either where the slope is flat enough for deposition to occur or where a channel forms from concentrated runoff. Runoff often concentrates in less than 120 m, but this is not necessarily the case (Renard et al. 1997). As slope length increases, the amount of runoff increases. Similarly, as slope steepness increases, the runoff velocity increases. The increase in amount and velocity of runoff increases erosion (Ghosal & Bhattacharya 2020). Slope steepness is considered to contribute greater to soil loss than slope length (Renard et al. 1997). Improvements from USLE include

a more linear slope steepness equation and the ability to represent complex slopes through a number of segments. These improvements result in RUSLE soil loss estimates being half those estimated by USLE on steep slopes (Renard & Ferreira 1993).

2.8.3.1. Variations in Measurement

Renard et al. (1997) suggest measuring or pacing in the field to determine the L-factor while using an inclinometer for the S-factor. Contour maps may be used for slope determination but are not suggested for slope length because they are not detailed enough. There is a lot of variation in equations used to determine the LS-factor. The L-factor is often determined as in the equation developed by Wischmeier and Smith (1957).

$$L = (\frac{\lambda}{22.13})^m$$

Where:

- λ = slope length
- 22.13 = RUSLE plot length in metres
- m = $\frac{\beta}{(1+\beta)}$ = variable slope exponent, which in steep landscapes ranges from 0.2 to 0.5
- β = $\frac{sin\theta/0.0896}{[3(sin\theta)^{0.8}+0.56]}$ = ratio of rill to interrill erosion
- θ = slope angle

This equation considers the ratio of soil lost on the studied slope to that of a 22.13 m slope with a 9% slope steepness, which is given an LS-factor of 1.0 (Wischmeier & Smith 1957).

While Wischmeier and Smith's equation is commonly used, there are still variations in how it is calculated. This includes the popular L-factor calculation methods:

- The grid cumulation (GC) method
- The contributing area (CA) method

The grid cumulation method, initially developed by Hickey (2000) and based on the earlier work by Hickey et al. (1994), was further refined by Van Remortel, Hamilton, and Hickey (2001) and Van Remortel, Maichle, and Hickey (2004). It considers the slope length (λ) to be the length calculated along flow path. The method uses a D8 flow routing algorithm to sum up the non-cumulative slope length (NCSL) following flow direction from high points. The flow path begins from high points, which have no in-flow and thus only the downhill half of the cell has a flow length.

The contributing area method uses the upslope contributing area instead of the slope length. This method is based on the principle that flow accumulation and divergence across the landscape influence the flow reaching a specific point. Desmet and Govers (1996) proposed this method for use in GIS using Quinn et al.'s (1991) FD8 multiple flow direction flow routing algorithm with the equation:

$$L_{i,j} = \frac{(A_{i,j-in} + D^2)^{m+1} - A_{i,j-in}^{m+1}}{D^{m+2}(x_{i,j}^{m})22.13^{m}}$$

Where,

- L is the L-factor at coordinates i,j
- $A_{i,j\text{-}in}$ is the contributing area at the inlet of that grid cell in meters squared
- D is the grid cell size in meters
- $x_{i,j}$= sin($a_{i,j}$) + cos($a_{i,j}$) where $a_{i,j}$ is the aspect direction
- m = length exponent of the USLE's L-factor

Liu et al. (2011) in their study compared CA algorithms to GC algorithms. They found that CA algorithms resulted in higher L-factors and greater error rates. They suggested that the reason behind this is that the GC methods include a cutoff for the L-factor which limits its maximum attainable value. Liu et al. (2011) also found that as the spatial resolutions of DEMs gets coarser, the difference between the two methods gets even more enhanced. This can be attributed to the fact that the CA method gets a larger area to use under coarse spatial resolutions, and this in turn increases the L-factor. The authors thus determined that GC methods are more suited than CA methods, especially when using coarse resolution DEMs (Liu et al. 2011).

Regarding the S-factor, other than Wischmeier and Smith's (1957) equation, there are also those by Moore and Burch (1986), McCool et al. (1987), and McRoberts et

al. (2002). McCool et al.'s (1987) equation is used in the RUSLE, and it depends on the slope angle as follows:

- If θ is less than 9%, S = 10.8sinθ + 0.03
- If θ is more than 9%, S = 16.8sinθ – 0.5

Where,

- θ = slope angle

Slope angle calculation methods include the neighbourhood (NBR) method and the maximum downhill slope method (MDS). The NBR method involves a 3x3 window moving over the DEM and averaging the elevation's rate of change of the adjacent cells to find the slope of the central cell. The equation for the NBR method is as follows:

$$\theta = \tan^{-1}\left(\sqrt{\left(\frac{dz}{dx}\right)^2 + \left(\frac{dz}{dy}\right)^2}\right)$$

Where,

- $\frac{dz}{dx}$ is the east to west slope
- $\frac{dz}{dy}$ is the north to south slope

This method has two main problems, which are:

- Inaccuracies can arise since this method averages the slope across a neighbourhood, leading to underestimations in steep areas and overestimations in flat areas

- The NBR method's slope angle calculation can be inconsistent with flow direction, which can be problematic for models that heavily utilize flow direction.

(Dunn and Hickey 1998).

The maximum downhill slope method does not utilise averaging techniques and so is more adept for small features and variability in the landscape. Hand in hand with this advantage is the disadvantage that it is susceptible to DEM errors (Hickey 2000). Like the NBR method, it utilizes a 3x3 window, but calculates slope based on the elevation difference between the centre cell and the single neighbouring cell with the steepest downslope, thereby reducing the risk of overestimation (Dunn & Hickey 1998; Hickey 2000). The equation for MDS is:

$$\theta = \tan^{-1}(max\frac{z_9 - z_i}{L_e})$$

Where,

- Z_9 is the centre cell
- Z_i is the adjacent cell 1-8
- L_e is the distance between the centres of the two cells being considered (if the cells are diagonal, multiply by √2)

A study by Srinivasan and Engel (1991) compared these two methods, the neighbourhood and maximum downhill slope, as well as the quadratic surface best fit plane methods to observed results. They found that while it had better results in flat areas rather than in steep areas, the neighbourhood method was always the closest to observed values. The maximum downhill slope method estimated higher slopes, and it led to USLE's LS-factor being 2x greater on flat areas and 1.6x more on steep areas when using the maximum downhill slope method over using the neighbourhood method (Srinivasan & Engel 1991). This is contradicted by a later study by Moody (2020) which suggested the use of the maximum downhill slope method instead as it maintained variability in the landscape and small features, which were lost using the neighbourhood method. The use of this method was especially recommended at fine resolutions. The author also mentioned that using coarse resolutions, the difference between the two methods is not as great. It is also suggested by the author to use a spatial resolution for the DEM of 5 m, as finer resolutions produce a busy LS-factor and might detect small-scale erosion patterns, not just established trends. On the other hand, coarser DEMs can have a smoothing effect on the data (Moody 2020).

2.8.3.2. Flow Routing

Flow routing is the way the flow is transferred down the slope. Flow routing algorithms are divided into two main classifications: single flow direction (SFD), and multiple flow direction (MFD) (Moody 2020). SFD directs all flow in a cell to one

downslope cell. It includes the common D8 algorithm which transfers the flow to the steepest downslope adjacent cell (O'Callaghan & Mark 1984) and the Rho8 algorithm which weighs the probability that one cell gets all the flow as per its gradient from the centre cell respectively (Fairfield & Leymarie 1991). MFD algorithms transfer the flow to at least two downslope adjacent cells. Some algorithms include the FD8 (Freeman 1991) and the D-infinity (Tarboton 1997).

While SFD algorithms usually result in low L-factor values and low contributing area values, the MFD algorithms using all downslope adjacent cells have higher values than those using fewer cells because using more cells distributes the flow to more areas and thus leads to a higher contributing area amount (Desmet & Govers 1996). Under steep terrain, the difference between SFD and MFD is also seen to be larger thereby suggesting that determining which algorithm to use is more influential in upslope areas than in flatter areas. SFD algorithms create sharper features and they have a banding effect, which is when it is part of a flow path, the area cannot be distributed to another flow path later (Moody 2020). This is more representative of valleys since permanent drainage systems are much more easily established there. MFD algorithms do not usually have banding effects and are more representative of hilly areas (Moody 2020).

2.8.3.3. Spatial Resolution of the LS-Factor

Digital elevation models (DEMs) are often used to compute the LS-factor, with the L-factor being reliant on the accuracy of the DEM (Liu et al. 2011). Using GIS, the common method for determining LS is: filling the sinks to create a depression-less DEM, flow direction, flow path (using an algorithm such as the D-8 algorithm), flow accumulation, L-factor and S-factor using their respective equations (using the raster calculator in a GIS environment), and finally multiplying the L- and S-factor maps (Ibetsberger 2020). A study by Raj et al. (2018) using several random points for different slope classes and using break values of 10, 25, and 50 respectively, were utilized for extraction of LS-factor values for each slope class. The computed statistics reveal that coarser DEMs of 10 m and 30 m spatial resolution are not able to capture micro-topographical differences which the fine resolution DEM (18 cm) captures. However, across the different slope classes, comparable results were achieved for each class by all the DEMs (Raj et al. 2018).

Another study by Bircher et al. (2019) investigated the effect of spatial resolution on the L- and S- factors using DEMs of 2 m and 25 m spatial resolution. They found that using the S-factor method suggested by Renard et al. (1997) for the RUSLE equation, the 25 m DEM had significantly lower S-factor values (maximum, mean and standard deviation values). This is mainly attributed to an increased smoothing effect in coarse resolution DEMs. Since S-values are lower, coarse resolutions can lead to decreases in reported soil erosion (Bircher et al. 2019). On the other hand, the 25 m DEM

resulted in slightly higher L-factor values. Regarding the LS-factor, the two methods compared, the MFD and the WAT, which had a convergence value of 1.1 and 5 respectively, produced conflicting results. The MFD 1.1 had lower values on the 2 m DEM while the WAT 5 had higher values for the 2m DEM (Bircher et al. 2019).

Another study by Fu et al. (2015) also investigated the effects of spatial resolution of DEMs on the LS-factor. They found that average slope steepness (S-factor) of their AOI diminished in a linear decay function as spatial resolution gets coarser. On the other hand, the average slope length (L-factor) increased when using a coarser resolution. The average LS-factor decreased with a coarser resolution and when continuing to use the LS-factor in a soil loss equation, Fu et al. (2015) found that estimated soil loss was higher for finer resolution DEMs. However, for DEMs with a spatial resolution of 10 m or less, results of the S-, L- and LS-factor, as well as soil erosion, were similar to the results obtained by the 2 m DEM (Fu et al. 2015).

2.8.3.4. Topography

Sabzevari and Talebi (2019) conducted a study to explore the effect of slope topography on soil erosion. They studied slopes with different plans and curvatures and found that convex hillslopes had higher erosion rates than concave and straight slopes, an increase by a factor of 1.43 and 1.19 times respectively. They also found that profile curvature had a more marked effect on erosion than plan shape.

However, in general, erosion was found to be lowest on divergent-concave slopes and highest on divergent-convex slopes (Sabzevari & Talebi 2019).

Rieke-Zapp & Nearing (2005) also conducted an experiment on topography and its effect on soil erosion. They constructed five different slope shapes: uniform, convex-linear, concave-linear, head slope, and nose slope, made of silt loam soil and applied artificial rainfall to them for a duration of 90 min. They found that the slope shape had a significant effect on runoff, sediment yield, and rill patterns. Notably, head slopes and concave-linear slopes deposited sediment on their toe slopes and thus yielded less sediment than the other slope types tested. Furthermore, the study revealed a correlation between slope steepness and the distribution of rill erosion (Rieke-Zapp & Nearing 2005).

2.8.4. C-Factor

The C-factor refers to the crop and vegetative cover effect on soil erosion. It is a very important factor in RUSLE because it can be improved through human management and is not an inherent characteristic. It is determined as a deviation from the standard clean-tilled continuous fallow plot. It is then worked through a number of soil loss ratios (SLRs) which are the ratio of soil loss in the studied area to soil loss under the standard (Renard et al. 1997). RUSLE uses the following subfactors:

- Canopy's protection of the soil (CC)
- Surface cover (SC)
- Surface roughness (SR)

- Previous cropping and tillage (PLU)
- Soil moisture (SM)

These effects are given a subfactor value which are then multiplied together to obtain a SLR. A SLR value is worked out for each time period in where the parameters are constant. Each SLR is weighted by the fraction of the EI value at their respective time period. The combination of the weighted values creates the C-factor. Under slow changing conditions, the subfactors are multiplied together to obtain the C-factor and no weighting is performed as it is assumed that the subfactors are annual averages (Renard et al. 1997).

Vegetation is highly influential in determining soil loss because it has many effects. These include its interception capabilities which serve to doubly protect the soil by increasing the total surface which needs to be wetted before the soil surface is, and also by decreasing detachment from raindrop impact and reducing runoff from the reduction of surface seal formation. Another protective aspect of vegetation are the roots which increase infiltration and resistance to detachment. Friction caused by the presence of vegetation reduces the flow's velocity as well as absorbs some erosive energy. These effects of vegetation mean that as vegetation density increases, soil erosion decreases (FAO 2019; de Baets et al. 2007).

2.8.5. P-Factor

The P-factor is the field management factor which refers to the soil loss ratio between the soil loss using a specific practice to that using up-downslope tillage (Renard et al. 1997). It includes practices which alter the direction, amount, and pattern of surface runoff. Practices include:

- Terracing
- Contouring
- Strip-cropping
- Sub-surface drainage

These respective subfactors are multiplied together to obtain an overall P-factor which ranges between 0-1 (Renard et al. 1997).

Proper determination of the P-factor exists, such as that by Wischmeier and Smith (1978), but most studies take it to be 1 due to the lack of conservation practices applied in their study area (Ghosal and Bhattacharya 2020).

2.9. Soil Erosion Models and Climate Change

Many different soil erosion models are used to research climate change and its effects on soil erosion. These models work differently from each other and thus can have different results. This depends on the forcing used leading to which soil erosion processes are considered by the model, with the major hillslope processes being

raindrop impact detachment and runoff detachment (Morgan 2005). The empirical models RUSLE (Renard et al. 1997) and USLE (Wischmeier & Smith 1978) consider forcing by precipitation, i.e. raindrop impact, meanwhile process-based soil erosion models such as SWAT and MUSLE often consider runoff detachment instead (Morgan 2005). There also exist models with a combination of both precipitation and runoff forcing, such as EUROSEM, WEPP, and SPHY-MMF, which is the integration of Spatial Processes in HYdrology (SPHY) with the Morgan-Morgan-Finney model (MMF) (Eekhout et al. 2018). Eekhout and De Vente (2019) compared current and projected soil loss under RCP8.5 at two sites using RUSLE, MUSLE, and SPHY-MMF. The results were very different spatially and numerically, with RUSLE projecting the highest soil loss rate which is spatially based on precipitation and slope. MUSLE projects a lower rate with a spatial pattern based on water accumulation areas, and SPHY-MMF projecting the lowest amount with a spatial pattern similar to RUSLE's at one site and similar to MUSLE's at the other. Under an RCP8.5 scenario, RUSLE projects a mainly reduced soil loss rate; MUSLE projects a higher soil loss rate; and SPHY-MMF also projects a mainly higher soil loss rate. The decrease in soil erosion reported by RUSLE is most likely due to the projected precipitation decrease (Eekhout & De Vente 2019). Many studies assess the effectiveness of the soil erosion model and the soil loss predictions by comparing the predictions to sediment yields at the catchment outlet and measured plot data. The better performance was sometimes recorded by the empirical models and sometimes by the process-based models. These assessments were however, often conducted on small spatial scales and so cannot be generalised (Eekhout & De Vente 2019).

2.10. Satellite Data for RUSLE Modelling

Satellite data comes from a type of remote sensing technology, i.e. satellites. Satellites utilise sensors to remotely capture different types of data through bands. A number of different products can then be made available. Commonly used satellites include the MODIS, Landsat, and Sentinel series (Zhao et al. 2022). Sensors aboard the satellites can be specialized for a specific product.

When it comes to using satellites and their products, one needs to consider what their needs are. This involves both considering what type of imagery is needed as well as other considerations such as for how long data has been being collected, as well as temporal and spatial resolution. For example, if historic data is required, the Landsat satellites, operated by NASA and the US geological survey (USGS), are a good option. This is due to the fact that Landsat has been in operation since 1972 with Landsat 1 (ERTS-1). Since then, 8 more satellites have been launched, with only Landsat 6 failing to achieve orbit. Currently, Landsat 8 and 9 are in operation and Landsat 7 is on an extended science mission, with a lowered orbit in order to make way for Landsat 9. Landsat 8 and 9 have Operational Land Imagers (OLI) and Thermal Infrared Sensors (TIRS) onboard while Landsat 7 has the Enhanced Thematic Mapper Plus (ETM+). These sensors capture a number of bands which can be used to derive several satellite products and indices, which include the NDVI (Normalised

Vegetation Index), EVI (Enhanced Vegetation Index), and SAVI (Soil Adjusted Vegetation Index), among others. The next Landsat mission, Landsat Next, is planned for 2031 with sensors picking up a total of 26 spectral bands (NASA 2025; USGS n.d.).

While Landsat has a 30 m spatial resolution on most bands and a temporal resolution of 8 days for Landsat 9, and 16 days for Landsat 8, Sentinel's combined revisit rate is 5 days and its bands have a spatial resolution ranging from 10 m to 60 m. This makes the Sentinel series a good option for users who require high resolutions. The Sentinel missions are a series of satellites by the European Space Agency (ESA) and provide a large amount of data for Copernicus. Sentinel-1, which includes both Sentinel-1A and Sentinel-1B, are radar imaging satellites; and Sentinel-2A, and Sentinel-2B are high resolution multispectral imaging satellites. Other satellites in the series include Sentinel-3 and Sentinel-6. However, despite their high resolution, the Sentinel series are recently launched satellites, going as far back as 2014, and thus do not have a large data archive like the Landsat satellites (European Space Agency n.d.).

Another important satellite product is the MODIS (Moderate Resolution Imaging Spectroradiometer) sensor aboard NASA's Terra and Aqua satellites. MODIS caters for a different need than the Sentinel and Landsat series. Terra and Aqua pass over the equator at the same time every day and can cover the entirety of the globe in 1 to 2 days. The sensor has 36 spectral bands but its spatial resolution is coarser than that of Landsat or Sentinel, with products having a resolution of either 250 m, 500 m, or 1 km, depending on the product (NASA n.d.).

Satellites can also be used to produce RGBs and enhanced images. This is done through the combination of satellite images from different channels. Enhanced satellite images are often used for weather forecasting with InfraRed images that help in visualizing cloud top temperatures and convective cloud systems. On the other hand, RGB is the combination of three bands, allocated to red, green, and blue. RGBs can be made differently to monitor specific phenomena (EUMeTrain 2013; NOAA 2019). The Natural Colour RGB helps in visualizing surface features such as vegetation and soil, as well as clouds and ice. This RGB looks similar to a True Colour image of the Earth and so makes for easy interpretation. The True Colour RGB is the closest RGB to colour photography (EUMETSAT 2023).

The Advanced Spaceborne Thermal Emission and Reflection Radiometer, or ASTER for short, is an imaging sensor aboard the satellite Terra. Its data is used for detailed maps concerning elevation, reflectance, and land surface temperature (NASA 2024). ASTER collects 14 bands of visible and near-infrared, short-wave infrared, and thermal infrared, with spatial resolution ranging from 15 m to 90 m, depending on the instrument (Satellite Imaging Corporation 2022). The sensor is the product of a joint collaboration between the National Aeronautics and Space Administration (NASA), Japan's Ministry of Economy, Trade and Industry (METI), and Japan Space Systems (J-spacesystems) (NASA 2024). Another sensor providing elevation data is the Shuttle Radar Topography Mission (SRTM), which was aboard the Endeavour Space Shuttle in February 2000. This sensor is by NASA and the National Geospatial-Intelligence Agency (NGA). It uses Interferometric Synthetic Aperture Radar (InSAR)

technology to acquire two signals from two radar antennas to create the first elevation dataset with almost global coverage. It has a spatial resolution of either 30 m or 90 m (EROS 2018). ASTER GDEM V3 has global coverage while SRTM has a coverage ranging from 60° N and 56° S. However, ASTER has voids over Antarctica and Greenland and may be obscured by cloud cover. Meanwhile, SRTM does not have a cloud cover problem since it is not an optical sensor, but it has more voids in mountainous areas than ASTER (USGS 2020).

Khasanov (2020) compared SRTM and ASTER over a mountainous and a flat area and found that SRTM performs better and is more accurate than ASTER over mountainous areas, but ASTER outperforms SRTM over flatter topography. Forkuor and Maathuis (2012) found contradicting results where ASTER tends to underestimate elevation, but it is more evident in flat areas. Meanwhile, SRTM has a tendency to overestimate. The underestimation by ASTER is greater than the overestimation by SRTM and so it was concluded that SRTM has greater accuracy. When compared to a reference DEM, ASTER and SRTM obtained the same correlation coefficient for the flatter area but SRTM had a higher correlation than ASTER for the more mountainous topography (Forkuor & Maathuis 2012). Nikolakopoulos et al. (2006) compared ASTER and SRTM over two areas in Crete. They found that the SRTM dataset had a displacement but once fixed, the ASTER and SRTM DEMs had similar shape and a strong correlation (Nikolakopoulos et al. 2006). Krishnan et al. (2017) used SRTM and ASTER to derive landslide susceptibility index maps. The conclusion was also that SRTM performed better with elevation values of

both DEMs correlating well with reference data, but SRTM-derived terrain variables outperformed ASTER-derived terrain variables (Krishnan et al. 2017).

Satellites can be used to obtain a number of products, not just DEMs, with one such product being precipitation. The problem with precipitation satellite data is that it often has a spatial resolution over 10 km (Filippucci et al. 2022). This is especially problematic for small areas of interest such as Maltese valleys and Malta in general. Another problem faced by precipitation satellites is that they provide indirect estimates of precipitation, often with a lot of variability. In mountainous terrain, satellite estimates are less representative of real data, possibly due to the high spatiotemporal variability in these areas. Infrared (IR) sensors have difficulty in mountainous areas and with light rain events, while passive microwave sensors have more difficulty in the cold season in mountainous regions (Derin & Yilmaz 2014). One of the satellites which obtains observed precipitation data is the Global Precipitation Measurement (GPM) Mission, a joint endeavour by NASA and JAXA. The GPM follows the Tropical Rainfall Measuring Mission (TRMM) and has a temporal resolution of 30 minutes and a spatial resolution of 11.1 km. The Integrated Multi-satellitE Retrievals for the Global Precipitation Measurement (IMERG) is the algorithm which NASA applies to TRMM-era and GPM-era data to obtain almost-global coverage precipitation data for over 20 years (Huffman et al. 2023).

Some soil products can also be obtained via satellites. One of these is soil moisture content. ESA's Heritage Envisat uses the Advanced Synthetic Aperture Radar (ASAR)

at C-band to collect data on soil moisture content. This is possible as radar can detect a soil's dielectric constant, which mirrors changes in soil water content. ESA's Earth Explorer Soil Moisture and Ocean Salinity (SMOS) Mission uses its Microwave Imaging Radiometer with Aperture Synthesis (MIRAS) sensor for the same purpose (ESA 2023). When a study compared data from the International Soil Moisture Network (ISMN) with five satellite-derived products (SMAP, ESA CCI, and AMSR2 (ascending, descending, and average)), they were seen to overestimate soil moisture. Land cover type also affected the satellites' estimates, with bad performance being recorded over forests and better performance was seen over grasslands and shrublands (Feng et al. 2022).

Remote sensing is a non-destructive non-invasive way of getting soil measurements, and while it still has limitations, such as in determining soil depth and heterogeneity, it has many advantages. Benefits include their extensive coverage, accuracy, cost, repeatability, and their non-destructive nature as well as the ability to use such methods in difficult terrain. Assessments can be conducted on a variety of scales, such as at watershed and individual field level (Abdulraheem et al. 2023). A number of different remote sensing techniques are used to gather data on several soil aspects. One of the techniques, spectral reflectance analysis, includes determining electromagnetic radiation reflectance over visible light and infrared wavelengths. Since soil properties have unique spectral signatures, the reflectance pattern obtained can identify and quantify these properties (Mohamed et al. 2018). Another technique is thermal infrared imaging, which measures longwave infrared (8-14 um)

emitted from Earth. This technique measures soil temperature but since soil temperature is affected by a number of other variables, thermal infrared imaging can also estimate and determine some of these variables. This mainly includes soil moisture, but this in turn produces information on porosity, compaction and fertility as surface temperatures reflect water availability, which in turn reflects the water infiltration rate and therefore soil porosity and compaction, and thus fertility (Khanal et al. 2017). Remote sensing via radar technologies is another technique which can be used for soil property assessment. This is especially useful since the microwaves can permeate the surface of the soil and obtain measurements related to moisture content and texture (Petropoulos et al. 2015). Remote sensing can also provide the input to methods and indices in determining soil erosion, soil salinity, soil organic carbon content, and crop health (Abdulraheem et al. 2023).

2.11. International and Local Legislation Relating to Soil Erosion

Legislation is an important aspect to soil erosion as it serves as a basis for management. Soil loss estimates and related studies are important as they provide the necessary information to policymakers to develop effective laws. Subsequently, effective legislation implements strategies and policies which promote erosion-reducing practices and technologies. For example, subsidies could incentivize sustainable land practices such as rubble wall maintenance, contour ploughing, and conservation or no-tillage.

2.11.1. International Law

Soil is globally recognised as an important asset and therefore laws and policies relating to soil can be found globally. Despite this, it is important to note that soil has no overarching law or authority at international level, and policies need to be implemented by the individual states (Bodle 2022).

An important legally binding, with 197 parties, document is the UNCCD, United Nations Convention to Combat Desertification, which aims to address the issue of desertification. This document considers land-related issues, with soil conservation being linked to desertification's definition. One of the main issues of this document is that the obligations are very generic (Bodle 2022). The UNCCD also gives direction over the execution and management of Sustainable Development Goal (SDG) 15.3. SDG 15 and its target 15.3 stipulate that land degradation neutrality should be achieved by 2030, although this is not binding. In fact, the UNCCD seems to focus more on capacity-building, rather than on legally binding documents (Ruppel 2022). In terms of SDG 15.3, the UNCCD offers help in progress measurement, reporting, and guidance (Bodle 2022).

Another important UN institution when it comes to soil is the Food and Agricultural Organisation (FAO). FAO is mainly concerned with providing technical guidelines and sharing knowledge relating to soil. These documents are not legally binding. Some

important work of theirs include the World Soil Charter in 1981 and its revised version of 2015, as well as the Voluntary Guidelines for Sustainable Soil Management (VGSSM). They are also credited with the establishment of the Intergovernmental Technical Panel on Soils (Bodle 2022).

2.11.2. EU Law

The European Union (EU) is one of the entities trying to tackle issues pertaining to soil. 60% to 70% of EU soils were considered to be not healthy in 2021 estimates. This is due to soil erosion, salinisation, biodiversity loss, compaction, pollution, sealing, and organic matter reduction (EC 2021b). Europe is set to be influenced by more droughts, thereby increasing the desertification process. This process is mainly visible in the Mediterranean, and in central and eastern European countries (EC 2021a). While the Single European Act of 1987 makes it possible for soil legislation to be passed, EU-wide soil protection is still lacking. Any soil protection comes as a by-product from other policies aimed at other aspects, such as nature, water, and waste (Heuser 2022). The European Court of Auditors stated that the Commission's and member states' actions have not been enough, and the EU lacks a shared vision on how to obtain land degradation neutrality by 2030 (European Court of Auditors 2018).

The European Green Deal is a framework which aims to apply certain green measures across different sectors in the EU to help a green transition within the continent and become the first climate-neutral continent by 2050 (Heuser 2022). The targets of the European Green Deal also consider soil protection. The European Green Deal has several sub-strategies which consider different sectors. These strategies include the:

- Zero Pollution Strategy
- EU Climate Law
- Biodiversity Strategy
- Farm to Fork Strategy
- EU Soil Strategy

These strategies consider soil in different ways as part of an overarching aim. The Zero Pollution Strategy is meant to prevent and remedy environmental pollution. Soil is considered part of the environment and so part of this strategy is aimed at soil pollution. Similarly, the EU Climate law considers soil as an important carbon sink; the Biodiversity Strategy considers soil biodiversity a key part in ecosystem services such as nutrient cycling and soil fertility; the Farm to Fork strategy tackles soil from an agricultural perspective and includes the need for food security (Heuser 2022).

The EU Soil Strategy (2021) is the main aspect of the European Green Deal which considers soil. It outlines a number of objectives (EC 2021a) which it aims to reach by 2030 and 2050 respectively.

By 2030, the EU aims to:

- Combat desertification,
- Restore degraded soils and land,
- Remove 310 million tonnes of CO_2 annually for the land use, land use change and forestry (LULUCF) sector within the EU,
- Achieve good ecological and chemical surface water status and good chemical and quantitative groundwater status by 2027,
- Decrease nutrient loss by 50%,
- Decrease use and risk of chemical and hazardous pesticides by 50%,

By 2050, the aims are:

- Obtain no net land take,
- Decrease soil pollution to non-harmful levels to both humans and ecology,
- Obtain a climate neutral Europe,
- Obtain a climate resilient society in the EU which is ready to deal with the impacts of climate change.

The EU Soil Strategy for 2030 is a framework concerning the protection, restoration, and sustainable use of soils (EC 2023b; EC 2023c). It was adopted in 2021 to replace the Soil Thematic Strategy from 2006. The Soil Thematic Strategy had included a proposal for a Soil Framework Directive, but this directive was never passed. Now, the EU Soil Strategy, is calling for the introduction of a Soil Health Law. Such a step is

important as while the strategy interacts with other EU policies, soil legislation comes as a by-product from other laws and there is no EU-wide soil specific law (Kolpak & Fornabaio 2022). The law which came from the EU Soil Strategy is the Soil Monitoring Law which aims to provide the legal framework for healthy soils by dealing with soil threats including erosion, landslides, salinisation, etc. It will set up a monitoring framework and encourage sustainable soil management practices across all member states as well as require member states to identify contaminated sites (EC 2023a).

The soil monitoring law (Directive 2023/0232 (COD)) proposes that member states are obliged to establish soil districts throughout the country. These districts require a monitoring framework to be created for them. The framework aims to monitor the soil's health in each district. The Commission and the European Environment Agency (EEA) will help the member state in its monitoring efforts by conducting in-situ soil sampling regularly and using remote sensing technologies to develop soil monitoring products. Member states are to analyse the samples with the aim of determining the soil descriptors' values in Annex I, any additional soil descriptors' values, and land take values and soil sealing indicators as in Annex I part D. Member states are obliged to use the methods listed in Annex II parts B and C. A healthy soil is when the soil descriptor's values meet the criteria in the Annex. If one criterion is not met, a soil is considered unhealthy. The proposed Directive also sets out a reporting system with reporting to the Commission and EEA being done every 5 years. Reports need to consist of the results of the monitoring, a trend analysis of the descriptors, and a summary of the progress regarding sustainable soil management principles which are

coming into practice ad the identification and management of contaminated sites. Online access to the Commission and EEA is also to be ensured (EC 2023a). Based on Directive 2008/99/EC, the protection of the environment through criminal law, violations are dealt with by the member state through fines which should be proportionate to the violation. The proposal for the Soil Monitoring Directive has already been criticised for lacking legally binding targets (Kolpak & Heinzel 2023).

Another new EU regulation which is related to soil management is the nature restoration law (Regulation (EU) 2024/1991). This law works in tandem with other soil measures set by the EU to restore and manage soil. This law passed into force on the 18th of August 2024 (Directorate-General for Environment 2024). The proposed law requires member states to:

- Put in place adequate restoration measures to improve the habitat types mentioned in Annex I and II to a good condition status.
- Apply appropriate restoration measures for freshwater, marine, coastal, and terrestrial habitats of species found in Annex III and Annexes II, IV, and V of the Habitats Directive (92/43/EEC) and the Birds Directive (2009/147/EC).
- Ensure habitats listed in Annexes I and II do not degenerate.
- Increase the habitat area with good condition status of those under Annexes I and II and increase the quality and quantity of the habitats of the species listed in Annex III and in Annexes II, IV, and V of the Habitats Directive (92/43/EEC) and the Birds Directive (2009/147/EC).

- Guarantee no overall loss of urban green space and urban tree canopy cover between 2021 and 2030.
- Increase the total area of urban green space by 3% of the total urban area in 2021 by 2040 and by 5% by 2050, while also ensuring there is at least an urban tree canopy cover of 10%.
- Undo the reduction in pollinator populations by 2030.
- Set up restoration measures for biodiversity enrichment in agricultural ecosystems.
- Obtain an improving trend in the:
    - Stock of organic carbon in cropland mineral soils.
    - Grassland butterfly index.
    - Share of agricultural land with high-diversity landscape features.
- Establish restoration measures on organic soils in drained peatlands, including rewetting.
- Establish restoration measures to improve forest biodiversity.
- Improve the trends as per Annex VI in the following forest indicators:
    - Lying deadwood.
    - Standing deadwood.
    - Forest connectivity.
    - Share of the forest with uneven-aged structure.
    - Stock of organic carbon.
    - Common forest bird index.

- Prepare national restoration plans and preparatory monitoring and research necessary to help in identification of the restoration measures required so that the targets and obligations of Articles 4-10 may be met.
- Quantify the area which requires restoration as per the targets in Articles 4 and 5.

(Regulation (EU) 2024/1991)

The EU's Common Agricultural Policy (CAP) also considers soil within its remit. The latest version of the CAP, CAP 2023-27, attempts to protect soil through concepts such as crop rotation, which is a new condition for farmers and thus should take place on 85% of the CAP's arable land. This will disturb diseases and pests, thereby decreasing pesticide use, as well as increase soil fertility, thus improving water retention capacity of the soil and the soil's resilience to drought conditions. This is among other conditions to improve and support agriculture and its relationship with the environment (EC 2022). This period of the CAP has €387 billion from the European agricultural guarantee fund (EAGF) and the European agricultural fund for rural development (EAFRD). For farmers to benefit from financial aid, they must meet a set of requirements (European Commission n.d.).

2.11.3. National Law

In Malta one of the main environmental laws is the Environment Protection Act of 2016. In its definition of the environment, this act specifically mentions soil as an

aspect of the environment and so this means that soil is included within its remit. Furthermore, soil is listed as being included in the terms land and natural resources within the act. The Environment Protection Act (2016) states that it is the duty of the government, every entity, and every person to protect the environment. It also sets up the Environment and Resources Authority (ERA) which has several functions:

- Forms and implements environmental polices,
- Conducts environmental monitoring,
- Promotes research on environmental topics,
- Issues information and guidelines to other entities and to the public relating to environmental issues,
- Establishes environmental measures,
- Monitors compliance and enforces it,
- Assess and issues permits for activities influencing the environment,
- Advises the Minister in charge on formulation of environmental policy.

Another Maltese law which relates to soil is the Fertile Soil (Preservation) Act of 1973. While this law does not directly mention soil erosion, it mentions other soil related activities. It prohibits a number of harmful activities such as transportation of soil, covering fertile soil with stones or concrete, make fertile soil unsuitable for agricultural purposes by mixing it with stones among other activities, or build on fertile soil. When a building is to be built, the Fertile Soil (Preservation) Act states that the soil is to be removed as per the proper regulations beforehand. It also gives

the inspectors the right to enter a building site or any land where a building is going to be built.

Malta also has a number of management plans for Natura 2000 sites. While the area of interest for this study is not explicitly within a Natura 2000 site, it is adjacent to one. The site, il-Qortin tal-Magun u l-Qortin il-Kbir, which is a special area of conservation (SAC) with the code MT0000026, includes a number of aims and actions which seek to conserve and manage the site, its habitats, and its species. The management plan also identifies threats to the site, one of which being the risk of increased soil erosion arising from walking and trampling off the tracks (ERA 2014).

3. METHODOLOGY

3.1. Introduction

This chapter focuses on the methods used during this study. It includes the methods used to derive the 5 factors for the RUSLE equation. The methods used are mainly based on spatial data analysis that includes raster and GIS data processing, using a number of software, namely: the Aeronautical Reconnaissance Coverage Geographic Information System (ArcGIS) ArcMap v. 10.8 (esri 2020) and ArcPro v. 3.1 (esri 2023a), the System for Automated Geoscientific Analysis (SAGA GIS) v. 9.3.0 (Conrad et al. 2023), and the Quantum Geographic Information System (QGIS) v. 3.26.3 (QGIS Development Team 2023). Figures 3-1, 3-2, and 3-3 graphically explain the methodology of each aim.

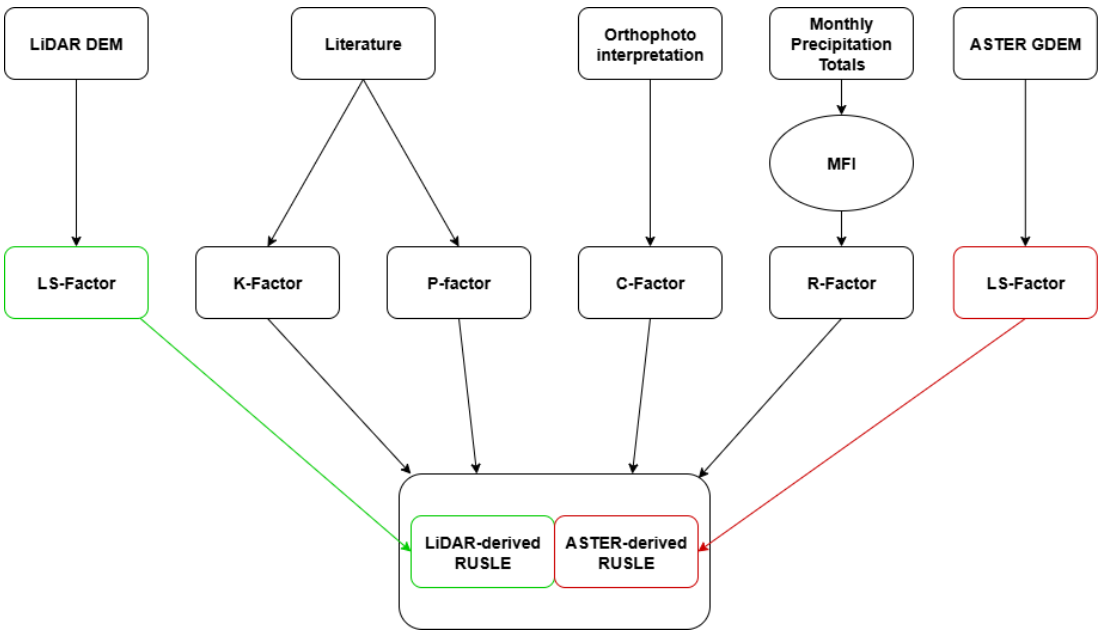

Figure 3-1: Flowchart of Methodology for Aim 1: Estimating the Soil Erosion at Different Spatial Resolutions, Using Both Coarse and Fine Data.

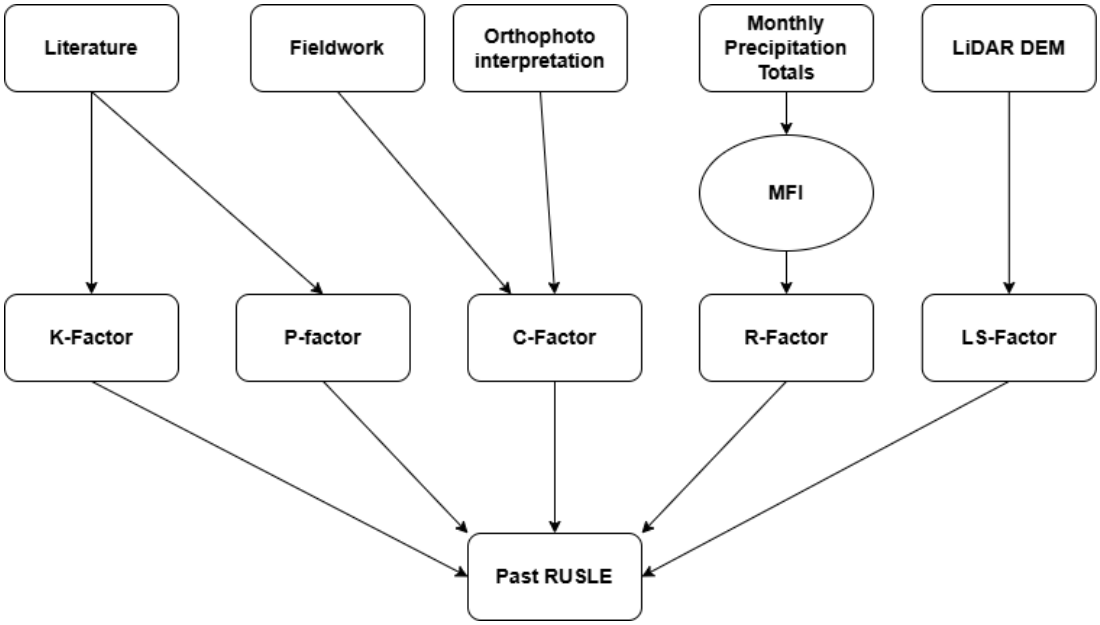

Figure 3-2: Flowchart of Methodology for Aim 2: Mapping Soil Erosion Patterns and Estimating Total Annual Soil Loss for Intermediate Years from 1957 up to 2021.

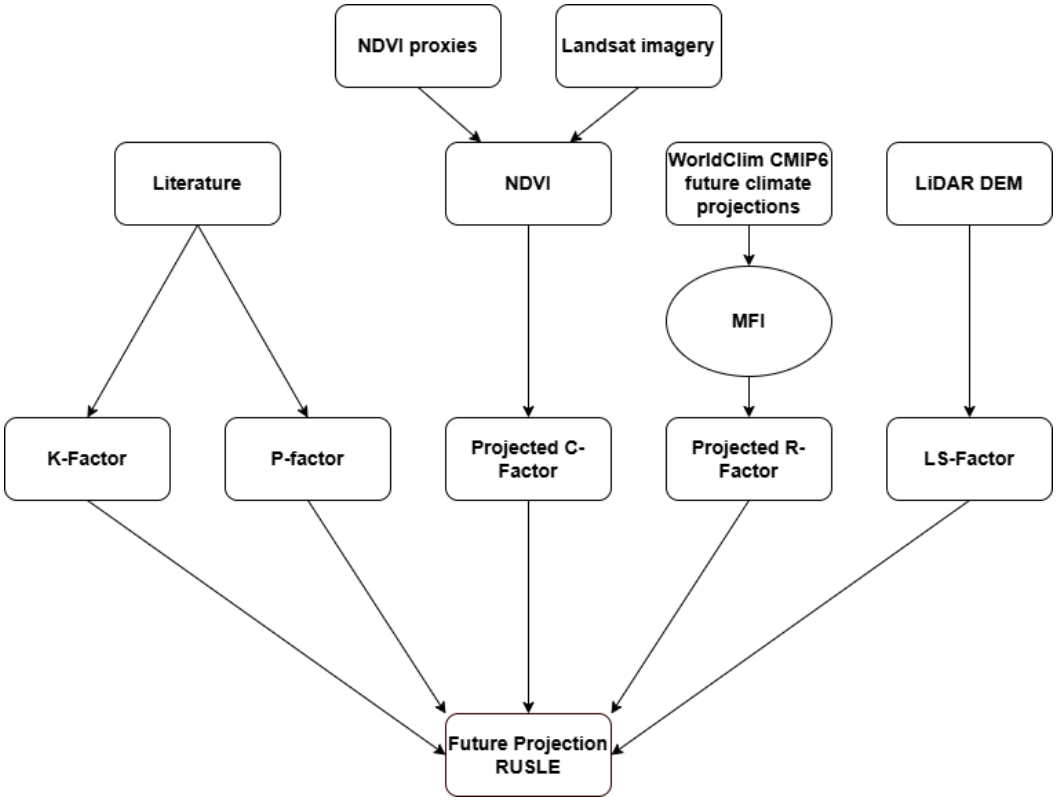

Figure 3-3: Flowchart of Methodology for Aim 3: Estimating the Future Potential Soil Erodibility on the Basis of Variables Derived from Multi-Model Climate Projections.

3.2. Data Sources

Table 3-1: Data Sources for the RUSLE Equation.

Factor	Influence on erosion	Source
R-factor	Rainfall erosivity	Monthly precipitation in mm from Malta International Airport (MIA) Meteorological Office Projected monthly precipitation from CMIP6 Climate Models from WorldClim (Fick & Hijmans 2017)
K-factor	Soil erosivity	Fieldwork and lab analysis
LS-factor	Topography	LiDAR DEM 1 m resolution (Planning Authority 2018) ASTER GDEM 30 m resolution (2013) (NASA/METI/AIST/Japan Spacesystems and U.S./Japan ASTER Science Team 2019)
C-factor	Vegetative cover	Muscat, 2022 Orthophotos (Planning Authority 1978, 1988, 1998, 2004, 2018) Landsat 5 TM (USGS/NASA Landsat 5 TM Surface Reflectance Tier 1 2023) Landsat 7 ETM+ (USGS/NASA Landsat 7 ETM+ Surface Reflectance Tier 1 2023) Landsat 8 OLI/TIRS (USGS/NASA Landsat 8 Surface Reflectance Tier 1 2023)
P-factor	Management	Panagos 2015b; Muscat 2022

3.3. RUSLE Factors

3.3.1. R-Factor

The R-factor was determined via the method introduced by Arnoldus (1980) and modified by Renard and Freimund (1994) to result in the modified Fournier index (F) which is shown in the following equation:

$$F = \frac{1}{N}\sum_{j=1}^{N}(\sum_{i=1}^{12}\frac{pi^2}{p})$$

Where:

- F = modified Fournier index
- N = number of months
- pi = monthly rainfall in mm
- p = mean annual rainfall in mm

The data obtained from the Meteorological Office contained monthly precipitation values for 1947-2021. For each year that required an R-factor, i.e. each year that the RUSLE is being worked for, the above equation was used with 4 past years of data. Thereby, N was set to 48 months. This determines the modified Fournier index but a subsequent step is necessary to calculate the R-factor. The following two equations by Ferro et al. (1999) and Renard and Freimund (1994) for Italy-Sicily and Morocco respectively were used for this purpose.

$$R_{Italy-Sicily} = 0.612 * F^{1.56}$$

$$R_{Morocco} = 0.264 * F^{1.5}$$

As in Malta Environment and Planning Authority (MEPA) (2013), the Moroccan equation underwent a correction by dividing the resulting R-factor by 0.587. The result of this correction and the result of the Italy-Sicily equation were averaged together to calculate an estimate for the Maltese Islands. This specific method was used because Sicily and Morocco have similar climates to Malta since they are geographically close to the Maltese Islands. Therefore, it was assumed that an average of their respective equations would be good for Malta as it lies approximately between them, in terms of latitude. Table 3-2 below displays the resulting R-factors for the different years.

Table 3-2: R-factors for Each Relationship for Each Year.

Relationship and reference	**R-factor**						
	1957	**1978**	**1988**	**1999**	**2004**	**2018**	**2021**
$R_{(Italy-Sicily)}$ Ferro et al. (1999)	1135.7	698.7	1049.6	949.3	792.2	573.5	969.7
$R_{(Morocco)}$ Renard and Freimund (1994)	366.8	229.9	340.0	308.7	259.4	190.1	315.1
$R_{(Morocco\ correction)}$ (MEPA 2013)	624.8	391.7	579.2	525.9	441.9	323.9	536.8
$R_{(Malta)}$	880.3	545.2	814.4	737.6	617.1	448.7	753.2

The R-factor for Malta for each year was used and each value was inputted into the attribute table of a separate vector layer in ArcGIS, which covered the entire valley as one polygon. The vector layers were exported as shapefiles from ArcGIS and imported into SAGA GIS.

3.3.2. K-Factor

The K-factor was calculated using Sharpley and Williams' (1990) EPIC model's K-factor equation. While this is not the standard RUSLE approach to calculating the K-factor, this method was chosen due to data constraints and a well-documented use of this equation for the RUSLE in cases where there is not enough data to use the standard nomograph or equation (Wischmeier 1971; Wischmeier & Smith 1978; Yang et al. 2024; Ghosal & Bhattacharya 2020; Xu et al. 2013; Guduru & Jilo 2023; Jin et al. 2021). This method was chosen over other potential K-factor calculation methods as it's use in RUSLE is more well-documented and because all data required for this method was available, unlike for other methods. Soil samples were collected based on site access and permission, with at least two samples taken per category from Lang's (1960) soil map. The EPIC equation requires soil texture and soil organic matter percentages, which were determined in a lab as in Muscat (2022) (Appendix 6), which were often found to have a high sand content and a low organic matter content. The equation is as follows:

$$K = \left(0.2 + 0.3 * \exp\left(-0.0256 * SAN * \left(1 - \frac{SIL}{100}\right)\right)\right) * \left(\frac{SIL}{CLA + SIL}\right)^{0.3}$$

$$* \left(1 - \frac{0.25 * C}{C + \exp(3.72 - 2.95 * C)}\right)$$

$$* \left(1 - \frac{0.7 * SN1}{SN1 + \exp(-5.51 + 22.9 * SN1)}\right)$$

Where:

- K = K-factor
- SAN = percentage sand
- SIL = percentage silt
- CLA = percentage clay
- C = percentage organic matter
- SN1 = $1 - \frac{SAN}{100}$

The equation was calculated for each soil sampling site and the result was multiplied by 0.1317 to convert the units from the American units ton.acre.hr/hundreds of acre.ft.tonf.in to the SI units t.ha.hr/ha.MJ.mm. In ArcGIS a new point feature class was created and a new record was created in each soil sampling location. In the attribute table, the K-factor values were inputted, with care that each value corresponds to the location it was taken from. The vector layer was then exported as a shapefile and imported into SAGA GIS. Ordinary kriging interpolation of the points was then performed to create a continuous raster covering the entire area of interest.

Interpolation was a necessary step in the processing and analysing of the data as it is impossible to manually sample every spot in the AOI to have a continuous surface unless you use satellite imagery. Since field samples were taken, interpolation had to be used to estimate the values between the sample points based on some type of weighting system. The weighting system chosen for this study was kriging as it is a geostatistical method, based on statistical models using statistical relationships between the data points to weigh them based on distance between the measured point and the missing value, and the spatial distribution of the points. This makes it more capable of predicting the missing values as well as help it produce an element of accuracy to these predictions. It assumes that the direction or distance between the given point values is indicative of a spatial relationship that describes the variation present in the area. Hence, it is used when bias based on distance is present in the data (esri 2023c). This is a very useful technique to interpolating soil-related attributes as soils have a spatial pattern, whose variation needs to be reflected in the interpolation. Inverse distance weighting (IDW) and spline are also interpolation techniques. They were not chosen for this study as IDW is highly distance-based, weighing the neighbouring values according to distance; and spline is ideal for surfaces with gentle variation; thereby making them less suited for soil interpolation than kriging (esri 2023b; esri 2023d).

3.3.3. LS-Factor

The LS-factor was determined via GIS methods in SAGA GIS (Conrad et al. 2023). The LiDAR data obtained was in .las format and thus the first step of processing was converting it to a grid. This was done using the point cloud to grid conversion tool in SAGA GIS. The second step was using the LS Factor (One Step) tool to calculate a raster grid of the LS-factor. This method involves sink removal as preprocessing and uses the method of Desmet and Govers (1996). A post-processing step was applied to the result of the LS-Factor (One Step) result. The raster calculator was used to apply a command to remove any values larger than 3 and thus help to filter out any rubble walls or small trees which may still be present. For proper comparison purposes, a copy of the LiDAR data was resampled to match the spatial resolution of the ASTER GDEM data.

The ASTER GDEM data was obtained from NASA Earthdata in TIFF format and thus the initial part of the processing was unnecessary. It was decided to use ASTER GDEM data as it is easily available but slightly coarser elevation data, thereby making it part of the methodology used to meet aim 1. The data was first clipped to match the extent of the AOI, the aforementioned LS Factor (One Step) tool was then used to determine the LS-factor from the ASTER GDEM data. Since the spatial resolution of this dataset is 30 m, no command was applied because at 30 m, such small details like rubble walls are averaged across the entire cell.

3.3.4. C-Factor

The C-factor includes the type of vegetation growing in the plot as well as the type, if any, of tillage method used. The C-factor changes annually as farmers change the land use and the tillage method used. This means that for every year that the RUSLE equation is being calculated, the C-factor needs to be reworked. This is done by using old orthophotos from the specific years that are being used in the calculation and determining what is growing in each field in each year. The first step to doing this is to obtain the orthophotos and then to georeference them into the GIS software being used. Georeferencing is the process by which images and maps with no coordinate system are placed on a coordinated map and fixed in place, thereby giving the uncoordinated map or image the same coordinate system as the underlying map. The process uses reference points from both the image and the coordinated map to ensure that the image is positioned properly. Therefore, each orthophoto was added to the GIS file and using the georeferencing toolbar in ArcGIS, fixed into its correct position on the map. Spline georeferencing was used as it uses a large number of reference points to enhance the local georeferencing positioning, which is what is ideal for this project.

Once the old aerial images were georeferenced in place, a new polygon vector layer was created in ArcGIS. This layer was made the first time by plotting each field in the valley as a polygon. It was then copied for each year as necessary. Each vector layer

has an attribute table, with each row representing a polygon – i.e. a field – and which includes the following columns:

- Fid (field ID)
- Classification
- Crop factor
- Tillage method
- Tillage factor
- C-factor

The Fid is an automatically generated column which identifies each individual field, with an identification number starting from 0 and increasing upwards. The classification field is filled in manually. This was achieved by checking row by row what is growing in each field, as per the old orthophotos, and filling the column accordingly. This is a difficult process as some of the orthophotos are black and white, and of relatively bad quality. This makes the land use difficult to determine. The crop factor column is then filled in automatically via a python code (Appendix 1.1) according to what is growing in the field. The crop factor values vary between 0-1 and were obtained from a number of sources and are as per table 3-3 below.

Table 3-3: Classification and Crop Factor (Adapted from Galdies et al. 2022; Panagos et al. 2015d; Schürz et al. 2020; Benavidez et al. 2018).

Classification	Crop factor
Bare soil	1.0
Seasonal crops	0.5
Fallow	0.5
Grain	0.35
Vines	0.35
Palms	0.3
Fruit trees/Citrus/Young trees/Reeds/Other trees	0.1
Prickly pears	0.02
Abandoned	0.02
Abandoned with trees	0.01

Due to difficulties in identification of land use, not all of the classifications were used for all of the orthophotos. For example, in black and white imagery, it is difficult to determine fallow fields.

Regarding the tillage method field, two options were available: tilled or not tilled. This limited choice is because it is impossible to determine certain other tillage methods, such as conservation tillage, through orthophotos. Bare soil, seasonal crops, grain, and vines were considered tilled while fallow, palms, reeds, other trees, prickly pears, abandoned, and abandoned with trees were considered not tilled. This

was done automatically using a python code similar to that in Appendix 1.1. Since fruit trees, citrus, and young trees can be both tilled or untilled, each field containing them was checked manually to determine whether it was tilled or not. The tillage factor is the value given to each tillage option, as per table 3-4.

Table 3-4: Tillage Method and Factor (Adapted from Galdies et al. 2022).

Tillage method	Tillage factor
Tilled	1.0
Not tilled	0.25

The above methods regarding obtainment of the crop factor and the tillage factor were repeated for every year that is being studied. The C-factor is the final value used in the RUSLE calculation which represents the soil's erosivity according to what is being grown and to how the field is tilled. It is obtained automatically by multiplying the crop factor by the tillage factor using the field calculator in ArcGIS. The layer is then exported as a shapefile from ArcGIS.

3.3.5. P-Factor

The P-factor for this entire study was kept constant at 0.5 as in Muscat 2022 and as found in Panagos et al. 2015b due to the presence of rubble walls and terracing throughout the valley. A polygon covering the entire valley was created and the p-

value of 0.5 was entered into its attribute table in ArcGIS. This layer was then exported as a shapefile so that later it can be used in the final RUSLE calculation.

3.3.6. RUSLE Calculation

The shapefiles of the R-, C-, and P-factor layers were imported into SAGA GIS and they were rasterized using the shape to grids tools. Along with the rasters of the K-, and LS-factors, they were also clipped to match the extent of the AOI using the clip grids with polygon module in SAGA GIS. The grid calculator was then used to multiply the shapefiles together as per the RUSLE equation. The equation includes the R-, K-, LS-, C-, and P-factor layers. It was repeated with these five factors for each year, i.e. for 1957, 1978, 1988, 1998, 2004, 2018, and 2021. Another RUSLE was also worked with the 2018 data but using the LS-factor obtained from the ASTER GDEM. All the RUSLE calculations were named accordingly and exported as GeoTIFFs. ArcGIS was used for symbology and map layout purposes.

3.4. Future Soil Loss Projections

Another aspect of the study was to predict future soil loss estimates. This is an important outlook to consider in the face of today's climate change challenges and it is essential to study potential outcomes to aid in their mitigation and management. While soil types and topography are slow-changing processes, rainfall and vegetation are two major aspects which are likely to change with a changing climate. Therefore this study considered some possible methods, outlined below, to adjust these two factors accordingly to best represent future changes. The management factor was not adjusted as this is a very difficult factor to estimate, especially for the future, because it has several affecting factors, including those relating to human choices.

3.4.1. Models

Future climate projections were obtained from WorldClim v2.1 (Fick & Hijmans 2017), which downscales future climate projections from CMIP6. Its products include monthly minimum and maximum temperature, precipitation, and bioclimatic variables, averaged over 20-year periods for different GCMs, spatial resolutions, and SSP scenarios (WorldClim 2024). CMIP6 itself includes several models and has a wide range of products to choose from. Some products, among many others, include (Copernicus 2021):

- Air temperature, in K
- Precipitation, in kg m-2 s-1

- Sea surface salinity, in PSU
- Surface air pressure, in Pa
- Relative humidity, in %

CMIP6 has a varying spatial resolution depending on the model. It has data from 1850 to 2014 as past experiments and 2015 to 2100 as future projections. CMIP6 also offers different emission scenarios as discussed in section 2.6 of this study. The data from CMIP6 is obtained in a NetCDF4 format (Copernicus 2021). Products and scenarios available differ from model to model. For this study the following models from CMIP6 were used to obtain the monthly total precipitation in mm:

- CMCC-ESM2 (Lovato et al. 2022)
- EC-Earth3-Veg (EC-Earth Consortium 2019)
- IPSL-CM6A-LR (Boucher et al. 2018)
- UKESM1-0-LL (Tang et al. 2019)

Furthermore, each model was used to obtain a dataset for the SSP 2-4.5 and SSP 5-8.5 scenarios for the years 2041-2060, resulting in 8 datasets overall. The data was obtained at a 30 second spatial resolution, which is about 1 km, from WorldClim v2.1 (Fick & Hijmans 2017).

The four chosen models are all European models. This relative proximity of their origin to Malta is the reason why they were chosen. CMCC-ESM2 is an Italian model from the Centro Euro-Mediterraneo sui Cambiamenti Climatici. EC-Earth3-Veg originates from the EC-Earth consortium, which is made up of 27 partners from 10

European countries. IPSL-CM6A-LR is from the Institut Pierre-Simon Laplace in France. UKESM1-0-LL is a UK model by the Met Office Hadley Centre.

3.4.2. R-Factor

Rainfall measurements in mm over the area of interest was extracted from the downloaded data. A total of 6 pixels were used to cover the area of interest at the 30 seconds spatial resolution which the data was in. The value tool in QGIS was used to determine the rainfall measurement per month for each dataset.

The R-factor for the datasets was determined using MS Excel. Using the Modified Fournier Index (Renard & Frimund 1994) and the aforementioned Sicily-Italy and Morocco equations by Ferro et al. (1999) and Renard and Freimund (1994), the same process applied to the past data was applied to each model for both the SSP 2-4.5 and the SSP 5-8.5 scenarios for each model. The results of the models were then averaged to determine one R-factor per pixel for each SSP scenario.

2 layers were created in ArcGIS for the different SSP projections of the data. The resulting R-factors were then inputted into the respective ArcGIS attribute tables according to their pixels. The layers were exported from ArcGIS as shapefiles.

3.4.3. C-Factor

Since vegetation is not constant, the C-factor is a factor which changes with time. To obtain a more accurate estimate of future soil loss, the future C-factor had to be adjusted. This was done using the Normalised Vegetation Index (NDVI). This index helps determine plant health and areas of vegetation undergoing stress. It can thus be used as a proxy for the C-factor. It is calculated with the following equation:

$$\frac{NIR - Red}{NIR + Red}$$

Where:

- NIR = Near InfraRed Band
- Red = Red Band

NDVI estimates for the future are not readily available and so two methods were used to predict the estimates. One of the methods offers spatial variation while the other does not, and thus in this study they are referred to as the spatial method and the non-spatial method. The non-spatial method uses past NDVI data calculated from Landsat 5, 7, and 8 surface reflectance imagery (USGS/NASA Landsat 5 TM Surface Reflectance Tier 1 2023; USGS/NASA Landsat 7 ETM+ Surface Reflectance Tier 1 2023; USGS/NASA Landsat 8 Surface Reflectance Tier 1 2023) and regresses it against specific humidity and air temperature data from CMIP 5 (Copernicus Climate Change Service, Climate Data Store 2019). Landsat data was downloaded for a specific day in early spring, so that green vegetation would be present, as opposed to dry vegetation

in summer. The images were also chosen on a day which had minimal cloud cover over the AOI, this was preferred over downloading annual averages so that a year's worth of averaged cloud cover does not alter the real NDVI values. The images were found using Earth Engine (Appendix 1.2) (Gorelick et al. 2017), were downloaded with only the red and NIR band, and were visually inspected before downloading to ensure cloud cover was minimal. Different dates were chosen because of the cloud cover issue and thus image date ranges from February to April, with one of the years being studied having an image from a different year as no images with minimal cloud cover were available within that date range. Table 3-5 displays the years being studied and the dates of each Landsat image representing it.

Table 3-5: Landsat Images Date and Bands.

Year	Landsat image date	Landsat satellite	Bands for red and NIR
1985	3rd March	5	3 and 4
1991	27th March	5	3 and 4
1995	18th February	5	3 and 4
2000	5th April	7	3 and 4
2005	18th March	7	3 and 4
2010	8th April	7	3 and 4
2015	29th March	8	4 and 5
2021	29th March	8	4 and 5

The specific humidity and air temperature data were downloaded from CMIP5's data store for the years being studied (Copernicus Climate Change Service, Climate Data

Store 2019). The years 2010, 2015, and 2021 did not have any historical data so instead data from RCP 2-4.5 was downloaded. The data for 2050 under RCP 2-4.5 and RCP 5-8.5 was also downloaded. This data was loaded into SAGA GIS and the mean of each year being studied for both datasets was extracted and inputted into MS Excel. The Landsat images were also loaded into SAGA GIS and the NDVI was calculated using the above equation in the grid calculator. Some preprocessing was done before the NDVI was calculated, this included interpolating the faulty scan lines in Landsat 7 images, clipping the images to the AOI, and resampling them to match the other RUSLE grids. The mean of the NDVI over the AOI was then found and inputted into MS Excel with the specific humidity and air temperature data. Multiple regression was then performed in MS Excel between the means of the three datasets, with specific humidity and air temperature acting as predictors for NDVI (table 4.4.5-5). It should be noted that other relationships with other variables were also explored, but this was data that gave the best fitting model and was thus chosen to be used. The resulting NDVI value was inputted into the below equation to determine the C-factor and one C-factor was used for the entire valley. The use of the proxies to determine NDVI, which is then further used to determine the C-factor was repeated for both SSP scenarios, resulting in a C-factor for SSP 2-4.5, and a C-factor for SSP 5-8.5 for 2050.

For the spatial method, only the Landsat images for 1991 and 2021 were used. The NDVI was calculated as aforementioned and the 1991 grid was then subtracted from the 2021 grid using the grid calculator to determine the difference in the NDVI which

occurred in the 30 years. The annual rate of change was then determined by dividing the difference in the NDVI by 30. The NDVI for the future was then projected based on this annual rate of change using the following equation:

$$NDVI_{2050} = NDVI_{2021} + (Rate\ of\ change\ of\ NDVI * Number\ of\ years)$$

This calculation was performed with SAGA GIS's grid calculator. The resulting grid was then classified to exclude any values larger than 1 and any values smaller than -1, since the NDVI is an index which ranges from -1 to 1. This was accomplished using the reclassify grid values tool in SAGA GIS, which changed any value over 1 to 1 and any value less than -1 to -1 while keeping all other values the same.

Both of the NDVI maps, and the NDVI constants require transformation into C-factor values maps. This was done using the relationship and equation by Van der Knijff et al. (1999), which is as follows:

$$C = \exp\left(-\alpha \frac{NDVI}{(\beta - NDVI)}\right)$$

Where:

- C = C-factor
- α = a parameter that helps define the shape of the NDVI-C curve, given a value of 2 as in Van der Knijff et al. (1999)
- β = another parameter that also helps define the shape of the NDVI-C curve, given a value of 1 as in Van der Knijff et al. (1999)

For the non-spatial method, the equation was calculated in MS Excel, whereas for the spatial method the grid calculator in SAGA GIS was used to apply this relationship between the NDVI and C-factor and thereby estimate the C-factor values from the calculated NDVI maps for 2021 and 2050.

3.4.4. Other Factors

The other RUSLE factors needed for the equation were kept constant since they do not undergo a lot of change within a small number of years. Therefore the same K-, LS- (from LiDAR), and P-factor layers were used. These layers were multiplied by each other using the raster calculator in SAGA GIS as per the RUSLE equation:

$$A = R * K * LS * C * P$$

This equation was used to calculate a RUSLE for each SSP scenario. It should be noted that for the non-spatial method, a constant value was inputted as the C-factor for each SSP, whereas for the spatial method, a grid was inputted as the C-factor in the calculation. The spatial method also calculated a RUSLE for 2021 using the C-factor from the 2021 NDVI for comparison purposes.

3.5. Statistical Analysis of the Three Aims

The next chapter will display the results and statistics of this study. The chapter is divided into 3 parts, one for each aim for clarity. Here, a breakdown of each test listed in the next chapter will be provided.

Two difference maps are present in the next chapter. These are maps which highlight the changes between two maps. The first map presented is a comparison between soil loss estimates from ASTER and LiDAR at 30 m spatial resolution. This highlights areas where the two datasets differ. The second map is between the soil loss estimates for 2021 and 1957. This serves to highlight the changes in soil erosion the valley went through as well as visually depict areas undergoing erosion increase and erosion decrease. Time series plots are found with the results of the third aim. They present an easy-to-read graph showing changes in soil erosion in the AOI in time. The future predictions are included. A trendline of the past data is also included on the graphs to further illustrate the changes in erosion in the valley in a very general way.

The descriptive statistics are another aspect presented in the next chapter. This is a numerical breakdown of the maps – highlighting the mean and maximum so that a better idea of the soil erosion changes throughout the years and under different scenarios is understood. The results of Moran's I are also presented. This test is a type of spatial autocorrelation test which is used to determine whether there is clustering in the data, and whether this clustering is statistically significant. This is an

important test to consider for this study as the spatial dimension is very important in soil erosion and clusters tend to be present, thus spatial statistics and patterns are of the utmost importance.

Some sections also have normality and statistical tests presented. Normality tests and Q-Q plots for the data tested are first displayed. This is an essential step to determine if parametric or non-parametric tests should be used. The statistical tests are then presented. These tests relate to aim 3 of this study, i.e. soil loss estimates at different spatial resolutions. This is why the Wilcoxon signed-ranks test was chosen as it compares the mean of two related datasets, such as when the datasets are of the same location. The second test is Spearman's rank correlation coefficient. This test was used to investigate the strength of the relationship between the soil loss estimates from ASTER and LiDAR datasets. Each test had related graphs produced to further illustrate the statistical findings. Another statistical test presented is the multiple regression, which was mentioned in section 3.4.3. This test was necessary as a relationship between NDVI and two proxies was required so that a relationship could be used to estimate a future value for NDVI over the AOI.

It is important to note that throughout all the tests, H_0 represents the null hypothesis, where there is no statistical significance and thus there is no significant difference; meanwhile, H_1 is the alternative hypothesis which means that there is a statistically significant difference between the datasets being tested. Please find the full list of hypotheses for each test in Appendix 3.1.

4. RESULTS

This section displays the results obtained from this work. This section is divided into 3 subsections, one for each aim, with each section including its own descriptive statistics and Global Moran's I – a test to determine if similar data values are spatially clustered together. The first subsection displays the results for the first aim, i.e. the soil erosion predictions using the same method but a different spatial resolution. The section includes the map results obtained, as well as a map highlighting the changes between the two datasets; and some statistical tests, including normality tests. The second subsection relates to the second aim of the study, and it includes the map results of the RUSLE equation, i.e. the soil loss estimates in t/ha/yr, as well as one of the final estimates' influencing factor – the C-factor. This subsection illustrates the spatial trends of erosion throughout the years, in approximately 10-year intervals, between 1957 and 2021. The maps show both patterns in the AOI as well as quantities of erosion in the valley being studied. The third subsection shows the results obtained for the third aim, the future predictions of soil erosion in the AOI – based on future rainfall and NDVI estimates. This subsection displays the soil loss estimates for both the non-spatial and the spatial methods, as well as for both scenarios studied: SSP 2-4.5 and SSP 5-8.5 for 2050. This section also displays time series plots showing past estimates from 1957 to projections for 2050; and the multiple regression used in Chapter 3 of this study.

4.1.Soil Loss Estimates at Different Spatial Resolutions

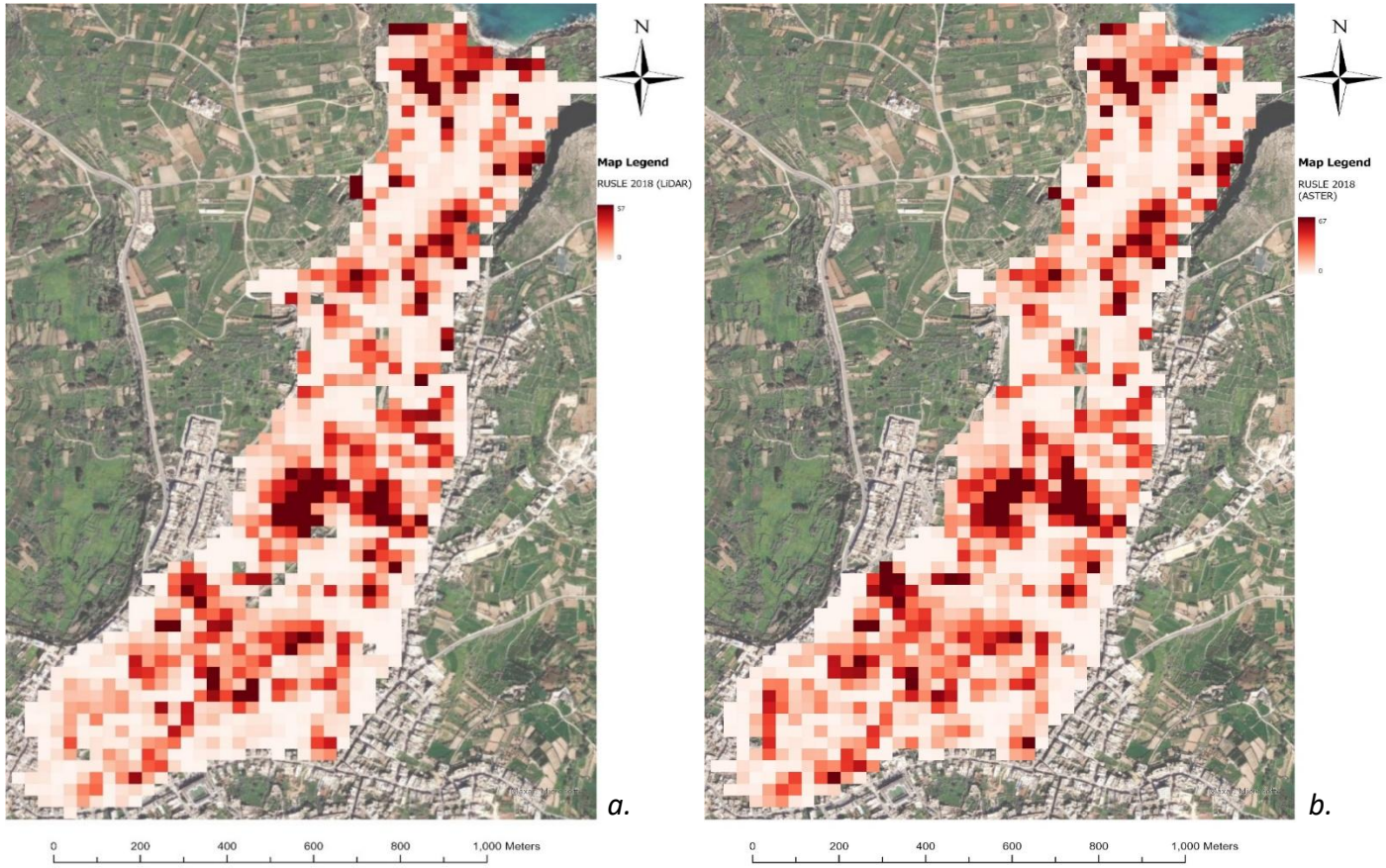

Figure 4-1: Estimated Soil Loss in in t/ha/yr for 2018 over the AOI at 30 m Spatial Resolution with (a) Showing Results from LiDAR, (b) Showing Results from ASTER GDEM.

Figure 4-1 displays the soil loss results at 30 m resolution from (a) LiDAR-derived DEM upscaled from 1 to 30 m, and (b) ASTER GDEM. Hotspots of soil loss are evident in both figures in the same locations. The figures are also very similar, spatially and quantitatively, with (b) having a slightly higher maximum.

4.1.1. Difference Map of Lidar-Derived vs ASTER-Derived Soil Loss Estimates

Difference maps have been made by subtracting one map from another to bring out changes present between two maps. Figure 4.2 illustrates a difference map where the soil loss estimate map obtained through a LiDAR DEM (figure 4-1 (a)) was subtracted from that obtained by ASTER GDEM (figure 4-1 (b)). The resulting map displays overestimations and underestimations made by ASTER GDEM, with only slight changes being observed.

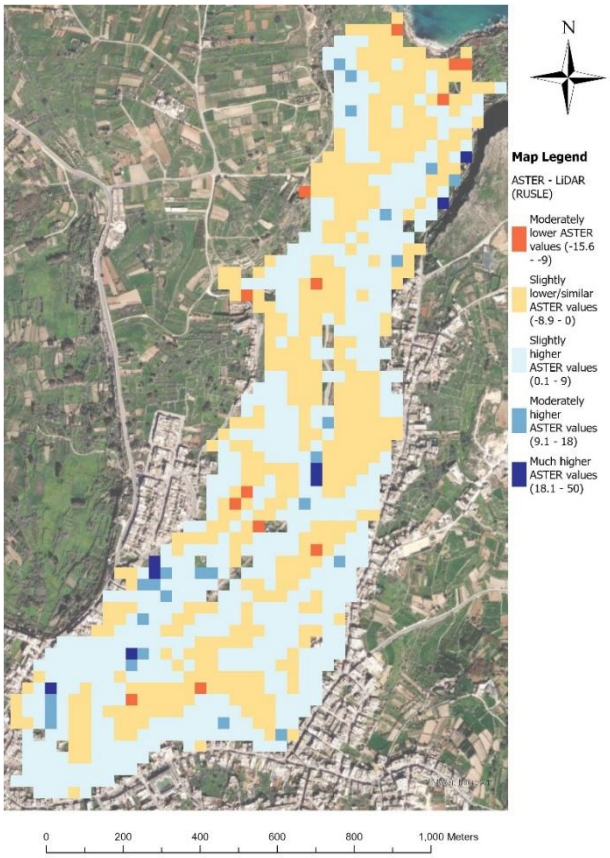

Figure 4-2: Difference Map of Soil Loss Estimates in t/ha/yr from ASTER GDEM – LiDAR.

4.1.2. Descriptive Statistics for LiDAR-Derived vs ASTER-Derived Estimates

Table 4.1 displays the mean, standard deviation, and maximum in t/ha/yr for the soil loss estimates obtained using a 1 m DEM from LiDAR, the same DEM but upscaled to 30 m, and ASTER GDEM at 30 m spatial resolution. The soil loss estimates obtained at a 1 m spatial resolution are much lower than those at 30 m, with the mean being more than half, and the standard deviation and maximum being approximately half for the 1 m resolution dataset when compared to the 30 m resolution datasets.

Table 4-1: Descriptive Statistics for Soil Loss Estimates at Different Spatial Resolutions.

	Mean in t/ha/yr	**Standard deviation in t/ha/yr**	**Maximum in t/ha/yr**
LiDAR 1 m (2018)	2.12	4.32	32.03
LiDAR 30 m (2018)	8.30	9.83	57.32
ASTER 30 m (2018)	9.03	10.49	66.64

4.1.3. Spatial Autocorrelation – Global Moran's I for LiDAR-Derived vs ASTER-Derived Soil Loss Estimates

Global Moran's I tests for spatial autocorrelation, i.e. clustering of data values, this is important for this study as soil erosion is often found in clusters. The Moran's index for the 1 m LiDAR-derived soil loss estimates is very close to 1 and is thus strong and positive, indicating the presence of clustering of data values. This is further reinforced by the very high z-score. The very low p-value of almost 0 means that the

data is statistically significant, i.e. it is highly unlikely that the clustering of data values is occurring due to chance, and H_1 is accepted.

Table 4-2: Results of Global Moran's I for Soil Loss Estimates at Different Spatial Resolutions.

	Moran's Index	**z-score**	**p-value**
LiDAR 1 m (2018)	0.847596	1625.197	0.000
LiDAR 30 m (2018)	0.359639	22.02317	0.000
ASTER 30 m (2018)	0.364924	22.20902	0.000

4.1.4. Normality and Statistical Tests for LiDAR-Derived vs ASTER-Derived Soil Loss Estimates

Normality tests are an important aspect to consider when doing statistical analysis as through them it is decided whether to use parametric or non-parametric tests. The statistical tests themselves are important as they test for statistical significance, i.e. whether something is likely to have occurred by chance or not.

Normality:

Table 4-3 shows the result for the normality test conducted on the soil loss estimates from LiDAR and ASTER at 30 m spatial resolution. Since the p-value of both LiDAR and ASTER-derived soil loss is almost 0 for both the Kolmogorov-Smirnov and Shapiro-Wilk tests, the normality assumption is violated, and the data is not normally distributed. This is further reinforced by the Q-Q plots in figures 4-3 and 4-4, where

the data points deviate from the reference line; as well as in the normal distribution plot displayed over the histogram (Appendix 3.2), which clearly shows the skewness of the data. Since the data is not normal, non-parametric tests will be used.

Table 4-3: Normality Tests for Soil Loss Estimates from LiDAR and ASTER Datasets.

	Kolmogorov-Smirnov			Shapiro-Wilk		
	Statistic	df	p-value	Statistic	df	p-value
LiDAR	.194	1006	.000	.804	1006	.000
ASTER	.193	1006	.000	.802	1006	.000

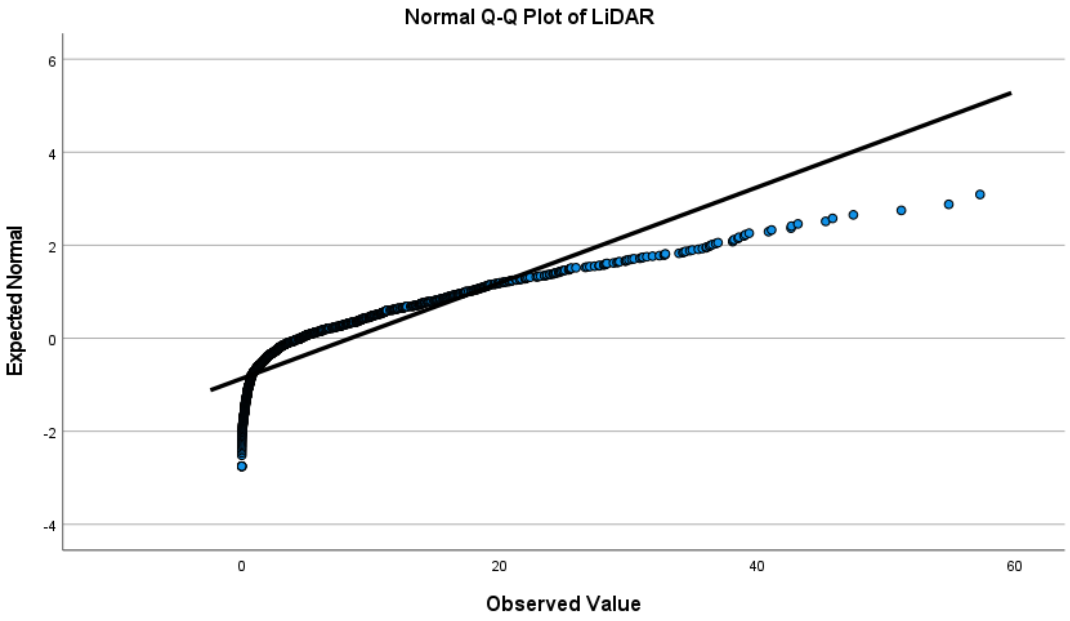

Figure 4-3: Q-Q Plot for Soil Loss Estimates from LiDAR at 30 m.

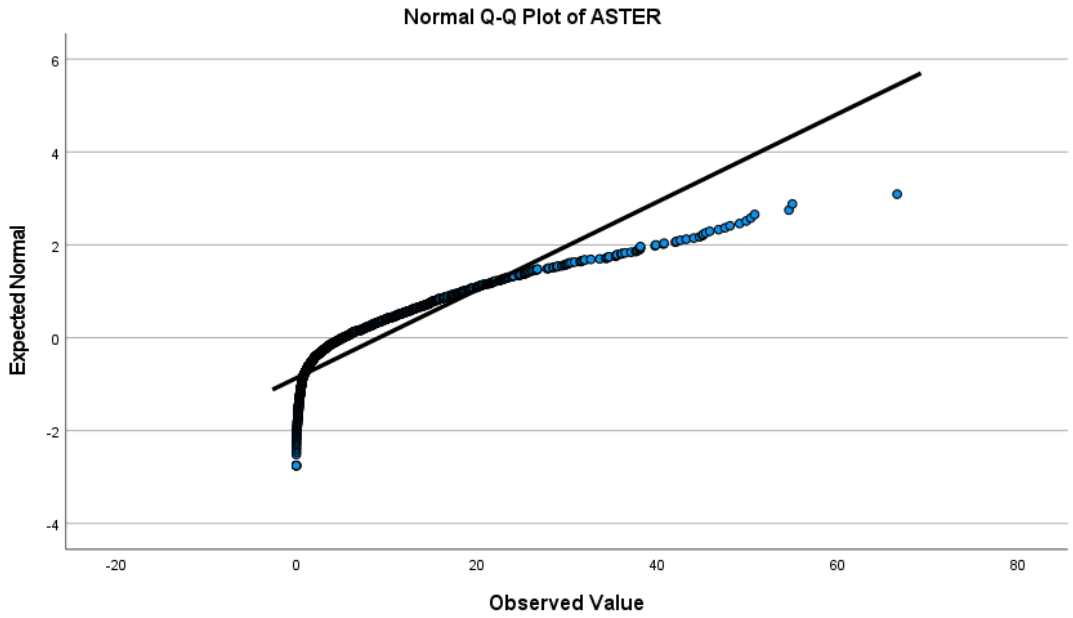

Figure 4-4: Q-Q Plot for Soil Loss Estimates from ASTER GDEM at 30 m.

Wilcoxon Signed-Ranks Test:

Table 4-4 and table 4-5 are the results of the Wilcoxon signed-ranks test from SPSS for the soil loss estimates from ASTER and LiDAR datasets at 30 m spatial resolutions. The Wilcoxon signed-ranks test was used as it compares paired datasets together, such as datasets located over the same area. The former table shows the ranks result, with negative ranks showing the number of pixels with a higher LiDAR value and positive ranks showing the opposite. It can be seen that there are more positive ranks, revealing that ASTER-derived values are higher more often than LiDAR-derived values. This is in line with the descriptive statistics, as ASTER-derived values had a slightly higher mean and a higher maximum. Table 4-5 shows the z-score and p-value for the Wilcoxon signed-ranks test for the same dataset. The p-value of almost 0 means that H_1 is accepted and H_0 is rejected. The error bar graph in figure 4-5 graphically displays the results of the Wilcoxon signed-ranks test, with a graphical

representation of the lower LiDAR values. It visualizes the overestimation produced by ASTER GDEM as its mean is higher than LiDAR's mean. The 95% confidence intervals around the means for the two datasets overlap, suggesting that the means are not very different from each other, despite the result of the Wilcoxon signed-rank test suggesting statistical significant difference between the means. This could be because while there is some difference present between the two means, this is minimal.

Table 4-4: Ranks' Results for Wilcoxon Signed-Ranks Test for ASTER – LiDAR Datasets.

		N
ASTER – LiDAR	Negative Ranks	431[a]
	Positive Ranks	570[b]
	Ties	5[c]
	Total	1006

a. ASTER < LiDAR

b. ASTER > LiDAR

c. ASTER = LiDAR

Table 4-5: Statistics Result for Wilcoxon Signed-Ranks Test for ASTER – LiDAR Datasets.

	ASTER – LiDAR
Z	-5.528[b]
p-value	.000

b. Based on negative ranks.

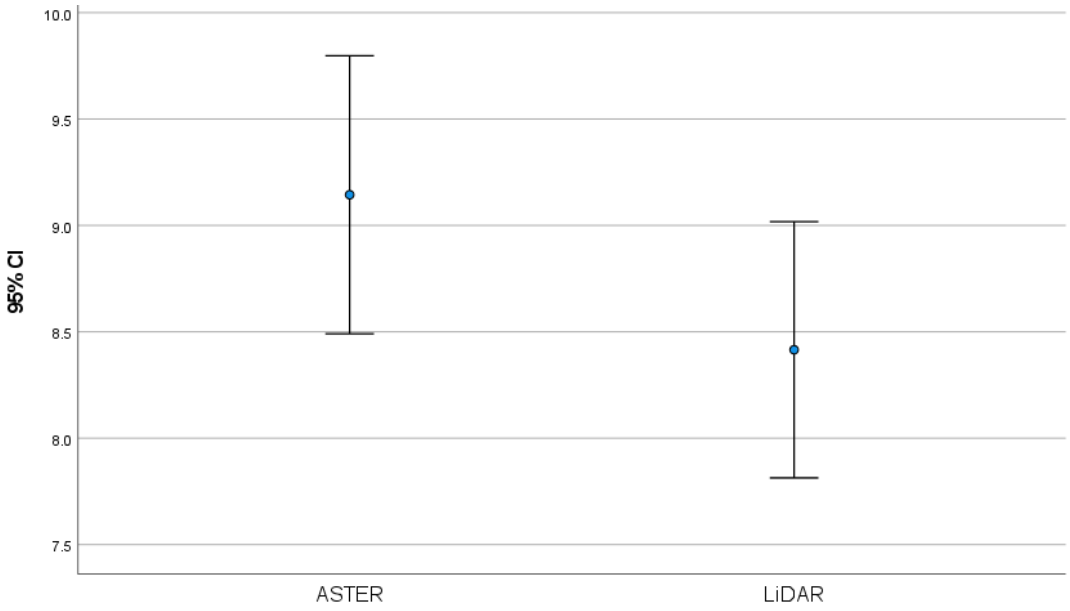

Figure 4-5: Error Bar Graphs for ASTER and LiDAR Datasets.

Spearman's Rank Correlation Coefficient:

Another test conducted was Spearman's rank correlation (table 4-6) to compare the soil estimates from ASTER and LiDAR at 30 m spatial resolution. The table displays the correlation coefficient and the p-value while the scatterplot in figure 4-6 displays this relationship in graphical format. The high, almost 1 correlation coefficient suggests a strong positive relationship between the two datasets. Meanwhile, the very low p-value of almost 0 means H_1 is accepted and H_0 is rejected. The R^2 value and a trendline were added to the scatterplot to further illustrate the relationship between the ASTER and LiDAR derived soil loss estimates. While there are a few outliers, the majority of the data points are clustered around the trendline, indicating that the two datasets are strongly correlated. The R^2 of the scatterplot is 0.8, further

confirming the strong correlation between the ASTER- and LiDAR-derived soil loss datasets.

Table 4-6: Results for Spearman's Rank Correlation for ASTER and LiDAR Datasets.

			LiDAR
Spearman's rho	ASTER	Correlation coefficient	.966
		p-value	.000

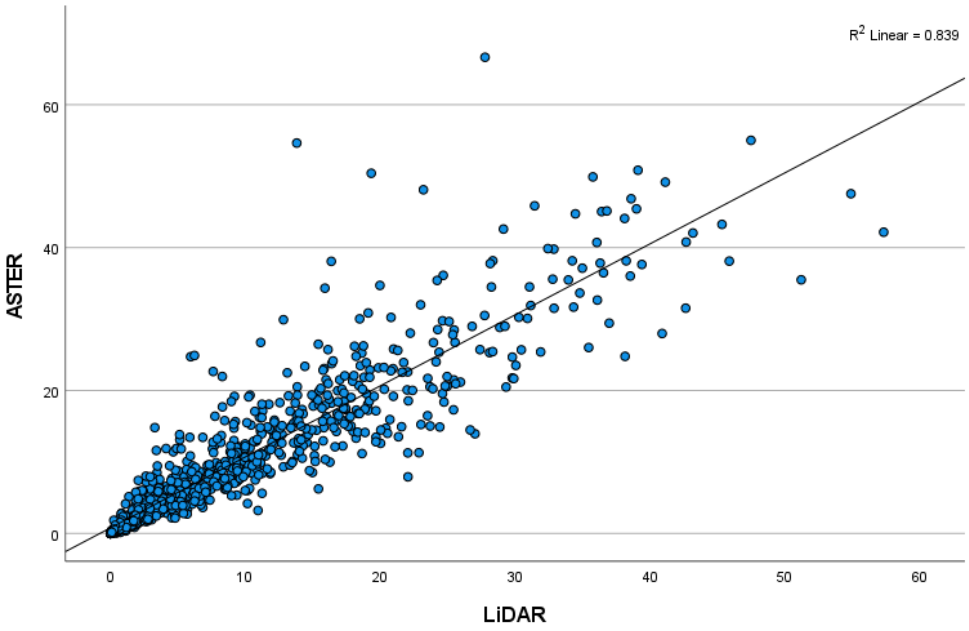

Figure 4-6: Scatterplot of RUSLE Results Obtained Using ASTER GDEM Against Those Obtained by the Upscaled (1 m to 30 m) LiDAR Data.

4.2. Past Soil Loss Estimations

The following maps (a) are the estimated soil loss in t/ha/yr calculated with the RUSLE equation between 1957 and 2021 at approximately 10-year intervals. Each soil loss estimate map is adjacent to its C-factor map (b), which represents vegetation cover and is one of the factors influencing soil loss estimates. This was done for ease of reference as the C-factor is possibly the main spatial influence on the soil loss estimates. The soil erosion figures (a) display the highest estimates of soil loss in red. Through the years, these red hotspots are seen to spatially change, but some trends remain constant through the years. The C-factor maps (b) mirror the soil loss maps (a) with high C-factor areas in white corresponding to red areas highlighting high soil erosion in figures (a).

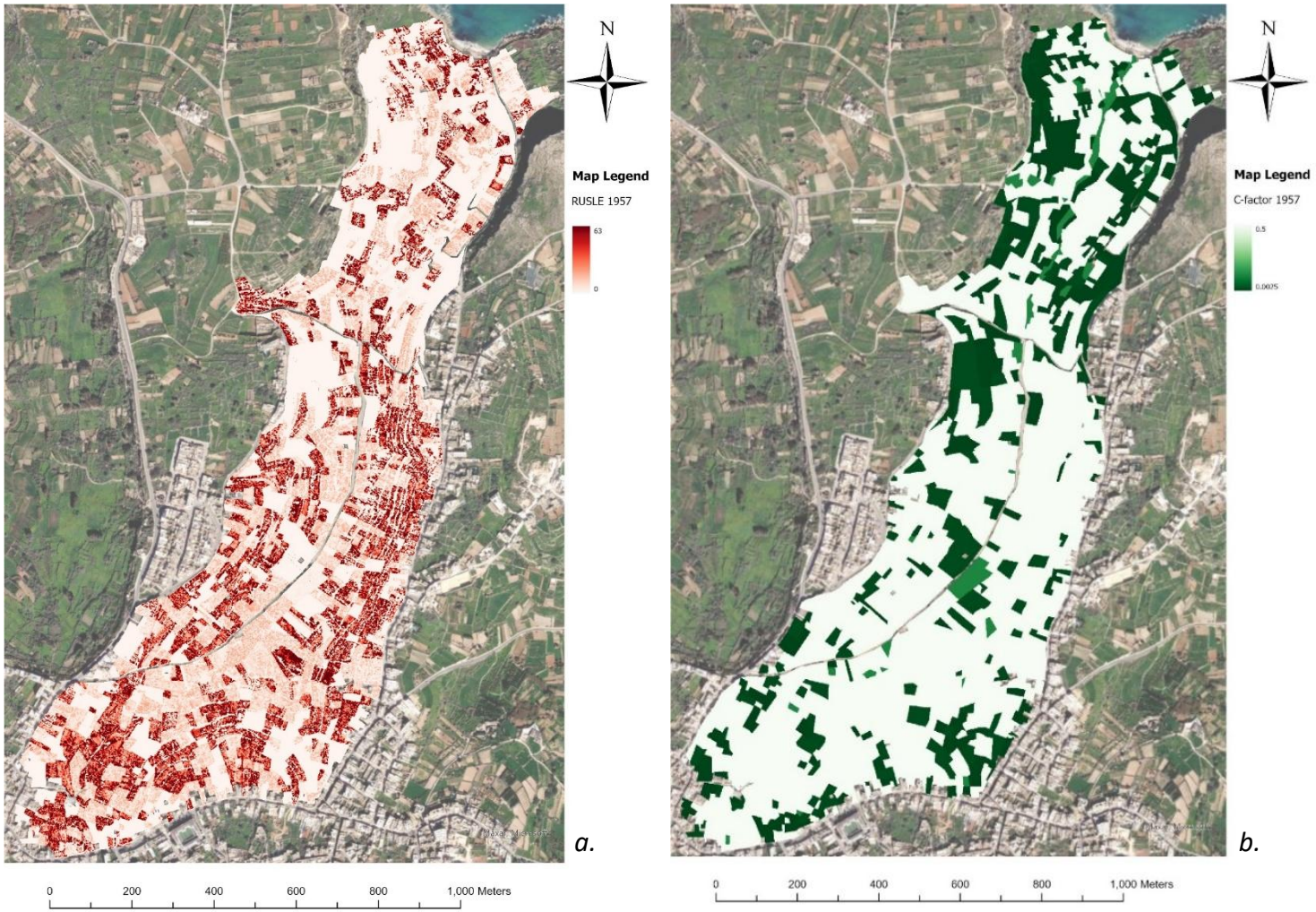

Figure 4-7: 1957 (a) Soil Loss Estimates in t/ha/yr, (b) C-factor.

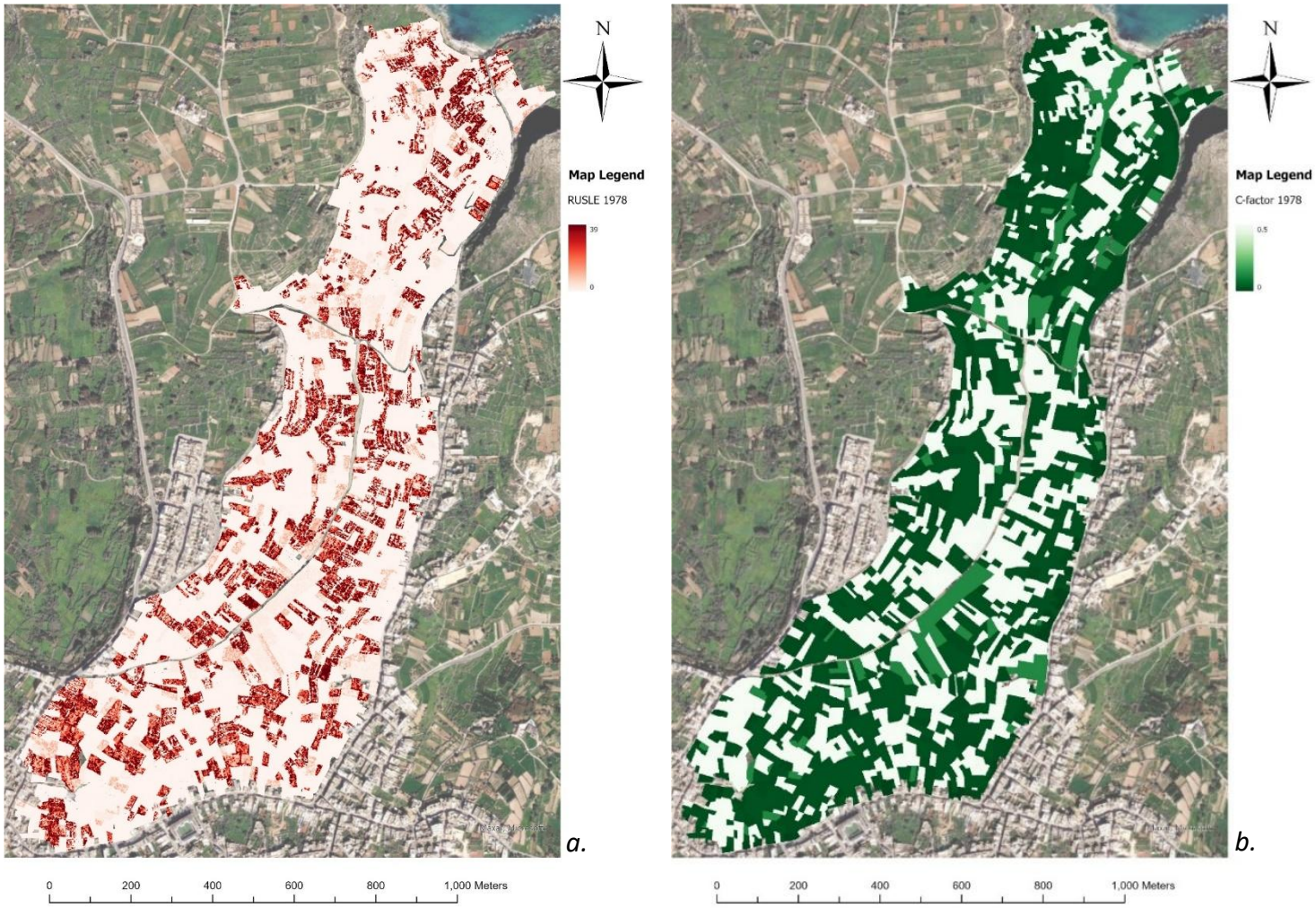

Figure 4-8: 1978 (a) Soil Loss Estimates in t/ha/yr, (b) C-factor.

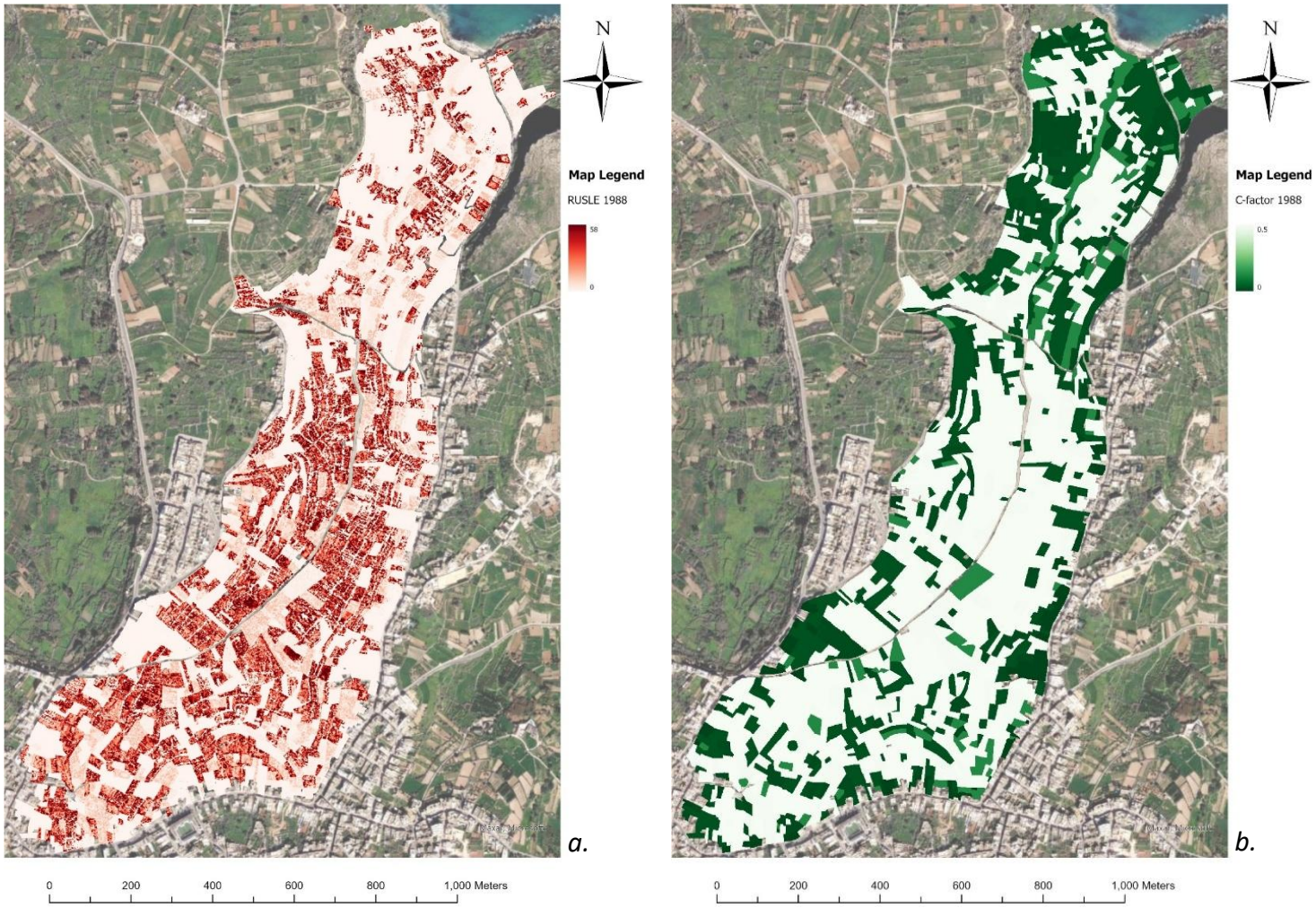

Figure 4-9: 1988 (a) Soil Loss Estimates in t/ha/yr, (b) C-factor.

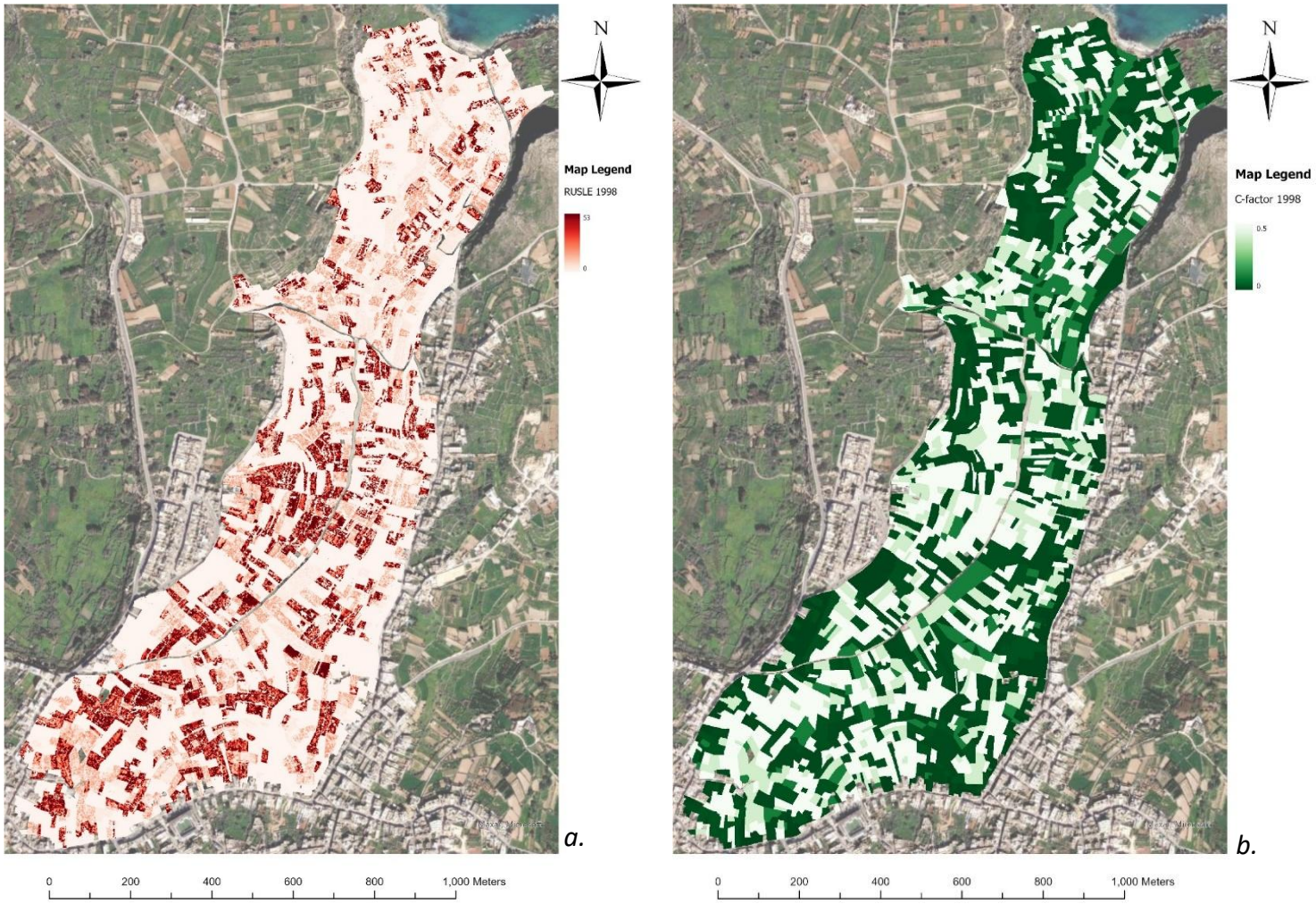

Figure 4-10: 1998 (a) Soil Loss Estimates in t/ha/yr, (b) C-factor.

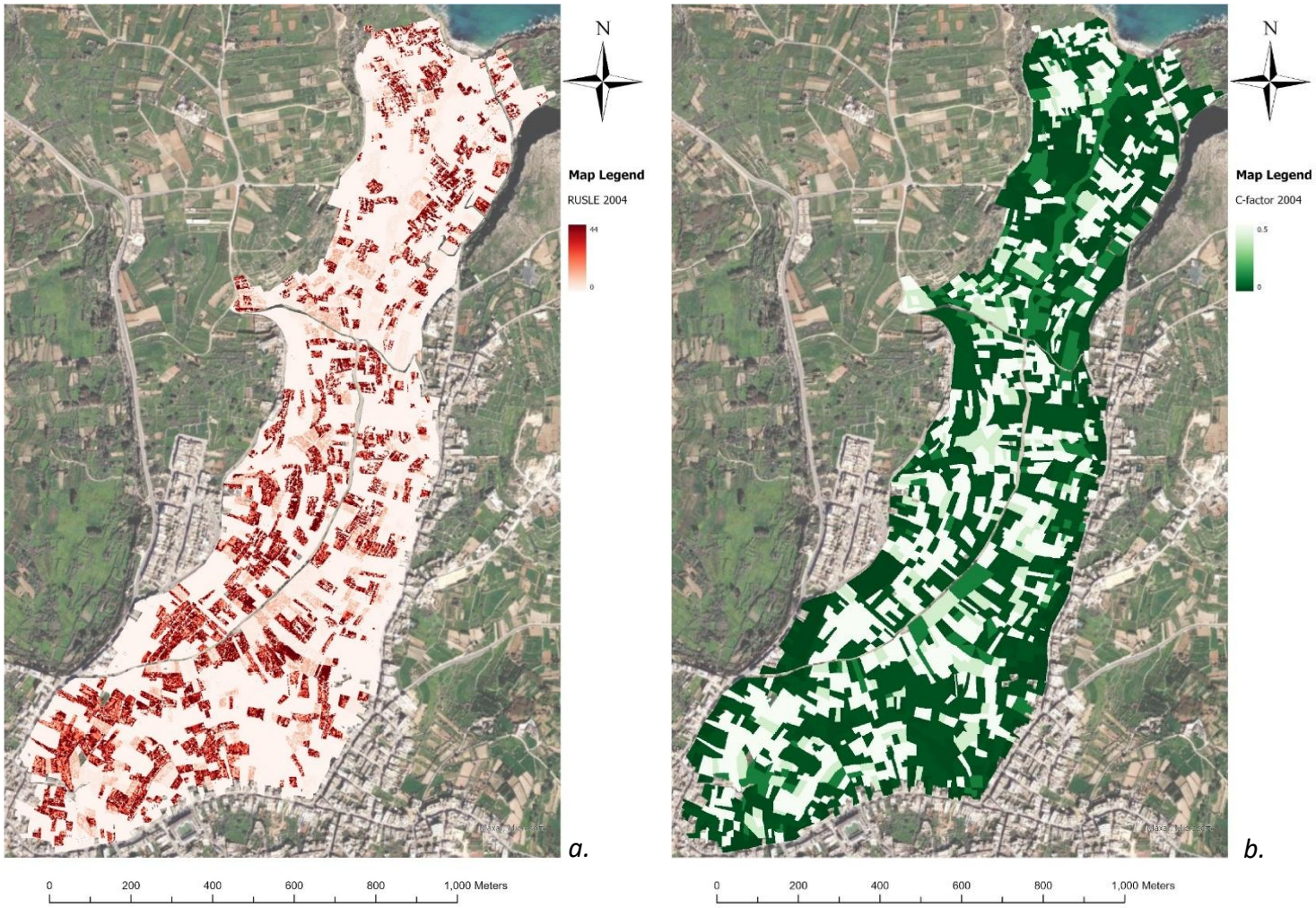

Figure 4-11: 2004 (a) Soil Loss Estimates in t/ha/yr, (b) C-factor.

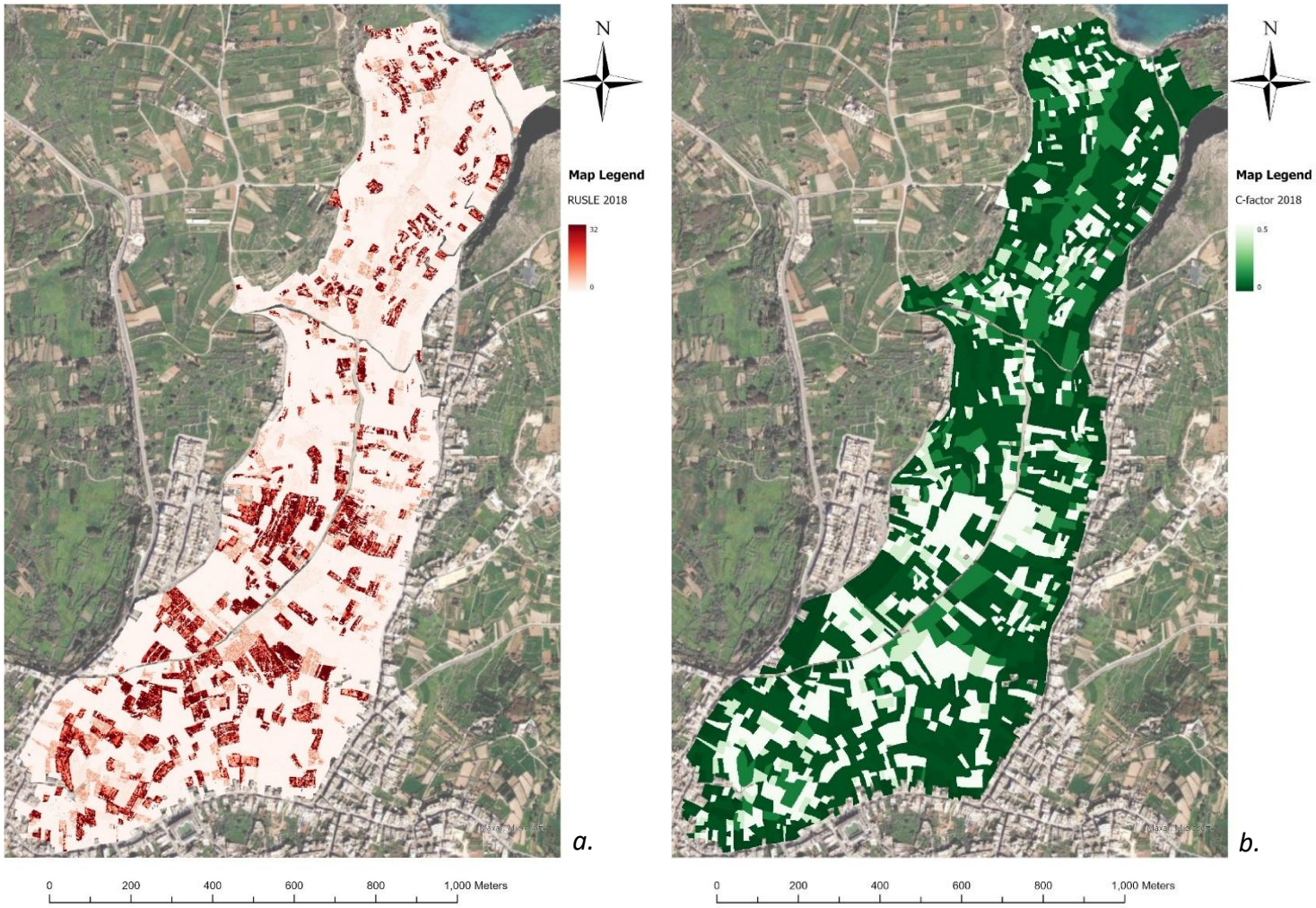

Figure 4-12: 2018 (a) Soil Loss Estimates in t/ha/yr, (b) C-factor.

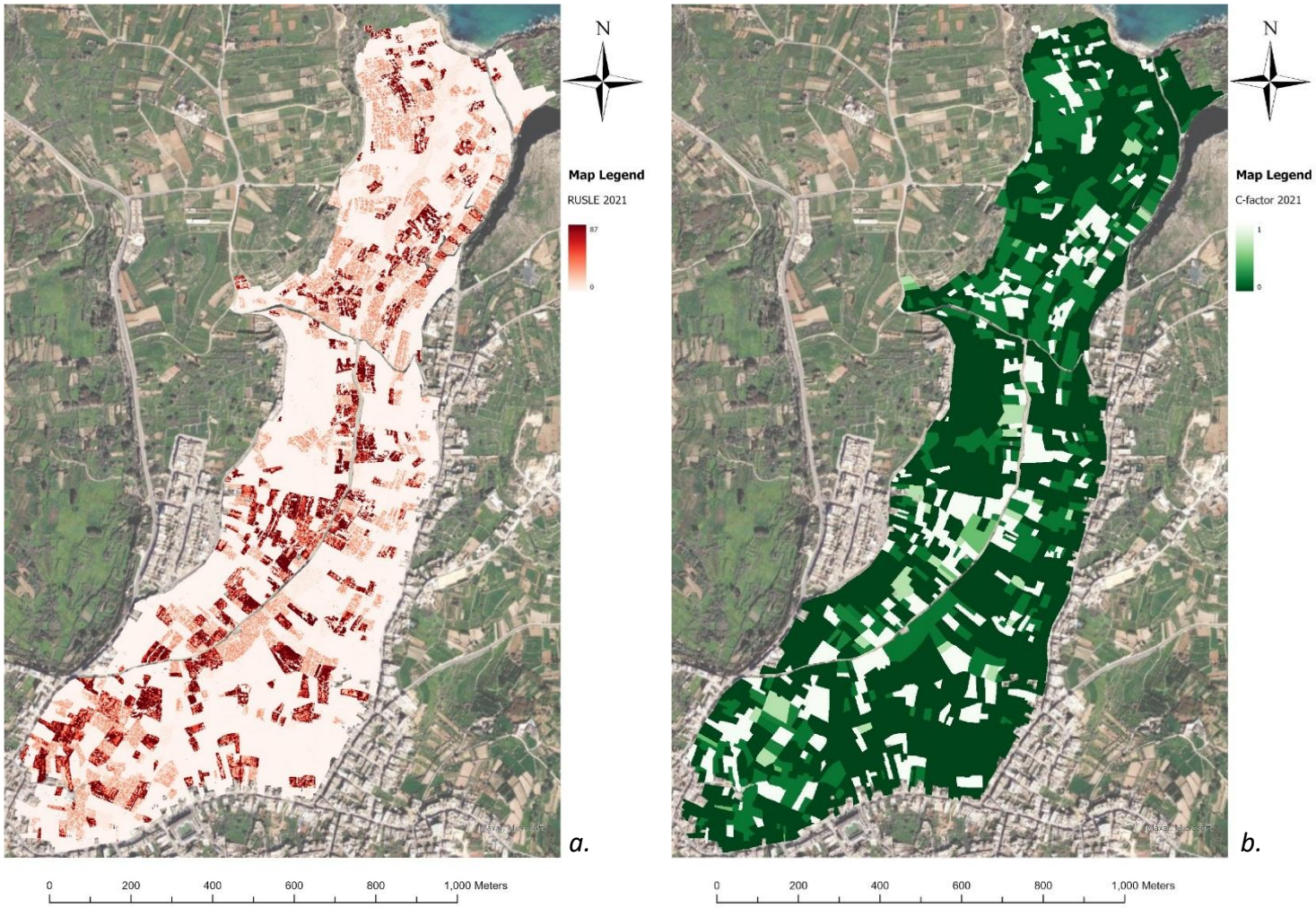

Figure 4-13: 2021 (a) Soil Loss Estimates in t/ha/yr, (b) C-factor.

Results for 1957:

Figure 4-7 illustrates the (a) soil loss estimates, and (b) the C-factor for 1957. Areas highlighted in white in (b) are seen to have a higher soil loss estimate in (a). The landwards side of the valley is seen to have higher erosion values, as well as higher C-factor values. High soil loss values seem to be common, covering most of the AOI's landward side.

Results for 1978:

Figure 4-8 displays the (a) soil loss estimates, and (b) the C-factor for 1978. Soil loss estimates are much lower than in 1957, with a lower maximum and a more dispersed spatial pattern. This spatial pattern of the soil loss estimates once again mirrors the C-factor, with much less high C-factor values.

Results for 1988:

Figure 4-9 shows the (a) soil loss estimates, and (b) C-factor for 1988. Soil loss estimates have increased from 1978, with a higher maximum and more areas marked in red in (a). These soil erosion hot spot areas are mirrored in (b) in white which show areas of high C-factor. High soil loss values are especially concentrated around the valley floor.

Results for 1998:

Figure 4-10 displays (a) the soil loss estimates, and (b) the C-factor for 1998. The maximum soil loss estimate value is similar to that in 1988 but the spatial pattern is much less dense, showing less areas with a high soil erosion estimate. This could be due to there being less high C-factor areas in (b). Despite this, there are still high erosion hotspots.

Results for 2004:

Figure 4-11 shows the (a) soil loss estimates, and (b) the C-factor for 2004. Erosion is spatially similar to that in 1998 but the maximum in 2004 is slightly lower. Despite the lower maximum, hot spot areas of high erosion are still present in the valley, especially on the landward side (southern side).

Results for 2018:

Figure 4-12 shows (a) soil loss estimates, and (b) C-factor for 2018. A decrease in erosion is evident, with a lower maximum – similar to 1978 levels. Despite the lower estimates, hotspots, displaying high erosion values are still present. These areas correspond to high C-factor areas in (b). These hotspots are less dense than in other years.

Results for 2021:

Figure 4-13 displays (a) soil loss estimates, and (b) the C-factor for 2021. The maximum soil erosion value has increased greatly from 2018 but spatially, there are still many areas displaying low erosion values. It is important to note that the C-factor (b) ranges from 0-1 in 2021 instead of from 0-0.5. Despite this, the C-factor is often low.

4.2.1. Difference Map for the Study Period 2021-1957

Figure 4-14 relates to aim 2 of this study and displays the changes occurring in soil loss estimates over the AOI between 1957 and 2021. The map does not consider any fluctuations throughout the years, nor does it break down how the changes occurred through the 10-year intervals studied. This map simply shows the difference one can see if a snapshot of soil erosion in 1957 is compared to one in 2021. The map shows an increase in erosion along the valley floor and on the seaward (north) side of the valley. Meanwhile, the landward (south) side of the valley, with the exception of the valley floor seem to be undergoing a decrease in erosion with time. The majority of the changes are either decreases in erosion, with changes up to 30 t/ha/yr, or increases in erosion of up to 40 t/ha/yr. There are also exceptions which involve larger decreases or increases.

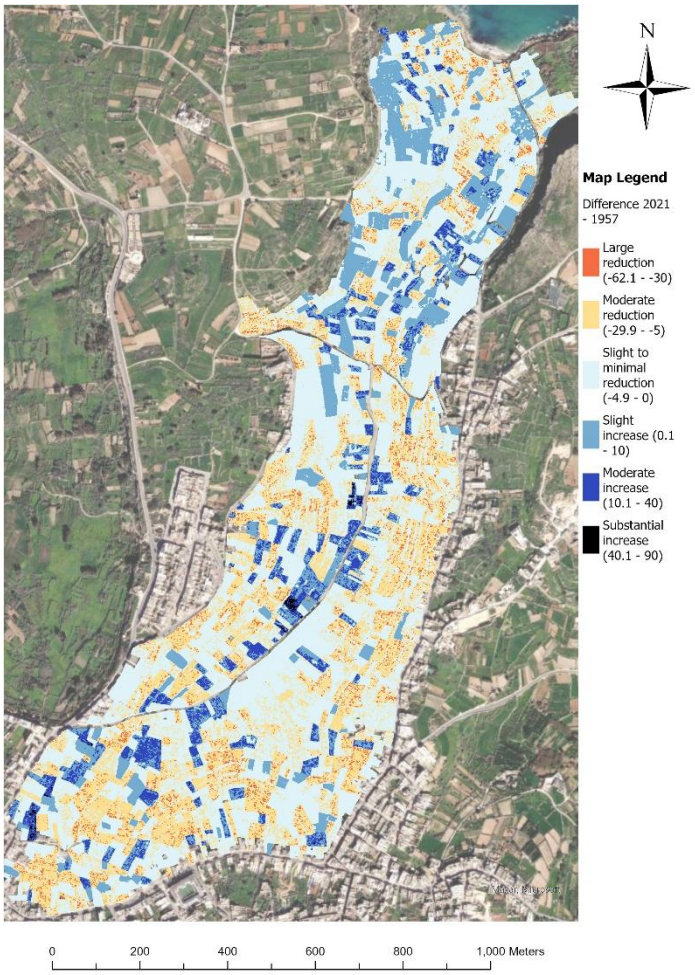

Figure 4-14: Difference Map of Soil Loss Estimates in t/ha/yr in 2021 - in 1957.

4.2.1. Descriptive Statistics for Past Soil Loss Estimates

Table 4-7 groups together the mean, standard deviation, and maximum for past soil loss estimates at a 1 m spatial resolution. The maximum and the mean can be seen to fluctuate slightly throughout the years studied, despite a decreasing trend being visible. The maximum mean rate recorded is in 1988, followed closely by that in 1957. On the other hand the highest maximum rate recorded is in 2021. This is over 20

t/ha/yr more than the second maximum rate recorded in 1957. Meanwhile the 2021 mean soil erosion rate is only 3.51 t/ha/yr, suggesting the presence of outliers.

Table 4-7: Descriptive statistics of the results obtained.

	Mean in t/ha/yr	**Standard deviation in t/ha/yr**	**Maximum in t/ha/yr**
1957	7.52	10.38	62.78
1978	3.55	6.17	38.93
1988	7.60	10.24	58.07
1998	4.46	7.59	52.65
2004	3.85	6.78	44.02
2018	2.12	4.32	32.03
2021	3.51	7.13	87.01

4.2.2. Spatial Autocorrelation – Global Moran's I for Past Soil Loss Estimates

Global Moran's I tests clustering of data values and tests whether the clustering is statistically significant or not. Table 4-8 summarizes the results for Global Moran's I test conducted in ArcGIS Pro for the past soil loss estimates. All the Moran's indices obtained are positive, with a very high index of almost 1 being obtained for all years studied. Similarly, all the p-values obtained where almost 0 and thus were lower than the 0.05 level of significance. This means that the alternative hypothesis, H_1, is accepted.

Table 4-8: Results of Global Moran's I Test from ArcGIS Pro.

	Moran's Index	**z-score**	**p-value**
1957	0.803395	1540.450	0.000
1978	0.819837	1571.532	0.000
1988	0.802753	1539.207	0.000
1998	0.826322	1583.403	0.000
2004	0.828227	1587.031	0.000
2018	0.847596	1625.197	0.000
2021	0.846630	1623.357	0.000

4.3. Future Soil Erosion Predictions

This section presents the future soil loss prediction maps in t/ha/yr for 2050 under SSP 2-4.5 and SSP 5-8.5. The rainfall erosivity (R-) factor was adjusted as estimated from WorldClim CMIP6 climate models and the vegetation cover (C-) factor was altered using two methods. The first presented method is the non-spatial method (figure 4-15), where one NDVI value for the whole AOI was estimated using proxy data; the second method is the spatial method (figure 4-16), where future NDVI values were estimated from past NDVI values (section 3.4.3). The resulting maps display minimal spatial differences between the two scenarios, but the two methods resulted in highly different maps.

RUSLE (Non-Spatial):

Figure 4-15 displays the estimated soil loss for 2050 using the non-spatial method for (a) SSP 2-4.5, and (b) SSP 5-8.5. Figures (a) and (b) are spatially very similar as they have no spatially varying factor as the C-factor is the same number for the entire AOI. The figures differ in scale with (a) recoding a higher maximum erosion rate.

RUSLE (Spatial):

Figure 4-16 shows the soil loss estimates for 2050 using the spatial method for (a) SSP 2-4.5, and (b) SSP 5-8.5. The figures are once again very similar due to the C-factor being the same for both scenarios. This limits spatial and quantitative variation between the two scenarios. Despite this, hotspots are still visible, highlighting areas of highest concern.

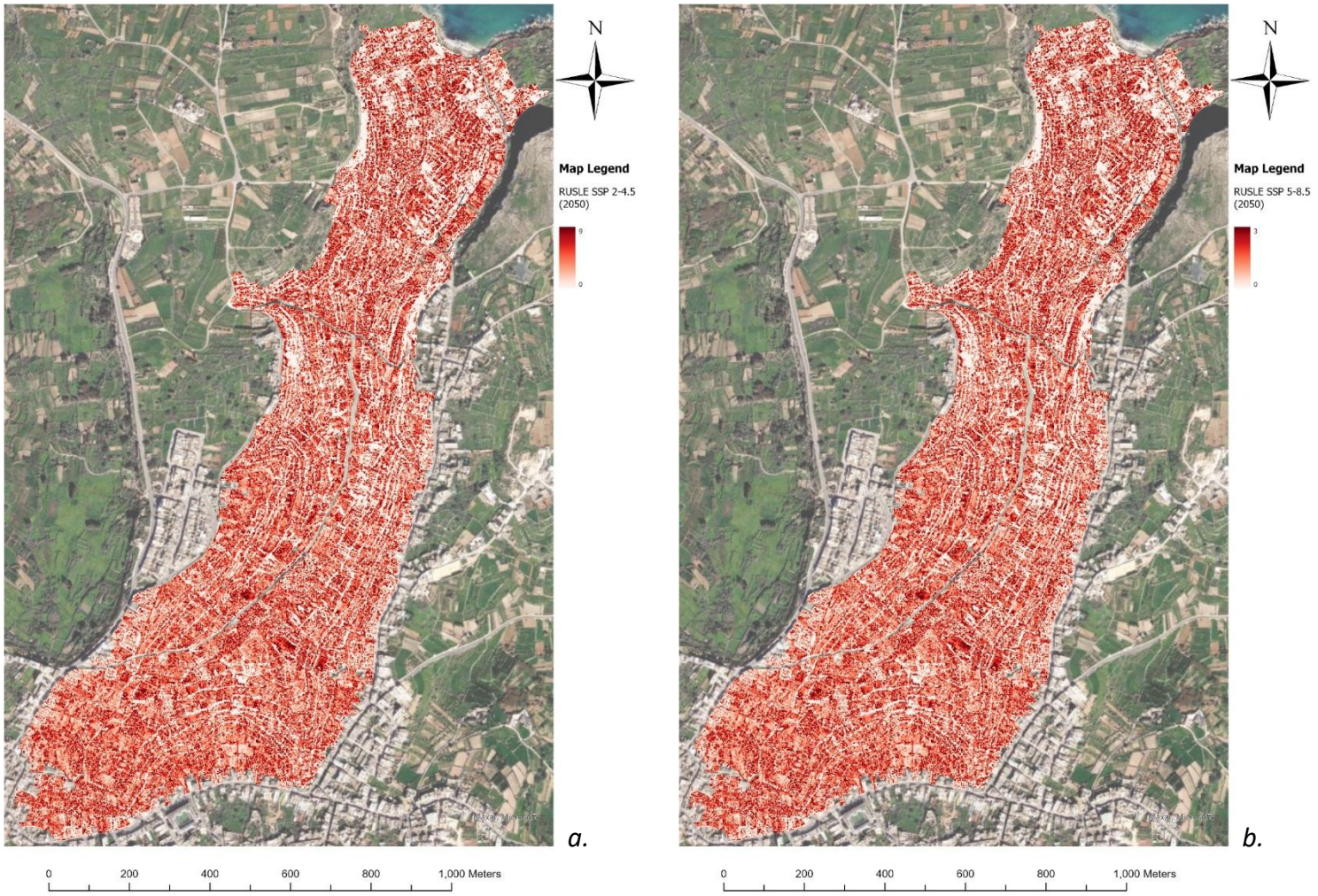

Figure 4-15: Estimated Soil Loss in t/ha/yr for 2050 Using the Non-Spatial method for (a) SSP 2-4.5, (b) SSP 5-8.5.

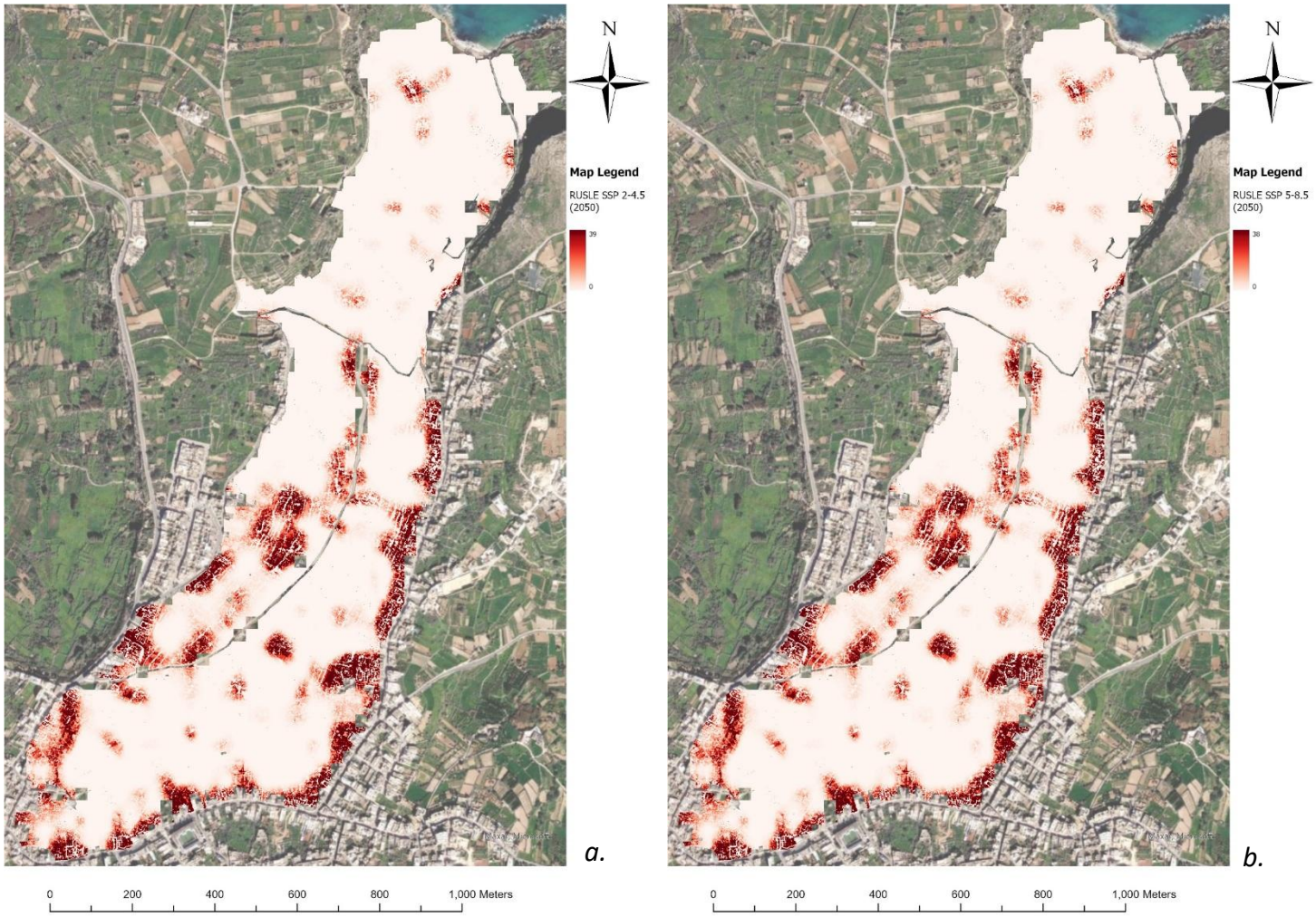

Figure 4-16: Estimated Soil Loss in t/ha/yr for 2050 Using the Spatial Method for (a) SSP 2-4.5, (b) SSP 5-8.5.

4.3.1. Time Series Plots for Past and Future Soil Loss Estimates

Figures 4-17 and 4-18 are time series plots of the mean and maximum results obtained for past soil erosion (over the years 1957, 1978, 1988, 1998, 2004, 2018, and 2021), as well as future predictions for 2050 under SSP 2-4.5 and SSP 5-8.5. The graphs also indicate the general trend that the past estimates have been following through the years and display the R^2 of the plotted trendline. Figure 4-17 shows a trend of decreasing soil erosion over the AOI through the years, despite some fluctuations. While the future scenarios have no trendline plotted, it is still visible that erosion will either minimally change (SSP 2-4.5) or continue decreasing (SSP5-8.5). Meanwhile, figure 4-18 shows that the maximum is set to continue slightly increasing. However, the future predictions both predict very low maximums in comparison with past estimates.

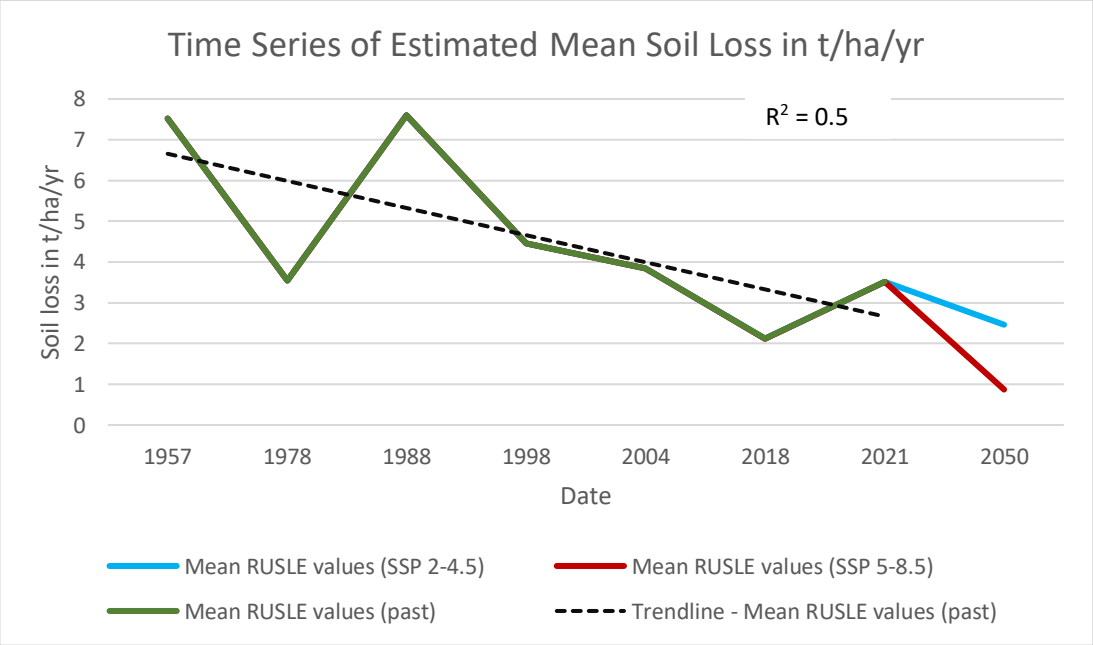

Figure 4-17: Time Series of Estimated Mean Soil Loss in t/ha/yr over the AOI, Including the Future Predictions for 2050 under Two Different SSP Scenarios.

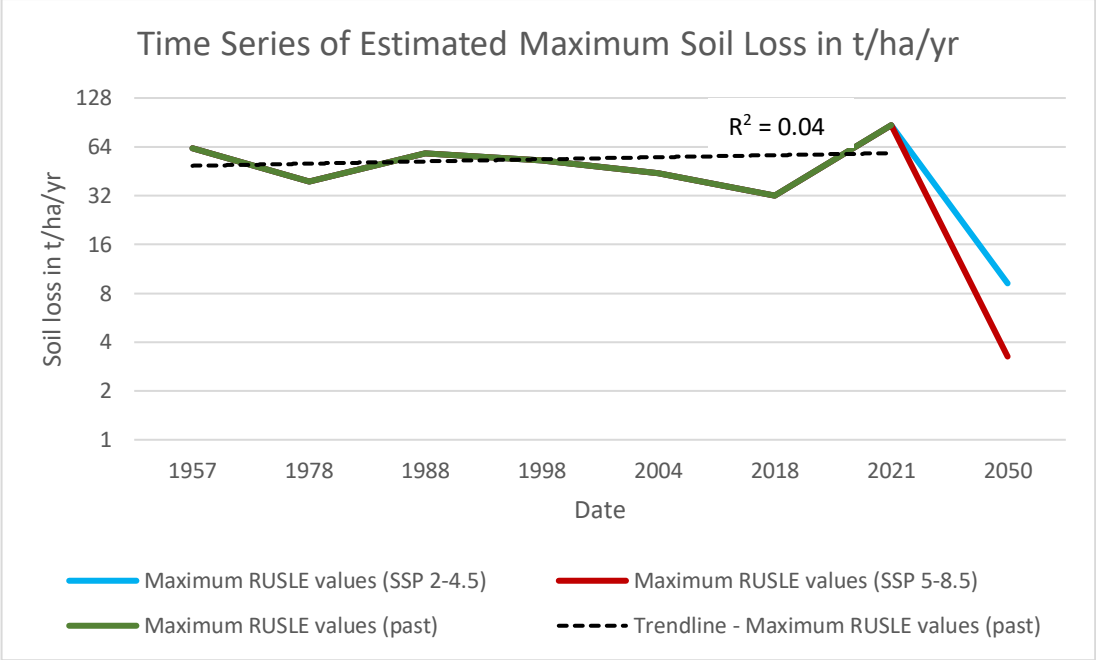

Figure 4-18: Time Series of Estimated Maximum Soil Loss in t/ha/yr over the AOI, Including the Future Predictions for 2050 under Two Different SSP Scenarios.

4.3.2. Descriptive Statistics for Future Soil Loss Predictions

Table 4-9 displays the mean, standard deviation, and maximum for 2050 for SSP 2-4.5 and SSP 5-8.5. Soil loss is projected to be lower for SSP 5-8.5, with SSP 2-4.5 having a similar mean to past soil loss estimates, but maximum soil loss rates for both scenarios is projected to be much lower than those estimated for past soil loss rates.

Table 4-9: Descriptive Statistics for Future Soil Loss Predictions for 2050 under Different SSP Scenarios.

	Mean in t/ha/yr	**Standard deviation in t/ha/yr**	**Maximum in t/ha/yr**
2050 SSP 2-4.5	2.46	1.84	9.21
2050 SSP 5-8.5	0.87	0.65	3.26

4.3.3. Spatial Autocorrelation – Global Moran's I for Future Soil Loss Predictions

Table 4-10 shows the results for Global Moran's index. The high positive Moran's index suggests the presence of clustering, further reinforced by the high z-score, while the very low p-value indicates statistical significance. Since the p-value is lower than the 0.05 level of significance, the alternative hypothesis is accepted, and the clustering of similar data values is assumed to not be by chance.

Table 4-10: Results for Global Moran's Index for Future Soil Loss Predictions.

	Moran's Index	**z-score**	**p-value**
2050 SSP 2-4.5	0.656281	1258.369	0.000
2050 SSP 5-8.5	0.848413	1598.505	0.000

4.3.4. Statistical Tests for Future Soil Loss Predictions

Multiple Regression:

Table 4-11 displays the results of the multiple regression done during the methods for aim 3 (section 3.4.3). This regression was required to determine a relationship between NDVI and two proxies. This relationship would be determined via past data and would then be applied to future data to estimate a future NDVI value for the AOI. Past NDVI is regressed against past specific humidity and air temperature to determine a relationship between them. Since the R^2 (0.86) was relatively high, this

relationship was used, and specific humidity and air temperature were used as proxies to determine future NDVI as per the equation determined by the regression.

Table 4-11: Results of the Multiple Regression between NDVI, Air Temperature, and Specific Humidity in MS Excel.

Regression Statistics								
Multiple R	0.924900665							
R Square	0.85544124							
Adjusted R Square	0.797617736							
Standard Error	0.032149574							
Observations	8							
ANOVA								
	df	*SS*	*MS*	*F*	*Significance F*			
Regression	2	0.030582024	0.015291012	14.79400556	0.007945313			
Residual	5	0.005167976	0.001033595					
Total	7	0.03575						
	Coefficients	*Standard Error*	*t Stat*	*P-value*	*Lower 95%*	*Upper 95%*	*Lower 95.0%*	*Upper 95.0%*
Intercept	18.49077975	6.379230846	2.898590786	0.033846213	2.092444812	34.88911469	2.092444812	34.88911469
tas	-0.070298589	0.022962921	-3.06139573	0.028057356	-0.129326657	-0.011270521	-0.129326657	-0.011270521
huss	236.8373611	43.76029364	5.412152007	0.002913502	124.3479451	349.326777	124.3479451	349.326777

5. DISCUSSION

This section of the study discusses and interprets the results found and presented in chapter 4. The chapter discusses the findings of each aim separately; summarises the effects of each RUSLE factor on the final soil loss estimates; compares the study to other similar studies; and lists a number of recommendations which should be taken to further safeguard against erosion as well as highlights areas of potential future research.

5.1. Soil Loss Estimates at a Different Spatial Resolution

Aim 1 of this study considers soil erosion estimates from the RUSLE equation at a different spatial resolution. The LiDAR-obtained DEM used for the past and future soil loss estimates is upscaled to a 30 m DEM to match the resolution of ASTER GDEM. The LS-factor is calculated from these two DEMs, and two RUSLE equations are calculated – one for LiDAR and one for ASTER. The results were then compared together to determine if the use of ASTER data is sufficient for soil erosion estimates over a small watershed.

5.1.1. Comparison between the Original 1 m LiDAR-Derived Soil Loss Estimates and the Upscaled 30 m LiDAR-Derived Estimates

Figure 4-1 (a) illustrates the results of the RUSLE equation using LiDAR 1 m data upscaled to a 30 m spatial resolution. The resulting soil loss map is visibly coarser and looks more pixelated than its 1 m resolution counterpart. Despite this, the map still shows hotspot areas of higher values (figure 5-1 (a)) – on the western slope closest to the sea (A); on the eastern slope on the seaward side of the valley heading towards the centre of the valley (B); in the centre of the valley, starting on the valley floor and going up the slope (C); further landwards at the valley floor going up the slope (D). Each of the four hotspots, especially (A) and (B), are also visible in figure 5-1 (b), which is the 1 m spatial resolution version of soil loss estimates for 2018 using a LiDAR DEM. Hotspot (B) is the least visible of the four hotspots on figure 5-1 (b) as adjacent to it there are similar values. In figure 5-1 (a) the hotspots near area (B) are more separate, unlike in figure 5-1 (b) where there seems to be a larger area of relatively higher values of soil erosion.

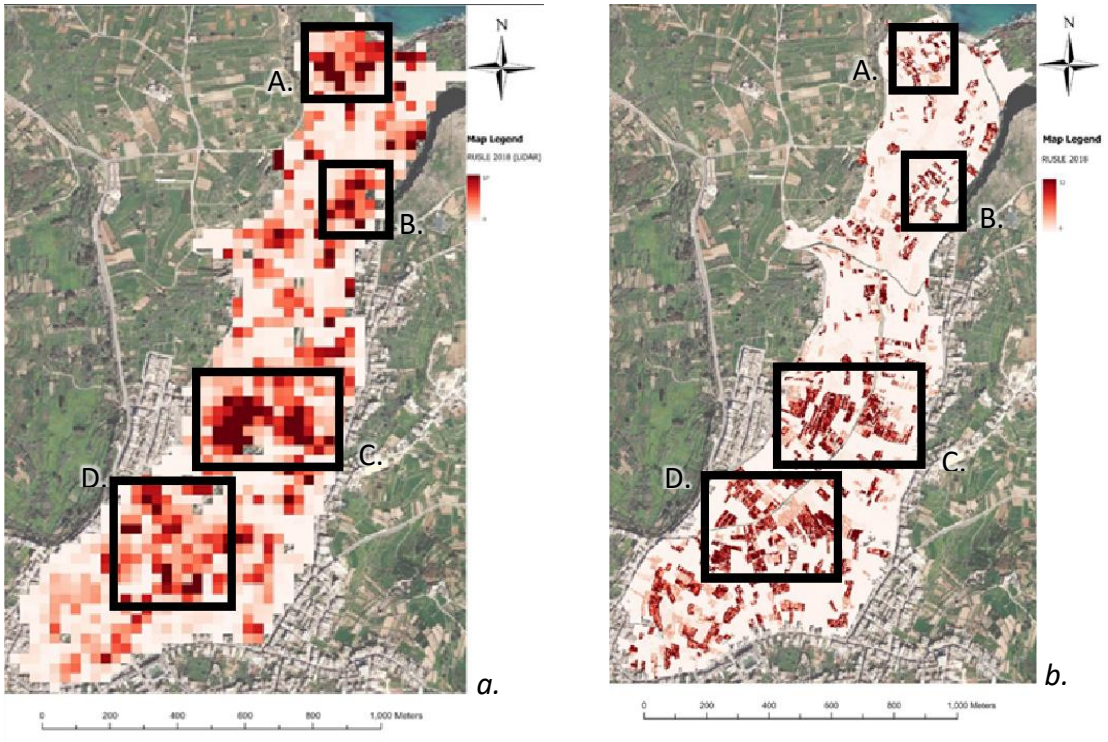

Figure 5-1: Soil Loss Estimates with Marked Hotspots (a) at 30 m spatial Resolution from Upscaled LiDAR, (b) at 1 m Spatial Resolution from Original 1 m LiDAR.

All five factors used to create figure 4-1 (a) are the same as the ones used to create figure 4-12, but they are upscaled. These factors affect the spatial pattern and the numerical values of the resulting soil loss maps. Patterns were not very visible in the 1 m resolution LS-factor (Appendix 2.4), however, when it was upscaled, the patterns were more decipherable (Appendix 2.10). Generally, the seaward side of the valley showed a higher LS-factor than the landwards side. This is likely because the landwards side of the valley has gentler slopes than the seaward side of the valley, which has much steeper slopes. The highest LS-values are found on the sides of the valley, with certain hotspot areas – another logical aspect as the middle of the valley is the valley floor and is thus not very steep. It is noticeable, however, that the mouth of the valley has a very high LS-factor. However, the LS-factor's pattern is not consistent with the pattern of the RUSLE output – indicating that another one of the

factors is the main influence on the visible pattern of soil erosion in the valley. Given that the R- and P-factors are constant throughout the valley, and the K-factor has little variation, the influencing factor is likely to have been the C-factor.

While in this case the lack of variation of the other factors is an important contribution to the fact that the C-factor is the biggest spatial influencer on the RUSLE, it is still valid that the C-factor greatly affects soil erosion. The C-factor represents vegetation cover and vegetation has several soil-protecting mechanisms that help hinder erosive processes. The canopy of the vegetation itself increases interception and thus decreases raindrop splash, meanwhile the roots of plants bind the soil together increasing its resistance to erosion. The denser the vegetation, the lower the C-factor (de Baets 2007). Another aspect is tillage. Tillage operations loosen and break the structure of soil and can even create a precursor to rills, especially if tillage is done up-and-down a slope, with soil erosion occurring on the plough lines (Van Oost et al. 2006).

When comparing the mean soil loss rates of the 30 m LiDAR-derived estimates to the 1 m data for 2018, it is immediately evident that the upscaled data is resulting in higher values (table 4.1). The mean soil loss rate of the upscaled data is quadruple that of the 1 m, while the standard deviation and maximum are almost double. This suggests that while coarser datasets can determine hotspot locations well when compared to finer data, numerical quantification of erosion is not as accurate and reliable as that of finer datasets. Therefore, caution must be taken when using coarse

datasets for quantitative purposes. It is important to note that this is still LiDAR data, it is just upscaled and so differences in the soil loss estimates stem from the coarseness of the data and not from any inaccuracies or differences of the DEM.

When quantifying soil erosion, an important step is to classify it into several classes that help determine its severity. This can be used for easy comparison between different areas and studies. The following table (table 5-1) by Stone and Hilborn (2012) was used for classification purposes. For 2018 upscaled soil loss estimates from LiDAR DEM, the mean soil loss value of 8.3 t/ha/yr is over the 6.7 t/ha/yr tolerable threshold and thus is classified as low. Meanwhile, the maximum falls into the severe category as it exceeds the 33.6 t/ha/yr threshold. This differs from the categorization of 2018 1 m soil loss estimates which has a tolerable mean soil loss rate and a maximum soil loss rate falling in the high classification. This difference in categorization further reinforces the difference in quantitative measurement between fine and coarse datasets with regards to soil loss estimates.

Table 5-1: Severity Classification Table as per Stone and Hilborn (2012).

Classification	Soil loss in t/ha/yr
Severe	>33.6
High	22.4 – 33.6
Moderate	11.2 – 22.4
Low	6.7 – 11.2
Tolerable (very low)	<6.7

Table 4-2 displays the results of Moran's I spatial autocorrelation test. Moran's index is 0.36, contrasting with the values obtained for the 1m spatial resolution data of the same year which had a much higher Moran's index of 0.85. Therefore, while this is technically the same data, just at a different spatial resolution, the upscaled data showed less clustering and grouping together of similar values than the original data. Despite this, 0.36 still indicates a positive spatial autocorrelation so grouping together of similar values, while less than before, still occurs. Clustering of soil erosion values is a logical result as many of the factors which affect soil erosion occur over whole areas and not single points. This includes slopes and soil types, among other factors, as both are often, but not always, found to change gradually.

5.1.2. Comparison between Upscaled LiDAR-Derived Soil Loss Estimates and ASTER-Derived Soil Loss Estimates

Figure 4-1 (b) shows the soil erosion estimates from ASTER GDEM at a spatial resolution of 30 m. The hotspots visible and the spatial pattern in figure 4-1 (b) are similar to those in figure 4-1 (a), which were created using the LiDAR DEM. This suggests that spatially, ASTER GDEM can be used in soil loss predictions with relatively good accuracy. The same R-, K-, C-, and P-factors as for the LiDAR-derived predictions were used for the ASTER-derived predictions, and only the LS-factor differed. The LS-factor (Appendix 2.10) used was calculated from ASTER GDEM (Appendix 2.9). The LS-factor for ASTER GDEM is seen to be very similar to the LiDAR one, but it appears to be smoother and has a slightly lower range. However, all the hotspots of the LiDAR LS-factor are visible as hotspots of the ASTER LS-factor. Again,

the pattern of the LS-factor does not seem to match that of the RUSLE output and thus one of the other factors, likely the C-factor, is influencing the pattern of the soil loss more.

A difference map of ASTER-derived soil loss – LiDAR-derived soil loss was created to check where and how the two maps differ spatially from each other. The map is mainly covered by two categories: slightly higher ASTER values, and slightly lower/similar ASTER values, with values ranging between -9 to 9 t/ha/yr. There are then very few pixels throughout the valley which show moderate or large differences. This again shows the similarity between the two RUSLE products and show that spatially ASTER behaves very well and produces good results.

The mean and the standard deviation are approximately 1 t/ha/yr higher for ASTER-derived predictions than for LiDAR-derived ones, while the maximum differs with approximately 10 t/ha/yr, with ASTER-derived predictions being higher. This suggests that while spatially ASTER-derived predictions are quite accurate, magnitude-wise ASTER-derived estimates are slightly higher than LiDAR-derived ones, suggesting that ASTER GDEM tends to overestimate when estimating soil erosion values in the AOI. The classifications of the ASTER-derived predictions match the classifications of the LiDAR-derived dataset. The mean soil loss is categorized as low since it is between 6.7 – 11.2 t/ha/yr, and the maximum soil loss is categorized as severe since it exceeds 33.6 t/ha/yr. The spatial autocorrelation test (table 4-2) obtained results that are very

similar to the results obtained by the LiDAR-derived predictions, with differences only seen with more decimal places.

Wilcoxon Signed-Ranks Test:

The Wilcoxon signed-ranks test compares the soil loss estimates derived from LiDAR with those derived from ASTER GDEM, both at 30 m spatial resolution. Table 4-4 illustrates the overestimation of the ASTER-derived soil loss estimates since these estimates are higher more often than LiDAR derived estimates. Despite the difference between the LiDAR-derived and the ASTER-derived soil loss estimates being statistically significant, figure 4-5 shows us that the means do not have a high degree of difference. This is further reinforced by table 4-1. This means that using ASTER GDEM in soil loss estimation instead of LiDAR technology can result in a slight overestimation of soil erosion values. However, this overestimation over the AOI was not very large. It is important to keep in mind that this test compared estimates obtained using 30 m spatial resolution data for both ASTER GDEM and LiDAR. This means that the slight overestimation of ASTER GDEM is when compared to LiDAR estimates of the same spatial resolution. Table 4-1 shows that if LiDAR at 1 m was compared with LiDAR at 30 m, different results might have been obtained as their descriptive statistics were different despite being the same dataset, just over a different spatial resolution.

Spearman's Rank Correlation Coefficient:

This test correlates the soil loss estimates obtained using LiDAR and ASTER GDEM. Since both datasets represent the same variable over the same location at the same time, a high correlation coefficient close to 1 is expected. Since the value of 0.966 is very close to 1, the datasets are strongly correlated, suggesting that ASTER-derived soil loss is a valid alternative to upscaled LiDAR-derived soil loss. This conclusion is supported by several results. Figure 4-1 visually shows that both datasets identify similar areas as hotspots for soil erosion, and figure 4-1 illustrates the low amount of differences between the two maps in figure 4-1. Spatial autocorrelation between the two datasets is also very similar. This means that in terms of hotspots, both DEMs perform well. When it comes to descriptive statistics, LiDAR-derived and ASTER-derived soil loss estimates at 30 m are similar, but ASTER-derived estimates are slightly higher. The biggest difference is between fine resolution LiDAR estimates and upscaled LiDAR estimates. The overestimation of ASTER-derived soil loss estimates is confirmed with the Wilcoxon signed-ranks test. However, the error bar graph in figure 4-5 and the result of Spearman's rank correlation suggest that despite the overestimation, ASTER-GDEM can still be used instead of the upscaled LiDAR DEM. This is because the overestimation is not very high.

5.1.3. Conclusion for LiDAR vs ASTER GDEM-Derived Soil Loss Estimations

Despite the conclusion that ASTER GDEM can be used instead of an upscaled LiDAR DEM, it is important to note that this is a comparison between 30 m resolution

datasets. When compared to the 1 m dataset, the results are quite different. While statistical tests were not conducted, maps and descriptive statistics were used to compare the datasets. The descriptive statistics are different enough between the datasets that the fine resolution data has a different severity category than the coarse resolution data. The hotspots themselves on the maps were quite similar to each other (figure 5-1). The spatial autocorrelation was positive for all three datasets, showing that all datasets experienced clustering of similar values, but the 1 m dataset had a much higher degree of clustering than the 30 m resolution datasets. This suggests that while ASTER GDEM can be used for small watersheds in cases where finer data is unavailable, it performs better spatially than quantitatively. This means that it can detect hotspots of higher soil erosion values, but it is not as accurate as fine data when it comes to numerical measurements of erosion as it tends to overestimate. This overestimation is not just the one between the 30 m datasets, but also the one seen within the descriptive statistics, where the mean soil loss rates for the 30 m datasets are quadruple that of the 1 m dataset. This stems from the coarseness of the data itself – as even upscaled LiDAR suffered from it. A possible solution would be downscaling the ASTER GDEM, as this would remove the issue of coarseness and ASTER GDEM performed well when compared to LiDAR at the same resolution. In downscaling, it is imperative to be cautious of artifacts as these are often introduced into the downscaled DEM and can alter the soil loss estimates.

In comparison of these conclusions with other studies, a slight conflict between studies is evident. Bircher et al. (2019) reported that a 25 m DEM, similar to ASTER GDEM's 30 m, resulted in a higher L-factor and a lower S-factor when compared to a

2 m DEM due to the smoothing effect. Fu et al. (2015) also found that the S-factor decreased, and the L-factor increased with a coarse resolution DEM. Fu et al. (2015) continued to find that the LS-factor decreased and thus, the estimated soil loss was lower for the coarse resolution DEM. This is in contrast with this study's findings as the soil loss estimates, through observation – and not statistical tests – are higher for the coarse resolution DEMs. This difference of overestimation instead of underestimation of soil loss estimates by coarser resolution DEMs could have occurred due to the specific topography of the AOI. While the AOI does have hilly areas and slopes, the change in terrain is relatively gradual, and thus smoothing of the terrain may lead to longer slopes (higher L-factor) and larger slope angles (higher S-factor) to be calculated than what is present – thereby exaggerating the LS-factor.

5.2. Past Soil Loss Estimations

Aim 2 of this study considers soil loss estimations over past years to determine the general trends in erosion and whether there are fluctuations. The years considered range from 1957 to 2021, in approximately 10-year intervals. With the data constraints available, the years considered in this study were: 1957, 1978, 1988, 1999, 2004, 2018, and 2021. Data availability relied on orthophotos available from the Planning Authority, their 1960s aerial imagery run did not cover Gozo and so no data was available; 2004 was considered instead of 2008 as it was the closest year with data available; and 2021 uses fieldwork-derived data conducted at the start of this study.

5.2.1. Overall Trend

The second aim, mapping and estimating the total annual soil loss for intermediate years between 1957 and 2021, is to further increase the understanding of the mechanisms and trends of soil erosion in the AOI. In fact, an important aspect is to determine whether soil erosion in the AOI fluctuates over the years or whether it undergoes gradual increase or decrease. Figure 4-17 graphically illustrates this behaviour in a time series graph of the mean values of each year under study. 7 years were used in this study and while it can be seen that the mean values seem to fluctuate, 4 of the years studied (1988-2018) show a clear decrease in soil loss without any break in the trend. Despite the outliers of 1978 and 2018, a negative

trend was obtained showing erosion over the AOI decreasing with time. This suggests that soil erosion is decreasing throughout the AOI, thereby resulting in an overall lower mean soil loss rate with time. It is important to note that this trend has not been tested for statistical significance due to the very small sample size of only 7 samples.

Figure 4-18 shows the maximum values of the 7 years studied instead of the mean. This graph is also seen to fluctuate despite having 4 years obtaining a constantly lower value than the previous one studied. This decrease in maximum erosion over 1988-2018 is especially contradictory when compared to the trendline of the graph which is showing a positive trend – thereby an increase in maximum erosion over the years. This trendline might have been the result of the 2021 maximum value – which is a strong outlier. The trendlines obtained indicate that the severity of the maximum soil loss rates will increase as the maximum will increase but more areas will get less and less erosion as the mean will decrease over time. However, it is important to note that neither trendline was tested for significance due to the small sample size. There is also the presence of outliers in the data, these might be either normal fluctuations or abnormal outliers, but it is difficult to determine which due to the small sample size.

Figure 4-14 is the difference map for the entire time period under study. The map (2021 – 1957) – aiming to see the overall changes which occurred – displays a lot of areas which underwent minimal change in the 64-year difference that this map is

investigating. The landward side of the valley has many areas which through the years have undergone a moderate reduction in soil erosion. There are, however, a few hotspots all throughout the valley which are marked as a moderate increase and even substantial increase in erosion. These hotspots are areas where the maximum might continue increasing as the maximum soil erosion rate trend suggests. These areas are the areas most in need of erosion control measures as they are most at risk – with their erosion rate having increased greatly. Many of these hotspot areas can be found along the valley floor, and areas which have undergone a slight increase in erosion can be found mainly on the seaward side of the valley. In general, this map illustrates a small decreasing trend in erosion between 1957 and 2021 – further reinforcing the time series plot of figure 4-18. This is in stark contrast to the pattern revealed by figure 5-7 which showed an increase in erosion in the past 20 years. Given that the other two difference maps (figures 5-3, 5-5) both illustrate decreases in erosion, it is only the past 20 years that display an increase in erosion in the difference maps created. This is an important result as it shows that while erosion was decreasing in the valley, it is once again increasing.

This trend could be the result of either the R- or C-factor. Rainfall totals make up part of the R-factor, along with rainfall intensity, and decreasing precipitation totals could be part of the reason why soil loss estimates have been decreasing. 2021 and the 3 years prior had a relatively higher total precipitation and thus a higher R-factor was obtained for 2021. The mirroring effect between the R-factor and the mean soil loss rate over the AOI is further explained in section 5.4.1 of this study. Rainfall erosivity

is known to have a large impact on soil loss and thus, it is a logical conclusion that it is one of the major reasons why soil loss is changing in this way. The C-factor is seen to affect the spatial pattern of the soil loss in each of the years studied. If a year has large areas with a high C-factor, the same place is seen to record high soil loss values. This directly shows the influence that the C-factor has on the soil loss estimates.

5.2.2. Analysis for 1957

Spatial Pattern:

The spatial pattern of the soil loss estimates is seen to change throughout the years, with some hotspot areas shifting and some remaining as hotspots throughout the study period. Hotspot area of higher erosion values can be compared with the individual factors making up the soil loss estimates so there is more understanding of the processes at work. This can aid in management and soil erosion control measures as the control measure chosen can directly affect the most influential factor in that hotspot. In this study, the R-factor and the P-factor are constant throughout the entire valley, therefore, any variation within the valley within the same year of study is the result of the K-, LS-, and C-factors. The LS-factor ranges between 0 and 3, however, spatial variation is very difficult to determine as there is no clear pattern or distribution. This could be due to the fact that most of valley is terraced. Where higher values are actually visible, there is no obvious relationship between them and the high RUSLE values upon inspecting them visually.

The K-factor doesn't have a large variation with the maximum being 0.10 and the minimum being 0.091. In contrast with the RUSLE soil loss findings, the higher K-factor values are found on the seaward side of the valley – where there is generally lower estimated soil loss. On the other hand, the lowest K-factor values are found on the landward, western side of the valley, which is one of the places recording higher RUSLE values. Regarding soil texture, high RUSLE values were often recorded in areas with a sandy loam and with a clay loam. It is important to note that despite this, not all sampled areas with sandy loam or clay loam soils experienced higher levels of erosion. While soil texture is a major aspect of the K-factor, it is not the only factor considered. However, it is of great importance with fine silty soils tending to erode more than sandy or clayey soils. This is because sand particles are larger, heavier, and thus are more difficult to entrain. Their high permeability rate also decreases the amount of surface flow which can wash it away. Meanwhile, clay soils have a high cohesion and are thus difficult to detach and wash away. On the other hand, silty soils are neither large and heavy enough to hinder transportation processes nor small enough to have strong cohesive forces (FAO 2019).

The C-factor values for 1957 are more in line with the RUSLE findings. Figure 5-2 displays the high and low soil erosion areas of 1957 with the corresponding area on the C-factor map. Sites A and C display low erosion estimates on figure 5-2 (a) and corresponding low C-factor values on figure 5-2 (b). Sites B, D, and E illustrate that the opposite is also true. The values range from a maximum of 0.5 to a minimum of 0.0025. Most of the valley is recording high C-factor values in 1957, and this is likely

due to the much higher percentage of land being under crop production. In fact, the combination of seasonal crops and presence of tillage can greatly increase the C-factor. On the other hand, abandoned plots, and plots abandoned but with trees suffer from less erosion due to the higher amount of vegetation cover and so have a higher C-factor. However, most plots in 1957 were either under crop production or tree cultivation. While most of the valley has a high C-factor close to the 0.5 maximum, the landward side of the valley has the highest values and has only few areas with a lower C-factor. This could be a good explanation as to why the RUSLE values in the landward side of the valley are higher than in the seaward side.

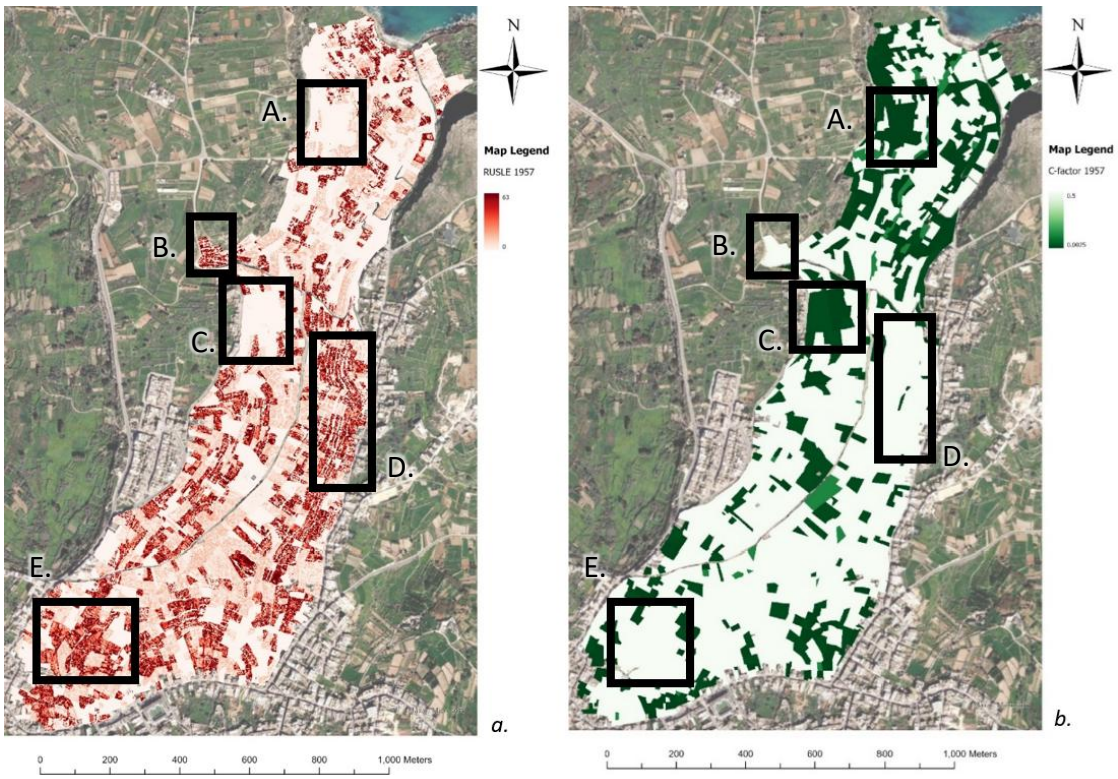

Figure 5-2: 1957 Hotspot Links between (a) Soil Erosion Estimates, (b) C-factor.

Descriptive Statistics and Classification:

The descriptive statistics for 1957 display a big difference between the mean and the maximum as the overall mean erosion rate of the entire valley is 7.52 t/ha/yr while the maximum is a much higher 62.78 t/ha/yr. According to Stone and Hilborn (2012) (table 5-1), who classified soil loss rates into different scales of severity, the mean erosion rate for 1957 falls into the low category. On the other hand, the maximum erosion rate for 1957 exceeds the 33.6 t/ha/yr minimum threshold for the severe category and is thus classified as severe. The standard deviation for this dataset was 10.38 t/ha/yr, which is relatively high when compared to the mean. It further reinforces the fact that the data is dispersed, which can be seen by the large difference between the mean and the maximum. The 1957 histogram (Appendix 3.2) graphically illustrates the distribution of the data, the mean, and the standard deviation. The data is clearly skewed towards 0 with a large majority of the data found between 0-2 t/ha/yr of estimated soil loss. This is in line with the mean value of 7.52 t/ha/yr and with the normality distribution curve.

Moran's I, a spatial autocorrelation test, checks whether values are clustered, dispersed or randomly distributed. It ranges between -1 to 1, with -1 indicating a perfect clustering of dissimilar values, i.e. a negative spatial autocorrelation; 1 indicating a perfect clustering of similar values, i.e. a positive spatial autocorrelation; and 0 indicating a random spatial distribution. With a high Moran's index of 0.8, the data displays a strong positive spatially clustered pattern. This is a reasonable finding as soil erosion is often found in clusters as influencing factors are often located close

to each other. In this case, the valley only has few sudden slope changes, the rainfall erosivity and management factors are constants, and the soil erosivity factor is based on interpolation. These four factors would contribute to the clustering of similar data values in the soil loss estimates. Meanwhile, the C-factor, which is visibly the main spatial influence on the soil loss estimates, has the most potential variance for spatial autocorrelation. However, the high Moran's index suggests that in all, the five factors lead to highly clustered data values. This is expected for soil erosion values as even without the potential variance of the C-factor, the other factors change gradually or not at all. The C-factor itself can also be clustered with fields near each other growing similar crop types. This can be because a certain area is good for growing specific crops due to factors such as water resources, soil type, land ownership, etc.

5.2.3. Analysis for 1978

Spatial Pattern:

The spatial pattern for 1978 is quite different to that of 1957 (figure 4-8), with more dispersion of high erosion values throughout the valley. There is still a general trend where the landward side of the valley is displaying higher erosion levels, however, unlike in 1957 estimates, there is a patch of high erosion values on the northern side of the valley.

Regarding correlation between the different layers and how they affect the final RUSLE values. The R-, and P- factors are again constant throughout the valley for the entire year and so do not offer variation within the year itself. The LS-factor, as in 1957, has minimal visible patterns and so it is difficult to determine its influence. The same K-factor that was used for 1957 was used for 1978. Again, for 1978, there are no obvious visible trends between the K-factor and the final RUSLE values. Higher RUSLE values are still recorded mainly on the landward side of the valley while the K-factor has higher values on the seaward side. Again, it is important to note that variation in the K-factor itself is minimal.

On the other hand, the C-factor for 1978 is much different than that for 1957. The range is still the same between 0-0.5, however, there are much more low values recorded in this year than in 1957. The high C-factor values present are spread out throughout the valley – similar to the high RUSLE values' dispersion. This change in vegetation cover could explain the lower soil loss rates as the C-factor is generally lower. This change in C-factor values could be due to land abandonment, leaving the land fallow, a shift to orchards, and a number of other potential factors.

Descriptive Statistics and Classification:

Table 4-7 shows that the mean and maximum for 1978 are very different than 1957's, which were higher than 1978's. The mean of 1957 was double that of 1978, and the maximum was slightly less than double but still much higher. This shows that 1978

suffered much less erosion than 1957 and even the areas marked in red, which show high erosion relative to the rest of the erosion in the valley in the same year, suffered much less soil losses in 1978.

According to Stone and Hilborn (2012) the data recorded in 1978 can be classified as very low for the mean, as it falls underneath the 6.7 t/ha/yr minimum threshold; and severe for the maximum as it slightly exceeds the 33.6 t/ha/yr minimum (table 5-1). Therefore, while the majority of the valley can be classified as suffering very low or low soil erosion, there are areas which are undergoing severe erosion. Moran's index for the testing of spatial autocorrelation was found to be very high as in 1957 (table 4-8). The index of 0.82 indicates a strong positive spatial autocorrelation – and thus indicates that similar values are grouped together.

Changes with Time:

In comparison with the RUSLE results of 1957, there is less overall erosion in 1978 with both maximum and mean values being lower. There are also less areas experiencing severe erosion in 1978. Similarly to 1957, there are higher erosion values estimated on the landward side of the valley than on the seaward side. However, visually cases of severe erosion look more dispersed in 1978 than in 1957. This could be due to the smaller number of severe cases estimated. According to Moran's I, both in 1957 and in 1978, there was a similar high amount of clustering of soil erosion values.

Figure 5-3 is graphically illustrating the difference in RUSLE estimates of soil loss between 1978 and 1957. The map highlights areas which saw an erosion increase or an erosion decrease during the approximately 20-year time gap. It can be noted that the seaward side of the valley, which suffered less erosion in both years studied in relation to the rest of the valley, recorded mostly minimal reduction or no change in erosion. Meanwhile, the landward side of the valley recorded mostly moderate reduction. Large reductions and moderate increases were present but minimal and dispersed throughout the valley.

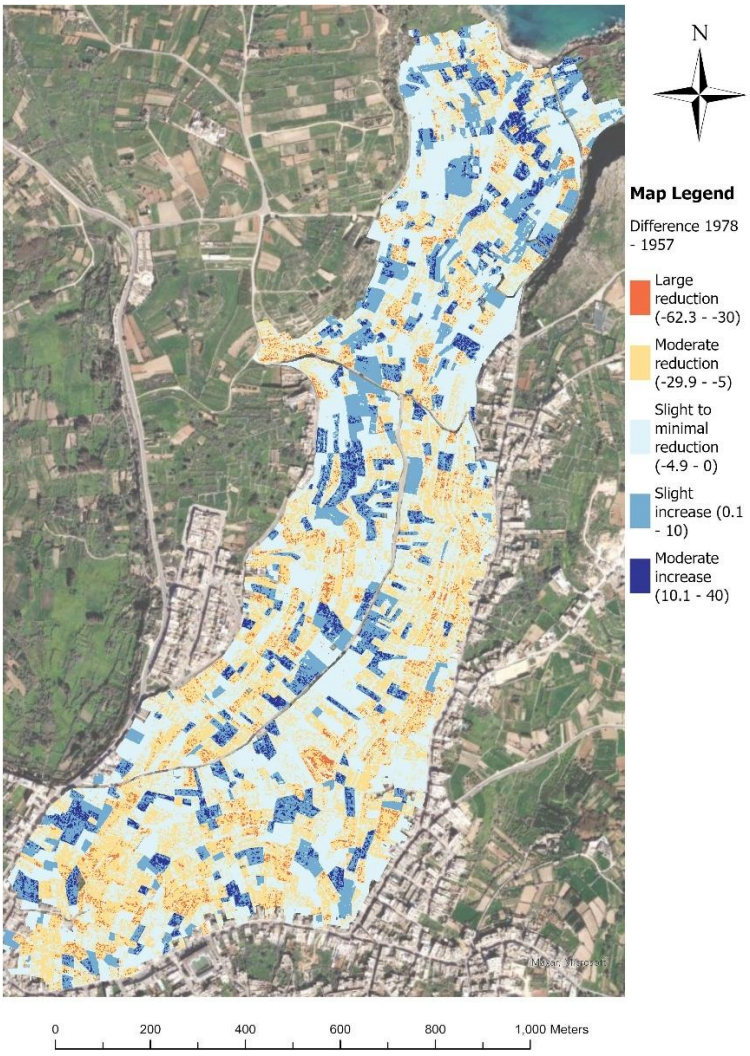

Figure 5-3: Difference Map of Soil Loss Estimates between 1978 - 1957 in t/ha/yr.

A major reason behind the decrease in soil loss can be attributed to the R-factor. The R-factor is the same throughout the valley for the entire year, but it changes annually. The R-factor in 1957 is 880 MJ mm ha^{-1} hr^{-1} yr^{-1} while in 1978 the R-factor decreased to 545 MJ mm ha^{-1} hr^{-1} yr^{-1}. This change is likely to have occurred due to a decrease in precipitation in 1978 and in the 3 years prior, which are used to calculate the R-factor. In fact, total rainfall in the 4-year period for 1957 is 2725.62 mm while the total for the 4-year period for 1978 is 2242 mm. Since the R-factor is multiplied with

the other factors in the RUSLE equation, a decrease in its value will result in a decrease in the final RUSLE result, if all other factors were constant. This means that while it is a contribution to the final RUSLE, it is not the only change. The K-, LS-, and P-factors are kept constant throughout the years studied, but the C-factor is not. Visibly, there is a drastic change in the C-factor (figures 4-7 (b) and 4-8 (b)). Both maps have the same range of values with a maximum of 0.5, but in 1957 there were many more instances where the maximum was reached than in 1978. This can be seen as the map for 1957 has a lot more white – the colour of the maximum – than the map for 1978. Given that only the C- and R-factors are contributing to change between different years, this change in the C-factor is likely to also be a contribution to the decrease in RUSLE values.

5.2.4. Analysis for 1988

Spatial Pattern:

The spatial pattern of soil loss estimates in 1988 is more similar to that of 1957 than that of 1978 (figure 4-9). Soil erosion is higher on the landward side as in both 1957 and 1978, but there are many more cases where soil erosion reaches higher values. Soil erosion is also highly concentrated closer to the valley floor on the landward side of the valley. It is imperative to investigate the individual factors which affect the RUSLE soil loss estimate to help in understanding the variation occurring within the valley within the same year, as well as between years. As in 1957, the C-factor in 1988, shows more areas with high values of 0.5 than in 1978. However, there are still

more areas with lower C-factor values than in 1957. The C-factor in 1988 also shows a general trend of higher values on the landward side of the valley, although there are exceptions. This could be due to the fact that the landward side of the valley has a gentler slope than the seaward side and so is used more for agricultural production. This would increase the C-factor as seasonal crops have a higher C-factor value than trees and especially more so than abandoned land. Tillage of agricultural fields further increases the C-factor value. It is particularly noteworthy that the floor of the valley on the landward side has a high C-factor value and is in fact represented in white – meaning the C-factor is 0.5. This is interesting because the RUSLE output at this spot recorded some relatively high values.

Descriptive Statistics and Classification:

Table 4-7 shows the mean and maximum soil loss rates for 1988 to be much higher than those of 1978 and are in fact, more similar to the descriptive statistics of 1957. This could explain why the soil loss map for 1988 at first glance looks much more similar to that of 1957, rather than that of 1978. Regarding soil erosion classification, according to Stone and Hilborn (2012) (table 5-1), the mean soil erosion rate for 1988 falls in the low category. However, since the maximum is 58.07 t/ha/yr, this is more than the 33.6 t/ha/yr minimum threshold and so it needs to be classified into the severe category. These are the same categories that the mean and maximum of 1957 were classified in. On the other hand, the mean for 1978 was classified into very low or tolerable soil erosion, while 1978's maximum soil erosion was still classified into the severe category. Table 4-8 shows Moran's I to be 0.8. This is in line with the

findings for spatial autocorrelation of 1957 and 1978, and indicates a strong positive spatial autocorrelation, showing that in the dataset, similar values are grouped together.

Changes with Time:

When comparing with other years, visually the map of soil estimates of 1988 looks very similar to that of 1957. The R-factor for 1988 is 814 MJ mm ha^{-1} hr^{-1} yr^{-1}, slightly less than the 880 MJ mm ha^{-1} hr^{-1} yr^{-1} of 1957. Despite this, total rainfall in the 4-year period is much less than that of 1957, with 1988 having only 2190.7 mm of rainfall as compared to 1957's 2725.62 mm. The higher R-factor could be one of the contributors to the higher RUSLE output. The other time-varying factor is the C-factor. As aforementioned, the C-factor for 1988 is generally higher with the map displaying much more white values, which represent the maximum of 0.5.

5.2.5. Analysis for 1998

Spatial Pattern:

The values for soil loss estimates for 1998 can be found in figure 4-10 (a), with a spatial pattern slightly similar to that of figure 4-8 (a), which displays the soil loss estimates for 1978. As with all the years studied before, the landward side of the valley is seen to suffer more from erosion, with the seaward side of the valley having less instances of high erosion estimated. Regarding hotspots (figure 5-4), the most obvious concentration of high erosion values lies in the centre of the valley, on the

landward side, near the valley floor (A); and on the landwards western side (B). In general, visibly high erosion hotspot areas are not as frequent as in 1957 and 1988.

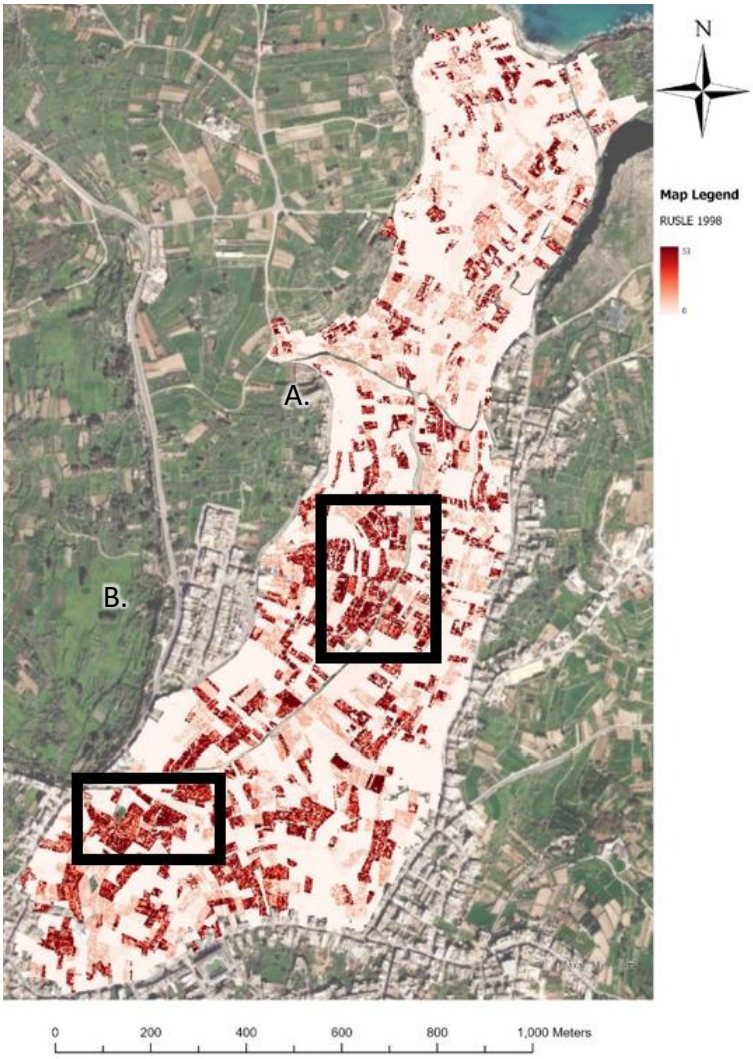

Figure 5-4: 1998 Soil Loss Estimates Hotspot Areas.

As with other years, the R- and P-factors are constant throughout the valley, while the LS- and K-factors do not visibly show enough direct correlation to the RUSLE output map. While all these factors still affect the soil loss rates calculated by the RUSLE in some way, the final output map visibly looks similar pattern-wise to the map displaying the C-factor. In fact, 1998 was another year where the C-factor values in

the valley seemed to be generally lower than the values of 1957 and 1988. Large areas of uninterrupted high C-factor values are not visible and instead looking at the map you notice a lot of green – the symbology used to represent low C-factor values. In fact, areas which are showing a C-factor value of 0.5 (the maximum), are showing high RUSLE values, while areas displaying low C-factor values are found to have low RUSLE soil loss values.

Descriptive Statistics and Classification:

The mean soil loss over the AOI in 1998 is slightly higher than the mean soil loss in 1978, but lower than the mean soil loss of 1957 and 1988 (table 4-7). This is in line with the visual observations from figure 4-10 (a) which clearly shows less high erosion areas, with the map being much paler in colour – symbolizing lower erosion values. However, the maximum soil loss for 1998 is very similar to that of 1988, only slightly less, but quite higher than the maximum soil loss of 1978. This suggests that while there are less high erosion areas, these areas still have a relatively high soil erosion rate. It is important to note that while the maximum of 1998 is relatively high, it is still 10 t/ha/yr lower than the maximum soil loss rate of 1957. The mean value of 4.46 t/ha/yr falls into the very low (tolerable) soil loss classification. Meanwhile, the maximum value falls once again into the severe classification class. This is the same classification as that obtained by 1978. So far, soil erosion over the AOI is seemingly fluctuating with time. The Moran's index for 1998 is 0.83 (table 4-8), indicating a strong positive spatial autocorrelation, thereby meaning that similar values are clustered together.

Changes with Time:

When compared with previous years studied, the C-factor values map of 1998 (figure 4-10 (b)) is quite similar to that of 1978 (figure 4-8 (b)). An important difference between them is that while figure 4-8 (b) is mainly divided into white (high C-factor), green (moderately low C-factor), and dark green (low C-factor), figure 4-10 (b) also has many areas under a light green colour scheme, representing moderately high C-factor values. This means that some high erosion areas had a decrease in erosion, but some moderately low or low erosion areas had an increase in soil erosion. Meanwhile, the R-factor, the only other annually changing factor, was calculated to be 738 MJ mm ha^{-1} hr^{-1} yr^{-1}. This is lower than both 1957's and 1988's R-factors, but higher than 1978's relatively low R-factor. This could also have contributed to the general trend of more or less erosion on this specific year being studied. The total rainfall for the 4-year period used for 1998's R-factor is 2557.5 mm, higher than 1978's and 1988's rainfall totals. This shows that the R-factor is not only affected by the rainfall amount, but also by other factors such as rainfall intensity.

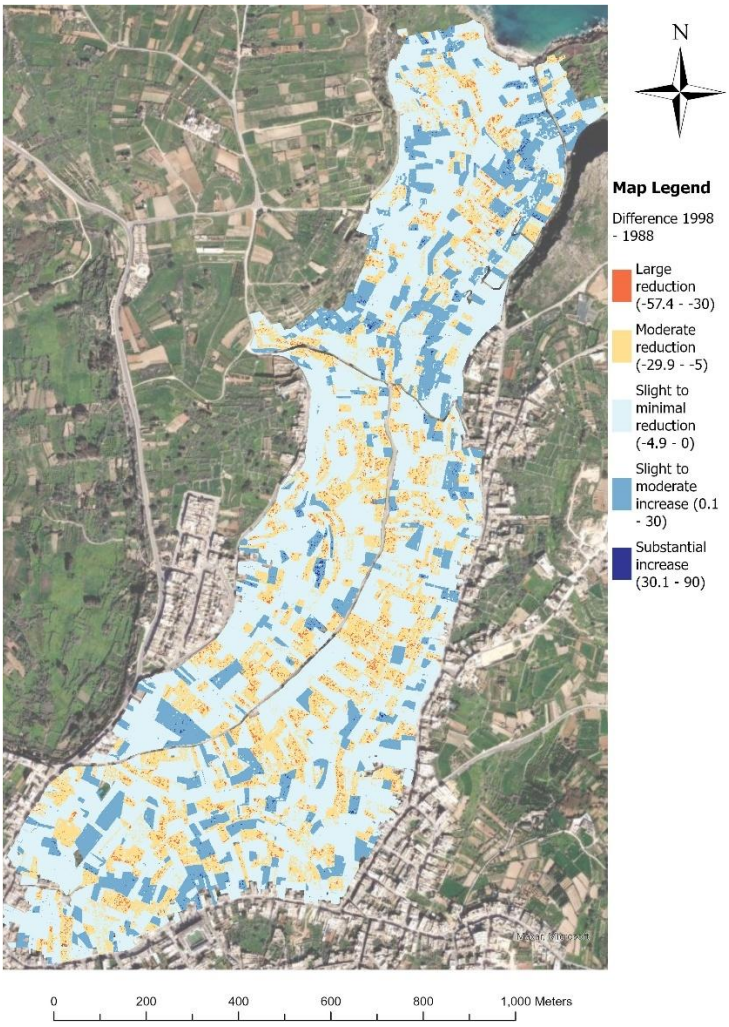

Figure 5-5: Difference Map of Soil Loss Estimates between 1998 – 1988 in t/ha/yr.

Figure 5-5 is a difference map between 1998 and 1988, and it serves to highlight areas which had a shift in erosion during this 10-year time period. This specific 10-year period was chosen as it is in the middle of the whole study period between 1957-2021 and hence it can provide a glimpse into the changes occurring in the middle of the study. The map suggests that a lot of the valley underwent minimal changes in the 10-year period under study in this map. However, erosion increase, and erosion decrease are also both detected in this timeframe, with areas undergoing such changes being dispersed throughout the valley. It can be noted that the seaward side

of the valley had more areas undergoing erosion increase than the central part of the valley which had mainly erosion decrease.

5.2.6. Analysis for 2004

Descriptive Statistics and Classification:

The mean soil loss in 2004 was quite low and is very similar to that of 1978, with only 0.3 t/ha/yr of difference. The maximum is also quite lower than 1998's and 1988's. It is instead only slightly higher than in 1978 (table 4-7). These values mean that there is less erosion in 2004 than in most of the years studied, apart from 1978. Figure 4-11 (a) shows that there are quite a few low erosion areas, and the lower maximum shows that even high erosion areas do not suffer as much erosion as high erosion areas in previous years such as in 1988. The lower mean also suggests the decrease in erosion which occurred in 2004.

With a mean of 3.85 t/ha/yr, the mean soil loss rate of 2004 can be classified as very low or tolerable since it is lower than the 6.7 t/ha/yr maximum threshold of the category. The maximum fits into the severe category as it is higher than 33.6 t/ha/yr. These are the same categories obtained by soil loss in 1998 and 1978, two years where soil erosion estimates were relatively lower than of other years studied. The spatial autocorrelation test Moran's I resulted in a strong positive spatial autocorrelation and the presence of clusters in the data – just like in previous years.

Changes with Time:

When compared with other C-factor maps, 2004's is possibly the greenest. 1978 has many dark green areas (low), but it also has a good number of white areas (high) and essentially no light green areas (moderately high). 1998 seems to have quite a few areas with a moderately high C-factor but 2004 seems to have more areas with a low C-factor while many areas which in 1978 were white (high), in 2004 they are light green (moderately high). While moderately high is not the optimal C-factor, it is still lower than high C-factor values and thus it can lead to lower soil erosion estimates.

The R-factor is the other factor which affects variability over the years. 2004 had a calculated R-factor of 617 MJ mm ha^{-1} hr^{-1} yr^{-1}. This is lower than all the other year's R-factor except 1978's, and it can explain why the descriptive statistics of 2004 are in general higher than 1978's but lower than all the other years studied. The total amount of rainfall over the 4 years considered for the calculation of the R-factor is 2154.30 mm. This is a lower rainfall total than all the previous 4-year timeframes, however, it is important to note that rainfall totals are not the only thing which influence the R-factor. In fact, while 1978 has a higher rainfall total over the 4 years, it has a lower R-factor than 2004.

5.2.7. Analysis for 2018

Descriptive Statistics and Classification:

These values in table 4-7 are the lowest values recorded for the mean, maximum, and standard deviation of all the years studied so far. The low maximum means that the high values seen in figure 4-12 (a) are still relatively low when compared to the high values of other years. In fact, the maximum of 2018 is almost half that of 1957. The mean is also very low, being more than half the mean of 1998, which was an already relatively low mean. Overall, it can be said that 2018 suffered less estimated erosion than other years due to the lower descriptive statistics, and the relatively paler map showing lower values (as white means low soil erosion). It is important to note that there are still quite a few hotspots where erosion reaches the highest values of around 30 t/ha/yr.

Due to the lower mean and maximum for 2018, the classification is different from that of other years studied so far. The very low mean of 2.12 t/ha/yr falls into the very low or tolerable soil erosion rate while the maximum of 32.03 t/ha/yr is just under the 33.6 t/ha/yr threshold of the severe category, thereby falling instead into the high soil loss rate. This is the only year studied so far which had a maximum in any category but the severe one. For 2018, the global Moran's test obtained an index of 0.85 (table 4-8). This means the data has strong spatial clustering and data points of similar values are found near each other.

Changes with Time:

The C-factor map for 2018 is another map which is largely coloured in green. Whilst there are still some hotspots of high C-factor values in white on the landward side, as well as a few spots on the seaward side, there is a much greater area of dark green (low), especially when compared to previous years. The seaward side also has many areas represented in green (moderately low). This change in C-factor throughout the years could potentially be due to an increase in land abandonment or in the switch in agriculture from crop production to fruit tree and citrus cultivation. Another potential change could be a reduction in tillage operations – such as ploughing less underneath tree cultivation.

The R-factor is the other variable which changes with time. For 2018 the R-factor was calculated to be 449 MJ mm ha^{-1} hr^{-1} yr^{-1}, while the rainfall total was 1631.2 mm. This makes the 4-year period used for 2018 relatively dry, with none of the years included (2015-18) being extremely wet. In fact, none of the years even reached 500 mm, which is Malta's annual average. While the R-factor is not only affected by the rainfall amount, it is still one of the factors influencing it, therefore the R-factor is understandable lower. This is actually the lowest R-factor of all the years studied so far. The lower R-factor is also a good explanation as to why the RUSLE outputs of 2018 were in general lower than all of the other years.

5.2.8. Analysis for 2021

Spatial Pattern:

The results in figure 4-13 (a) are quite different from the soil loss results of other years. The seaward side of the valley suffers more erosion than in other years. Otherwise, the erosion is mainly focused on the valley floor. Figure 5-6 shows the location of the soil loss estimates hotspots in the AOI. These hotspots could arise because of a number of reasons, including higher accessibility leading to more tillage and crop cultivation; steeper slopes on the seaward side of the valley; etc.

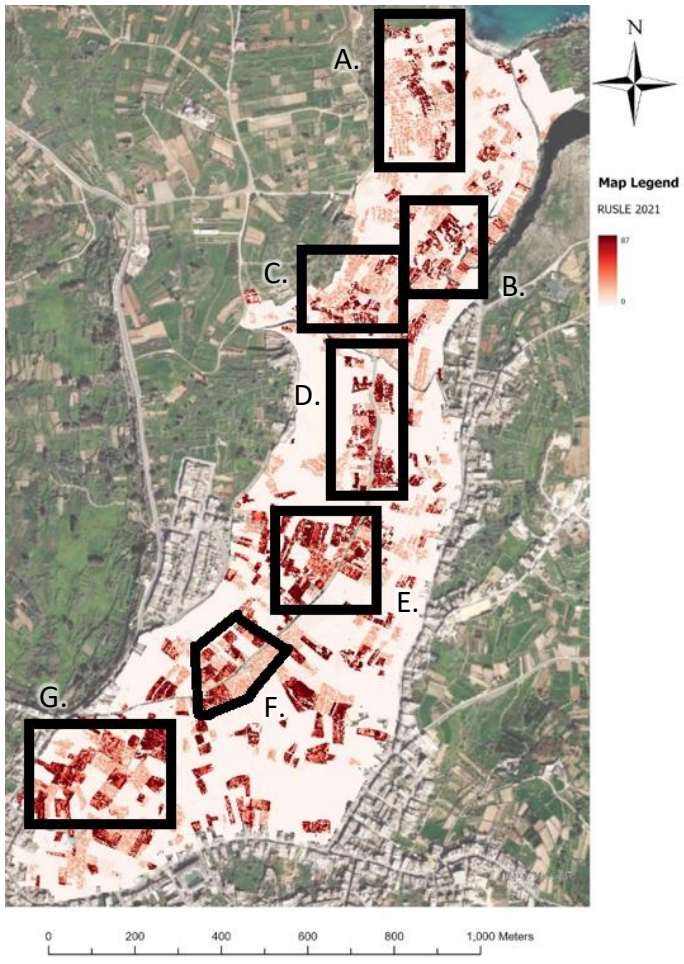

Figure 5-6: 2021 Soil Loss Estimates Hotspot Areas.

Descriptive Statistics and Classification:

The descriptive statistics in table 4-7 are also a bit different than other years'. The mean erosion is similar to other years which had relatively low erosion rates, however, the maximum soil erosion was estimated to be 87.01 t/ha/yr. This is a very large difference from the other years. It is the highest estimate, but even when compared with the second highest estimate of 1957, it is still over 20 t/ha/yr more. This means that caution must be taken when looking at the map in figure 4-13 (a) as red areas have much higher erosion estimated than those highlighted in the same colour for previous years. It also means that while some areas are highlighted in pink and may seem like they have moderately high erosion, in reality, these values would be about 30 t/ha/yr. This is still a lot, especially when considering that some of the previous years studied had maximums close to 30 t/ha/yr. An area which is coloured in this way is the majority of the seaward side of the valley – thereby showing that there was an increase in erosion here when compared to earlier years. The low mean, however, suggest that maximum values are minimal. The high abundance of pink on the map further reinforces this as most areas are not experiencing the maximum soil erosion estimated.

Regarding classification of the soil erosion taking place, the mean soil erosion rate can be classified into the tolerable or very low category as it is less than 6.7 t/ha/yr. The maximum soil loss rate needs to be classified into the severe category as it far exceeds the 33.6 t/ha/yr threshold. This is the same classification as 1978, 1998, and 2004, however, it is important to note that despite this, the maximum of 2021 is far

higher than that for any of the other years. The results for the spatial autocorrelation test indicate a Moran's index of 0.85 (table 4-8), suggesting the presence of spatial clustering of the data values, where similar values are more likely to be found near to each other.

Changes with Time:

The C-factor map in figure 4-13 (b) was visually inspected to determine if and how the C-factor is affecting the results of the RUSLE equation in terms of variation within the valley within the same year. The first important aspect to note is that the legend of the C-factor is different for 2021 than for other years. The legend's scale for other years ranges between 0-0.5, however, for 2021 it ranges between 0-1. This means that areas represented by white in 2021 have a much higher C-factor value than the ones represented by white in other years. Despite this change in scale, there are still a lot of areas which are represented by green, especially on the seaward side of the valley. While the higher range of C-factor values compliments the higher maximum of the final RUSLE, the abundance of green areas reflects the low frequency of maximum values and the low mean. Regarding the R-factor, the value of 753 MJ mm ha^{-1} hr^{-1} yr^{-1} is quite high, albeit not the highest of the R-factors calculated for the previous years studied. The total rainfall was 2050.2 mm for the 4-year time period used for the R-factor calculation. This is lower than all the other years' studied totals, except for 2018. This is an example of how the R-factor is not just based on rainfall totals, but also on rainfall intensity.

Two difference maps were created for 2021. One looks at the difference that occurred between 2004 and 2021 – aimed at catching a glimpse of the changes of the past 20 years; the other, figure 4-14, looks at the difference between 1957 and 2021 and is discussed in section 5.2.1. Figure 5-7 (2021 – 2004) investigates the soil erosion changes which occurred with time in recent years. A 20-year timeframe was used to see long-term changes. At first glance, the map displays many areas undergoing erosion increase. The seaward side of the valley is particularly interesting as it is shown to suffer mainly from slight erosion increase but also some moderate erosion increase and moderate decrease in other areas. It is important to mention that the slight increase category, which is categorizing the vast majority of the valley, is an increase between 0.1 and 5 t/ha/yr. The landward side of the valley saw more areas with minimal change than the seaward side, however, it also saw areas of substantial erosion increase. This is a category which is showing areas which had an increase of erosion between 30.1 and 90 t/ha/yr. In fact, these are areas which in 2021 showed some of the highest erosion rates. In general this map illustrates a pattern of slight erosional increase in the past 20 years in the AOI. This is an important aspect to the study as it reveals that while there is a general trend of erosion decrease, the past 20 years have deviated from this, and soil erosion is seeing an increase again. It is important to note that since statistical tests were not conducted, statistical significance is unknown, and results are simply based on visual observation of the maps and the soil erosion rates.

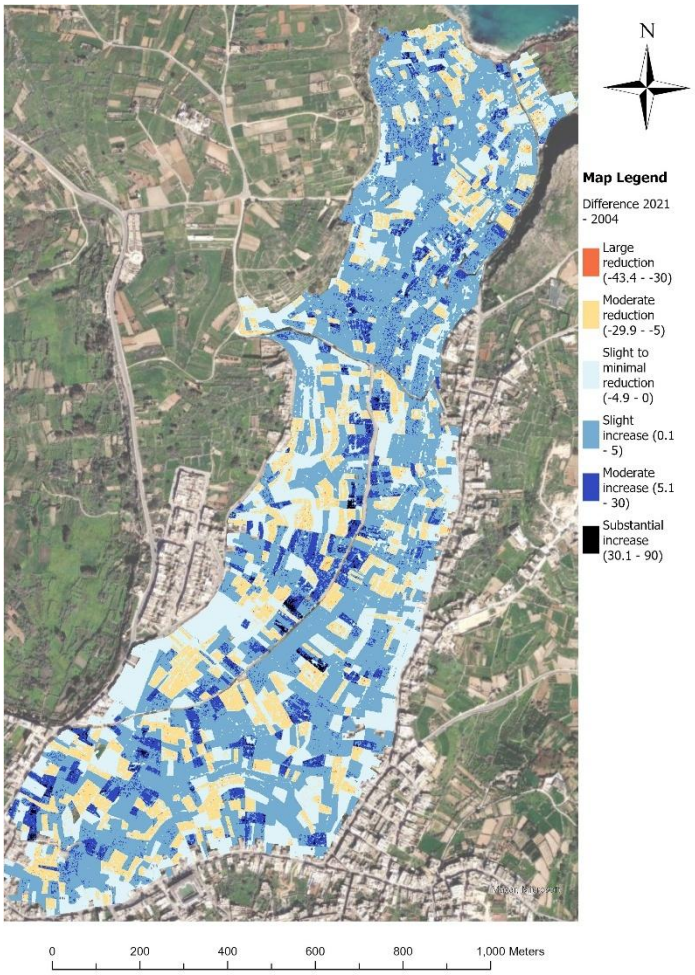

Figure 5-7: Difference Map of Soil Loss Estimates between 2021 - 2004 in t/ha/yr.

5.3. Future Soil Loss Predictions

The third aim of the study was to predict future soil losses over the AOI for 2050 under SSP 2-4.5 and SSP 5-8.5. This was achieved using rainfall data from CMIP6 models to predict an R-factor for the future, NDVI calculated through Landsat imagery, and proxies for future NDVI estimates from Copernicus Climate Data Store to estimate a future C-factor. A second method was also used to achieve a spatially varying C-factor – the spatial method. This used the past NDVI to estimate NDVI change over the years and apply the same rate to the future. The other factors in the RUSLE equation were kept the same as those used for the past as it was determined that the K- and LS-factors do not undergo many changes on the short-term, and the P-factor is very difficult to determine for the future due to its being based on many managerial components, which in turn rely on several other factors.

5.3.1. 2050 SSP 2-4.5

Descriptive Statistics and Classification:

Table 4-9 shows us the descriptive statistics for future soil loss predictions. The mean soil loss rate is in line with low soil erosion rates estimated for past years, with 2018 even having a slightly lower mean estimated. However, both the maximum and the standard deviation are much lower for the 2050 SSP 2-4.5 prediction than they were in any of the past years studied. The low maximum can be the result of smoothing of extreme values in climate models which in turn affect the R-factor. This was evident

when analysing the CMIP6 data and calculating the R-factor – storm events were not visible in the data despite these being very important to soil erosion and being relatively common in Malta. The removal of storm-related values can lower the maximum as less erosion is taking place as these storms often result in high amounts of soil loss.

Regarding the classification of the mean and maximum soil erosion estimated, the mean falls into the very low or tolerable category while the maximum falls into the low category. This is in contrast with the category of the maximum for all the past years. The category was always severe, except for one instance where the category was high – with the 2050 SSP 2-4.5 estimate the maximum soil erosion prediction has been lowered so much that it completely skips the moderate category between high and low. Moran's index for this dataset is 0.66 (table 4-10) meaning that while the correlation is less strong than that of the past years, a positive autocorrelation is still present – therefore there is less, but still present, clustering of similar values.

Spatial Pattern:

The R-factor for the future predictions is not constant throughout the valley, however, it has only little variation. It ranges between 341-353 MJ mm ha^{-1} hr^{-1} yr^{-1}, which is a range quite lower than R-factors calculated from past rainfall data. This is most likely due to the lack of storm events modelled in the CMIP6 data, which unfortunately, is a limitation of the study. The general trend of the R-factor is that it

is slightly higher on the landward side of the valley. The C-factor is calculated through regression between specific humidity, air temperature, and NDVI. Unfortunately, the specific humidity and air temperature datasets are too coarse to give any variation to the C-factor within the same year. The variables used in the regression, the resulting NDVI, and the calculated C-factor for the entire valley for 2050 SSP 2-4.5 can be seen in table 5-2. It is a huge oversimplification to have only one NDVI value for the entire study area, however, this is another limitation of the study as the only data available was too coarse. However, an NDVI value of 0.455 indicates moderate vegetation, which is a logical conclusion for the state of the valley. A C-factor of 0.188 is relatively low. For comparison purposes, fruit trees and citrus have a value of 0.1 in past estimates while seasonal crops have a value of 0.5. It is important to remember that this value is multiplied by the tillage factor to obtain the C-factor. Tilled fields have a factor of 1.0 while untilled fields have a factor of 0.25. This means that seasonal crops have a C-factor value of 0.5 as they are often tilled while abandoned plots (0.02) have a C-factor value of 0.005, as they are untilled.

Table 5-2: Regression Variables, Resulting NDVI, and C-factor for 2050 under SSP 2-4.5 over the Entire AOI.

	2050 SSP 2-4.5
Air temperature	292 K
Specific humidity	0.01052 kg/kg
NDVI	0.455
C-factor	0.188

The spatial variation of figure 4-15 (a) is difficult to decipher and visually, it seems to mimic the pattern of the LS-factor (Appendix 2.4). This would be understandable as the past estimates seemed to follow the C-factor's spatial pattern, but the future predictions have only one C-factor for the whole valley and thus cannot do this. The P-factor is also a constant for the whole valley and thus does not offer spatial variation. The K- and R-factors have little variation within the same year and this variation does not seem to be visible in figure 4-15 (a). This means that not many patterns or trends emerge for easy visualization through the map.

Changes from 2021:

The lack of an easy decipherable spatial pattern also means that upon visual comparison with the past estimates' maps, such as that of 2021, it is difficult to see where the changes occurred. It is important to note that the range of values is much lower and thus there were definitely changes in the hotspot areas of 2021. Upon creating an actual difference map between 2050 SSP 2-4.5 and 2021, the changes that occurred became much more evident (figure 5-8). The landward side of the valley shows mainly a slight increase in soil erosion values (up to 10 t/ha/yr), however, there are also quite a few areas which underwent erosion reduction, including substantial reduction of up to 60 t/ha/yr on the hotspots of 2021. The seaward side of the valley also had some increases in erosion, especially in the northernmost part. However, it is also predicted that it will undergo slight decreases in erosion and in some cases even moderate decreases.

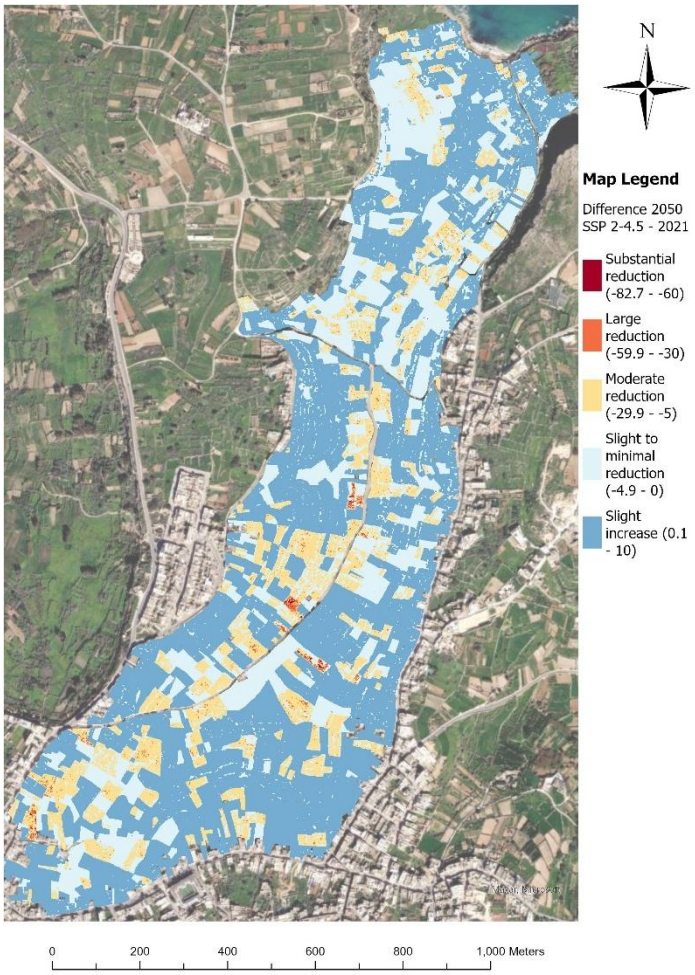

Figure 5-8: Difference Map of Soil Loss Estimates between 2050 SSP 2-4.5 - 2021 in t/ha/yr.

These changes are highly likely to be due to the R-factor as this was the biggest change that the soil loss predictions underwent. The smoothing of climate data removed rainfall extremes and created a much lower R-factor, which in turn would create lower soil loss predictions as it would consider rainfall to be less erosive – from both a rainfall total and a rainfall intensity aspect, as the R-factor includes both. However, it is unlikely that it is the only affecting factor which caused the major changes between the 2050 predictions and the 2021 estimates. The C-factor also had major changes, even being calculated in a different way. A C-factor of approximately

0.2 is quite low, since this value was used throughout the AOI, it could have lowered the soil erosion predictions as well. The other factors were kept as in 2021 and thus are not influencing the change which occurred.

5.3.2. 2050 SSP 5-8.5

Descriptive Statistics and Classification:

Erosion estimates for 2050 were created also under SSP 5-8.5. The predictions in table 4-9 are the lowest values obtained throughout the entire study – even lower than those for SSP 2-4.5, which had quite low values. The very low maximum reflects the lack of storm data found in the CMIP6 models. This contrasts with the expectations of climate change which is expected to increase the frequency of heavy-precipitation storms in many parts of Europe, among other impacts (Ciarlo et al. 2017; Stocker et al. 2013). Extreme storms are especially bad for soil erosion, especially if the soil was very dry beforehand from lack of rainfall as this leads to surface sealing (Wang et al. 2020; Ran et al. 2012). However, since extreme storms are not visible in the CMIP6 data used, such predictions of soil erosion from extreme storms are not present in this study. The mean soil loss rate for SSP 5-8.5 shows how generally, in the AOI, soil erosion will keep falling, which is in line with the trendline of figure 4-17.

Regarding classification of the mean and maximum soil erosion values. Both the mean and maximum soil loss rates fall into the tolerable or very low category of soil loss. This is the only instance where the maximum soil loss rate is categorized as very low. Table 4-10 displays a Moran's I of 0.85, a result that is very similar to the results of the past estimates, indicating that data is clustered, with data points of similar values grouped together – just like in past estimates.

Spatial Pattern:

Variations within the year must come from the R-, K- or LS-factors as the C- and P-factors are constant throughout the valley. The R-factor has little variation, ranging from 333 to 344 MJ mm ha^{-1} hr^{-1} yr^{-1}; and the K-factor has even less variation, ranging from 0.091 to 0.1 t ha hr ha^{-1} MJ^{-1} mm^{-1}. The spatial variation visible in figure 4-15 (b) likely occurs from the LS-factor (Appendix 2.4), making variation difficult to decipher from visual observation alone.

Regarding variation between the different SSP scenarios, the range of the R-factor of SSP 5-8.5 is lower than that of SSP 2-4.5, but it is spatially similar with the landwards side of the valley having a slightly higher R-factor value. The C-factor is a constant for the whole valley but unlike the K-, LS- and P-factors it varies between scenarios and different years. Table 5-3 displays the regression variables, NDVI, and C-factor for 2050 SSP 5-8.5. The air temperature is very similar under both scenarios with only a 0.3 difference; and the specific humidity is slightly higher under SSP 5-8.5. The

resulting NDVI from the regression equation was higher than that of SSP 2-4.5 indicating slightly denser vegetation – moderate to high vegetation cover. This contrasts with the expected increase of drought-like conditions. The C-factor obtained is very low – only slightly higher than the C-factor value for untilled soil underneath tree cultivation. Such a low C-factor value, coupled with the relatively low R-factor, is an understandable reason why such low soil erosion values were obtained from the RUSLE equation.

Table 5-3: Regression Variables, Resulting NDVI, and C-factor for 2050 under SSP 5-8.5 over the Entire AOI.

	2050 SSP 5-8.5
Air temperature	291.7 K
Specific humidity	0.01093 kg/kg
NDVI	0.57
C-factor	0.068

Changes from 2021:

A difference map of 2050 SSP 5-8.5 – 2021 (figure 5-9) was created to help in visualizing the changes which are predicted to occur. This map is very similar to figure 5-8, the difference map for SSP 2-4.5 – 2021. Figure 5-9 shows mainly a slight increase in erosion, however, hotspot areas in 2021 are predicted to undergo minimal to substantial decrease in erosion. These areas are mainly found along the valley floor

and on the seaward side of the valley. So far, the trends suggest that erosion will be more uniform throughout the valley with less extreme maximums. It is, however, of utmost importance to consider the limitations of using CMIP6 data and its implications, as well as any other limitations of this study when interpreting the trends and patterns of the predicted soil erosion.

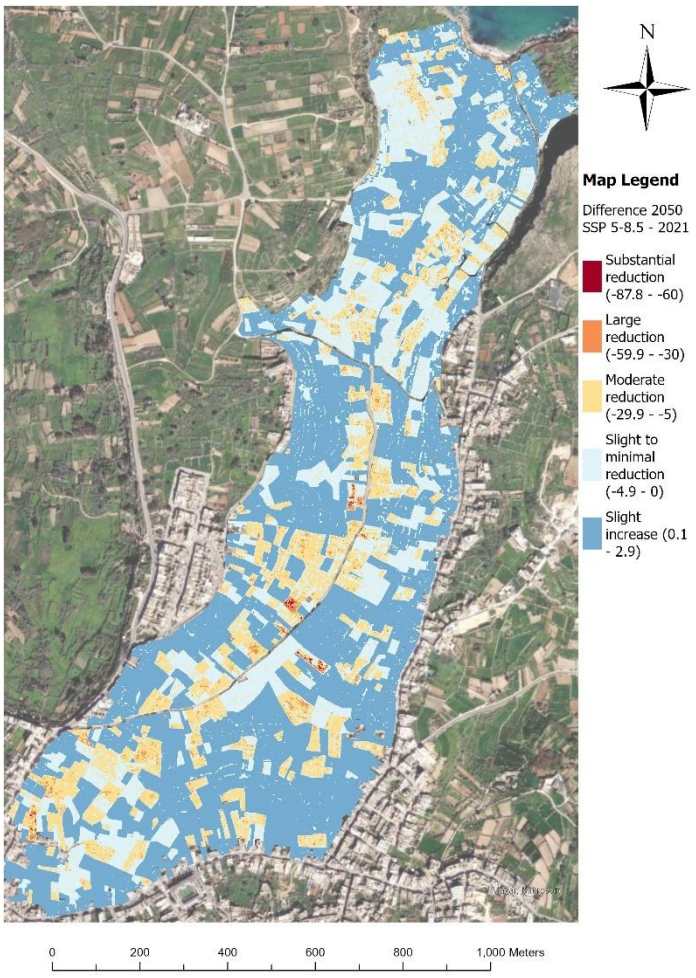

Figure 5-9: Difference Map of Soil Loss Estimates between SSP 5-8.5 - 2021 in t/ha/yr.

Time Series Plots:

Figures 4-17 and 4-18, the time series plots display the mean and maximum soil erosion values for past soil estimates, SSP 2-4.5, and SSP 5-8.5. Figure 4-17 illustrates how the mean soil erosion rate will continue to decrease in 2050 – following the trend that was calculated for past estimates. The mean for SSP 5-8.5 is seen to be much lower than that of SSP 2-4.5, being in fact the lowest mean on the graph. Figure 4-18 displays the time series for the maximum soil loss, revealing the large difference the maximum soil loss values have between past estimates and future predictions. The future predictions are much lower than the past estimates, with SSP 5-8.5 being even lower than SSP 2-4.5. This means that they do not follow the trend based on past data where maximum values were seen to slightly increase over time. This trendline could be the result of both outliers and a small sample size, while future predictions also suffer from the data limitations of future rainfall predictions from climate models. These limitations are likely to be the reason for the large discrepancy between the maximums of the past estimates and the future predictions.

5.3.3. Spatial Method

The spatial method was conducted because the non-spatial method results in only one C-factor for the whole valley, and it has resulting soil loss maps which lack a simple decipherable pattern. The method considers NDVI in 1991 and in 2021 and calculates the rate of change. This rate is then applied to 2050 to determine NDVI per pixel. While this method considers variation of NDVI within the valley, it does not

consider the influence the changing rainfall pattern has on the vegetation – which is why the non-spatial method was also conducted.

Spatial Pattern:

The soil loss estimates obtained from the spatial method are in figure 4-16 (a) for SSP 2-4.5, and (b) for SSP 5-8.5. Both scenarios have very similar looking soil loss maps with hotspots located at the top of the hillslopes and on the valley floor on the landward side of the valley, with very little high erosion values on the seaward side.

Using the NDVI for 2021, a map for 2021 soil loss estimates was also created. This is for direct comparison purposes with soil loss estimates from fieldwork data to determine if NDVI can also accurately determine soil erosion hotspot areas. Figure 5-10 displays the soil loss estimates for 2021 using NDVI (a) adjacent to the soil loss estimates for 2021 using fieldwork data (b). Visually, the maps are seen to be relatively similar, with many hotspots being visible on both maps, despite slight differences. The locations are more or less the same for all the hotspots with the exceptions of sites F and G, which include the entire slope all the way to the top of the valley in the NDVI estimate; and site H, which includes only the top of the slope in the NDVI estimate. Another difference is that the NDVI estimate included much of the top of the slope as a hotspot as well.

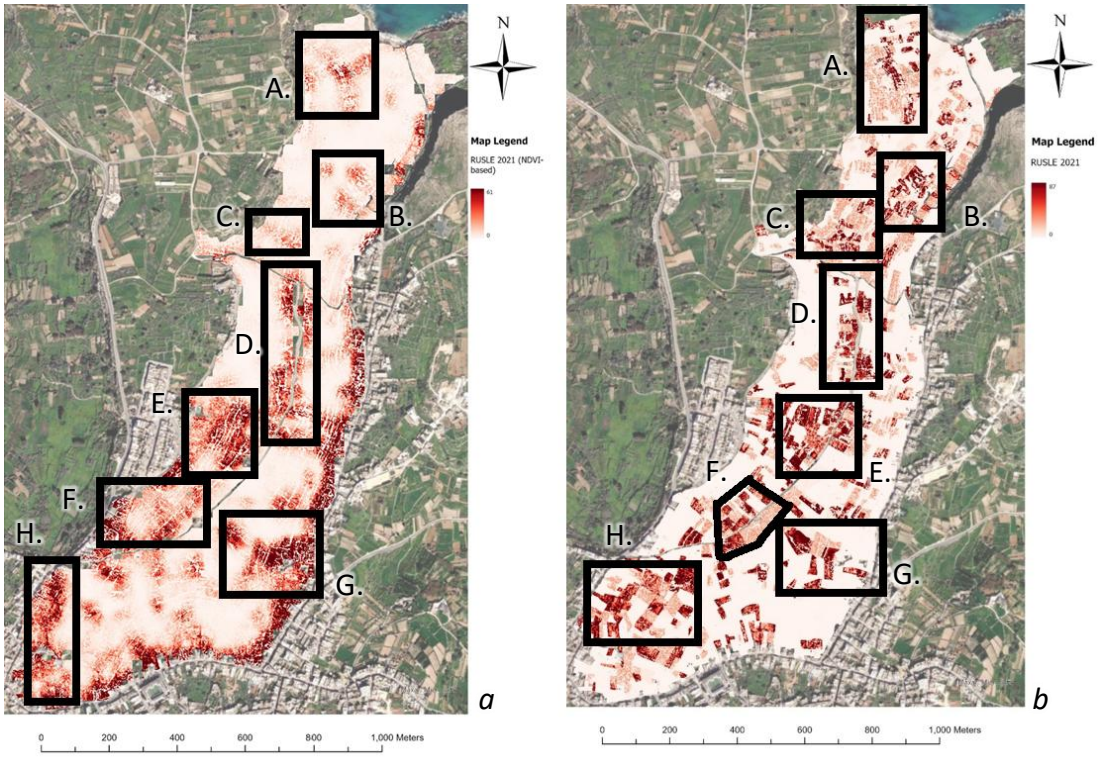

Figure 5-10: Hotspot Location Comparison for 2021 between (a) the NDVI-Derived Soil Loss Estimates, and (b) the Fieldwork-Derived Soil Loss Estimates.

The two SSP scenarios have similar spatial patterns together and with that of 2021. This is likely to be because the spatial pattern seems to be influenced by the C-factor, which is based on the NDVI. Since the NDVI is adjusted for the future according to the rate of change in NDVI between 1991-2021, for 2050 both scenarios share the same NDVI map. This means that the only change they have between them is the R-factor, which undergoes only little variation.

Descriptive Statistics and Classification:

It is important to note that while the non-spatial method resulted in soil loss maximums of 9.21 t/ha/yr and 3.26 t/ha/yr, the spatial method resulted in maximums of 39.07 t/ha/yr and 38.17 t/ha/yr for SSP 2-4.5 and SSP 5-8.5 respectively. These maximums are more in line with the results of the past soil loss estimates – showing generally lower, but still similar results to the past estimates. This is also seen in the 2021 estimates, where NDVI-derived estimates have a maximum of 60.8 t/ha/yr while fieldwork-based estimates have a maximum of 87.01 t/ha/yr. The mean for 2021 NDVI-derived estimates is 2.5 t/ha/yr – a value similar to the 3.51 t/ha/yr mean of the fieldwork-derived estimates. The means for SSP 2-4.5 and SSP 5-8.5 are 0.9 t/ha/yr and 0.88 t/ha/yr respectively. The SSP 5-8.5 mean values for spatial and non-spatial methods are very similar, unlike the means for SSP 2-4.5. When classifying the mean soil loss estimates, the spatial method values can be classified similarly to the non-spatial method, with the means for both SSP scenarios falling in the very low or tolerable category but both maximums fall in the severe category. These values, which are more in line with past estimates, could be because the effect of the change in rainfall on vegetation is not being considered, and therefore the C-factor is more like that of the past estimates. This is not realistic as reduced rainfall amounts can reduce or change the vegetation available due to increased dryness.

5.3.4. Conclusion and Comparison for Future Soil Loss Predictions

In conclusion, all methods used to determine future soil loss predictions estimated a decrease in soil loss to occur over the AOI. The non-spatial method, which considered the effect the changing rainfall will have on vegetation change, estimated very low soil erosion losses. Meanwhile, the spatial method, which did not consider the effect of precipitation change on vegetation and only considered it as part of the R-factor, estimated soil losses more in line with past and current estimates. This is likely due to how the future NDVI was calculated.

In comparison with other studies, a local study conducted in the adjacent valley to the AOI, found similar results, where soil erosion was estimated to decrease under future SSP scenarios. This was attributed to the decrease in precipitation and resulting increase of drought conditions which are expected to affect the Maltese Islands because of climate change (Galdies et al. 2022). The same reasoning where a reduction in precipitation leads to reduced estimates of soil erosion can be applied to this study, as the four climate models used predicted much lower monthly precipitation values than those recorded in the past. This greatly reduced rainfall amount in monthly averages is likely what led to substantially lower soil loss estimates under the future SSP scenarios.

Another study in Crete considered the change in rainfall erosivity under the RCP scenarios. Grillakis et al. (2020) found that RCP2.6 is estimated to suffer from an increase in rainfall erosivity, but RCP8.5 is estimated to undergo a decrease in rainfall erosivity. This study used SSP scenarios instead of RCP scenarios. It found that rainfall erosivity in the AOI decreased under both SSP2-4.5 and SSP5-8.5, with the R-factor being calculated at 753 MJ mm ha^{-1} hr^{-1} yr^{-1} for 2021 and ranging between 341-353 MJ mm ha^{-1} hr^{-1} yr^{-1} for SSP2-4.5, and between 333-344 MJ mm ha^{-1} hr^{-1} yr^{-1} for SSP5-8.5. This substantial difference could be due to the lack of extreme storms predicted by the climate models, which provided smoothed monthly averages and no data of possible individual storms. It is important to note that not all studies find that rainfall erosivity is expected to decrease under future SSP predictions, in fact, many studies find that rainfall erosivity will likely increase, such as in the studies by Shiono et al. (2013), and Wang et al. (2023b). Whether rainfall erosivity will decrease or increase with time depends on a number of factors, including where the study was conducted and how climate change is expected to affect that location in particular.

5.4. Summary of RUSLE Factors' Effect on Soil Erosion

Each RUSLE factor influences the final value of the soil loss estimate. Therefore, determining how the factors change spatially and temporally is imperative to properly understand how soil erosion changes throughout the valley on both a spatial and a temporal scale.

5.4.1. R-Factor

This is the factor responsible for the erosive power of the rainfall on soil erosion. It is mainly affected by rainfall intensity and rainfall totals, however, factors like raindrop size are a contributing aspect to rainfall intensity (Panagos et al. 2015a; Nearing et al. 2017). In this study the R-factor was a constant value over the whole AOI for each year being studied, but it was changed for each year. This is due to a lack of data. This meant that no variation within the same map was provided by this factor, however, it contributed to changes between the different years studied. In fact, the high or low R-factor is mirrored in the soil loss estimates, with years recording a high R-factor value also recording a higher mean (and maximum) soil loss value. Figure 5-11 displays this mirroring between the mean soil loss and the R-factor.

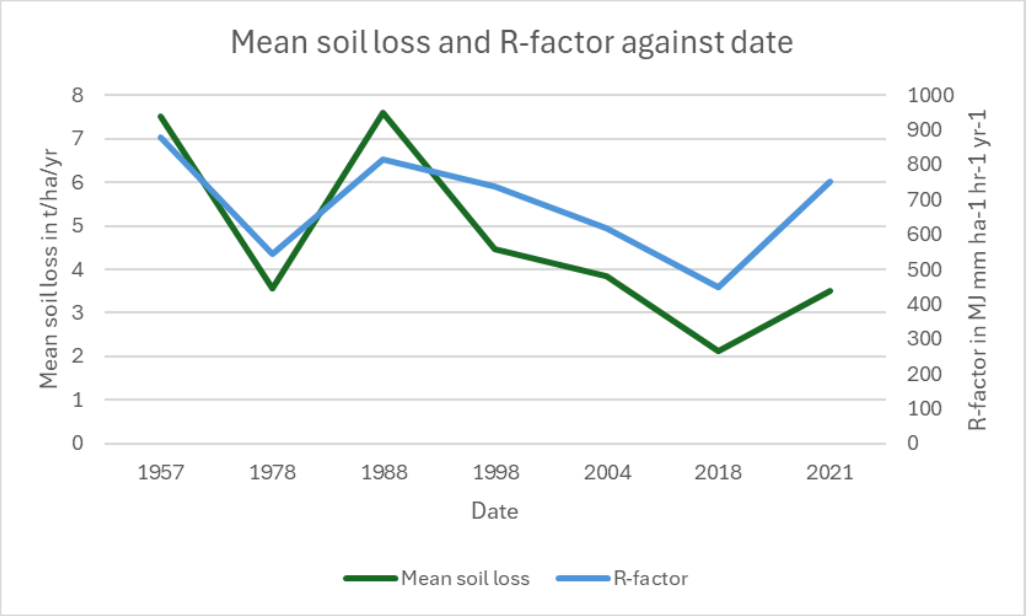

Figure 5-11: Mean soil loss and R-factor for past estimates against date.

When the R-factor is plotted against rainfall totals (of the 4-year period which was considered for the R-factor), a similar relationship but less prominent is revealed (figure 5-12). The graph shows the same mirrored relationship between the R-factor and rainfall as between mean soil loss and the R-factor. However, there are some obvious deviations – such as 1988 and 1998, where the R-factor first increased then decreased – opposite to the rainfall. This is because while rainfall totals are an important aspect of the R-factor, it is not the only influencing factor, with rainfall intensity being a major aspect to the R-factor.

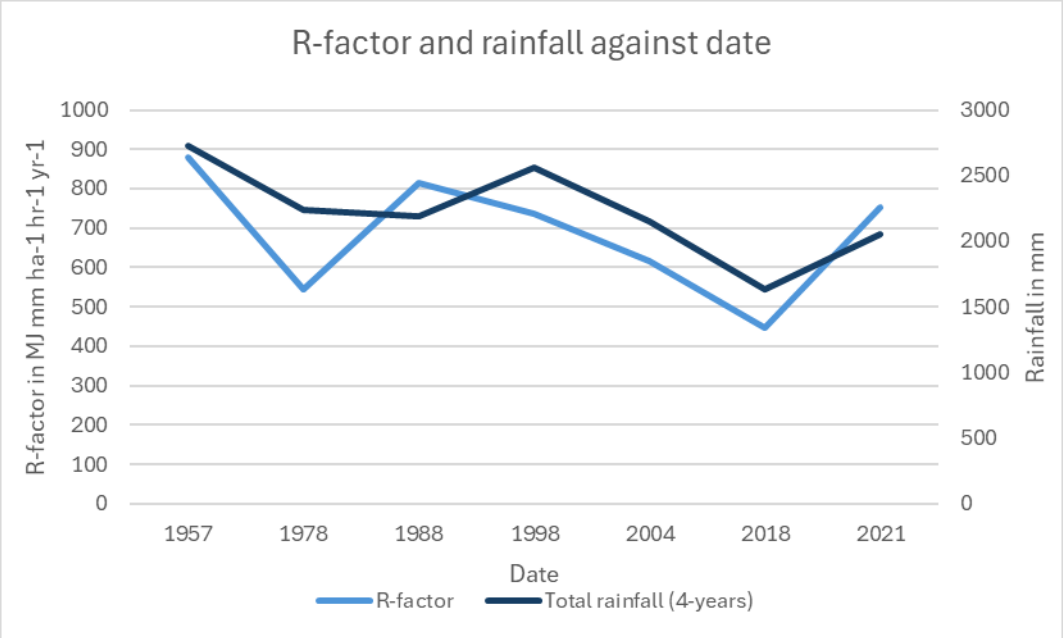

Figure 5-12: R-Factor and Rainfall for Past Estimates against Date.

Despite the obvious influences from other factors for both the R-factor itself, as well as for the soil loss estimates, the R-factor – and thus the rainfall totals – are an important aspect to the soil loss estimates. Many studies mention the R-factor as having a major impact on the soil loss estimates of their study (Meng et al. 2021; Yuan et al. 2021). The large impact rainfall erosivity has on soil loss is an understandable concept. Rainfall directly breaks up soil particles and aggregates through processes like rain splash erosion, and it also washes away any loose soil particles which it has the energy to move through several mechanisms, like sheet wash or rill erosion (Meng et al. 2021). Rainfall erosivity and the severity of its impact also depends on other factors – such as runoff generation, which in turn depends on not only rainfall amount and duration of rainfall, but also on antecedent soil moisture

conditions and surface sealing; and interception, which depends on vegetation present (Meng et al. 2021).

The most erosive type of rainfall is that of high intensity and short duration as a lot of energy is hitting the soil over a short period of time (Meng et al. 2021). This is especially problematic as in a climate change context, the Mediterranean is likely to see an increase in extreme events with higher rainfall intensities (Camarasa-Belmonte et al. 2020; Romera et al. 2017). Despite this, the future soil loss predictions were much lower than the past soil loss estimates. This could be due to the large uncertainties when using future climate projections, and the fact that the datasets obtained from WorldClim CMIP6 did not seem to be predicting extreme events, but where instead much smoother, predicting lower precipitation totals.

5.4.2. K-Factor

The K-factor is the soil's erodibility, i.e. how resistant it is to erosion. This relies on several soil characteristics which when considered together make up the K-factor. Major soil characteristics which play a role in a soil's resistance to detachment and transport are soil texture and organic matter content. In fact, these are the two factors considered in this study. Other factors such as permeability and soil structure can also contribute to soil loss estimates but were not considered in this study due to a lack of data.

In general, larger sand particles are more resistant to transport and small clay particles have high cohesion between themselves, thereby resisting detachment. This means loam soils and silty soils are usually the most erodible soils in terms of soil texture (FAO 2019). In general, in this study the AOI is highly sandy, with only few sample points having a majority of particles as silt or clay (figure 5-13). In this study, there is not much of a visible relationship between soil loss estimates and the soil texture from observation, however, this could be due to the low sample size of only 14 sample points.

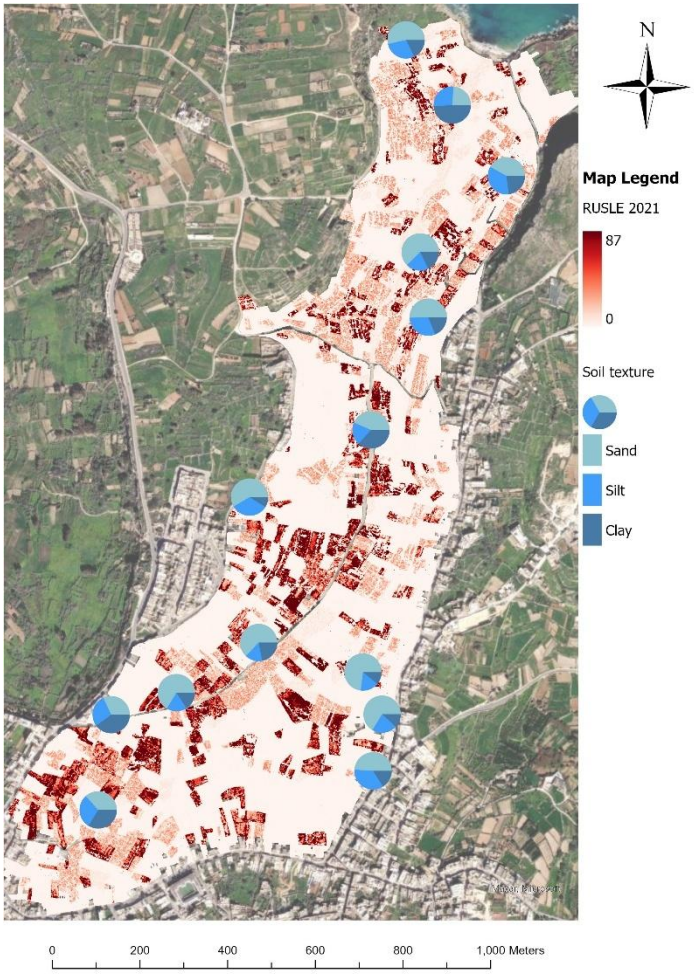

Figure 5-13: Soil Texture Percentages Superimposed over Soil Loss Estimates of 2021.

Another major aspect of soil erodibility is the percentage of organic matter in the soil. This is because organic matter helps to bind the soil aggregates together – similarly to clay particles. Higher organic matter content means more erosion resistant aggregates (FAO 2019). In this study, the highest organic matter content found was in a loam soil with 5.7% and the least was in a sandy loam with 1.46%. As with the soil texture, this study showed no trends between soil loss estimates and organic matter content from visual observation alone.

5.4.3. LS-Factor

The LS-factor is the slope length and angle factor and represents the topography of the land. This is a very important factor which both directly affects soil losses but also influences other factors. The length of a slope directly affects erosion with longer slopes leading to higher soil losses (Bagio et al. 2017). The slope gradient is also of utmost importance. Steeper slopes have higher runoff amounts leading to higher soil losses (Li et al. 2019; FAO 2019). Steeper slopes also promote a higher runoff velocity, which in turn can transport particles easier. While soil particles on steep slopes are likely to detach and be transported with the higher velocity flow, gentler slopes are more likely to form a crust as soil particles fill larger soil pores (Wang et al. 2023a). While slope gradient is very important, with increasing rainfall intensity, its influence on erosion can decrease (Li et al. 2019).

In this study, the LS-factor is difficult to decipher as it contains a lot of data since it is a DEM of 1 m spatial resolution. Patterns are hard to see by visual observation alone, especially since this is a factor which can operate on relatively small scales – i.e. smaller than a field scale if necessary. An important aspect to the LS-factor in the AOI is that it is affected by the presence of terraces. Terraces help reduce both the slope length and slope gradient. This can be seen in the LS-factor map as the higher values are mostly on the fields' perimeter with the centre having lower LS-values. This could be the stepped terraces while the centre of the field remains more level.

5.4.4. C-Factor

This factor represents the vegetation cover and its protection from erosion. This factor considers both tillage and vegetation present. Conservation tillage can result in much lower soil loss estimates than conventional tillage methods, with a study in Calabria finding a decrease of 67% (Preiti et al. 2017). In this study only two tillage methods were considered: no tillage applied and conventional tillage. This is due to difficulty deciphering different tillage methods from orthophotos. However, it is evident through visual observation that plots which are untilled, have suffered higher soil losses in the 2021 soil loss estimates using the 2021 tillage data (figure 5-14).

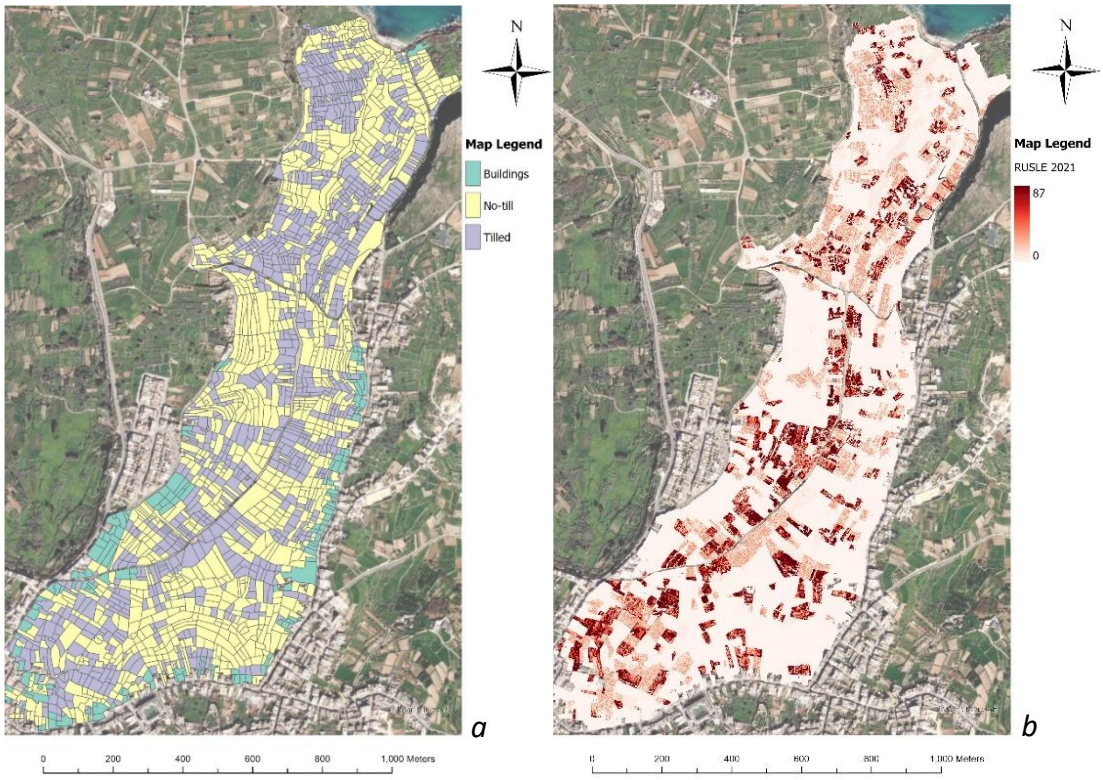

Figure 5-14: 2021 (a) Tilled vs Non-Tilled Fields (b) Soil Loss Estimates

The plant type is also important to the final C-factor value. Denser crops, such as fodder crops, and trees lead to lower C-factor values as they produce more cover for interception purposes. On the other hand, low density crops, such as potatoes, cauliflower, etc. produce less protective cover and thus can lead to higher soil loss values (Preiti et al. 2017; Zhang et al. 2022). Plant cover is a major influencer of soil erosion because of interception. Interception can interact with the kinetic energy of the rainfall and reduce its erosivity as raindrops are stopped by foliage instead of falling on the ground, leading to raindrop impact (Zore et al. 2022). Another aspect of vegetation which helps protect against soil erosion is plant roots. Plant roots can bind the soil particles and promote cohesion. Vannoppen et al. (2017) found that the type of root most effective against erosion depended on the soil type. Thick tap roots

were most effective in cohesive soils while fine roots were better suited for non-cohesive soils.

In this study, plant type was divided between several different categories, most notably seasonal crops, fruit trees and citrus, abandoned, and abandoned with trees. Seasonal crops have the highest C-factor, and they suffer the highest erosion values. This is because these are most often low-density crops, and the fields are tilled conventionally – the most used tillage method in the AOI. On the other hand, abandoned with trees is the category with the lowest C-factor. These are plots of land with no tillage and dense vegetation – both trees and shrubs – and thus have a good vegetative cover for both root binding and interception. Another part of this study used the NDVI instead of fieldwork to calculate the C-factor. This works on a similar concept where the index determines which areas have dense and which have sparse vegetation.

5.4.5. P-Factor

The P-factor is a notoriously difficult to estimate factor within the RUSLE equation. It is the management and practice factor, and it depends on human activities, which either hinder or promote erosion. Many studies take the P-factor to be 1, but this study used a constant value of 0.5, as suggested in Panagos et al. (2015b), due to the presence of rubble walls and terraces in most of the valley. These help in hindering erosion by creating a smaller slope length and a gentler slope angle. Rubble walls also serve as a barrier to soil being transported.

5.5. Comparison with Other Studies

There are some other studies which attempt to estimate soil loss over the San Blas and Binġemma valley. These studies are often coarse and consider more than just this valley as part of their AOI. One such study is that by Panagos et al. (2015c) which covers the entirety of the European Union. The mean soil loss rate for the EU's erosion-prone areas was found to be 2.46 t/ha/yr. This is a rate similar to this AOI's mean soil loss rates in years when erosion was low, with some years having higher rates of up to 7.52 t/ha/yr. The same study has a regional breakdown of soil loss rates per country. Malta was estimated to suffer from a mean soil loss rate of 6.02 t/ha/yr overall. This is in line with this study's findings as mean soil loss rates ranged between 2.12-7.52 t/ha/yr. It is important to note that these were found using the 1 m spatial resolution, using the 30 m resolution, the mean soil loss rate was 8.3 t/ha/yr for the same year that it was 2.12 t/ha/yr in the 1 m resolution. Meanwhile, Panagos et al.'s study had a much coarser spatial resolution of 100 m. Panagos et al. (2015c) could also provide comparisons with other EU countries due to the pan-European study they conducted. This revealed that Mediterranean countries have higher mean soil loss rates than other European countries. In fact, Malta has one of the highest rates, with only Italy, Slovenia, and Austria having a higher mean soil loss rate.

A similar study to this one was conducted in the adjacent watershed of Ramla, Gozo, Malta. The study by Galdies et al. (2022) used the RUSLE equation to estimate soil losses in the Ramla watershed for both present and future estimates. The majority

of the valley was found to have a soil erosion rate below 10 t/ha/yr for present estimates. This is similar to this study which had all mean soil erosion rates under 10 t/ha/yr for past estimates. Regarding future soil loss predictions, Galdies et al. (2022) did not consider a change in the C-factor as in this study, but just like this study, the future rainfall projections were based on monthly averages and not rainfall extremes. As in this study, Galdies et al. (2022) found decreasing soil erosion rates under future scenarios. The similar results between the two studies is understandable as the two valleys studied are exactly adjacent to each other and thus are likely to experience similar soil loss rates as certain factors like rainfall are likely to be similar.

This study builds directly on the findings of another study, Muscat (2022). The two studies have the same AOI but have slightly different methodologies on determining the five RUSLE factors, mainly the R-, K-, and LS- factors. The current study also increases its research to encompass more past years, future predictions, and a different spatial resolution. In general, Muscat (2022) estimated lower soil loss rates than the ones found in this study. For 2021, a maximum 13 t/ha/yr was found in contrast with this study's 87.01 t/ha/yr. However, it is mentioned that the majority of values are below 5 t/ha/yr – which is in line with this study which has a mean soil loss rate of 3.51 t/ha/yr. A different situation is evident for 1957, with Muscat (2022) finding a maximum of 5.5 t/ha/yr but with a majority of values being under 2 t/ha/yr. Meanwhile, this study found a much higher maximum of 62.78 t/ha/yr and a mean of 7.52 t/ha/yr, which is higher than the maximum found in Muscat (2022). The two studies have the same spatial resolution, but their methodologies differ and this is likely where these differences stem from.

5.6. Measures to Limit Erosion

In viewing the results in chapter 4 of this study, it is immediately noticeable that certain areas suffer more from erosion than other areas. Hotspot areas shift with time, but some areas seemed to be highlighted as a hotspot in more than one of the years studied. Such areas, which are more prone to erosion, could have several underlying factors as to why – such as soil type, vegetation cover, or slope. In determining which factor is affecting the area, appropriate management measures can be applied to limit erosion and help safeguard soil.

Several measures can be applied to erosion-prone areas, with varying degrees of cost and effectiveness. Measures vary according to what they aim to tackle – and this is why knowing the underlying issue causing the erosion is ideal. This is an example of why studies on soil erosion prediction are essential. Such studies can both highlight hotspots and areas most susceptible to erosion, as well as determine possible underlying factors which might be promoting soil loss in the area (Kumarasinghe 2021). This helps in determining where soil erosion control measures are most needed and which measure is the most suitable to be applied.

Many studies have found that the R-factor is a major influence on soil loss estimates. The R-factor itself cannot be adjusted as it depends on the characteristics of the rainfall. However, a number of measures can be applied to limit its influence. The C-factor itself is inherently tied to the R-factor as vegetation can be used to limit rainfall

erosivity. Measures revolving around soil surface protection from the force of the rain include planting a vegetation cover, reduced tillage, and mulching. All reduce the amount of exposed bare soil and intercepting the rainfall, thereby reducing raindrop splash, but a vegetation cover also serves to bind the soil particles with its roots, thus further protecting the soil from detachment. Mulch and residues can be held down by soil netting, so it is not blown or washed away. Other measures include strip cropping, which both provides vegetation for interception and root binding, as well as reduces runoff by acting as a barrier. Crop rotation is another measure as it provides a constant vegetation cover, this is especially useful when the vegetation is dense, such as that from a fallow field or grain crops like wheat (Kumarasinghe 2021; FAO 2017).

Measures could also be aimed at reducing the runoff. Runoff both detaches and transports soil particles, and it can be reduced often by means of a barrier as this slows down the flow. A common practice is to use hedges or rubble walls. These structures act as barriers and slow down the flow while also increasing infiltration, with hedges also binding soil with roots. Another hard engineering method is terracing, which is a very effective mechanism which reduces slope length and angle. A softer approach is contour planting, where crops are grown across slope so that they serve as a barrier to the flow and cause it to break and slow down. This is a very useful technique as even the ploughing itself helps in erosion control, with up-and-down slope ploughing often leading to rill formation in the plough lines. Another soft approach is the use of fibre rolls (wattles). These tube-shaped nets filled with grass

also help to reduce the flow's velocity by acting as barriers to the runoff (Kumarasinghe 2021; FAO 2017).

The AOI already has some erosion measures in place, but they can be increased. The presence of some erosion-control measures in the valley is the reason why the P-factor for the whole valley was taken as 0.5 and not 1. Most of the valley is terraced, with most terraces being intact and maintained – this is especially true where the land is still under agricultural production. Another common practice in the valley is the building of rubble walls or of planting prickly pear (*Opuntia ficus indica*). In the AOI this serves as both an erosion-control practice but also as a boundary between plots. The often-small plots mean rubble walls and prickly pears planted along the perimeter are a very common sight and while their main function is often to serve as a boundary, both structures help in erosion control by reducing runoff velocities, improving infiltration, and in the case of the prickly pear, binding soil with its roots.

While the above-mentioned practices are very good erosion control measures, other practices like contour planting, or even contour ploughing, are not well-practiced. The most used tillage method is the easiest one the farmer finds to implement, which unfortunately is often up-and-down slope. A good practice which is sometimes, but always done, is that under trees, the land is not always ploughed, and it is left untilled. This depends on the individual farmer and so it varies from field to field. Another practice which depends on the individual farmer and varies greatly is strip cropping. Strip cropping is quite rare, but it is sometimes evident in a few fields,

although this could be done for a different purpose. Other measures such as soil netting and fibre rolls are not used in the AOI.

These soil erosion control measures are very important, and they greatly help to reduce soil erosion. They are especially needed in erosion hotspots and in areas more susceptible to erosion. This will be even more needed under a climate change scenario of more extreme weather. This is an expected scenario even though the climate change projections used in this study did not use climate extremes to project future soil loss predictions. To fully understand the effects extreme weather can have on soil erosion, Appendix 4 describes a short case study conducted in the AOI before and after a strong storm to see its effects on the valley and on soil erosion.

5.7. Study Limitations

As with any research, this study has a number of limitations listed below:

- The R-factor for past estimates is calculated from monthly precipitation data recorded at Luqa because no records in the valley are available for all the years required. This resulted in only one R-factor for the entire area – with data recorded not in the AOI itself.
- Due to lack of data availability, the recommended nomograph by Wischmeier et al. (1971) could not be used and the equation from the EPIC model (Sharpley & Williams 1990) is used instead to calculate the K-factor.
- Only 14 samples were taken throughout the valley due to land ownership reasons.
- Interpreting the old orthophotos to determine the land use is difficult and prone to human error.
- Only two tillage methods were considered as it was not possible to determine any other tillage methods from orthophotos.
- Only one P-factor is considered for the entire valley throughout the entire study. This is because it is difficult to accurately determine and so it was taken from literature.
- CMIP6 climate projections are only projections and thus have a number of uncertainties. They also smooth the data and do not reveal any extreme events. To try to lessen the biases of using one climate model, four were used and their average was used instead.

- NDVI is not a perfect replacement for the C-factor. Furthermore, in projecting future NDVI, both the spatial and non-spatial methods have their limitations.
    - The spatial method does not consider the effect the changing precipitation pattern will have on the vegetation and instead assumes a constant change in NDVI – with a rate of change determined from past NDVI applied directly to future NDVI.
    - The non-spatial method uses proxies to determine future NDVI. This is not completely accurate (with the relationship having an R^2 of 0.86). Additionally, this method provides only one future NDVI value for the whole valley – an oversimplification of the NDVI – due to coarseness of the proxies.
- The K-factor was kept constant between present and future soil loss predictions, despite a possibility of a change in the SOM content. This was done due to feasibility issues in predicting future SOM values.
- ASTER GDEM and its LiDAR counterpart were compared on a 30 m basis as a downscaled ASTER GDEM produced artifacts in the DEM and so could not be used.
- ASTER GDEM is from 2013 as that was the freely available data while the LiDAR counterpart and the other factors are from 2018 as that is the closest year that was being studied.
- Most of the results presented in this study are maps from GIS and thus have not been tested for statistical significance and therefore generalizations cannot be made.

6. CONCLUSION

This study had three overall aims relating to soil erosion in the San Blas and Binġemma valley throughout the years. The first aim was to determine if a 30 m DEM (such as ASTER GDEM) can be used to accurately estimate soil loss over a small watershed such as the AOI. A 30 m DEM was compared with an upscaled 1 m DEM and results showed that the soil loss estimates were very similar between the two. However, the upscaled DEMs led to higher soil loss estimates than the original 1 m LiDAR-derived DEM. Statistical tests showed that while ASTER GDEM led to slightly higher soil loss estimates, the two datasets were still highly correlated together and thus, ASTER GDEM can be used in case there is no finer data available – albeit it will still have the limitations of a coarser dataset, such as the slightly higher estimates produced by both DEMs when at 30 m spatial resolution.

The second aim was to estimate the soil erosion in the valley between 1957 and 2021 in approximately 10-year intervals. The mean soil loss rate was found to slightly fluctuate despite a slightly decreasing trend. The spatial pattern was seen to slightly shift throughout the years studied, but soil loss was usually higher on the landwards (southern) part of the valley. The spatial pattern itself seems to have been highly influenced by the C-factor and upon visual comparison of the C-factor and soil loss maps, it was visible that the two maps have a similar spatial pattern. This is a logical effect as vegetation is highly influential in soil loss, depending on density and plant

type, with the AOI having varying plant densities and species making the C-factor well-varied.

The third aim was to predict future soil loss estimates over the AOI using future climate projections from climate models and a projected NDVI. Two methods for NDVI prediction were used, with the non-spatial method providing very low soil loss predictions for 2050, and the spatial method providing very low mean soil loss rates but maximum soil loss rates which are more similar to past estimates. Both methods show a decrease in soil erosion in the AOI for 2050 under both SSP scenarios studied. This is likely due to the lower rainfall projected by the climate models and the lack of predicted precipitation extremes.

To properly understand why such spatial and temporal changes were occurring in the AOI, the RUSLE factors and their influence on the soil loss estimates were investigated through visual observation and comparison, and it was found that the R- and C-factor show great influence on the estimates. The R-factor rises and falls throughout the years studied and this trend is mirrored by the mean of the soil loss estimates – with a high mean estimated every time a high R-factor is calculated. The C-factor is seen to affect the estimates spatially – with the soil loss map mirroring the patterns of the C-factor map. These are two factors, rainfall erosivity and vegetation cover, that are often found to greatly influence the soil loss occurring in an area.

Table 6-1: Summary of Research Questions and their Answers.

Research question	Summary of answer
Can coarse topographic data be used accurately for small valleys such as those found in the Maltese Islands, when finer data is unavailable?	30 m ASTER GDEM had a very good positive correlation with an upscaled LiDAR DEM and only slightly overestimated the soil loss estimates. Therefore, H_1 is accepted, and ASTER GDEM can be used when finer data is unavailable, although it is important to keep in mind the limitations of coarser data.
Has there been a substantial difference in the estimated annual total soil lost as well as its distribution during the period of analysis?	Estimated mean total soil loss has slight fluctuations, but there is a trend of a slight decrease in mean soil erosion in the AOI. Spatially, hotspots of high soil loss seem to shift slightly but are mainly concentrated on the landwards side of the valley.
Will there be a substantial change between estimated current soil erosion and predicted future soil erosion under climate change projections?	Future mean soil loss predictions for 2050 are set to decrease substantially under both scenarios (SSP 2-4.5 and SSP 5-8.5) with both methods used if not considering extreme rainfall events.

Potential for Future work:

Validate the soil loss estimates obtained from the RUSLE equation using different soil erosion models (Appendix 5).As with any study, this work leads to further studies related to the topic. Some potential areas for future work include investigating soil loss in the AOI prior to 1957 to further understand soil loss dynamics occurring in the valley, thereby improving its management. Another important area for future study is validation. Validation of the soil loss estimates could be done with in-situ measurements, as well as by using different models other than the RUSLE equation (Appendix 5). Soil loss measurements and estimates could also be determined for other valley systems in Gozo for comparison with the estimates obtained for the San Blas and Binġemma Valley. Another area for future work is regarding statistics. Statistical tests could be used to determine the significance of the observed changes. Finally, regarding future soil loss predictions, future studies could model the predictions using different SSP scenarios, timeframes, and potentially also using different models.

REFERENCES

Abdulraheem, MI, Zhang, W, Li, S, Moshayedi, AJ, Farooque, AA & Hu, J 2023, 'Advancement of Remote Sensing for Soil Measurements and Applications: A Comprehensive Review', *Sustainability*, vol. 15, no. 21. DOI: 10.3390/su152115444.

Abiodun, BJ & Adedoyin, A 2016, 'Chapter 23 - A Modelling Perspective of Future Climate Change' in TM Letcher, (ed), *Climate Change*, pp. 355-371. Elsevier, Boston.

Akbari, M, Neamatollahi, E, Noughani, MA & Memarian, H 2022, 'Spatial distribution of soil erosion risk and its economic impacts using an integrated CORINE-GIS approach', *Environmental Earth Sciences*, vol. 81, no. 287. DOI: 10.1007/s12665-022-10405-w.

Ali, E, Cramer, W, Carnicer, J, Georgopoulou, E, Hilmi, NJM, Le Cozannet, G & P, Lionello 2022, 'Cross-Chapter Paper 4: Mediterranean Region', Climate Change 2022: Impacts, Adaptation and Vulnerability. Contribution of Working Group II to the Sixth Assessment Report of the Intergovernmental Panel on Climate Change. Cambridge University Press, Cambridge, UK and New York, NY, USA.

Ann Arbor, MI, Briley, L, Dougherty, R, Wells, K, Hercula, T, Notaro, M, Rood, R, Andresen, J, Marsik, F, Prosperi, A, Jorns, J, Channell, K, Hutchinson, S, Kemp, C, & Gates, O 2021, *A Practitioner's Guide to Climate Model Scenarios*. Great Lakes Integrated Sciences and Assessments (GLISA).

Arnoldus, H 1980, 'An approximation of the rainfall factor in the Universal Soil Loss Equation' in MD Boodt & D Gabriels, (eds), *Assessment of Erosion*, pp. 127–132. Wiley, Chichester.

Asadi, H, Moussavi, A, Ghadiri, H & Rose, CW 2011, 'Flow-driven soil erosion processes and the size selectivity of sediment', *Journal of Hydrology*, vol. 406, pp. 73–81. DOI: 10.1016/j.jhydrol.2011.06.010.

Bader, D, Covey, C, Gutowski, W, Held, I, Kunkel, K, Miller, R, Tokmakian, R & Zhang, M 2008, *Climate Models An Assessment of Strengths and Limitations*. U.S. Climate Change Science Program, Washington D.C. Available from: https://www.wcrp-climate.org/images/modelling/WGCM/publications/sap3-climate-models.pdf. [20/05/2023].

Bagio, B, Bertol, I, Wolschick, NH, Schneiders, D & Santos, MA 2017, 'Water Erosion in Different Slope Lengths on Bare Soil', *Revista Brasileira de Ciência do Solo*, vol. 41. DOI: 10.1590/18069657rbcs20160132.

Baudry, J, Bunce, RGH & Burel, F 2000, 'Hedgerows: An international perspective on their origin, function and management', *Journal of Environmental Management*, vol. 60, no. 1, pp. 7–22. DOI: 10.1006/jema.2000.0358.

Belly, P 1964, *Sand Movement by Wind*. US Army Coastal Engineering Research Centre, US.

Benavidez, R, Jackson, B, Maxwell, D & Norton, K 2018, 'A review of the (Revised) Universal Soil Loss Equation ((R)USLE): with a view to increasing its global

applicability and improving soil loss estimates', *Hydrology and Earth System Sciences*, vol. 22, pp. 6059–6086. DOI: 10.5194/hess-22-6059-2018.

Benestad, RE, Hanssen-Bauer, I & Chen, D 2008, 'Downscaling Strategies' in *Empirical-Statistical Downscaling*, p. 22-24. World Scientific Publishing, Singapore.

Berendse, F, van Ruijven, J, Jongejans, E & Keesstra, S 2015, 'Loss of plant species diversity reduces soil erosion resistance', *Ecosystems*, vol. 18, pp. 881–888.

Berger, C, Schulze, M, Rieke-Zapp, D & Schlunegger, F 2010, 'Rill development and soil erosion: a laboratory study of slope and rainfall intensity', *Earth Surface Processes and Landforms*, vol. 35, no. 12, pp. 1456–1467.

Bernatek-Jakiel, A & Poesen, J 2018, 'Subsurface erosion by soil piping: significance and research needs', *Earth-Science Reviews*, vol. 185, pp. 1107–1128. DOI: 10.1016/j.earscirev.2018.08.006.

Bhat, SA, Dar, MUD & Meena, RS 2019, 'Soil Erosion and Management Strategies' in RS Meena, S Kumar, JS Bohra, & ML Jat, (eds), *Sustainable Management of Soil and Environment*, pp. 73-122. Springer, Singapore.

Bircher, P, Liniger, HP & Prasuhn, V 2019, 'Comparing different multiple flow algorithms to calculate RUSLE factors of slope length (L) and slope steepness (S) in Switzerland', *Geomorphology*, vol. 346. DOI: 10.1016/j.geomorph.2019.106850.

Boardman, J, Poesen, J & Evans, R 2003, 'Socio-economic factors in soil erosion and conservation', *Environmental Science & Policy*, vol. 6, no. 1, pp. 1–6. DOI: 10.1016/S1462-9011(02)00120-X.

Bodle, R 2022, 'International soil governance', *Soil Security*, vol. 6. DOI: 10.1016/j.soisec.2022.100037.

Borrelli, P, Robinson, DA, Panagos, P, Lugato, E, Yang, JE, Alewell, C, Wuepper, D, Montanarella, L, & Ballabio, C 2020, 'Land use and climate change impacts on global soil erosion by water (2015-2070)', Proceedings of the National Academy of Sciences, vol. 117, no. 36, pp. 21994–22001. DOI: 10.1073/pnas.2001403117.

Boucher, O, Denvil, S, Levavasseur, G, Cozic, A, Caubel, A, Foujols, MA, Meurdesoif, Y, Cadule, P, Devilliers, M, Ghattas, J, Lebas, N, Lurton, T, Mellul, L, Musat, I, Mignot, J & Cheruy, F 2018, *IPSL IPSL-CM6A-LR model output prepared for CMIP6 CMIP* (Version 20230220) [Data set]. Earth System Grid Federation. DOI: 10.22033/ESGF/CMIP6.1534.

Brevik, EC 2012, 'Soils and Climate Change: Gas Fluxes and Soil Processes', *Soil Horizons*, vol. 53, no. 4, pp. 12–23. Available from: 10.2136/sh12-04-0012.

Bryan, K & Albritton, CC 1943, 'Soil Phenomena as Evidence of Climatic Changes', *American Journal of Science*, vol. 241, no. 8, pp. 469–490. DOI: 10.2475/ajs.241.8.469.

Busico, G, Grilli, E, Carvalho, SC, Mastrocicco, M & Castaldi, S 2023, 'Assessing soil erosion susceptibility for past and future scenarios in semiarid Mediterranean agroecosystems', *Sustainability*, vol. 15, no. 17, p. 12992.

Busuttil, S 1993, 'Agriculture in Malta: a historical note' in S Busuttil, F Lerin, & L Mizzi, (eds), *Malta: food, agriculture, fisheries and the environment*, pp. 9-26. Montpellier:CIHEAM.

Camarasa-Belmonte, AM, Rubio, M & Salas, J 2020, 'Rainfall events and climate change in Mediterranean environments: an alarming shift from resource to risk in Eastern Spain', *Natural Hazards*, vol. 103, pp. 423–445.

Cerdà, A, Lucas-Borja, ME, Franch-Pardo, I, Úbeda, X, Novara, A, López-Vicente, M, Popović, Z & Pulido, M 2021, 'The role of plant species on runoff and soil erosion in a Mediterranean shrubland', *Science of The Total Environment*, vol. 799, p. 149218. DOI: 10.1016/j.scitotenv.2021.149218.

Choi, K, Arnhold, S, Huwe, B & Reineking, B 2017, 'Daily based Morgan–Morgan–Finney (DMMF) model: A spatially distributed conceptual soil erosion model to simulate complex soil surface configurations', *Water*, vol. 9, no. 4, p. 278.

Chokkavarapu, N & Mandla, VR 2019, 'Comparative study of GCMs, RCMs, downscaling and hydrological models: a review toward future climate change impact estimation.', *SN Applied Sciences*, vol. 1, no. 12, p. 1698. DOI: 10.1007/s42452-019-1764-x.

Ciarlo, J, Aquilina, N, Attard, M, Borg, S, Pace, PJ, Vassallo, S, Balzan, M, Camilleri, C, Deidun, A, Drago, A, Farrugia, S, Galdies, C, Moncada, S, Mule' Stagno, L, Muscat, J, Sapiano, M, Schembri, PJ, Schiavone, J, Sciberras, E, Stevens, D, Torpiano, A & von Brockdorff, P 2017, *The Seventh National Communication of Malta to the United National Framework Convention on Climate Change*, Institute for Climate

Change and Sustainable Development, University of Malta and Climate Change Unit, Malta Resources Authority. Available from: https://www.um.edu.mt/library/oar/bitstream/123456789/105742/1/The_seventh_national_communication_of_Malta_under_the_United_Nations_framework_convention_on_climate_change_2017.pdf. [03/03/2025].

Climate Change Committee for Adaptation 2010, *National Climate Change Adaptation Strategy*. Malta.

Conrad, O, Bechtel, B, Bock, M, Dietrich, H, Fischer, E, Gerlitz, L, Wehberg, J, Wichmann, V & Böhner, J 2023, *System for Automated Geoscientific Analysis (SAGA GIS)*, version 9.3, Hamburg.

Copernicus n.d., *Climate projections*. Available from: https://climate.copernicus.eu/climate-projections. [29/09/2023].

Copernicus 2021, *CMIP6 Climate Projections*. Available from: https://cds.climate.copernicus.eu/cdsapp#!/dataset/projections-cmip6?tab=overview. [17/01/2024].

Copernicus Climate Change Service, Climate Data Store 2019, CMIP5 daily data on single levels. Copernicus Climate Change Service (C3S) Climate Data Store (CDS). DOI: 10.24381/cds.d3513dbf [15/01/2025].

Critchley, W, Siegert, K & Chapman, C 1991, *A Manual for the Design and Construction of Water Harvesting Schemes for Plant Production*. Food and Agriculture Organization of the United Nations, Rome.

De Baets, S, Poesen, J, Galindo-Morales, P & Knapen, A 2007, 'Impact of root architectureon the erosion-reducing potential of roots during concentrated flow', *Earth Surface Processes and Landforms*, vol. 23, pp. 1323–1345.

De Oliveira Salumbo, AM 2020, 'A Review of Soil Erosion Estimation Methods', *Agricultural Sciences*, vol. 11, no. 8. DOI: 10.4236/as.2020.118043.

Derin, Y & Yilmaz, KK 2014, 'Evaluation of multiple satellite-based precipitation products over complex topography', *Journal of Hydrometeorology*, vol. 15, no. 4, pp. 1498–1516.

Desmet, P & Govers, G 1996, 'A GIS procedure for automatically calculating the USLE LS factor on topographically complex landscape units', *Journal of Soil and Water Conservation*, vol. 51, no. 5, pp. 427–433.

Directorate-General for Environment 2024, *Degraded ecosystems to be restored across Europe as Nature Restoration Law enters into force*. Available from: https://environment.ec.europa.eu/news/nature-restoration-law-enters-force-2024-08-15_en. [05/02/2025].

Dotterweich, M 2008, 'The history of soil erosion and fluvial deposits in small catchments of central Europe: Deciphering the long-term interaction between humans and the environment — A review', *Geomorphology*, vol. 101, no. 1, pp. 192–208. DOI: 10.1016/j.geomorph.2008.05.023.

Dudal, R, Nachtergaele, F & Purnell, MF 2002,'The human factor of soil formation', 17th World Congress of Soil Science, CD-ROM, paper 93., pp.1–6. Intern. Union Soil Sci., Bangkok, Thailand.

Dunn, M & Hickey, R 1998, 'The effect of slope algorithms on slope estimates within a GIS', *Cartography*, vol. 27, no. 1, pp. 9–15.

Earth Resources Observation and Science (EROS) Centre 2018, *USGS EROS Archive - Digital Elevation - Shuttle Radar Topography Mission (SRTM) 1 Arc-Second Global*. Available from: https://www.usgs.gov/centres/eros/science/usgs-eros-archive-digital-elevation-shuttle-radar-topography-mission-srtm-1. [17/01/2024].

Eash, N, Sauer, T, O'Dell, D & Odoi, E 2016, *Soil Science Simplified*, 6th edn, John Wiley & Sons, Inc., New Jersey.

EC-Earth Consortium (EC-Earth) 2019, *EC-Earth-Consortium EC-Earth3-Veg model output prepared for CMIP6 CMIP* (Version 20240927) [Data set]. Earth System Grid Federation. DOI: 10.22033/ESGF/CMIP6.642.

Eekhout, J, Hunink, JE, Terink, W & de Vente, J 2018, 'Why increased extreme precipitation under climate change negatively affects water security', *Hydrology and Earth System Sciences*, vol. 11, no. 22, pp. 5935–5946. DOI: 10.5194/hess-22-5935-2018.

Eekhout, J & de Vente, J 2022, 'Global impact of climate change on soil erosion and potential for adaptation through soil conservation', *Earth Science Reviews*, vol. 226. DOI: 10.1016/j.earscirev.2022.103921

Ellison, WD 1944, 'Studies of raindrop erosion', *Journal of Agricultural Engineering*, vol. 25, no. 4, pp. 131–136.

Ellison, WD 1945, 'Some effects of raindrops and surface-flow on soil erosion and infiltration', *Eos, Transactions American Geophysical Union*, vol. 26, no. 3, pp. 415–429. Available from: https://doi.org/10.1029/TR026i003p00415.

Environment and Resources Authority (ERA) 2014, *Il-Qortin tal-Magun u l-Qortin il-Kbir Natura 2000 Management Plan (SAC)*. Available from: https://era.org.mt/wp-content/uploads/2019/05/Il-Qortin_tal-Magun_u_l-Qortin_il-Kbir_ManagementPlan.pdf.

Environment Protection Act 2016. Available from: https://legislation.mt/eli/cap/549/eng/pdf.

Erskine, R, Sherrod, L & Green, T 2017, 'Measuring and Mapping Patterns of Soil Erosion and Deposition Related to Soil Carbonate Concentrations Under Agricultural Management', *Journal of Visualized Experiments*, vol. 127, p. 56064.

Environmental Systems Research Institute (esri) 2020, *Aeronautical Reconnaissance Coverage Geographic Information System (ArcGIS) ArcMap v 10.8*. Redlands, CA.

Environmental Systems Research Institute (esri) 2023a, *Aeronautical Reconnaissance Coverage Geographic Information System (ArcGIS) ArcPro v 3.1*. Redlands, CA.

Environmental Systems Research Institute (esri) 2023b, *How IDW works*. Available from: https://pro.arcgis.com/en/pro-app/latest/tool-reference/spatial-analyst/how-idw-works.htm. [17/01/2024].

Environmental Systems Research Institute (esri) 2023c, *How kriging works*. Available from: https://pro.arcgis.com/en/pro-app/latest/tool-reference/spatial-analyst/how-kriging-works.htm. [17/01/2024].

Environmental Systems Research Institute (esri) 2023d, *How spline works*. Available from: https://pro.arcgis.com/en/pro-app/latest/tool-reference/spatial-analyst/how-spline-works.htm. [17/01/2024].

EUMeTrain 2013, *RGB and Enhanced Channels*. Available from: https://resources.eumetrain.org/satmanu/Basic/RGB_Channels/print.htm#header. [14/01/2025].

EUMETSAT 2023, *Natural Colour RGB Quick Guide*. Available from: https://user.eumetsat.int/resources/user-guides/natural-colour-rgb-quick-guide. [14/01/2025].

European Commission (EC) n.d., *The common agricultural policy: 2023-27*. Available from: https://agriculture.ec.europa.eu/common-agricultural-policy/cap-overview/cap-2023-27_en. [30/03/2024].

European Commission (EC) 2021a, *Communication from the Commission to The European Parliament, The Council, The European Economic and Social Committee and The Committee of the Regions EU Soil Strategy for 2030 Reaping the benefits of healthy soils for people, food, nature and climate*, European Commission, Brussels. Available from: https://eur-lex.europa.eu/legal-content/EN/TXT/PDF/?uri=CELEX:52021DC0699. [30/03/2024].

European Commission (EC) 2021b, *European Missions: A Soil Deal for Europe: Implementation Plan*. Available from: https://research-and-innovation.ec.europa.eu/funding/funding-opportunities/funding-programmes-and-open-calls/horizon-europe/eu-missions-horizon-europe/soil-deal-europe_en#what-this-eu-mission-deals-with. [27/12/2024].

European Commission (EC) 2022, *Common Agricultural Policy for 2023-2027 28 cap strategic plans at a glance*. Available from: https://agriculture.ec.europa.eu/document/download/a435881e-d02b-4b98-b718-104b5a30d1cf_en?filename=csp-at-a-glance-eu-countries_en.pdf. [30/03/2024].

European Commission 2023a, *Proposal for a DIRECTIVE OF THE EUROPEAN PARLIAMENT AND OF THE COUNCIL on Soil Monitoring and Resilience (Soil Monitoring Law)*, COM(2023) 416 final, European Commission, Brussels. Available from: https://environment.ec.europa.eu/system/files/2023-07/Proposal%20for%20a%20DIRECTIVE%20OF%20THE%20EUROPEAN%20PARLIAMENT%20AND%20OF%20THE%20COUNCIL%20on%20Soil%20Monitoring%20and%20Resilience_COM_2023_416_final.pdf.

European Commission (EC) 2023b, *Soil and Land*. Available from: https://environment.ec.europa.eu/topics/soil-and-land_en#:~:text=The%20EU%20soil%20strategy%20for,to%20healthy%20soils%20by%202050. [13/01/2024].

European Commission (EC) 2023c, *Soil Health*. Available from: https://environment.ec.europa.eu/topics/soil-and-land/soil-health_en. [13/01/2024].

European Court of Auditors 2018, *Opinion No 7/2018: Concerning Commission Proposals for Regulations Relating to the common agricultural policy for the Post-2020 Period.* Available from: https://www.eca.europa.eu/en/publications?did=47751. [10/10/2024].

European Space Agency (ESA) n.d., *The Sentinel Missions*. Available from: https://www.esa.int/Applications/Observing_the_Earth/Copernicus/The_Sentinel_missions. [03/02/2025].

European Space Agency (ESA) 2023, *Remote sensing data underpin research on soil*. Available from: https://earth.esa.int/eogateway/news/remote-sensing-data-underpin-research-on-soil. [20/11/2024].

Eurostat 2020, *Agri-environmental indicator – soil erosion*. Available from: https://ec.europa.eu/eurostat/statistics-explained/index.php?title=Agri-environmental_indicator_-_soil_erosion. [06/08/2025].

Eyring, V, Cox, PM, Flato, GM, Gleckler, PJ, Abramowitz, G, Caldwell, P, Collins, WD, Gier, BK, Hall, AD, Hoffman, FM, Hurtt, GC, Jahn, A, Jones, CD, Klein, SA, Krasting, JP, Kwiatkowski, L, Lorenz, R, Maloney, E, Meehl, GA, Pendergrass, AG, Pincus, R, Ruane, AC, Russell, JL, Sanderson, BM, Santer, BD, Sherwood, SC, Simpson, IR, Stouffer, RJ, & Williamson, MS 2019, 'Taking climate model evaluation to the

next level', *Nature Climate Change*, vol. 9, no. 2, pp. 102–110. DOI: 10.1038/s41558-018-0355-y.

Fairfield, J & Leymarie, P 1991, 'Drainage networks from grid digital elevation models', *Water Resources Research*, vol. 27, pp. 709–717. DOI: 10.1029/90WR02658.

Faulkner, H 2006, 'Piping Hazard on Collapsible and Dispersive Soils in Europe' in J Boardman & J Poesen, (eds), *Soil Erosion in Europe*, pp. 537-562. John Wiley & Sons, Ltd.

Feng, S, Huang, X, Zhao, Shuaishuai, Qin, Z, Fan, J & Zhao, Shuhe 2022, 'Evaluation of Several Satellite-Based Soil Moisture Products in the Continental US', *Sensors*, vol. 22, no. 24. DOI: 10.3390/s22249977.

Ferro, V, Porto, P & Yu, B 1999, 'A comparative study of rainfall erosivity estimation for southern Italy and southeastern Australia', *Hydrological Sciences Journal*, vol. 44, no. 1, pp. 3–24. DOI: 10.1080/02626669909492199.

Fertile Soil (Preservation) Act 1973. Available from: https://legislation.mt/eli/cap/236/eng/pdf.

Fick, SE, Hijmans, RJ, 2017, 'Worldclim 2: New 1-km spatial resolution climate surfaces for global land areas', *International Journal of Climatology*, vol. 37, no. 12, pp. 4302–4315.

Filippucci, P, Brocca, L, Quast, R, Ciabatta, L, Saltalippi, C, Wolfgang, Wagner & Tarpanelli, A 2022, 'High resolution (1 km) satellite rainfall estimation from SM2RAIN applied to Sentinel-1: Po River Basin as case study', *Hydrology and*

Earth System Sciences, vol. 26, no. 9, pp. 2481–2497. DOI: 10.5194/hess-26-2481-2022.

Food and Agricultural Organization (FAO) 2017, *Voluntary Guidelines for Sustainable Soil Management*. Food and Agriculture Organization of the United Nations (FAO), Rome.

Food and Agricultural Organization (FAO) 2019, *Soil erosion: the greatest challenge to sustainable soil management*. Food and Agriculture Organization of the United Nations (FAO), Rome. Available from: http://www.fao.org/3/ca4395en/ca4395en.pdf.

Food and Agriculture Organization of the United Nations (FAO) & Intergovernmental Technical Panel on Soils (ITPS) 2015, *Status of the World's Soil Resources (SWSR) – Main Report*, p.100. Italy. Available from: https://www.fao.org/3/i5199e/i5199e.pdf.

Forkuor, G & Maathuis, B 2012, 'Comparison of SRTM and ASTER Derived Digital Elevation Models over Two Regions in Ghana – Implications for Hydrological and Environmental Modeling' in T Piacentini, (ed), *Studies on Environmental and Applied Geomorphology*, pp. 219-240. IntechOpen.

Foster, GR 1982, 'Chapter 8: Modelling the soil erosion process' in *Hydrological Modelling of Small Watersheds*, pp. 297-380.

Freeman, TG 1991, 'Calculating catchment area with divergent flow based on a regular grid', *Computers and Geosciences*, vol. 17, no. 3, pp. 413–422. DOI: 10.1016/0098-3004(91)90048-I.

Fryrear, D & Downes, J 1975, 'Estimating Seedling Survival from Wind Erosion Parameters', *Transactions of the ASAE*, vol. 18, no. 5. DOI: 10.13031/2013.36702.

Fu, S, Cao, L, Liu, B, Wu, Z & Savabi, MR 2015, 'Effects of DEM grid size on predicting soil loss from small watersheds in China', *Environmental Earth Sciences*, vol. 73, pp. 2141–2151.

Gabet, EJ & Dunne, T 2003, 'Sediment detachment by rain power', *Water Resources Research*, vol. 39, no. 1, p. ESG 1-1; ESG 1-12. DOI: 10.1029/2001WR000656.

Galdies, C, Said, A, Camilleri, L & Caruana, M 2016, 'Climate change trends in Malta and related beliefs, concerns and attitudes toward adaptation among Gozitan farmers', *European Journal of Agronomy*, vol. 74, pp. 18–28. DOI: 10.1016/j.eja.2015.11.011.

Galdies, C, Azzopardi, D & Sacco, A 2022, 'Estimates of soil erosion rates in a principal watershed in Gozo, Malta under current and future climatic conditions', *Catena*, vol. 210, p. 105900. DOI: 10.1016/j.catena.2021.105900.

Ghiloufi, W, Quero, JL, García-Gómez, M & Chaieb, M 2016, 'Potential impacts of aridity on structural and functional status of a southern Mediterranean Stipa tenacissima steppe', *South African Journal of Botany*, vol. 103, pp. 170–180. DOI: 10.1016/j.sajb.2015.09.004.

Ghosal, K & Bhattacharya, SD 2020, 'A Review of RUSLE Model', *Journal of the Indian Society of Remote Sensing*, vol. 48, pp. 689–707. DOI: 10.1007/s12524-019-01097-0.

Gilley, JE 2005, ‘Erosion: Water-Induced’ in D Hillel, (ed), *Encyclopedia of Soils in the Environment*, pp. 463-469. Elsevier, Oxford.

Gorelick, N, Hancher, M, Dixon, M, Ilyushchenko, S, Thau, D & Moore, R 2017, 'Google Earth Engine: Planetary-scale geospatial analysis for everyone', *Remote Sensing of Environment*, vol. 202, pp. 18-27.

Goudie, A 2013, *Encyclopedia of Geomorphology*. Routledge.

Govers, G & Poesen, J 1988, ‘Assessment of the interrill and rill contributions to total soil loss from an upland field plot’, *Geomorphology*, vol. 1, no. 4, pp. 343–354. DOI: 10.1016/0169-555X(88)90006-2.

Govers, G, Gimenez, R & Van Oost, K 2007, ‘Rill erosion: Exploring the relationship between experiments, modelling and field observations’, *Earth Science Reviews*, vol. 84, pp. 87–102. DOI: 10.1016/J.EARSCIREV.2007.06.001.

Grillakis, MG, Polykretis, C & Alexakis, DD 2020, ‘Past and projected climate change impacts on rainfall erosivity: Advancing our knowledge for the eastern Mediterranean island of Crete’, *Catena*, vol. 193, p. 104625. DOI: 10.1016/j.catena.2020.104625.

Guduru, JU & Jilo, NB 2023, ‘Assessment of rainfall-induced soil erosion rate and severity analysis for prioritization of conservation measures using RUSLE and Multi-Criteria Evaluations Technique at Gidabo watershed, Rift Valley Basin, Ethiopia’, *Ecohydrology & Hydrobiology*, vol. 23, no. 1, pp. 30–47. DOI: 10.1016/j.ecohyd.2022.09.002.

Guo, S, Zhu, Z & Lyu, L 2018, 'Effects of Climate Change and Human Activities on Soil Erosion in the Xihe River Basin, China', *Water*, vol. 10, no. 8, p. 1085. DOI: https://doi.org/10.3390/w10081085.

Hartley, IP, Hill, TC, Chadburn, SE & Hugelius, G 2021, 'Temperature effects on carbon storage are controlled by soil stabilisation capacities', *Nature Communications*, vol. 12, p. 6713. DOI: 10.1038/s41467-021-27101-1.

Hateffard, F, Mohammed, S, Alsafadi, K, Enaruvbe, GO, Heidari, A, Abdo, HG & Rodrigo-Comino, J 2021, 'CMIP5 climate projections and RUSLE-based soil erosion assessment in the central part of Iran', *Scientific Reports*, vol. 11, p. 7273. DOI: 10.1038/s41598-021-86618-z.

Hayhoe, K, Edmonds, J, Kopp, RE, LeGrande, AN, Sanderson, BM, Wehner, MF & Wuebbles, DJ 2017, 'Climate models, scenarios, and projections' in DJ Wuebbles, DW Fahey, KA Hibbard, DJ Dokken, BC Stewart, & TK Maycock, (eds), *Climate Science Special Report: Fourth National Climate Assessment, Volume I*, pp. 133-160. U.S. Global Change Research Program, Washington D.C.

Heuser, DI 2022, 'Soil Governance in current European Union Law and in the European Green Deal', *Soil Security*, vol. 6, p. 100053. DOI: 10.1016/j.soisec.2022.100053.

Hickey, R 2000, 'Slope angle and slope length solutions for GIS', *Cartography*, vol. 29, no. 1, pp. 1–8.

Hickey, R, Smith, A & Jankowski, P 1994, 'Slope length calculations from a DEM within ARC/INFO GRID', *Computers, Environment and Urban Systems*, vol. 18, no. 5, pp. 365–380.

Hu, Y & Liu, B 2021, *Measuring erosion and sediment yields on slopes and in small catchments*, UNESCO-ISI Online Training Workshop on Sediment Transport Measurement and Monitoring. China.

Huffman, GJ, Tan, J & National Centre for Atmospheric Research Staff (Eds) 2023, *The Climate Data Guide: IMERG precipitation algorithm and the Global Precipitation Measurement (GPM) Mission*. Available from: https://climatedataguide.ucar.edu/climate-data/gpm-global-precipitation-measurement-mission. [07/01/2025].

Ibetsberger, D 2020, *Soil Erosion Modeling (USLE)*. Available from: https://storymaps.arcgis.com/stories/98bf5b9024ce4110906370eb7b777ad6. [30/12/2024].

Igwe, PU, Ezeukwu, JC, Edoka, NE, Ejie, OC & Ifi, GI 2017, 'A review of vegetation cover as a natural factor to soil erosion', *International journal of Rural Development, Environment and Health Research*, vol. 1, pp. 21–28.

Intergovernmental Panel on Climate Change (IPCC) 2019, *IPCC Special Report on the Ocean and Cryosphere in a Changing Climate*, HO Pörtner, DC Roberts, V Masson-Delmotte, P Zhai, M Tignor, E Poloczanska, K Mintenbeck, A Alegría, M Nicolai, A Okem, J Petzold, B Rama & NM Weyer, (eds.). Cambridge University Press, Cambridge, UK and New York, NY, USA.

Intergovernmental Panel on Climate Change (IPCC) 2023 'Mediterranean Region', in *Climate Change 2022 – Impacts, Adaptation and Vulnerability: Working Group II Contribution to the Sixth Assessment Report of the Intergovernmental Panel on Climate Change*, pp. 2233–2272. Cambridge University Press, Cambridge.

International Organization for Standardization (ISO) 2017, *ISO 11272-2017, Soil Quality—Determination of Dry Bulk Density*. International Organization for Standardization, Geneva.

Issaka, S & Ashraf, MA 2017, 'Impact of soil erosion and degradation on water quality: a review', *Geology, Ecology, and Landscapes*, vol. 1, no. 1, pp. 1–11. DOI: 10.1080/24749508.2017.1301053.

James, LA 2013, 'Impacts of early agriculture and deforestation on geomorphic systems' in JF Shroder, (ed), *Treatise on Geomorphology*, pp. 48-67. Academic Press.

Jia, L, Fenli, Z, Guifang, L, Feng, B, & Juan, A 2016, 'The effects of raindrop impact and runoff detachment on hillslope soil erosion and soil aggregate loss in the Mollisol region of Northeast China', *Soil & Tillage Research*, vol. 161, pp. 79–85. DOI: 10.1016/j.still.2016.04.002.

Jia, H, Wang, X, Sun, W, Mu, X, Gao, P, Zhao, G & Li, Z 2022, 'Estimation of Soil Erosion and Evaluation of Soil and Water Conservation Benefit in Terraces under Extreme Precipitation', *Water*, vol. 14, no. 11, p. 1675. DOI: 10.3390/w14111675.

Jin, F, Yang, W, Fu, J & Li, Z 2021, 'Effects of vegetation and climate on the changes of soil erosion in the Loess Plateau of China', *Science of The Total Environment*, vol. 773, p. 145514. DOI: 10.1016/j.scitotenv.2021.145514.

Johnson, AI 1962, *Methods of Measuring Soil Moisture in the Field*, Geological Survey Water-Supply Paper 1619-U, United States Government Printing Office, Washington, D.C.

Kassam, AH, Velthuizen, HT, Mitchell, A, Fischer, GW & Shah, MM 1992, 'AgroEcological Land resources Assessment for Agricultural Development Planning. A Case Study of Kenya Resources Data Base and Land productivity', *Technical Annex 2. Soil Erosion and productivity*.

Ketema, A & Dwarakish, GS 2019, 'Water erosion assessment methods: a review', *ISH Journal of Hydraulic Engineering*, vol. 27, no. 4, pp. 434–441. DOI: 10.1080/09715010.2019.1567398.

Khasanov, K 2020, 'Evaluation of ASTER DEM and SRTM DEM data for determining the area and volume of the water reservoir'*, IOP Conference Series: Materials Science and Engineering 883*. Purpose-Led Publishing.

Khanal, S, Fulton, J & Shearer, S 2017, 'An overview of current and potential applications of thermal remote sensing in precision agriculture', *Computers and Electronics in Agriculture*, vol. 139, pp. 22–32. DOI: 10.1016/j.compag.2017.05.001.

Kilinc, M & Richardson, EV 1973, *Mechanics of soil erosion from overland flow generated by simulated rainfall*, PhD thesis, Civil Engineering Department, Colorado State University.

Kinnell, PIA 2005, 'Raindrop-impact-induced erosion processes and prediction: a review', *Hydrological Processes*, vol. 19, no. 14, pp. 2815–2844. DOI: 10.1002/hyp.5788.

Kinnell, PIA 2010, 'Event soil loss, runoff and the Universal Soil Loss Equation family of models: A review', Journal of Hydrology, vol. 385, no. 1, pp. 384–397. DOI: 10.1016/j.jhydrol.2010.01.024.

Kolpak, G & Fornabaio, L 2022, *EU Soil Health Law Legal principles underpinning the framework*. ClientEarth.

Kolpak, G & Heinzel, C 2023, *European Commission proposal for a Soil Monitoring Law Technical Briefing on establishing a robust governance structure*. Available from: https://eeb.org/wp-content/uploads/2023/10/Soil-Monitoring-Law_Technical-briefing-on-governance_EEB_ClientEarth-1.pdf. [16/01/2024].

Krishnan, MVN, Mohan, MAS, Pratheesh, P & Vijith, H 2017, 'Performance Evaluation and Sensitivity Analysis of ASTER and SRTM (30m) DEM-derived Terrain Variables in Landslide Susceptibility Assessment: A Case from the Western Ghats', *Journal of Environmental Research, Engineering and Management*, vol. 73, no. 2. DOI: 10.5755/j01.erem.73.2.16385.

Kumarasinghe, U 2021, 'A review on new technologies in soil erosion management', *Journal of research technology and engineering*, vol. 2, no. 1, pp. 120–127.

Lang, DM 1960, *Soils of Malta and Gozo*, His/Her Majesty's Stationary Office (HMSO), London.

Langbein, WB & Schumm, SA 1958, 'Yield of sediment in relation to mean annual precipitation', *Eos, Transactions American Geophysical Union*, vol. 39, no. 6, pp. 1076–1084. DOI: 10.1029/TR039i006p01076.

Lavee, H, Imeson, AC & Sarah, P 1999, 'The impact of climate change on geomorphology and desertification along a mediterranean-arid transect', *Land Degradation & Development*, vol. 9, no. 5, pp. 407–422. DOI: 10.1002/(SICI)1099-145X(199809/10)9:5<407::AID-LDR302>3.0.CO;2-6.

Laws, JO 1941, 'Measurements of the fall-velocity of water-drops and raindrops', *Eos, Transactions American Geophysical Union*, vol. 22, no. 3, pp. 709–721.

Li, J, Cai, Q, Sun, L & Chen, X 2010, 'Reviewing on Factors and Critical Conditions of Rill Erosion', *Progress in Geography*, vol. 29, no. 11, pp. 1319–1325. DOI: 10.11820/dlkxjz.2010.11.010.

Li, Z & Fang, H 2016, 'Impacts of climate change on water erosion: A review', *Earth-Science Reviews*, vol. 163, pp. 94–117. DOI: 10.1016/j.earscirev.2016.10.004.

Liu, H, Kiesel, J, Hörmann, G & Fohrer, N 2011, 'Effects of DEM horizontal resolution and methods on calculating the slope length factor in gently rolling landscapes', *Catena*, vol. 87, pp. 368–375. DOI: 10.1016/j.catena.2011.07.003.

Liu, Q, Chen, L & Li, J 2001, 'Influences of Slope Gradient on Soil Erosion', *Applied Mathematics and Mechanics*, vol. 22, pp. 510–519. DOI: 10.1023/A:1016303213326.

Lovato, T, Peano, D, Butenschön, M, Materia, S, Iovino, D, Scoccimarro, E, Fogli, P G, Cherchi, A, Bellucci, A, Gualdi, S, Masina, S & Navarra, A 2022, 'CMIP6 simulations with the CMCC Earth System Model (CMCC-ESM2)', *Journal of Advances in Modeling Earth Systems*, vol. 14, no. 3. DOI: 10.1029/2021MS002814.

Malta Environment and Planning Authority (MEPA) 2013, *Development of Environmental Monitoring Strategy and Environmental Monitoring Baseline Surveys*. Malta.

Marcinkowski, P, Szporak-Wasilewska, S & Kardel, I 2022, 'Assessment of soil erosion under long-term projections of climate change in Poland', *Journal of Hydrology*, vol. 607. DOI: 10.1016/j.jhydrol.2022.127468.

McCool, DK, Brown, LC, Foster, GR, Mutchler, CK & Meyer, LD 1987, 'Revised slope steepness factor for the Universal Soil Loss Equation', *Transactions of the ASAE*, vol. 30, no. 5, pp. 1387–1396.

McIntyre, DS 1958, 'Soil splash and the formation of surface crusts by raindrop impact', *Soil Science*, vol. 85, no. 5, pp. 261–266.

McRoberts, RE, Nelson, MD & Wendt, DG 2002, 'Stratified estimation of forest area using satellite imagery, inventory data, and the k-Nearest Neighbours technique', *Remote Sensing of Environment*, vol. 82, no. 2–3, pp. 457–468.

Meng, X, Zhu, Y, Yin, M & Liu, D 2021, 'The impact of land use and rainfall patterns on the soil loss of the hillslope', *Scientific Reports*, vol. 11. DOI: 10.1038/s41598-021-95819-5.

Merritt, WS, Letcher, RA & Jakeman, AJ 2003, 'A review of erosion and sediment transport models', *Environmental Modelling & Software*, vol. 18, no. 8, pp. 761–799. DOI: 10.1016/S1364-8152(03)00078-1.

Mohamadi, MA & Kavian, A 2015, 'Effects of rainfall patterns on runoff and soil erosion in field plots', *International Soil and Water Conservation Research*, vol. 3, no. 4, pp. 273–281. DOI: 10.1016/j.iswcr.2015.10.001.

Mohamed, ES, Saleh, AM, Belal, AB & Gad, A 2018, 'Application of near-infrared reflectance for quantitative assessment of soil properties', *The Egyptian Journal of Remote Sensing and Space Science*, vol. 21, no. 1, pp. 1–14. DOI: 10.1016/j.ejrs.2017.02.001.

Mohammad, AG & Adam, MA 2010, 'The impact of vegetative cover type on runoff and soil erosion under different land uses', *Catena*, vol. 81, no. 2, pp. 97–103. DOI: 10.1016/j.catena.2010.01.008.

Mondal, A, Khare, D & Kundu, S 2016, 'Change in rainfall erosivity in the past and future due to climate change in the central part of India', *International Soil and Water Conservation Research*, vol. 4, no. 3, pp. 186–194. DOI: 10.1016/j.iswcr.2016.08.004.

Moody, A 2020, *Comparing RUSLE LS Calculation Methods across Varying DEM Resolutions*, MSc. Thesis, All Master's Theses 1357, Central Washington University.

Moore, ID & Burch, GJ 1986, 'Physical basis of the length-slope factor in the universal soil loss equation', *Soil Science Society of America Journal*, vol. 50, no. 5, pp. 1294–1298.

Morgan, R, Morgan, D & Finney, H 1984, 'A Predictive Model for the Assessment of Soil Erosion Risk', *Journal of Agricultural Engineering Research*, vol. 30, pp. 245–253.

Morgan, R 2001, 'A simple approach to soil loss prediction: a revised Morgan–Morgan–Finney model', *Catena*, vol. 44, no. 4, pp. 305–322.

Morgan, RPC 2005, *Soil Erosion and Conservation*, 3rd edn, Blackwell Publishing Ltd.

Morgan, R & Duzant, JH 2008, 'Modified MMF (Morgan–Morgan–Finney) model for evaluating effects of crops and vegetation cover on soil erosion', *Earth Surface Processes and Landforms: The Journal of the British Geomorphological Research Group*, vol. 33, no. 1, pp. 90–106.

Morgan, R & Nearing, M 2010, *Handbook of Erosion Modelling*. Blackwell Publishing Ltd.

Muscat, S 2022, Understanding soil erosion patterns in San Blas and Binġemma Valley, BSc. Thesis, University of Malta.

Naipal, V, Reick, C, Pongratz, J & Van Oost, K 2015, 'Improving the global applicability of the RUSLE model – adjustment of the topographical and rainfall erosivity factors', *Geoscientific Model Development*, vol. 8, no. 9, pp. 2893–2913. DOI: 10.5194/gmd-8-2893-2015.

Naorem, A, Jayaraman, S, Dang, YP, Dalal, RC, Sinha, NK, Rao, CS & Patra, AK 2023, 'Soil Constraints in an Arid Environment—Challenges, Prospects, and Implications', *Agronomy*, vol. 13, no. 220, pp. 1–29. DOI: 10.3390/agronomy13010220.

NASA/METI/AIST/Japan Spacesystems and U.S./Japan ASTER Science Team 2019, *ASTER Global Digital Elevation Model V003*. NASA EOSDIS Land Processes Distributed Active Archive Centre (LP DAAC), Sioux Falls, South Dakota, USA. Available from: https://doi.org/10.5067/ASTER/ASTGTM.003.

National Aeronautics and Space Administration (NASA) n.d., *Terra & Aqua Moderate Resolution Imaging Spectroradiometer (MODIS)*. Available from: https://ladsweb.modaps.eosdis.nasa.gov/missions-and-measurements/modis/. [15/01/2025].

National Aeronautics and Space Administration (NASA) 2024, *ASTER*. Available from: https://asterweb.jpl.nasa.gov/. [17/01/2024].

National Aeronautics and Space Administration (NASA) 2025, *Satellites*. Available from: https://landsat.gsfc.nasa.gov/satellites/. [15/01/2025].

National Oceanic and Atmospheric Administration (NOAA) 2019, *Satellite Imagery RGBs: Adding Value, Saving Time*. Available from: https://www.nesdis.noaa.gov/news/satellite-imagery-rgbs-adding-value-saving-time. [14/01/2025].

Nearing, MA 2001, 'Potential changes in rainfall erosivity in the U.S. with climate change during the 21st century', *Journal of Soil and Water Conservation*, vol. 56, no. 3, pp. 229–232.

Nearing, MA, Pruski, FF & O'Neal, MR 2004, 'Expected Climate Change Impacts on Soil Erosion Rates: A Review', *Journal of Soil and Water Conservation*, vol. 59, no. 1, pp. 43–50.

Nearing, MA, Yin, S, Borrelli, P & Polyakov, VO 2017, 'Rainfall erosivity: An historical review', *Catena*, vol. 157, pp. 357–362. DOI: 10.1016/j.catena.2017.06.004.

Nikolakopoulos, KG, Kamaratakis, EK & Chrysoulakis, N 2006, 'SRTM vs ASTER elevation products. Comparison for two regions in Crete, Greece', *International Journal of Remote Sensing*, vol. 27, no. 21, pp. 4819–4838. DOI: 10.1080/01431160600835853.

Nordstrom, KF & Hotta, S 2004, 'Wind erosion from cropland in the USA: a review of problems, solutions and prospects', *Geoderma*, vol. 121, no. 3, pp. 157–167. DOI: 10.1016/j.geoderma.2003.11.012.

O'Callaghan, JF & Mark, DM 1984, 'The extraction of drainage networks from digital elevation data', *Computer Vision, Graphics, and Image Processing*, vol. 28, no. 3, pp. 323–344. DOI: 10.1016/S0734-189X(84)80011-0.

Ombadi, M, Risser, MD, Rhoades, AM & Varadharajan, C 2023, 'A warming-induced reduction in snow fraction amplifies rainfall extremes', *Nature*, vol. 619, pp. 305-310. DOI: 10.1038/s41586-023-06092-7.

Owoputi, LO & Stolte, WJ 1995, 'Soil detachment in the physically based soil erosion process: a review', *Transactions of the ASAE*, vol. 38, no. 4, pp. 1099–1110.

Panagos, P, Ballabio, C, Borrelli, P, Meusburger, K, Klik, A, Rousseva, S, Tadić, MP, Michaelides, S, Hrabalíková, M, Olsen, P, Aalto, J, Lakatos, M, Rymszewicz, A, Dumitrescu, A, Beguería, S & Alewell, C 2015a, 'Rainfall erosivity in Europe', *Science of The Total Environment*, vol. 511, pp. 801–814. DOI: 10.1016/j.scitotenv.2015.01.008.

Panagos, P, Borelli, P, Meusburger, K, Zanden, E van der, Poesen, J & Alewell, C 2015b, 'Modelling the effect of support practices (P-factor) on the reduction of soil erosion by water at European scale', *Environmental Science and Policy*, vol. 51, pp. 23–24.

Panagos, P, Borrelli, P, Poesen, J, Ballabio, C, Lugato, E, Meusburger, K, Montanarella, L & Alewell, C 2015c, 'The new assessment of soil loss by water erosion in Europe', *Environmental Science and Policy*, vol. 54, pp. 438–447. DOI: 10.1016/j.envsci.2015.08.012.

Panagos, P, Borrelli, P, Meusburger, K, Alewell, C, Lugato, E & Montanarella, L 2015d, 'Estimating the soil erosion cover-management factor at the European scale', Land Use Policy, vol. 48, pp. 38-50. DOI: 10.1016/j.landusepol.2015.05.021.

Panagos, P, Ballabio, C, Himics, M, Scarpa, S, Matthews, F, Bogonos, M, Poesen, J & Borrelli, P 2021, 'Projections of soil loss by water erosion in Europe by 2050',

Environmental Science & Policy, vol. 124, pp. 380–392. DOI: 10.1016/j.envsci.2021.07.012.

Parsons, A, Abrahams, A & Luk, S 1991, 'Size characteristics of sediment in interrill overland flow on a semiarid hillslope, southern Arizona', *Earth Surface Processes and Landforms*, vol. 16, pp. 143–152. DOI: 10.1002/esp.3290160205.

Peñuelas, J & Boada, M 2003, 'A global change-induced biome shift in the Montseny mountains (NE Spain)', *Global Change Biology*, vol. 9, no. 2, pp. 131–140. DOI: 10.1046/j.1365-2486.2003.00566.x.

Petropoulos, GP, Ireland, G & Barrett, B 2015, 'Surface soil moisture retrievals from remote sensing: Current status, products & future trends', *Physics and Chemistry of the Earth, Parts A/B/C*, vol. 83-84, pp. 36–56. DOI: 10.1016/j.pce.2015.02.009.

Preiti, G, Romeo, M, Bacchi, M & Monti, M 2017, 'Soil loss measure from Mediterranean arable cropping systems: Effects of rotation and tillage system on C-factor', *Soil and Tillage Research*, vol. 170, pp. 85–93. DOI: 10.1016/j.still.2017.03.006.

QGIS Development Team 2023, *Quantum Geographic Information System (QGIS),* version 3.26.3. Available from: https://www.qgis.org.

Quinn, P, Beven, K, Chevallier, P & Planchon, O 1991, 'The prediction of hillslope flow paths for distributed hydrological modelling using digital terrain models', *Hydrological Processes*, vol. 5, no. 1, pp. 59–79.

Raj, AR, George, J, Raghavendra, S, Kumar, S & Agrawal, S 2018, 'Effect of DEM resolution on LS factor computation', *The International Archives of the*

Photogrammetry, Remote Sensing and Spatial Information Sciences, vol. 42, no. 5, pp. 315–321. DOI: 10.5194/isprs-archives-XLII-5-315-2018.

Ran, Q, Su, D, Li, P & He, Z 2012, 'Experimental study of the impact of rainfall characteristics on runoff generation and soil erosion', *Journal of Hydrology*, pp. 99–111. DOI: 10.1016/j.jhydrol.2011.12.035.

Rasooli, D 2022, 'The rainfall erosivity factor: literature review' in *Predicting Rainfall Erosivity by Variable Models In a Region with a Non-Uniform Pluvial Regime*. Lap Lambert Academic Publishing.

Raza, A, Ahrends, HE, ur Rahman, MH & Gaiser, T 2021, 'Modeling Approaches to Assess Soil Erosion by Water at the Field Scale with Special Emphasis on Heterogeneity of Soils and Crops', *Land*, vol. 10, no. 422, pp. 1–35.

Regulation (EU) 2024/1991 of the European Parliament and of The Council of 24 June 2024 on nature restoration and amending Regulation (EU) 2022/869. Available from: https://eur-lex.europa.eu/legal-content/EN/TXT/?uri=CELEX%3A32024R1991&qid=1722240349976.

Reichle, DE 2023, 'Chapter 13 - Climate and climate models' in DE Reichle, (ed), *The Global Carbon Cycle and Climate Change (Second Edition)*. Elsevier.

Renard, KG, Foster, GR, Weesies, GA & Porter, JP 1991, 'RUSLE Revised universal soil loss equation', *Journal of Soil and Water Conservation*, vol. 46, no. 1, pp. 30–33.

Renard, K & Ferreira, V 1993, 'RUSLE model description and database sensitivity', *Journal of Environmental Quality*, vol. 22, pp. 458–466.

Renard, K & Freimund, J 1994, 'Using monthly precipitation data to estimate the R-factor in the revised USLE', *Journal of Hydrology*, vol. 157, no. 1–4, pp. 287–306.

Renard, K, Foster, G, Weesies, G, McCool, D & Yoder, D 1997, 'Predicting soil erosion by water: a guide to conservation planning with the revised universal soil loss equation (RUSLE)', *USDA Agriculture Handbook*. US Government Printing Office, Washington, D.C.

Richter, DB 2007, 'Humanity's transformation of earth's soil: pedology's new frontier', *Soil Science*, vol. 172, no. 12, pp. 957–967. DOI: 10.1097/ss.0b013e3181586bb7.

Rieke-Zapp, D & Nearing, MA 2005, 'Slope Shape Effects on Erosion', *Soil Science Society of America Journal*, vol. 69, no. 5, pp. 1463–1471. DOI: 10.2136/sssaj2005.0015.

Robinson, DA & Woodun, JK 2008, 'An experimental study of crust development on chalk downland soils and their impact on runoff and erosion', *European Journal of Soil Science*, vol. 59, no. 4, pp. 784–798. DOI: 10.1111/j.1365-2389.2008.01033.x.

Rodrigo-Comino, J, Martínez-Hernández, C, Iserloh, T & Cerdà, A 2018, 'Contrasted Impact of Land Abandonment on Soil Erosion in Mediterranean Agriculture Fields', *Pedosphere*, vol. 28, no. 4, pp. 617–631. DOI: 10.1016/S1002-0160(17)60441-7.

Romera, R, Gaertner, MÁ, Sánchez, E, Domínguez, M, González-Alemán, JJ & Miglietta, MM 2017, 'Climate change projections of medicanes with a large

multi-model ensemble of regional climate models', *Global and Planetary Change*, vol. 151, pp. 134–143. DOI: 10.1016/j.gloplacha.2016.10.008.

Römkens, M, Young, RA, Poesen, J, McCool, DK, El-Swaify, SA & Bradford, JM 1997, 'Soil erodibility factor (K)' in K Renard, G Foster, G Weesies, D McCool & D Yoder, (eds), *Agriculture Handbook no. 703*, pp. 65–99.

Roose, E 1977, 'Érosion et ruissellement en afrique de l'ouest vingt années de mesures en petites parcelles expérimentales', *Travaux et Documents de l'ORSTOM No. 78*. ORSTOM, Paris

Ruiz-Sinoga, JD & Diaz, AR 2010, 'Soil degradation factors along a Mediterranean pluviometric gradient in Southern Spain', *Geomorphology*, vol. 118, no. 3, pp. 359–368. DOI: 10.1016/j.geomorph.2010.02.003.

Ruppel, OC 2022, 'Overview of international soil law', *Soil Security*, vol. 6, p. 100056. DOI: 10.1016/j.soisec.2022.100056.

Sabzevari, T & Talebi, A 2019, 'Effect of hillslope topography on soil erosion and sediment yield using USLE model', *Acta Geophysica*, vol. 67, no. 6, pp. 1587–1597.

Satellite Imaging Corporation 2022, *ASTER Satellite Sensor*. Available from: https://www.satimagingcorp.com/satellite-sensors/other-satellite-sensors/aster/. [17/01/2024].

Schürz, C, Mehdi, B, Kiesel, J, Schulz, K, & Herrnegger, M 2020, 'Supplement of A systematic assessment of uncertainties in large-scale soil loss estimation from

different representations of USLE input factors – a case study for Kenya and Uganda', *Hydrology and Earth System Sciences*, vol. 24, pp. 4463–4489.

Segura, C, Sun, G, McNulty, S & Zhang, Y 2014, 'Potential impacts of climate change on soil erosion vulnerability across the conterminous United States', *Journal of Soil and Water Conservation*, vol. 69, no. 2, pp. 171–181. DOI: 10.2489/jswc.69.2.171.

Sharpley, AN & Williams, JR 1990, 'EPIC: Erosion/Productivity Impact Calculator. Part 1. Model documentation', *Technical Bulletin 1768*. USDA.

Shi, H, Fang, NF, Wu, FZ, Wang, L, Yue, BJ & Wu, GL 2012, 'Soil erosion processes and sediment sorting associated with transport mechanisms on steep slopes', *Journal of Hydrology*, pp. 123–130. DOI: 10.1016/j.jhydrol.2012.06.004.

Shi, H & Wang, G 2015, 'Impacts of climate change and hydraulic structures on runoff and sediment discharge in the middle Yellow River', *Hydrological Processes*, vol. 29, no. 14, pp. 3236–3246. DOI: 10.1002/hyp.10439.

Shiono, T, Ogawa, S, Miyamoto, T & Kameyama, K 2013, 'Expected impacts of climate change on rainfall erosivity of farmlands in Japan', *Ecological Engineering*, vol. 61, pp. 678–689. DOI: 10.1016/j.ecoleng.2013.03.002.

Srinivasan, R & Engel, BA 1991, 'Effect of slope prediction methods on slope and erosion estimates', *Applied Engineering in Agriculture*, vol. 7, no. 6, pp. 779–783.

Stocker, TF, Qin, D, Plattner, G-K, Tignor, MM, Allen, SK, Boschung, J, Nauels, A, Xia, Y, Bex, V & Midgley, PM 2014, 'Climate Change 2013: The physical science basis.

contribution of working group I to the fifth assessment report of IPCC the intergovernmental panel on climate change'. Cambridge University Press.

Stone, R & Hilborn, D 2012, *Universal soil loss equation factsheet*. Available from: http://www.omafra.gov.on.ca/english/engineer/facts/12-051.htm#4. [20/02/2025].

Stroosnijder, L 2005, 'Measurement of erosion: Is it possible?', *Catena*, vol. 64, no. 2–3, pp. 162–173. DOI: 10.1016/j.catena.2005.08.004.

Sultana, D 2015, 'Numerical Modelling of Soil Erosion Susceptibility in the Maltese Islands using Geographic Information Systems and the Revised Universal Soil Loss Equation (RUSLE)', *Xjenza Online*, vol. 3, pp. 41–50. DOI: 10.7423/XJENZA.2015.1.06.

Sun, L, Fang, H, Qi, D, Li, J & Cai, Q 2013, 'A review on rill erosion process and its influencing factors', *Chinese Geographical Science*, vol. 23, pp. 389–402. DOI: 10.1007/s11769-013-0612-y.

Sweeney, JC 2009, 'Climate Change' in R Kitchin & N Thrift, (eds), *International Encyclopedia of Human Geography,* pp. 147-155. Elsevier, Oxford.

Tabari, H 2020, 'Climate change impact on flood and extreme precipitation increases with water availability', *Scientific Reports*, vol. 10, p. 13768. DOI: 10.1038/s41598-020-70816-2.

Tang, J, Cheng, X, Zhu, B, Gao, M, Wang, T, Zhang, X, Zhao, P & You, X 2015, 'Rainfall and tillage impacts on soil erosion of sloping cropland with subtropical monsoon

climate — A case study in hilly purple soil area, China', *Journal of Mountain Science*, vol. 12, pp. 134–144. DOI: 10.1007/s11629-014-3241-8.

Tang, Y, Rumbold, S, Ellis, R, Kelley, D, Mulcahy, J, Sellar, A, Walton, J & Jones, C 2019, *MOHC UKESM1.0-LL model output prepared for CMIP6 CMIP* (Version 20230213) [Data set]. Earth System Grid Federation. DOI: 10.22033/ESGF/CMIP6.1569.

Tarboton, DG 1997, 'A new method for the determination of flow directions and upslope areas in grid digital elevation models', *Water Resources Research*, vol. 33, no. 2, pp. 309–319. DOI: 10.1029/96WR03137.

Toy, TJ, Foster, GR & Renard, KG 2002, *Soil Erosion: Processes, Prediction, Measurement, and Control*. John Wiley & Sons, Inc., USA.

Trenberth, K 2011, 'Changes in precipitation with climate change', *Climate Research*, vol. 47, pp. 123–138. DOI: 10.3354/cr00953.

U.S. Geological Survey (USGS) n.d., *Landsat Missions*. Available from: https://www.usgs.gov/landsat-missions. [15/01/2025].

U.S. Geological Survey (USGS) 2020, *Digital Elevation Model (DEM) Product Comparison Guide*. Available from: https://lpdaac.usgs.gov/documents/642/DEM_Comparison_Guide.pdf.

USGS/NASA Landsat 5 Thematic Mapper (TM) Surface Reflectance Tier 1 2023, Google Earth Engine, Accessed: 14/01/2025. Available from: LANDSAT/LT05/C02/T1_L2.

USGS/NASA Landsat 7 Enhanced Thematic Mapper Plus (ETM+) Surface Reflectance Tier 1 2023, Google Earth Engine, Accessed: 14/01/2025. Available from: LANDSAT/LE07/C02/T1_L2.

USGS/NASA Landsat 8 Surface Reflectance Tier 1 2023, Google Earth Engine, Accessed: 14/01/2025. Available from: LANDSAT/LC08/C02/T1_L2.

Vaezi, AR, Morvarid, A & Artemi, C 2017, 'Contribution of raindrop impact to the change of soil physical properties and water erosion under semi-arid rainfalls', *Science of the Total Environment*, vol. 583, pp. 382–392. DOI: 10.1016/j.scitotenv.2017.01.078.

Valentin, C 2004, 'The integrity of river and drainage basin systems: Challenges from environmental change' in P Kabat, M Claussen, P Dirmeyer, J Gash, L Deguenni, M Meybeck, RP Sr, C Vörösmarty, R Hutjes, & S Lutkemeier, (eds), *Vegetation, Water, Humans and the Climate*. Springer, New York.

Valentin, C, Poesen, J & Li, Y 2005, 'Gully erosion: Impacts, factors and control', *Catena*, vol. 63, no. 2, pp. 132–153. DOI: 10.1016/j.catena.2005.06.001.

Van der Knijff, J, Jones, R & Montanarella, L 1999, *Soil erosion risk assessment in Italy*. European Commission Directorate General JRC Joint Research Centre Space Applications Institute European Soil Bureau.

Van der Knijff, J, Jones, R & Montanarella, L 2000, *Soil Erosion Risk Assessment in Europe*. European Commission Directorate General JRC Joint Research Centre Space Applications Institute European Soil Bureau.

Van Oost, K, Govers, G, De Alba, S & Quine, TA 2006, 'Tillage erosion: a review of controlling factors and implications for soil quality', *Progress in Physical Geography*, vol. 30, no. 4, pp. 443–466.

Van Remortel, RD, Hamilton, ME & Hickey, RJ 2001, 'Estimating the LS Factor for RUSLE through Iterative Slope Length Processing of Digital Elevation Data within Arclnfo Grid', *Cartography*, vol. 30, no. 1, pp. 27–35. DOI: 10.1080/00690805.2001.9714133.

Van Remortel, RD, Maichle, RW & Hickey, RJ 2004, 'Computing the RUSLE LS Factor through Array- based Slope Length Processing of Digital Elevation Data Using a C++ Executable', *Computers and Geosciences*, vol. 30, no. 9–10, pp. 1043–1053.

Vannoppen, W, De Baets, S, Keeble, J, Dong, Y & Poesen, J 2017, 'How do root and soil characteristics affect the erosion-reducing potential of plant species?', *Ecological Engineering*, vol. 109, pp. 186–195. DOI: 10.1016/j.ecoleng.2017.08.001.

Verheijen, FGA, Jones, RJA, Rickson, RJ & Smith, CJ 2009, 'Tolerable versus actual soil erosion rates in Europe', *Earth-Science Reviews*, vol. 94, no. 1, pp. 23–38. DOI: 10.1016/j.earscirev.2009.02.003.

Wang, Y, Zhang, JH, Zhang, ZH & Jia, LZ 2016, 'Impact of tillage erosion on water erosion in a hilly landscape', *Science of the Total Environment*, pp. 522–532. DOI: 10.1016/j.scitotenv.2016.02.045.

Wang, N, Jiao, J, Bai, L, Zhang, Y, Chen, Y, Tang, B, Liang, Y, Zhao, C & Wang, H 2020, 'Magnitude of soil erosion in small catchments with different land use patterns

under an extreme rainstorm event over the Northern Loess Plateau, China', *Catena*, vol. 195, p. 104780. DOI: 10.1016/j.catena.2020.104780.

Wang, B, Zhang, Z, Wang, X, Zhao, X, Yi, L & Hu, S 2021, 'The Suitability of Remote Sensing Images at Different Resolutions for Mapping of Gullies in the Black Soil Region, Northeast China', *Remote Sensing*, vol. 13, no. 12, p. 2367. DOI: 10.3390/rs13122367.

Wang, Y, Tan, L, Wang, G, Sun, X & Xu, Y 2022, 'Study on the Impact of Spatial Resolution on Fractional Vegetation Cover Extraction with Single-Scene and Time-Series Remote Sensing Data', *Remote Sensing*, vol. 14. DOI: 10.3390/rs14174165

Wang, L, Li, Y, Wu, J, An, Z, Suo, L, Ding, J, Li, S, Wei, D & Jin, L 2023a, 'Effects of the Rainfall Intensity and Slope Gradient on Soil Erosion and Nitrogen Loss on the Sloping Fields of Miyun Reservoir', *Plants*, vol. 12, no. 3, p. 423. DOI: 10.3390/plants12030423.

Wang, W, Yin, S, He, Z, Chen, D, Wang, H & Klik, A 2023b, 'Projections of rainfall erosivity in climate change scenarios for mainland China', *Catena*, vol. 232, p. 107391. DOI: 10.1016/j.catena.2023.107391.

Webb, NP, Herrick, JE & Duniway, MC 2014, 'Ecological site-based assessments of wind and water erosion: informing accelerated soil erosion management in rangelands', *Ecological applications: a publication of the Ecological Society of America*, vol. 24, no. 6, pp. 1405–1420. DOI: 10.1890/13-1175.1.

White, RE 2006, *Principles and practice of soil science: the soil as a natural resource*, 4th edn. Blackwell Publishing.

Wichmann, V & Setiawan, M 2012, *Module MMF-SAGA Soil Erosion Model*. Available from: https://saga-gis.sourceforge.io/saga_tool_doc/2.2.6/sim_erosion_0.html. [17/01/2024].

Wischmeier, WH & Smith, DD 1957, 'Factors affecting sheet and rill erosion', *Eos, Transactions American Geophysical Union*, vol. 38, no. 6, pp. 889–896.

Wischmeier, W & Smith, DD 1958, 'Rainfall energy and its relationship to soil loss', *Transactions, American Geophysical Union*, vol. 39, pp. 285–291.

Wischmeier, W 1959, 'A rainfall erosion index for a universal soil loss equation', *Soil Science Society of America Journal*, vol. 23, pp. 246–249.

Wischmeier, WH, Johnson, CB & Cross, BV 1971, 'A soil erodibility nomograph for farmland and construction sites', *Journal of Soil and Water Conservation*, vol. 26, no. 5, pp. 189-193.

Wischmeier, WH & Smith, D 1978, Predicting Rainfall Erosion Losses - A Guide to Conservation Planning, *Agriculture Handbook No. 537*. United States Department of Agriculture (USDA), USA.

Woo, M, Fang, G & diCenzo, PD 1997, 'The role of vegetation in the retardation of rill erosion', *Catena*, vol. 29, no. 2, pp. 145–159. DOI: 10.1016/S0341-8162(96)00052-5.

WorldClim 2024, *Future climate data*. Available from: https://www.worldclim.org/data/cmip6/cmip6climate.html.

Wu, Xinliang, Wei, Y, Wang, J, Xia, J, Cai, C & Wei, Z 2018, 'Effects of soil type and rainfall intensity on sheet erosion processes and sediment characteristics along the climatic gradient in central-south China', *Science of The Total Environment*, vol. 621, pp. 54–66. DOI: 10.1016/j.scitotenv.2017.11.202.

Xu, L, Xu, X & Meng, X 2013, 'Risk assessment of soil erosion in different rainfall scenarios by RUSLE model coupled with Information Diffusion Model: A case study of Bohai Rim, China', *Catena*, vol. 100, pp. 74–82. DOI: 10.1016/j.catena.2012.08.012.

Yang, M, Yang, Q, Zhang, K, Pang, G & Huang, C 2024, 'Global soil erodibility factor (K) mapping and algorithm applicability analysis', *Catena*, vol. 239, p. 107943. DOI: 10.1016/j.catena.2024.107943.

Yao, H, Shi, C, Shao, W, Bai, J & Yang, H 2015, 'Impacts of Climate Change and Human Activities on Runoff and Sediment Load of the Xiliugou Basin in the Upper Yellow River', *Advances in Meteorology*, pp. 1–12. DOI: 10.1155/2015/481713.

Yoder, RE 1936, 'A Direct Method of Aggregate Analysis of Soils and a Study of the Physical Nature of Erosion Losses1', *Agronomy*, vol. 28, no. 5, pp. 337–351. DOI: 10.2134/agronj1936.00021962002800050001x.

Young, R & Onstad, C 1978, 'Characterization of Rill and Interrill Eroded Soil', *Transactions of the ASAE*, vol. 21, no. 6, pp. 1126–1130. DOI: 10.13031/2013.35454.

Yuan, L, Yue, K, Gu, Z, Chen, H & Chi, Y 2021, 'Analysis of Rainfall Factors and Soil Erosion in Different Soil and Water Conservation Measures in the Karst Plateau-Mountain', *Polish Journal of Environmental Studies*, vol. 30, no. 6, pp. 5343–5349.

Zachar, D 1982, *Soil Erosion: Developments in Soil Science*. Elsevier.

Zanchi, C & Torri, D 1980, Evaluation of rainfall energy in central Italy in M De Boodt & D Gabriels, (eds), *Assessment of Erosion*. Wiley, New York.

Zhang, Q, Lv, X, Yu, X, Ni, Y, Ma, L & Liu, Z 2022, 'Species and spatial differences in vegetation rainfall interception capacity: A synthesis and meta-analysis in China', *Catena*, vol. 213, p. 106223. DOI: 10.1016/j.catena.2022.106223.

Zhao, L, Fang, Q, Hou, R & Wu, F 2021, 'Effect of rainfall intensity and duration on soil erosion on slopes with different microrelief patterns', *Geoderma*, vol. 396, p. 115085. DOI: 10.1016/j.geoderma.2021.115085.

Zhao, Q, Yu, L, Du, Z, Peng, D, Hao, P, Zhang, Y & Gong, P 2022, 'An overview of the applications of earth observation satellite data: impacts and future trends', *Remote Sensing*, vol. 14, no. 8, p. 1863.

Ziadat, FM & Taimeh, AY 2013, 'Effect of rainfall intensity, slope, land use and antecedent soil moisture on soil erosion in an arid environment', *Land Degradation and Development*, vol. 24, no. 6, pp. 582–590. DOI: 10.1002/ldr.2239.

Zobeck, T & Fryrear, D 1986, 'Chemical and Physical Characteristics of Windblown Sediment II. Chemical Characteristics and Total Soil and Nutrient Discharge',

Transactions of the ASAE, vol. 29, no. 4, pp. 1037–1041. DOI: 10.13031/2013.30266.

Zobeck, T & Van Pelt, RS 2011, 'Wind Erosion', in J Hatfield & T Sauer, (eds), *Soil Management: Building a Stable Base for Agriculture*, pp. 209-227. ASA, CSSA, and SSSA Books.

Zore, A, Bezak, N & Šraj, M 2022, 'The influence of rainfall interception on the erosive power of raindrops under the birch tree', *Journal of Hydrology*, vol. 613, p. 128478. DOI: 10.1016/j.jhydrol.2022.128478.

APPENDIX 1. SCRIPTS

A1.1. Python Code Used for Automatic Filling of Attribute Tables in ArcGIS:

Updating the crop factor for the C-factor for 2021:

```
import arcpy

# Set the workspace
arcpy.env.workspace =
r"C:\Users\alsat\OneDrive\Desktop\GIS_Thesis"

# Set the feature class and the fields to update
fc = "C_fac21"
field_to_update = "Crop_fac"
field_to_check = "Class"

# Start an edit session
edit = arcpy.da.Editor(arcpy.env.workspace)
edit.startEditing(False, True)

# Start an edit operation
edit.startOperation()

# Use an update cursor to update the field
with arcpy.da.UpdateCursor(fc, [field_to_update,
field_to_check]) as cursor:
    for row in cursor:
        if row[1] == "Abandoned":
            row[0] = 0.5
        elif row[1] == "Seasonal crops":
            row[0] = 0
        elif row[1] == "Fruit trees":
            row[0] = 1
        elif row[1] == "Citrus":
            row[0] = 1
```

```
        elif row[1] == "Young trees":
            row[0] = 0.5
        elif row[1] == "Trees":
            row[0] = 1
        elif row[1] == "Tree":
            row[0] = 1
        elif row[1] == "Reeds":
            row[0] = 1
        elif row[1] == "Grain":
            row[0] = 0.5
        elif row[1] == "Abandoned with trees":
            row[0] = 1
        elif row[1] == "Vines":
            row[0] = 0.5
        elif row[1] == "Bare soil":
            row[0] = 0
        elif row[1] == "Fallow":
            row[0] = 0.5
        elif row[1] == "Olives":
            row[0] = 1
        elif row[1] == "Disturbed":
            row[0] = 0
        else:
            row[0] = 0 # Use numeric zero instead of "0"

        # Update the row
        cursor.updateRow(row)

# Stop the edit operation
edit.stopOperation()

# Stop the edit session and save the changes
edit.stopEditing(True)
```

A1.2. Earth Engine (JavaScript) Code to Download Landsat Imagery:

Landsat 8 2021 red and NIR bands:

```
var aoi = ee.Geometry.Rectangle([14, 35.7, 14.5, 36.3]);

var dataset =
ee.ImageCollection('LANDSAT/LC08/C02/T1_L2')
    .filterDate('2021-03-29', '2021-03-30')
    .filterBounds(aoi);

// Applies scaling factors.
function applyScaleFactors(image) {
  var opticalBands =
image.select('SR_B.').multiply(0.0000275).add(-0.2);
  var thermalBands =
image.select('ST_B.*').multiply(0.00341802).add(149.0);
  return image.addBands(opticalBands, null, true)
              .addBands(thermalBands, null, true);
}

var scaledDataset = dataset.map(applyScaleFactors);

// Select Red and NIR bands for visualization and export
var RedNIRBands = scaledDataset.select(['SR_B4',
'SR_B5']);

Map.setCentre(14, 36, 8);
Map.addLayer(RedNIRBands, {bands: ['SR_B4', 'SR_B5'],
min: 0, max: 0.3}, 'Red and NIR');
print('Number of images:', scaledDataset.size());

// Select the image as one image from the collection
var OneImage = RedNIRBands.first();
```

```
// Export the image
Export.image.toDrive({
  image: OneImage,
  description: 'Landsat8_21_Red_NIR',
  scale: 30,
  region: aoi,
  fileFormat: 'GeoTIFF',
  folder: 'EarthEngineImages'
});

print('Export started. Monitor the tasks in the Google
Earth Engine Code Editor under the Tasks tab.');
```

APPENDIX 2. EXTRA INPUT MAPS FOR THE RUSLE

A2.1. R-Factor (2021):

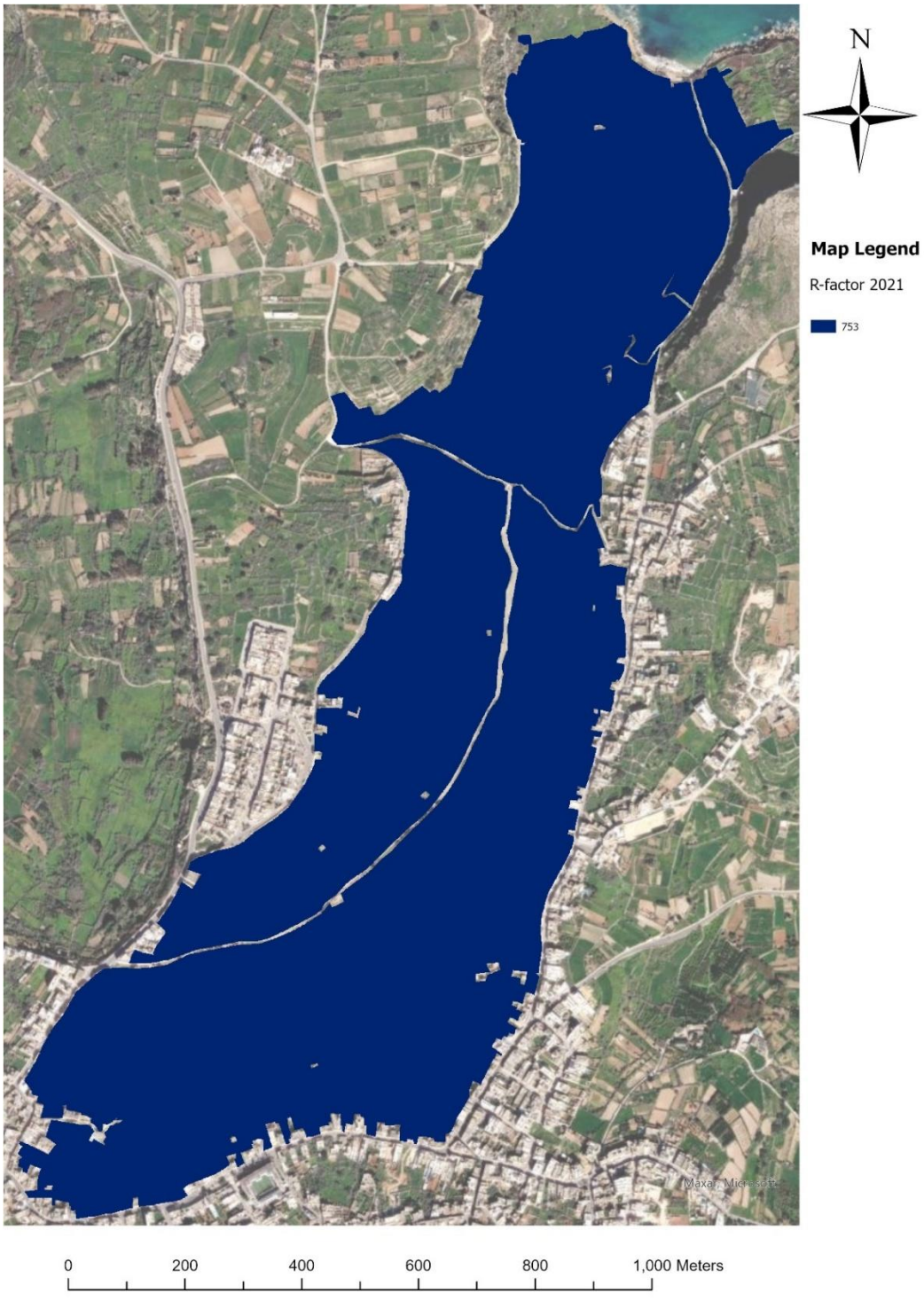

Figure A2-1: R-Factor for 2021

A2.2. K-Factor:

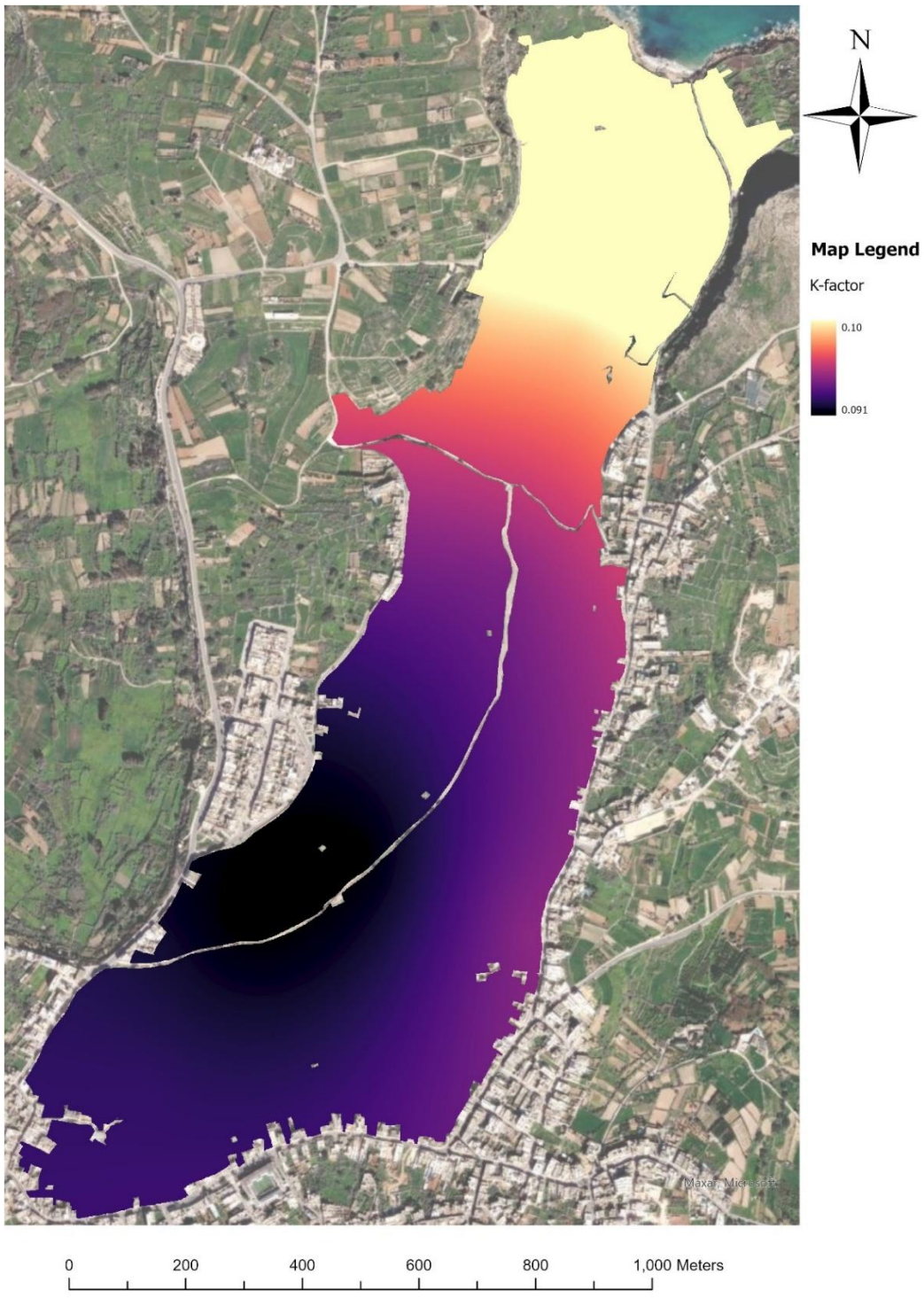

Figure A2-2: K-Factor for 2021

A2.3. DEM at 1 m Spatial Resolution:

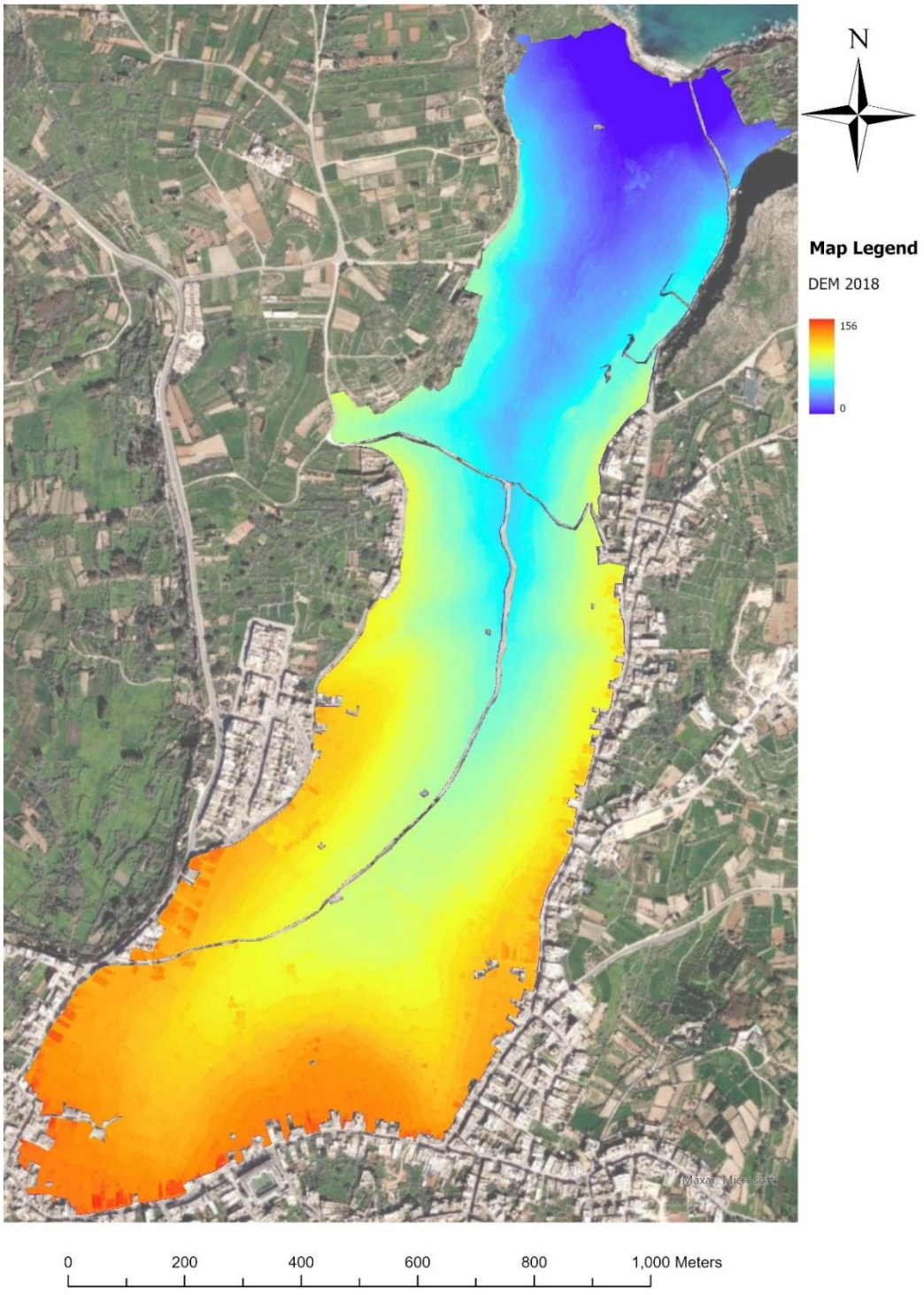

Figure A2-3: DEM for 2018

A2.4. LS-factor at 1 m Spatial Resolution:

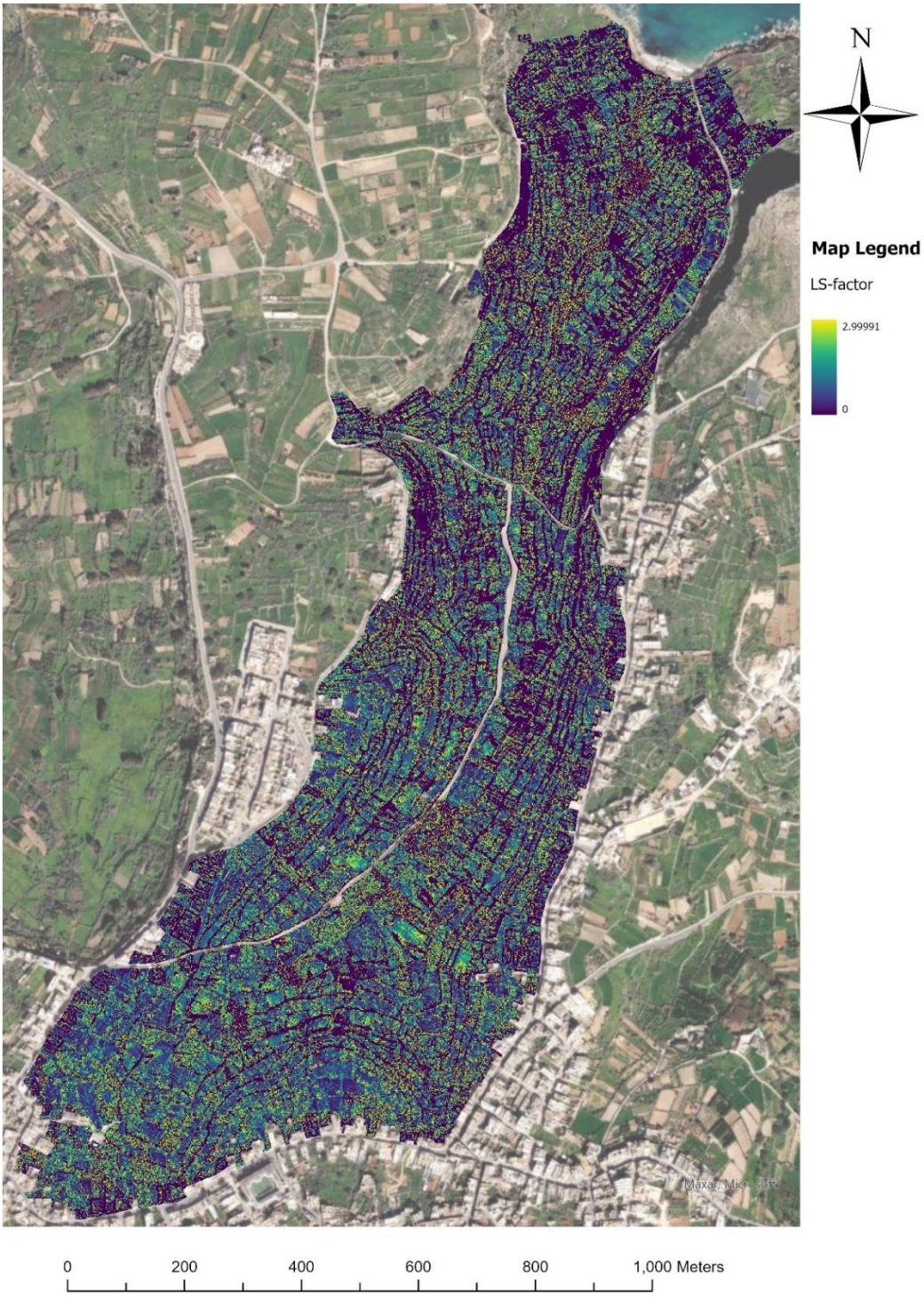

Figure A2-4: LS-Factor for 2018

A2.5. P-Factor:

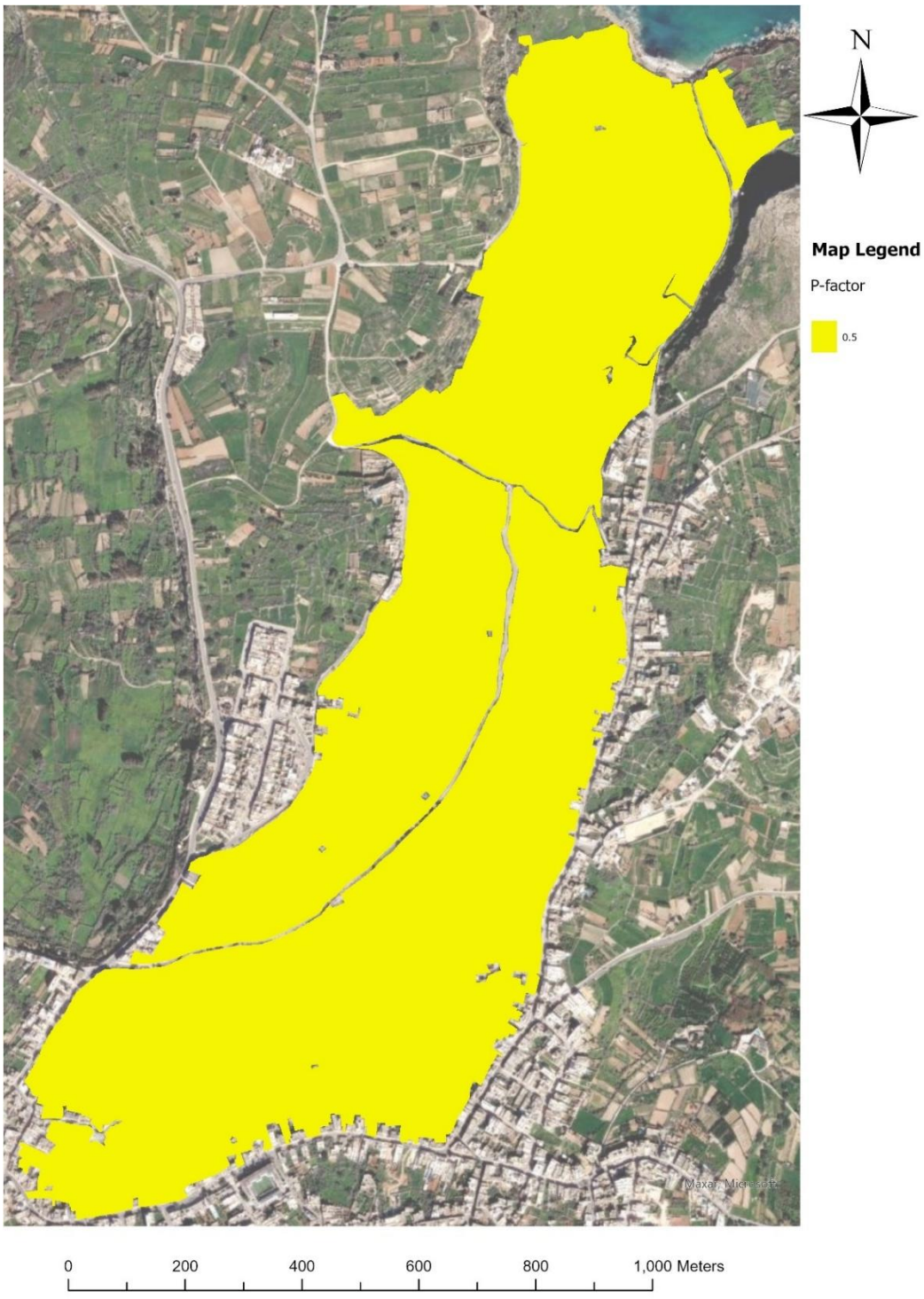

Figure A2-5: P-Factor for 2021

A2.6. R-Factor for 2050 under SSP 2-4.5:

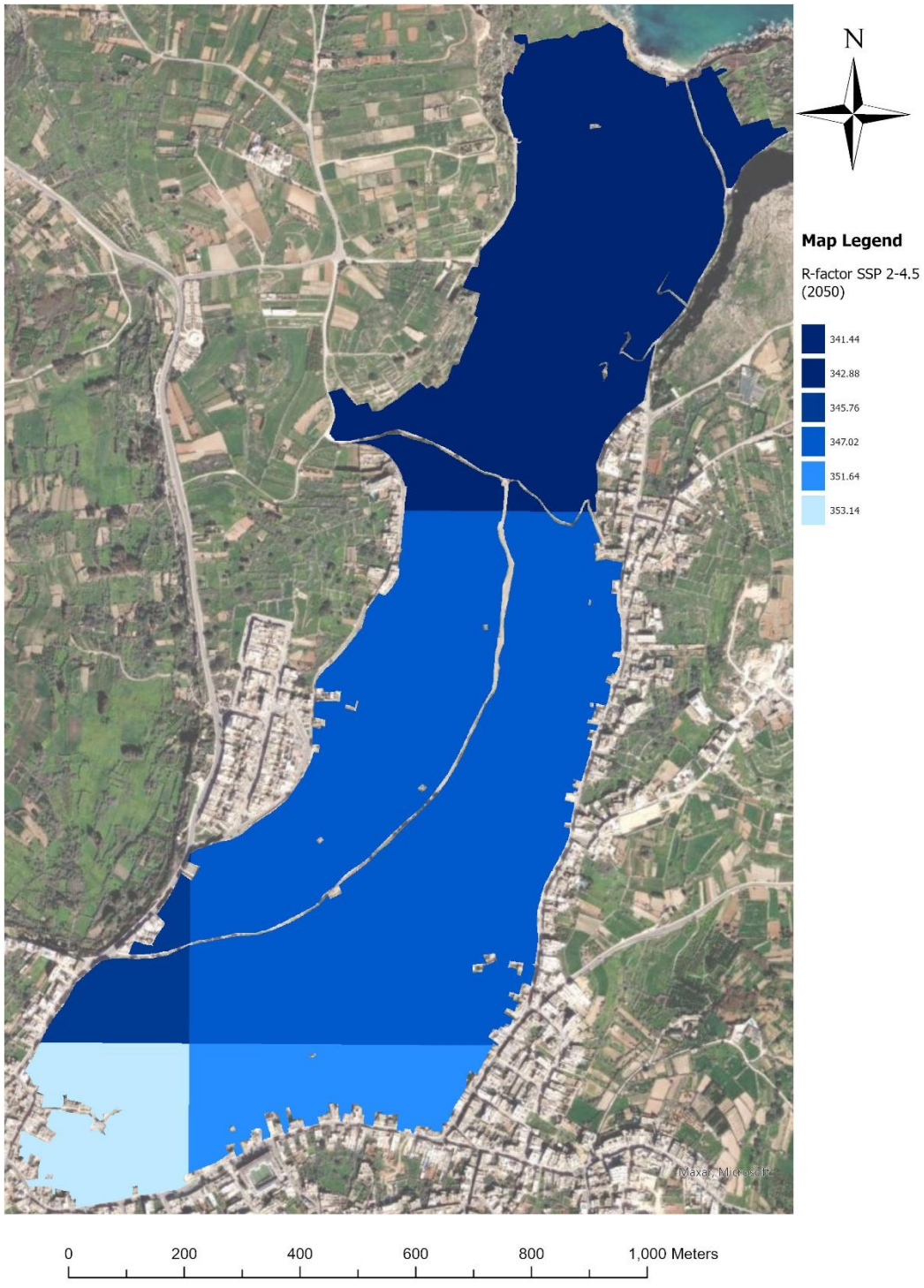

Figure A2-6: R-Factor for 2050 under SSP 2-4.5

A2.7. R-Factor for 2050 under SSP 5-8.5:

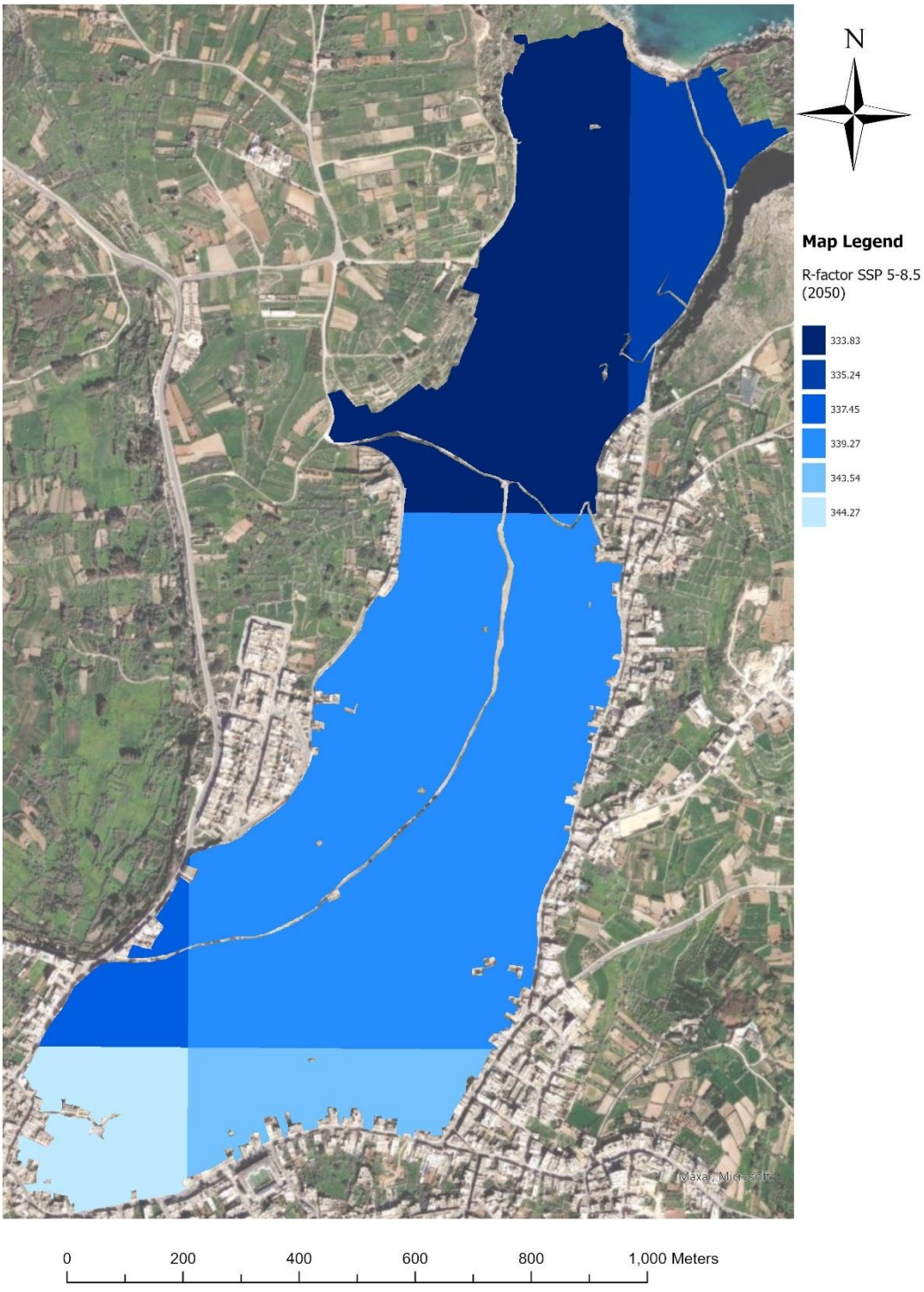

Figure A2-7: R-Factor for 2050 under SSP 5-8.5

A2.8. C-Factor for 2050 from the Spatial Method:

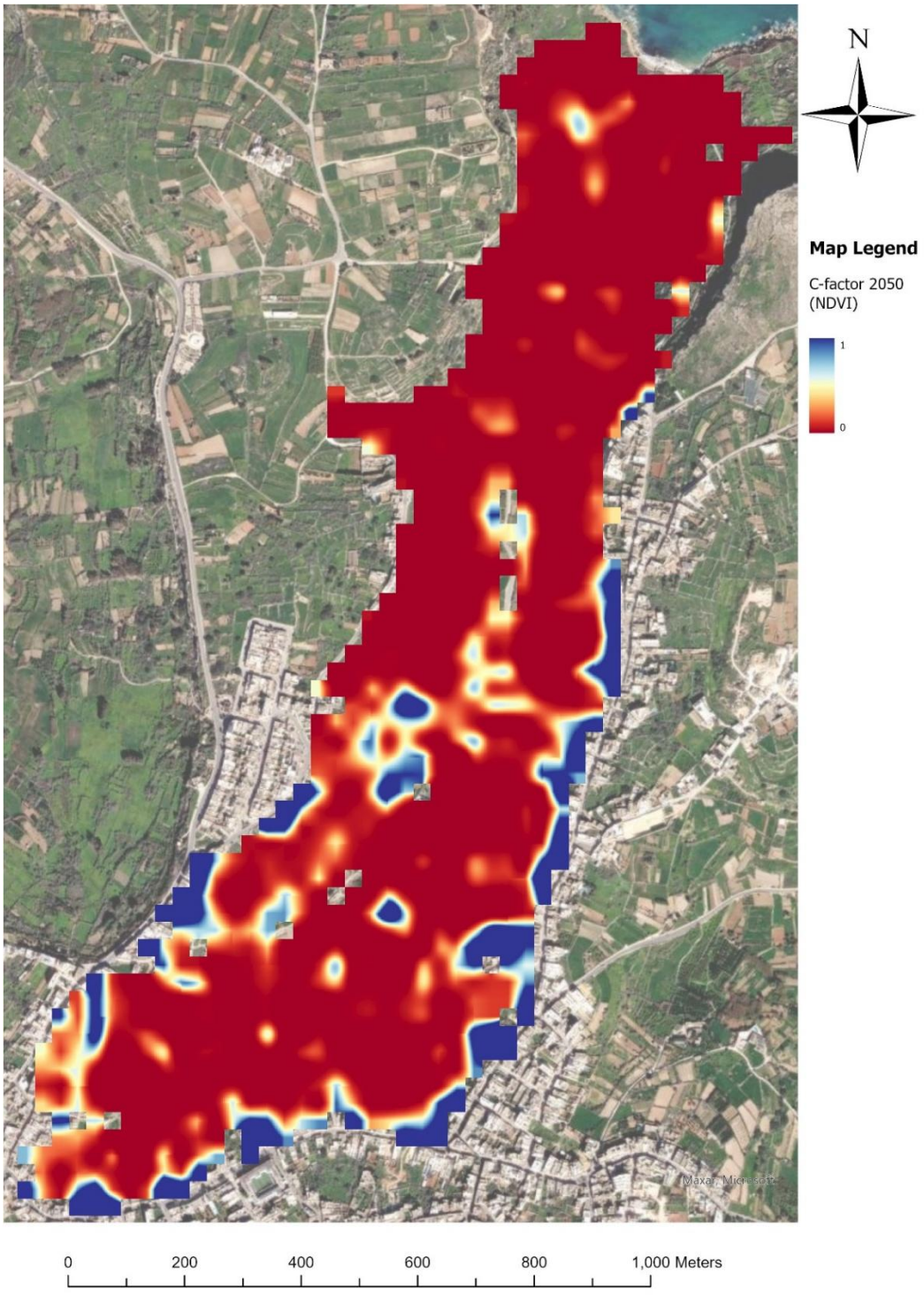

Figure A2-8: C-Factor for 2050 from NDVI

A2.9. DEM from ASTER GDEM at 30 m Spatial Resolution:

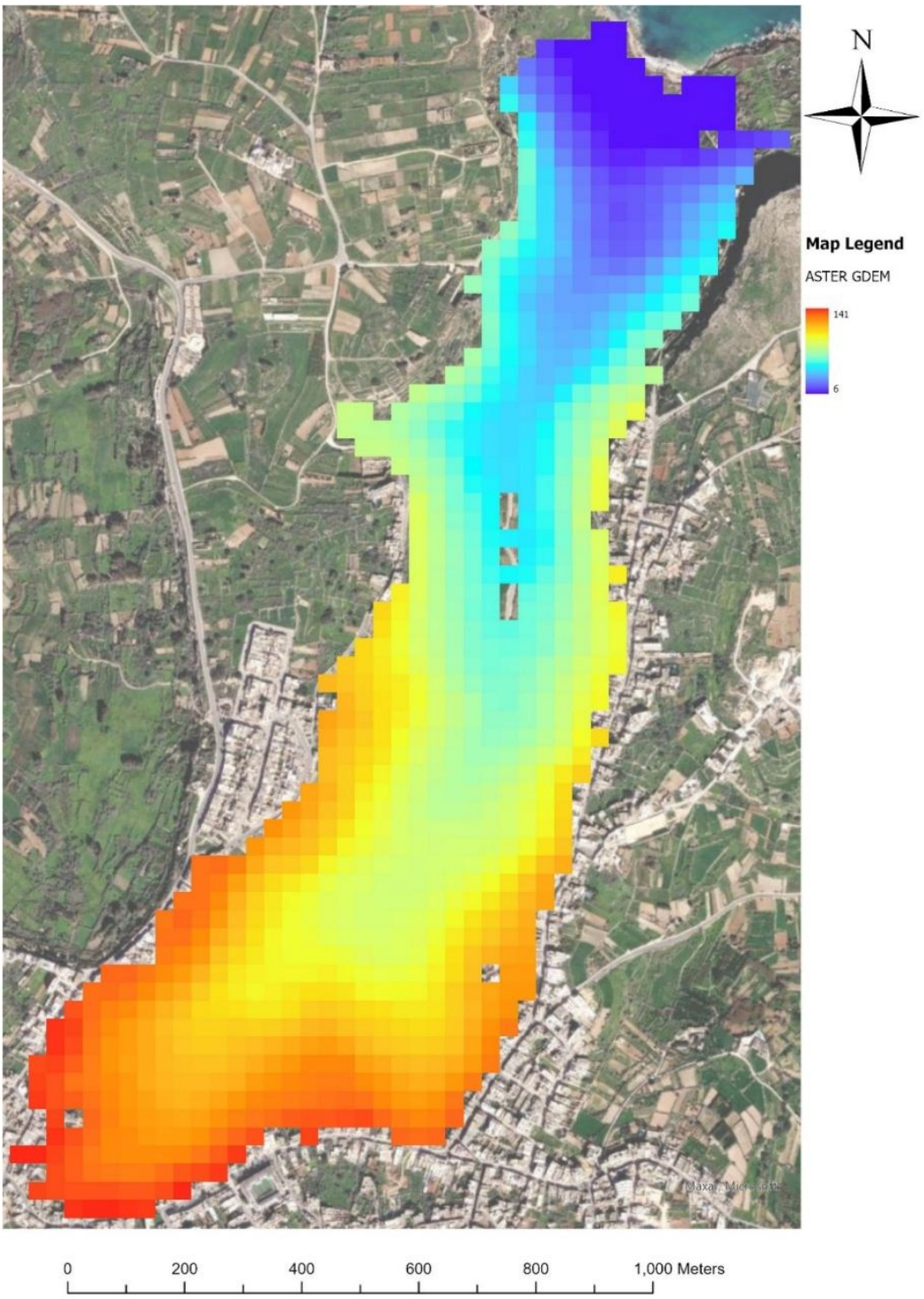

Figure A2-9: ASTER GDEM at 30 m Resolution

A2.10. LS-factor for 2018 at 30 m Spatial Resolution from Upscaled LiDAR vs ASTER GDEM:

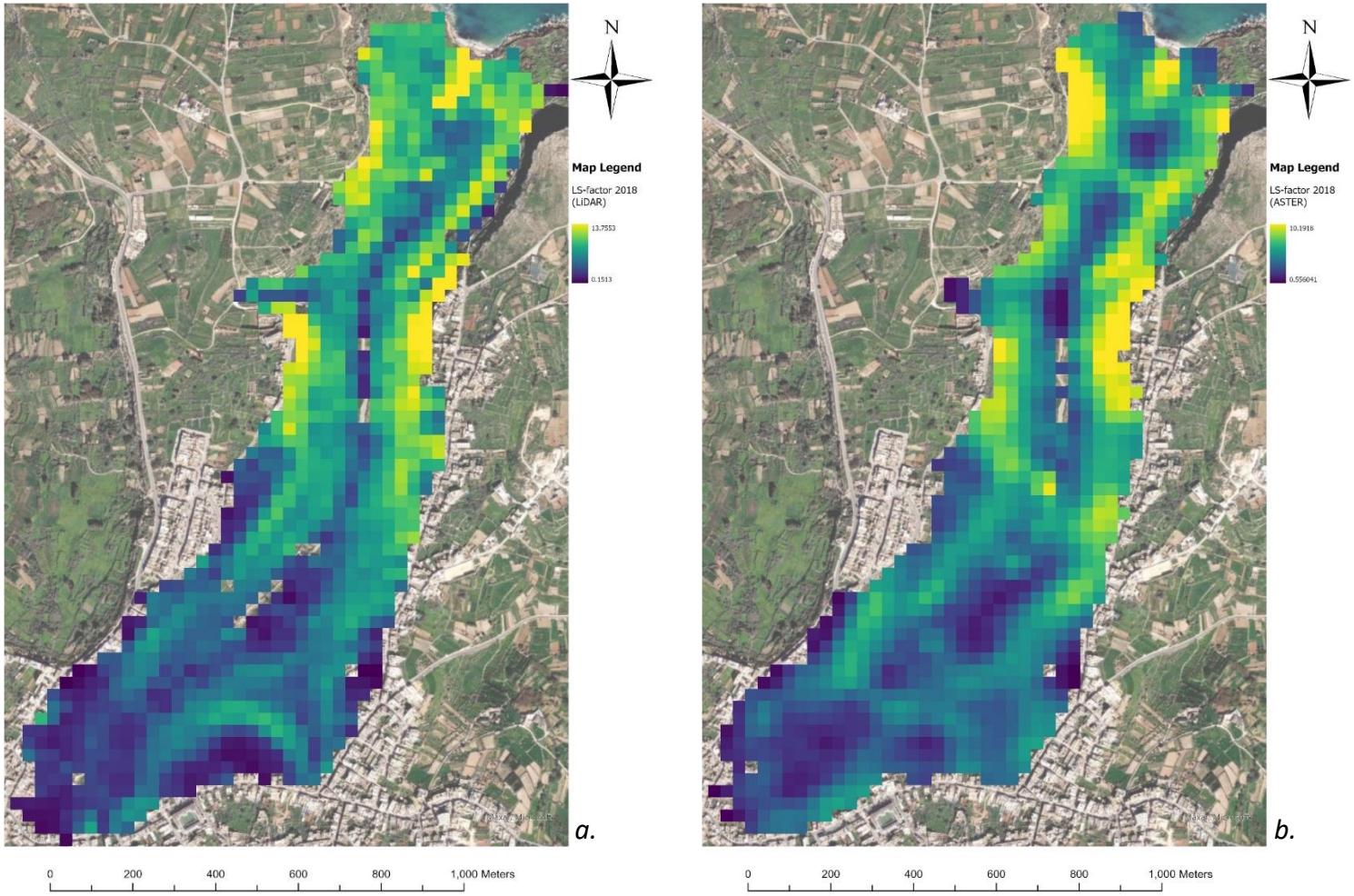

Figure A2-10: LS-Factor at 30 m Resolution Obtained from (a) LiDAR, and (b) ASTER GDEM

APPENDIX 3. EXTRA STATISTICS

A3.1. List of Hypotheses for the Statistical Tests:

Test	Hypotheses
Global Moran's I	H_0: The spatial distribution of the data is random.
	H_1: The spatial distribution of the data is not random.
Normality tests (Kolmogorov-Smirnov and Shapiro-Wilk)	H_0: The data is normally distributed.
	H_1: The data is not normally distributed.
Wilcoxon signed-ranks test	H_0: there is no significant difference in the soil loss estimates derived from a LiDAR DEM and ASTER GDEM.
	H_1: there is a significant difference in the soil loss estimates derived from a LiDAR DEM and ASTER GDEM.
Spearman's rank correlation coefficient	H_0: there is no relationship between LiDAR-derived and ASTER-derived soil loss estimates.
	H_1: there is a significant relationship between LiDAR-derived and ASTER-derived soil loss estimates.
Multiple regression	H_0: there is no relationship between the historic NDVI proxies, air temperature and specific humidity, and historic NDVI.
	H_1: there is a relationship between the historic NDVI proxies, air temperature and specific humidity, and historic NDVI.

A3.2. Histograms for the Soil Loss Estimates:

The histograms in this section all show the distribution of the data. A normality plot is drawn on them to further show the skewness of the data towards 0. The histograms also show the standard deviation in red and the mean in blue of their respective datasets. Histograms for the other datasets were also plotted but were found to have a very similar distribution to the ones present here and thus were not included.

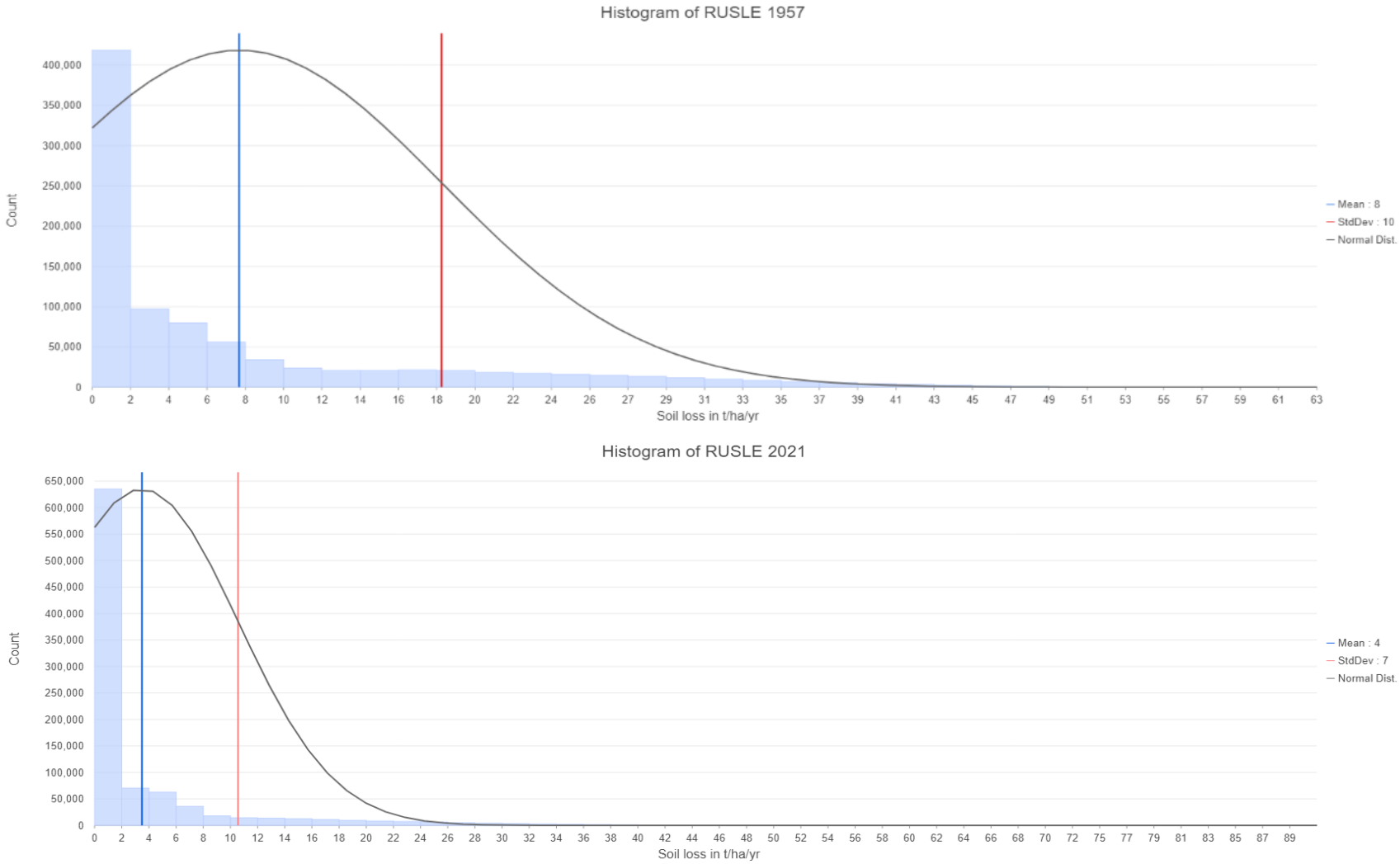

Figure A3-1: Histogram of Soil Loss Estimates for (a) 1957 (b) 2021

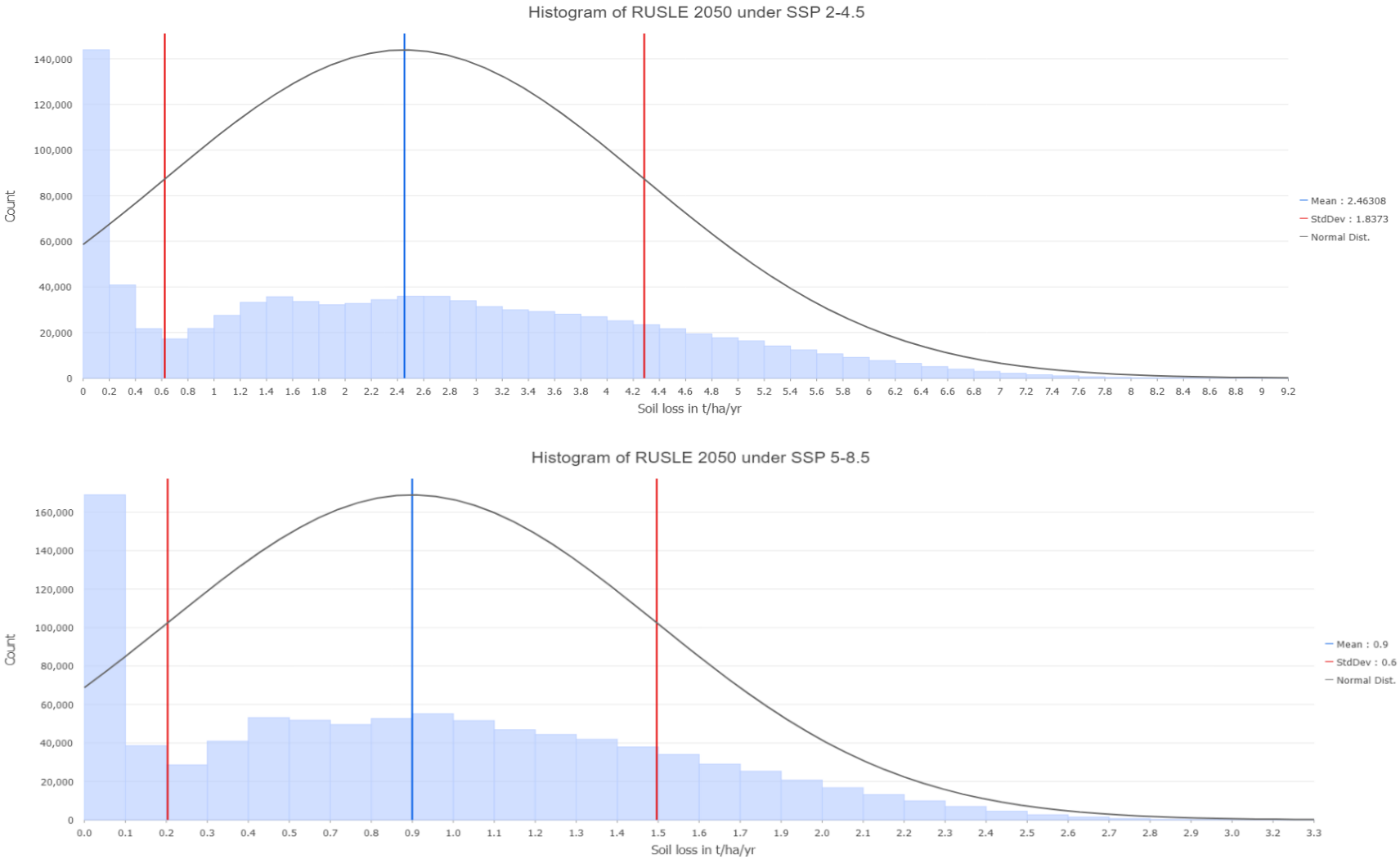

Figure A3-2: Histogram of Soil Loss Estimates for 2050 under (a) SSP 2-4.5 (b) SSP 5-8.5

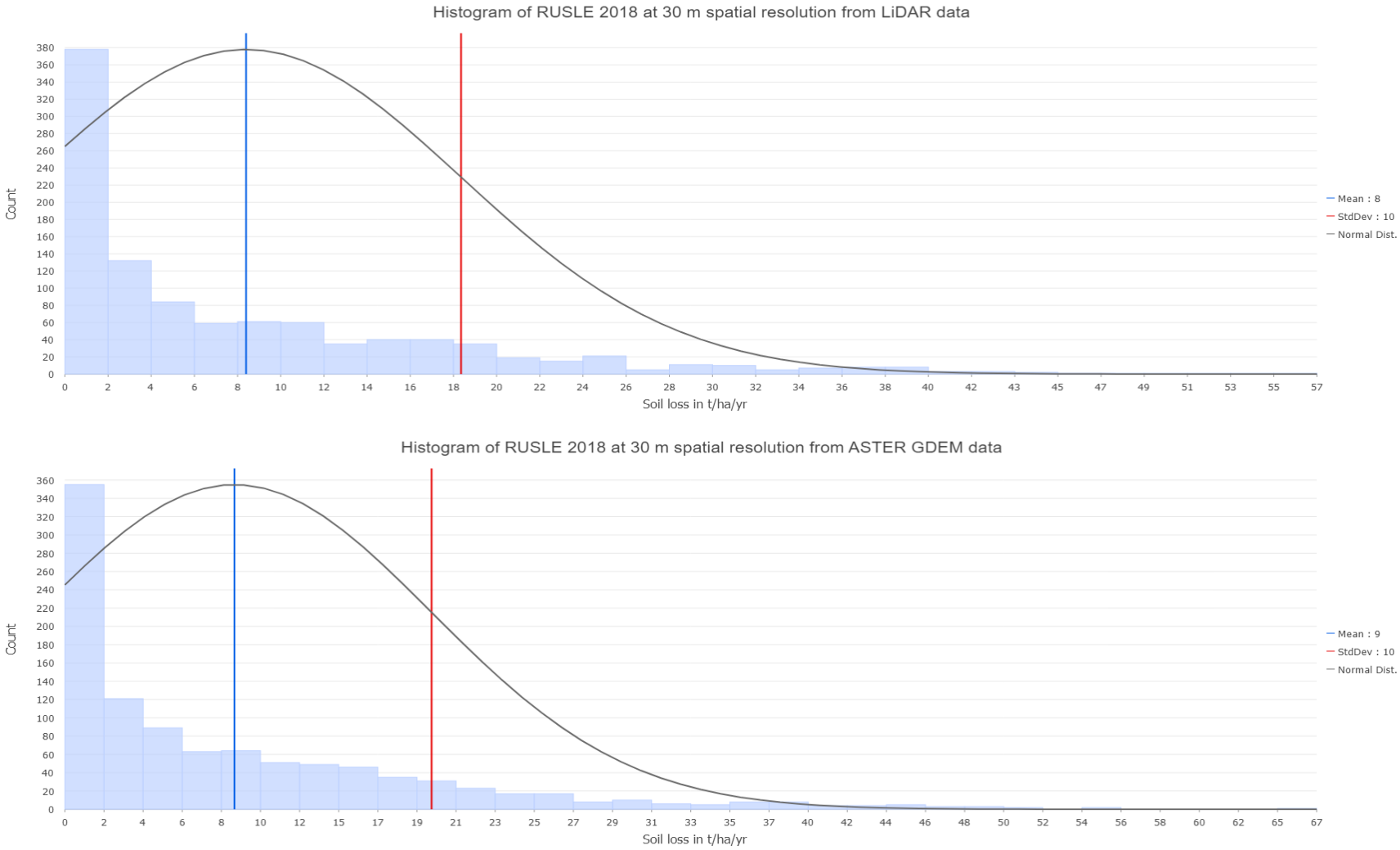

Figure A3-3: Histogram of Soil Loss Estimates at 30 m Spatial Resolution Obtained from (a) LiDAR (b) ASTER GDEM

APPENDIX 4. CASE STUDY OF A STORM EVENT

A4.1. Background:

In the duration of this study, a storm was forecasted to pass over the Maltese Islands and in order to see some visible signs and effects of soil erosion and storm damage, a fieldwork in the AOI was conducted to provide photographic evidence of visible soil erosion signs. The storm occurred between the 8th and 10th of February 2023, with most of the rainfall occurring on Thursday 9th February 2023, the second day of the storm. Rainfall over the three days was obtained from the Met Office's Xagħra station, which is relatively near to the AOI. The rainfall totals are in table A4-1.

Table A4-1: Rainfall Totals in mm per Day of the Storm.

Date	Rainfall in mm
08/02/2023	13.8
09/02/2023	100.2
10/02/2023	3.2

A4.2. Photographic Evidence:

Before the storm photos were taken on the 6th of February 2023 and after the storm photos were taken on the 11th of February.

a *b* *c*

Figure A4-1: Small Dams on the Side of the Valley (a) Muddy and Empty before the Storm (b) Muddy and Partially Empty before the Storm, and (c) Full of Water after the Storm.

Figure A4.1 displays the state of the small dams on the side of the valley floor before (a) and (b), and after (c). The dams are muddy and have only slight water amounts before the storm, however, they are completely full after. The dark line in the dams (a) and (b) shows the level the water often reaches. In fact, this line is under the water level after the storm (c). This shows the sheer amount of rainwater that fell during the storm as this level of water in the dams was achieved after one storm, despite all the runoff that already flowed away.

a

b

c

Figure A4-2: Sand Deposits (a) on the Side of the Valley Floor, (b) in a Field, (c) in a Rill.

Sand particles are heavier and bigger than other soil particles and are thus more resistant to transport, making them be deposited first – instead of continuing to be washed away with the flow.

a *b* *c*

Figure A4-3: Examples of Some of the Rills Found in the AOI. (a) Still has Water Ponding in the Rill, (c) Has Plant Roots Visible

Figure A4-3 shows photographic evidence of soil erosion happening in the AOI, in the form of rill formation.

Figure A4-4: Another Effect of the Storm: Broken Rubble Walls

Figure A4-5: Ponding and Waterlogging of Soils

APPENDIX 5. THE MODIFIED MORGAN-MORGAN-FINNEY MODEL (MMMF)

A5.1. Background:

This study initially had a fourth aim which was to use a different model to estimate soil loss in the AOI. The model chosen was the Modified Morgan-Morgan-Finney model (MMMF). The results of this model were to be compared with those of RUSLE as each model has its own strengths and weaknesses, which can make the use of a specific model better under certain circumstances. It also improves or reduces the models' credibility, depending on the estimates' similarity. Given the MMMF model's ability to estimate soil loss over a duration shorter than a year, this creates new possibilities in using it to estimate soil loss during a single storm event. This is in comparison with the RUSLE equation which is solely an annual model. This model, with its corresponding aim, are not included in the final presentation of the study due to computational and mathematical issues which occurred during processing. Resolving these issues required the use of methods which were out of scope of this study.

A5.2. Model Description:

The Modified Morgan-Morgan-Finney model (MMMF) is based on the earlier Morgan-Morgan-Finney model (MMF) by Morgan et al. (1984). Many different variations were done to improve the original MMF model, these include the MMMF by Morgan and Duzant (2008) as well as the revised Morgan-Morgan-Finney model

(rMMF) by Morgan (2001), and the Daily based Morgan-Morgan-Finney model (DMMF) by Choi et al. (2017). The GIS software SAGA GIS also has a module within the software for calculating the MMMF within a GIS environment. This module is called MMF-SAGA and while it is the MMMF by Morgan and Duzant (2008), it has a few changes from their original work (Wichmann & Setiawan 2012). These changes include:

- Adding a parameter for rainfall duration
- Adding a channel network layer
- Exposure to the parameter regarding flow depth
- Supporting spatially distributed modelling

The MMMF model is a physically-based empirical model making it relatively simple and requiring fewer input parameters than physically-based models, but is still more physically-based than the USLE family of models. The MMMF model requires a number of inputs to work, which can be classified into the following 4 major categories (Morgan & Duzant 2008).

Climate

Climate is a very important aspect to soil erosion. Soil erosion models usually consider an aspect of the climate to help estimate soil losses. The MMMF is no exception, it uses a number of climate related parameters to include the weather and climate aspect in the estimations (Morgan and Duzant 2008). These include:

- Mean annual rainfall in mm, R
- Mean annual temperature in °C, T
- Mean annual number of rain days, R_n
- Typical intensity of erosive rain in mm/h, I

For rainfall intensity, Morgan and Duzant (2008) suggest using a value depending on the climatic regime in which the soil loss is being estimated. They suggest:

- Temperate climates: 10
- Tropical climates: 25
- Strongly seasonal climates such as Mediterranean or monsoon: 30

The MMF-SAGA module includes additional input parameters, along with the aforementioned MMMF inputs. It also requires:

- A timespan in days, which is the duration you want the estimates to cover. The duration can have a minimum of 1 day and a maximum of 365 days.
- Relationship between kinetic energy and rainfall intensity. SAGA GIS provides a list of choices for this option which are as follows:
    - North America east of Rocky Mountains
    - North-western Europe
    - Mediterranean-type climates
    - Western Mediterranean
    - Tropical climates
    - Eastern Asia
    - Southern hemisphere climates

- Bogor, West-Java, Indonesia

Furthermore, all climate parameters are optional in SAGA GIS. However, when an optional parameter is left empty, SAGA GIS takes a default number and uses it for estimates, which may result in inaccuracies (Wichmann & Setiawan 2012).

Soil

Another important aspect to soil erosion is the soil itself and its characteristics. The MMMF includes the following soil characteristics in its estimations:

- Percentage clay, %c
- Percentage silt, %z
- Percentage sand, %s
- Percentage rock fragments on the soil surface, ST
- Soil moisture at field capacity in % w/w, MS
- Bulk density of the topsoil layer in Mg/m3, BD
- Effective hydrological depth of the soil in m, EHD
- Roughness of the soil surface in cm/m, RFR

(Morgan and Duzant 2008).

In addition to the above, MMF-SAGA also requires the saturated lateral permeability, LP of the soil in m/day. Another difference is that the surface roughness in MMF-SAGA is optional and if left blank, it is taken as 1 and thus the surface roughness of the soil is not considered (Wichmann & Setiawan 2012).

Slope

Topography is also of importance to soil erosion and so the MMMF also considers slope to determine soil loss estimations. There are three parameters:

- Slope steepness in °, S
- Slope length in m, L
- Slope width in m, W

(Morgan and Duzant 2008).

Since SAGA is a GIS software, the inputs to the MMF-SAGA are slightly different, albeit they serve the same purpose. They are:

- Digital Terrain Model in m, DTM
- Slope in radians, S

(Wichmann & Setiawan 2012).

Crop cover

The last major aspect which the MMMF model considers is the effect of vegetation and crop cover.

- Permanent interception expressed as a proportion between 0-1, PI
- Canopy cover expressed as a proportion between 0-1, CC
- Ground cover expressed as a proportion between 0-1, GC
- Ratio of actual to potential evapotranspiration, Et/E0

- Plant height in m, PH
- Average diameter in m of the individual plant elements at the ground surface, D
- Number of plant elements per unit area in number/m2 at the ground surface, NV

(Morgan and Duzant 2008).

A5.3. Methodology and Issue Experienced:

The Modified Morgan-Morgan-Finney model is calculated in SAGA GIS via the MMF-SAGA Soil Erosion Model module by V. Wichmann and M. Setiawan (2012). The module takes a number of grids as inputs and provides multiple grids as outputs. The outputs include soil loss, among other grids. The inputs can be classified into several categories and are described in more detail below.

Climate

Regarding climate, the MMMF model requires the following variables:

- Mean temperature in °C
- Amount of precipitation in mm
- Rainfall intensity in mm/hr
- Number of rain days
- Relationship between kinetic energy and rainfall intensity

The data for mean temperature, amount of precipitation, and number of rain days was obtained from the Malta International Airport (MIA) Meteorological Office and inputted into SAGA GIS. Rainfall intensity was set to 30 in SAGA GIS as suggested by Morgan and Duzant (2008) for strongly seasonal climates such as the Mediterranean climate. Relationship between kinetic energy and rainfall intensity was set to 2 for Mediterranean-type climates (Zanchi & Torri 1980).

Soil

Fieldwork

Site Selection

Sampling sites were chosen as in Muscat (2022). This meant that 14 sites were selected in all, from varying areas of the San Blas and Binġemma Valley. The same sites were used for all the sampling procedures.

Soil Moisture at Field Capacity

Soil was sampled by digging a V-shaped hole in the soil and taking a wedge from the side of the hole. This process was repeated 4 times in each field. These 4 samples were placed in a clean bucket and mixed together. The soil sample was then passed through a 2 mm sieve. The portion which passed through the sieve, i.e. was smaller than 2 mm, was placed into a plastic bag and transferred to the lab for further testing.

Bulk Density

A soil corer of known measurements (5 x 4.8) was used to take 4 soil cores from each site. The soil corer was pushed into the soil until it was full. A hole was then dug next to it and a flat piece of metal was pushed underneath it so that the soil core may be removed from the soil. Each soil core was deposited into a separate bag and taken to the lab for further analysis.

Lab Work

Lab analysis involved determining the soil moisture at field capacity and bulk density of the samples taken during the fieldwork. The soil moisture at field capacity was calculated by first reaching field capacity and then using the gravimetric method – an old method with first reported uses by Whitney in 1894 (Johnson 1962) – to ascertain the amount of soil moisture in the sample. The soil bulk density was determined using the core method, also known as the volumetric cylinder method. This method is based on the ISO (2017)'s procedure.

Soil Moisture at Field Capacity

Approximately 20 g of disturbed soil were placed in a cylinder with a mesh bottom of diameter 4.8 cm. This cylinder was placed in a container which was filled with distilled water to a level which was higher than that of the soil in the cylinder. Triples of each soil sample were made. The soil in the cylinder was left to saturate for 24 hours. The cylinder was then removed from the water-filled container and placed on

a drying rack for another 24 hours. This allowed the soil to reach field capacity. The gravimetric method was then used to determine the soil moisture content. The soil at field capacity was weighed and oven-dried at 105°C for 24 hours. When it was completely dry, it was weighed again.

The equation to determine the soil moisture percentage (% w/w) was as follows:

$$SM\% = \frac{M - M_d}{M_d} * 100$$

Where,

- SM% = soil moisture percentage
- M = mass of moist soil
- M_d = of oven-dried soil

Bulk Density

The soil cores were deposited into separate containers and oven-dried at 105°C for 24 hours. Once fully dry, they were weighed, and the measurements noted down.

The volume of the soil corer was determined using the equation:

$$V = \pi * r^2 * h$$

The bulk density was then determined using the following equation:

$$\rho_b = \frac{M_d}{V}$$

Where,

- ρ_b = bulk density
- M_d = mass of dry soil
- V = volume of soil

Percentage Rock Fragments

The soil sampling process mentioned in section 3.4.2.1.2 has two products: the finer portion which is made up of soil particles smaller than 2 mm, and the rockier portion consisting of material larger than 2 mm. This rockier portion is the part which remained in the sieve during the sieving process. To determine the percentage of rock fragments, the soil sample was weighed before sieving. The material larger than 2 mm was weighed again after the sieving process. The weight of the larger material was divided by the total weight of the soil sample and the answer was multiplied by 100 to become a percentage.

GIS Work

The data values for the saturated lateral permeability were determined according to Morgan and Duzant (2008) depending on the soil type present in each soil sampling location. The GIS work for saturated lateral permeability was the same as that for soil moisture at field capacity, bulk density, percentage sand, percentage silt, percentage clay, and percentage rock fragments. The data for each factor was inputted into an attribute table of a vector layer marking the location of the sampling site. Each factor

was then interpolated using kriging in SAGA GIS. This results in an interpolated raster grid for each function. Each grid was then clipped with the clip grids tool in SAGA GIS to match the extent of the AOI.

Topography

The MMF needed a DTM of the area and the slope in radians. The DTM was obtained via lidar imagery with a spatial resolution of 1m (Planning Authority 2018). The slope was calculated in radians using the slope, aspect and curvature tool in SAGA GIS from the DTM.

Land Use

Canopy Cover

The canopy cover layer refers to how much of the plot is covered by a canopy and it includes giving a value between 0-1 for each field. This represents the amount of canopy cover percentage present in the field, with 1 being 100% coverage and 0 being 0% coverage. This was determined using GIS software and an orthophoto of the area of interest. Supervised classification was used in SAGA GIS to divide the orthophoto into canopy cover, ground cover, and other. In QGIS, the raster calculator was used to create a mask layer which considered all the pixels under the division of canopy as 1 and everything as 0. The vector layer with polygons marking each field was used for zonal statistics to find the sum and count of the mask layer per polygon. The output was a new vector layer with sum and count columns in the attribute table.

A new field was added in this table and using the field calculator, sum was divided by count for each polygon to get the canopy values.

Ground Cover

The ground cover layer refers to how much of the ground in each field is covered by vegetation, with values ranging between 0-1 for each field. This represents the amount of ground cover percentage, with 1 referring to 100% coverage and 0 to 0% coverage. GIS software and an orthophoto of the area of interest were used to determine an estimate. The raster calculator was used to create a new mask layer from the classified orthophoto. This time the mask layer considered the ground cover as 1 and everything else as 0. The mask layer and the vector polygon layer were used to perform zonal statistics and calculate the sum and count of each polygon. The sum adds up all the cells with a value of 1 and the count counts all the cells regardless of their value. The field calculator was then used to divide the sum by the count to achieve the number of cells with a ground cover classification. This layer and the canopy cover layers are considered as estimates because the supervised classification process is not 100% accurate.

Permanent Interception

Permanent interception (PI) refers to the amount of rainwater which is intercepted by plants and not allowed to reach the ground during a rainfall event (Morgan & Duzant 2008). Each plot is given a value between 0-1 depending on the amount of rainwater they intercept. This value was decided on depending on the vegetation

growing in the field. ArcGIS was used to fill in the attribute table of a vector file containing polygons outlining each field. The crop cover type listed in this study was matched with a similar land cover type listed in the study by Morgan and Duzant (2008) and permanent interception values were taken from this study accordingly as listed in table A5-1.

Table A5-1: Crop Cover and Permanent Interception Value (Adapted from Morgan & Duzant 2008).

Crop cover	**Crop cover as in Morgan and Duzant (2008)**	**Permanent interception value**
Bare soil	Bare soil (no crust)	0
Seasonal crops	An average of forage crops, carrots, cabbage, peas, onions, and potatoes	0.17
Fallow	Moorland (mainly grass)	0.3
Grain	Winter cereals	0.4
Vines	Vineyards (with grass)	0.25
Fruit trees/Citrus/Young trees/Reeds/Other trees	Orchards	0.25
Abandoned	Moorland (mainly grass)	0.3
Abandoned with trees	Woodland (broadleaved)	0.2

Effective Hydrological Depth

The MMMF also requires the effective hydrological depth (EHD) which is expressed in metres (m). As was the case with the permanent interception, the effective hydrological depth was determined according to the vegetation growing in the field. ArcGIS was similarly used to input the EHD value into the attribute table of the vector file outlining each field as a polygon. The same study by Morgan and Duzant (2008) was used as reference values and so the crop cover classifications between this study and their study are the same as outlined in the permanent interception section above. The following table A5-2 lists the EHD value according to each crop cover classification used in this study.

Table A5-2: Crop Cover Classification and Effective Hydrological Depth Value (Adapted from Morgan & Duzant 2008).

Crop cover classification	**Effective hydrological depth value**
Bare soil	0.1
Seasonal crops	0.13
Fallow	0.13
Grain	0.13
Vines	0.13
Fruit trees/Citrus/Young trees/Reeds/Other trees	0.16
Abandoned	0.13
Abandoned with trees	0.21

Ratio Evapotranspiration

Ratio evapotranspiration, E_t/E_0 is the ratio of actual to potential evapotranspiration. Actual evapotranspiration is the amount of water which through evaporation and transpiration has been removed. On the other hand potential evapotranspiration is the amount of water which the atmosphere is capable of taking when there are no restrictions on water supply. This ratio between actual and potential evapotranspiration ranges between 0 and 1 (Morgan & Duzant 2008). This study used the reference values by Morgan and Duzant (2008) to classify ratio evapotranspiration according to crop type as per table A5-3. ArcGIS was also used to input the E_t/E_0 values into the attribute table of the polygon vector layer.

Table A5-3: Crop Cover Classification and Ratio Evapotranspiration Values (Adapted from Morgan & Duzant 2008).

Crop cover classification	**Ratio evapotranspiration value**
Bare soil	0.05
Seasonal crops	0.66
Fallow	0.90
Grain	0.60
Vines	0.30
Fruit trees/Citrus/Young trees/Reeds/Other trees	0.70
Abandoned	0.90
Abandoned with trees	0.95

Plant Height

Plant height is the height of the crop in meters, and it is used to consider the height which raindrops fall from the crop onto the soil underneath. The different plant classes were measured several times in the field using a tape measure, and then an average height was taken for each class. The classifications and their respective plant height values can be seen in the following table. ArcGIS was also used to input the height values into the attribute table of the polygon vector file outlining each field.

Tabe A5-4: Crop Cover Classification and Plant Height Values (Adapted from Morgan & Duzant 2008).

Crop cover classification	**Plant height value**
Bare soil	0.0
Seasonal crops	0.4
Fallow	1.2
Grain	0.9
Vines	0.8
Fruit trees/Citrus/Young trees/Reeds	2.5
Other trees	4
Abandoned	1.2
Abandoned with trees	3

Plant Diameter

Plant diameter is the average diameter of the crop in meters at the plant surface, and it can include plant stems and tree trunks. The different plant classes were measured several times in the field using a tape measure, and then an average diameter was taken for each class. The classifications and their respective plant diameter values can be seen in the following table. ArcGIS was also used to input the plant diameter values into the attribute table of the polygon vector file outlining each field.

Table A5-5: Crop Cover Classification and Plant Diameter Values (Adapted from Morgan & Duzant 2008).

Crop cover classification	**Plant diameter value**
Bare soil	0.0
Seasonal crops	0.014
Fallow	0.006
Grain	0.006
Vines	0.05
Fruit trees/Young trees	0.07
Citrus	0.15
Reeds	0.04
Other trees	0.164
Abandoned	0.006
Abandoned with trees	0.2

Number of Plant Elements

Number of plant elements is the number of the crops per unit area. Several sample areas of 1 meter squared of each crop were used to count the number of crops growing in it. An average amount was taken and used for each crop classification. The classifications and their respective number of plant elements values can be seen in the following table. ArcGIS was also used to input the number of plant elements values into the attribute table of the polygon vector file outlining each field.

Table A5-6: Crop Cover Classification and Number of Plant Elements Values.

Crop cover classification	**Number of plant elements value**
Bare soil	0.0
Seasonal crops	11.25
Fallow	100
Grain	400
Vines	0.44
Fruit trees	0.16
Citrus/Young trees	0.11
Reeds	100
Other trees	0.2
Abandoned	100
Abandoned with trees	100

MMMF Model

Each vector layer was exported as a shapefile from ArcGIS and imported into SAGA GIS. They were then rasterized and clipped to the extent of the AOI using the 'shapes to grid' and the 'clip grids' tools respectively. The MMF-SAGA Soil Erosion Model (Wichmann & Setiawan 2012) was then used to calculate the soil loss in kg using the MMMF model. When this tool in SAGA GIS was run, an issue was encountered as the resulting maps had a minimum and maximum of infinity, indicating that there was a division by 0 somewhere in the calculation. To find a solution to this problem, it was attempted to work the model step-by-step to determine where in the process the issue is occurring. However, working the model manually required a level of coding expertise which is out of scope for this study.

APPENDIX 6. PARTICLE-SIZE DISTRIBUTION AND SOIL ORGANIC MATTER CONTENT

A6.1. Particle-Size Distribution:

Sample	% Sand	% Silt	% Clay	Soil Textural Class
1A	57	35	8	Sandy loam
1B	61	30	9	Sandy loam
2A	53	28	19	Sandy loam
2B	54	30	16	Sandy loam
3A	43	21	36	Clay loam
3B	45	18	37	Clay loam
4A	48	33	19	Loam
4B	54	28	18	Sandy loam
5A	41	36	23	Loam
5B	43	34	23	Loam
6A	24	26	50	Clay
6B	24	28	48	Clay
7A	65	16	19	Sandy loam
7B	60	23	17	Sandy loam
8A	48	36	16	Loam
8B	50	34	16	Loam
9A	66	21	13	Sandy loam
9B	67	22	11	Sandy loam
10A	73	16	11	Sandy loam
10B	73	16	11	Sandy loam
11A	37	29	34	Clay loam
11B	36	31	33	Clay loam
12A	33	27	40	Clay
12B	31	29	40	Clay
13A	65	19	16	Sandy loam
13B	68	16	16	Sandy loam
14A	61	16	23	Sandy clay loam
14B	65	14	21	Sandy clay loam

Figure A6-1: Soil textural classes and percentage of sand, silt, and clay per soil sample.

A6.2. Soil Organic Matter Content (SOM):

Soil sample		Soil mass	Start	End	Difference	% Organic Matter	Average % Organic Matter
1	A	1.17	0	10.8	10.8	2.788	2.68
	B	1.1	10.8	23.3	12.5	2.405	
	C	1.04	23.3	34.9	11.6	2.857	
2	D	1.06	0	6.8	6.8	4.726	4.74
	E	1.2	6.8	12.6	5.8	4.496	
	F	0.94	12.6	20.2	7.6	5.001	
3	A	1.03	0	12.9	12.9	2.506	2.43
	B	1.13	12.9	/	/	/	
	C	1.03	24.9	38.2	13.3	2.360	
4	D	1.17	0	2.6	2.6	5.577	5.70
	E	0.99	2.6	7	4.4	5.901	
	F	1	7	12	5	5.614	
5	A	1.08	12	24.7	12.7	2.434	2.34
	B	1.01	24.7	38	13.3	2.383	
	C	1.03	0	13.7	13.7	2.192	
6	D	1.14	13.7	29	15.3	1.525	1.48
	E	1.01	29	45	16	1.454	
	F	1.12	0	15.6	15.6	1.449	
7	A	1.06	0	9.2	9.2	4.408	4.34
	B	1.04	9.2	19.1	9.9	4.254	
	C	0.98	19.1	29.4	10.3	4.370	
8	D	1.09	29.4	39.2	9.8	3.726	3.69
	E	1.1	0	9.8	9.8	3.692	
	F	1.01	9.8	20.8	11	3.638	
9	A	1.08	0	17.4	17.4	1.474	1.55
	B	1.11	17.4	33.7	16.3	1.749	
	C	0.98	0	18	18	1.429	
10	D	1.33	18	34.9	16.9	1.316	1.46
	E	1.25	0	16.7	16.7	1.451	
	F	1.35	16.7	32.3	15.6	1.603	
11	A	1.04	0	8.5	8.5	4.449	4.07
	B	1.15	8.5	16.8	8.3	4.081	
	C	1.02	16.8	27.9	11.1	3.687	
12	D	1.05	0	12.2	12.2	3.229	3.05
	E	1.01	12.2	25	12.8	3.160	
	F	1.02	25	38.9	13.9	2.770	
13	A	1.3	22.5	35.7	13.2	2.298	2.33
	B	1.04	0	14.8	14.8	2.378	
	C	1.2	14.8	28.6	13.8	2.329	
14	D	1.11	28.6	40.8	12.2	3.002	2.95
	E	1.16	0	11.9	11.9	2.957	
	F	1.27	11.9	23	11.1	2.904	

Figure A6-2: Titration readings and percentage organic matter per soil sample.